GEOTHERMAL RESEARCH, MONITORING AND TESTING: FINAL REPORT, GEOPHYSICS SUBTASK, MICROSEISMICITY STUDY

Prepared by P. Cooper and M. Dustman

1. INTRODUCTION

1.1. Proposed Work for Seismicity Study, Kilauea East Rift Zone

The proposed seismicity study was intended to address two problems important to geothermal resource assessment and management: (1) Baseline background seismicity prior to exploitation and (2) Geophysical characterization of upflow zones.

Through reconnaissance surveys, microearthquakes have been observed in many geothermal areas of the world, and microseismicity has been shown to correlate with geothermal activity. It is important to establish background seismicity levels prior to full-scale exploitation of a geothermal resource and especially before initiation of injection procedures. Underground fluid disposal by pressurized injection can induce seismicity on preexisting fractures at pressures lower than those necessary to fracture fresh rock. The normal stress on faults is reduced by increased pore pressure, triggering fault movement under existing (ambient) shear stresses (Simpson, 1986). In some cases seismic energy greatly exceeds injection energy, suggesting that induced earthquakes release tectonic strain. Microseismicity data have been shown to be very effective in evaluating the movement of reinjectate, as well. The most famous case is the Denver, Colorado, earthquakes studied in detail by Healy et al. (1968). Subsequent early studies of similar cases in Los Angeles, California, by Teng et al.

(1973), Matsushiro, Japan, by Ohtake (1974), and at Dale, New York, by Fletcher and Sykes (1977) came to the same conclusion: small microearthquake networks were effective in mapping the local seismicity, demonstrating its relationship to fluid injection, and in computing the focal mechanisms demonstrating that tectonic stress was released.

Geophysical research and exploration surveys that have been conducted along Kilauea's East Rift Zone during the past 15 years include aerial infrared scanning, gravity, airborne magnetic, vertical electric sounding, time-domain electromagnetic, ground noise, and seismic reflection/refraction studies, as summarized by Thomas (1986). No microearthquake surveys with sufficient resolution had been conducted previously in this region. Although the proposed seismic study would cover a smaller geographical area than that of Suyenaga and Furumoto (1978), it was hoped that the larger number of stations and smaller spacing between the seismometers would provide order-of-magnitude improvement in resolution of small heterogeneities at shallow, reservoir depth. Specifically, by detailed mapping of microearthquakes in the Puna region we hoped to locate active faults along which steam and hot water are brought to the surface. Active faulting is thought to be the major mechanism by which geothermal reservoirs are maintained and, in some cases, enlarged. Seismic observations of P- and S-wave travel-time delays and inversion for 3-dimensional Vp/Vs structure would be used to delineate the approximate dimensions of the geothermal field. The success of these geophysical techniques would provide a new method for locating drilling targets in the East Rift Zone.

The study was to be phased over a period of 2 years. Phases 1 and 2 were to include the construction of an initial velocity model for the rift zone and relocation of earthquakes previously reported by Hawaii Volcano Observatory using that initial velocity model. The travel times of the relocated earthquakes would then be inverted for an improved 3-dimensional velocity model. This velocity model was to be the jumping-off place for subsequent modeling efforts using new data. Problems with the HVO data made Phase 2 of this task fruitless. Although HVO currently has 52 active stations on the island of Hawaii, only four are located along the Lower East Rift Zone (LERZ). The inadequate azimuthal distribution of these four stations and the small number of earthquakes located along the LERZ (31 during the time period 1990-1992) combined to make the velocity inversion meaningless; there were not enough ray paths to resolve the velocity structure. Earthquake data recorded by HVO during the field portion of this experiment are included in this report.

Phase 3, the field experiment, was to include deployment of a small seismic network with a 4- to 7-km aperture for a 20-day period in the vicinity of HGP-A, later moving to a second location. These arrays were to have 14 sites spaced about 2 km apart, each instrumented with two sets of three-component, short-period geophones. The field experiment as modified and extended when the PANDA array was made available. Details of the field experiment are contained in the preliminary (1-year) report and are summarized briefly below in section 1.2. A gravity survey was to be undertaken within the boundaries of each array to help define shallow subsurface density variations associated with structural features.

This work was completed in collaboration with HVO and is discussed in section 2.

Phases 4 and 5 involved analysis of the data collected during Phase 3. The results of the data analysis, as summarized in the monthly reports, is discussed below in sections 3 through 7.

1.2. Seismicity Experiment

Between January 27 and May 03, 1993, the Portable Array for Numerical Data Analysis (PANDA) was used in a passive seismic array experiment in the Puna Geothermal Field, located in the Lower East Rift Zone (LERZ) of Kilauea Volcano. The instrumentation was leased from the Center for Earthquake Research and Information (CERI) at Memphis State University. Because the main purposes of the deployment of the PANDA instrumentation were to (1) establish background seismicity levels prior to full-scale exploitation of the resource and (2) create an "image" of the geothermal reservoir using the travel times of seismic waves from local earthquakes, the array was centered about Puna Geothermal Venture's (PGV) KS-8 well. Based on previous geophysical studies and well-log data this location was chosen as the approximate geographical center of the resource area. The PANDA instrumentation was deployed to provide ideal coverage of a target depth range of from 2 to 4 km (with the intention of sampling as many raypaths from local earthquakes as possible). This resulted in a very dense distribution of stations (0.4-

0.5 km spacing) near the PGV drill sites surrounded by a less-dense distribution (1.0-1.5 km spacing).

It was determined early-on in the project that earthquake data available from Hawaii Volcano Observatory would not be sufficient to determine a preliminary velocity model of the Puna region. This is primarily because HVO maintains only four single-component (vertical) short-period seismometer stations along the LERZ (names). The triggered response of these few stations to LERZ earthquakes is ignored unless other stations in the HVO detect the events; hence, HVO does not routinely locate and catalog events in the Puna region with magnitudes less than about 2.0. Four PANDA stations were co-sited with HVO stations both to provide greater depth resolution for the PANDA array and to facilitate integration of any available HVO data into the PANDA data set. Figure 1 shows the locations of all PANDA stations; complete background information on all stations is located in Appendix I.

1.2.1. General System Description

Individual stations consisted of pairs of three-component seismometers, FM radio transmitter with antenna, 12-V battery, solar panels, electronics and fiberglass field case (see e.g. Steiner, 1986; Chiu et al., 1991). The paired-station telemetry design places transmit-only "outer" stations along the outer edges of the array. "Inner" stations receive the radio signals from the outer stations and rebroadcast a multiplexed inner/outer signal. The voltage output from the instruments at the outer stations could be amplified by

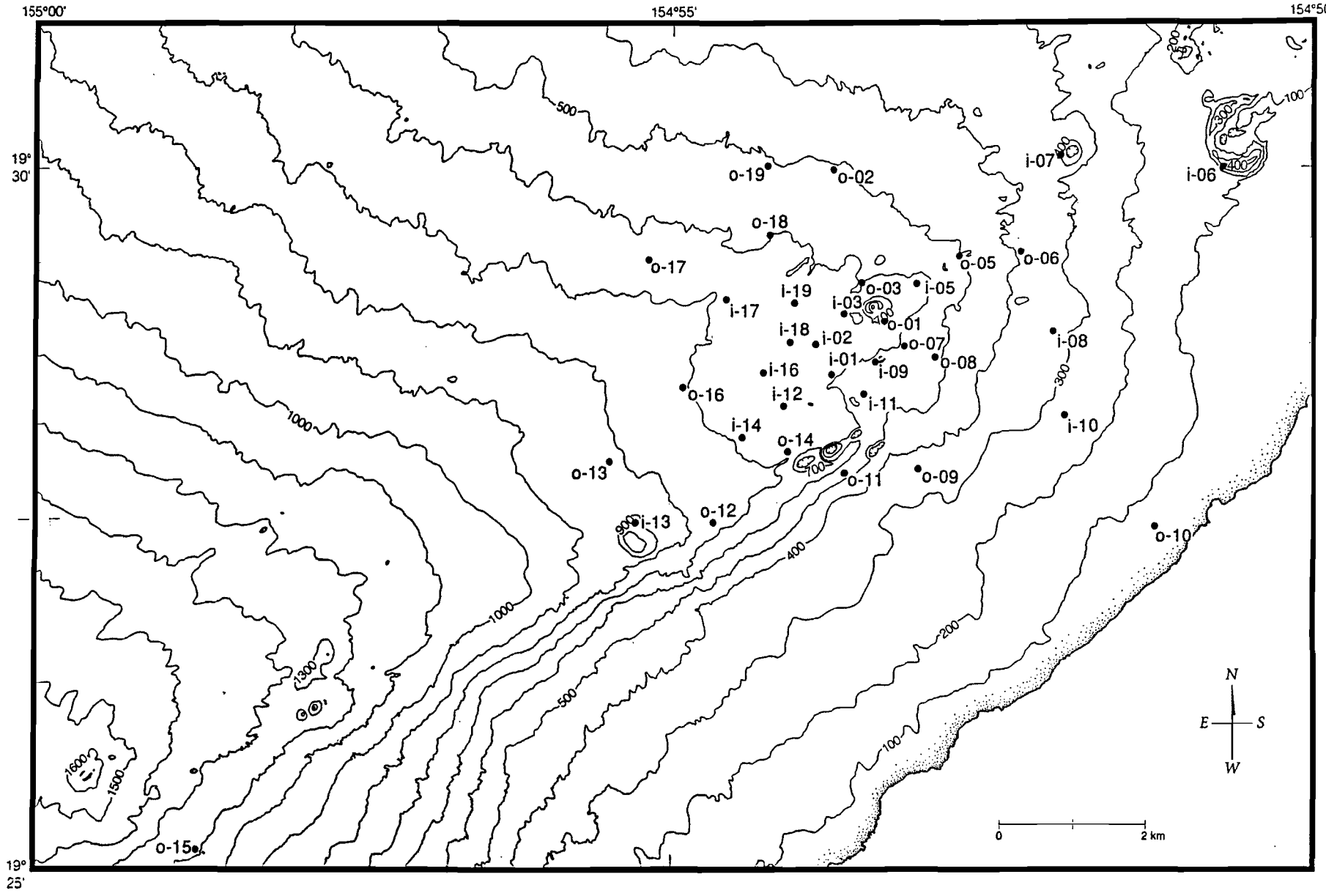

Figure 1. Station locations for PANDA array. The paired-station telemetry system, with inner, "i," and outer, "o," stations is explained in detail in the text. Contour intervals are in feet.

either a two-stage high-gain preamplifier or a single-stage low-gain preamplifier. Overlapping the high- and low-gain preamplifiers by 18 dB at a single site provided an effective dynamic range of up to 108 dB. Inner station preamplifiers were set to high-gain for both sets of components.

After amplification the data were passed through a four-pole analog Butterworth low-pass anti-aliasing filter. The cut-off frequency was set at 25 Hz for 100-Hz sampled data. A single-pole high-pass filter with cut-off frequency set to 0.033 Hz was used to remove DC offsets from the data (Figure 2).

A Voltage-Controlled Oscillator (Figure 3) with seven carriers spaced at 400 Hz converted the voltages to an FM signal. The first six carriers were used for the six signals (one per component) measured at each station. The seventh carrier was used only with the inner station configuration (Figure 4). The FM signal from the outer station was received and multiplexed with the six inner-station carriers. The inner stations, therefore, serve dual purposes as data acquisition sites and repeater stations.

The Puna Research Center, operated by the Natural Energy Laboratory of Hawaii Authority (NELHA; Lund, 1986) and located near the PGV lease was used as the central receive site, i-01, (Figure 1) because of its large storage area, work and office spaces, readily available power supply, and line-of-site location with respect to the planned array locations. All equipment and packaging was stored in approximately one-half of the covered facility; the remaining area was devoted to workspace for assembling the seismometer station components. One office housed the back-up power supply,

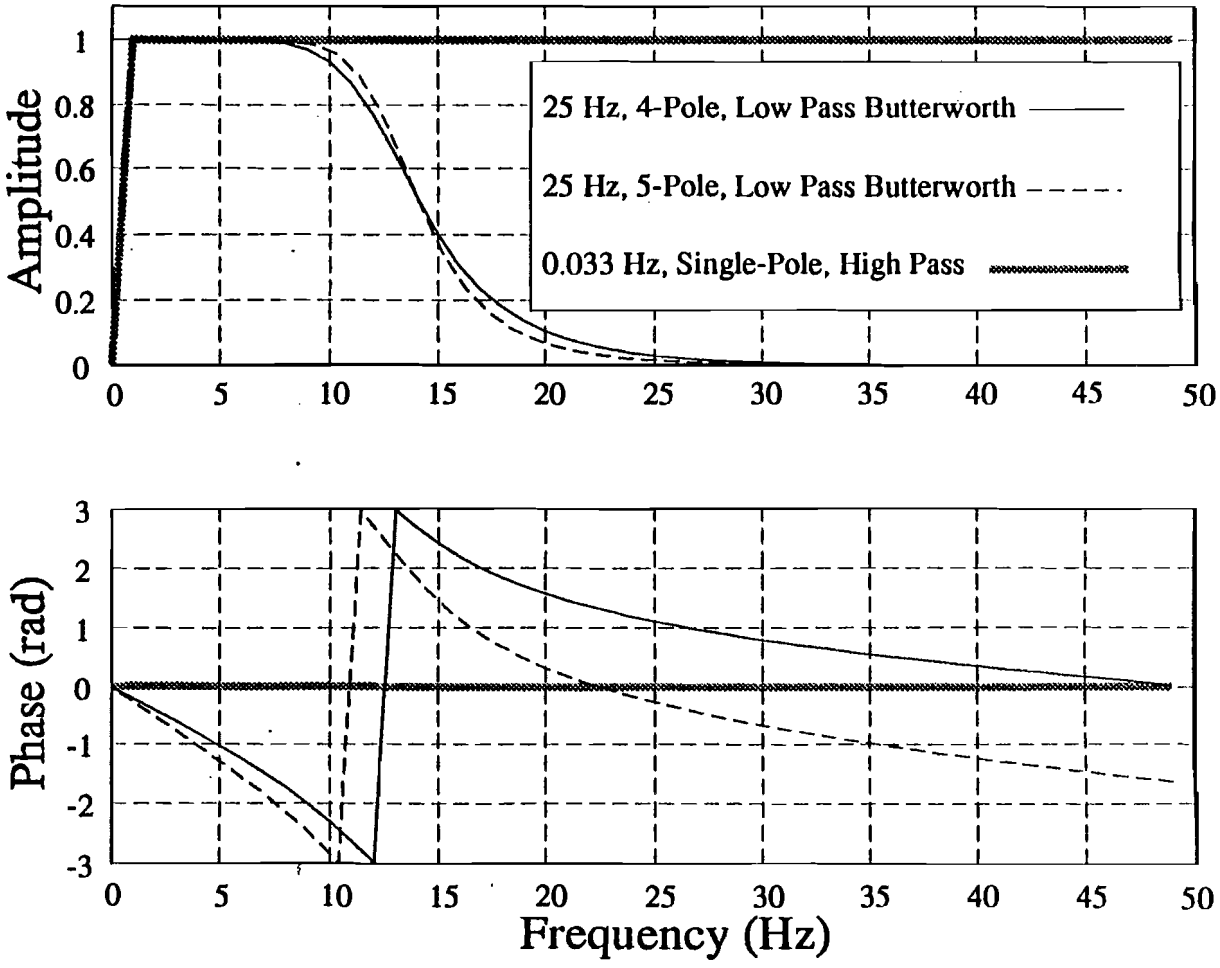

Figure 2. **Plots of the frequency and phase responses of the PANDA system filters.**

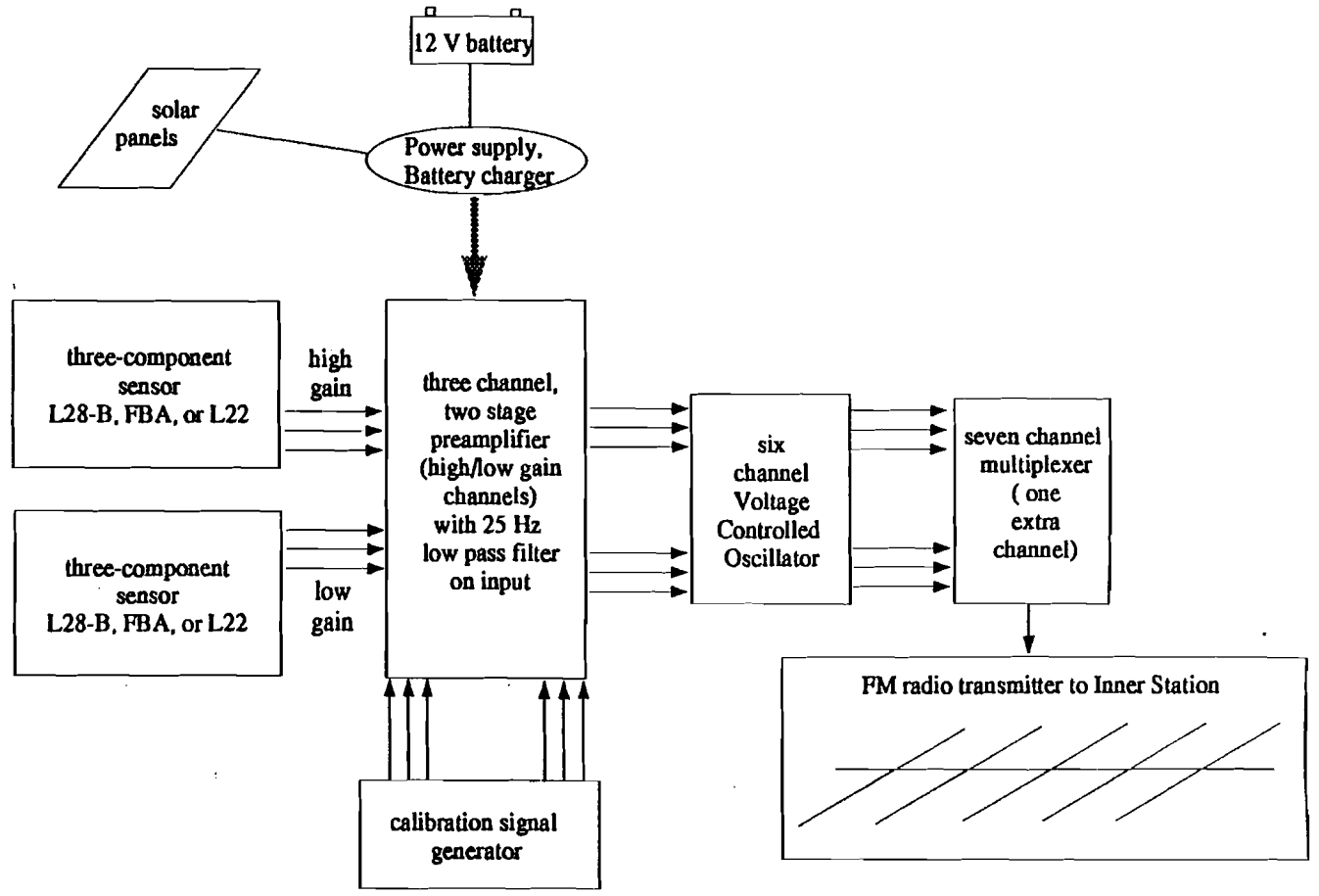

Figure 3. Data flow chart of an outer station, after Chiu et al., 1991.

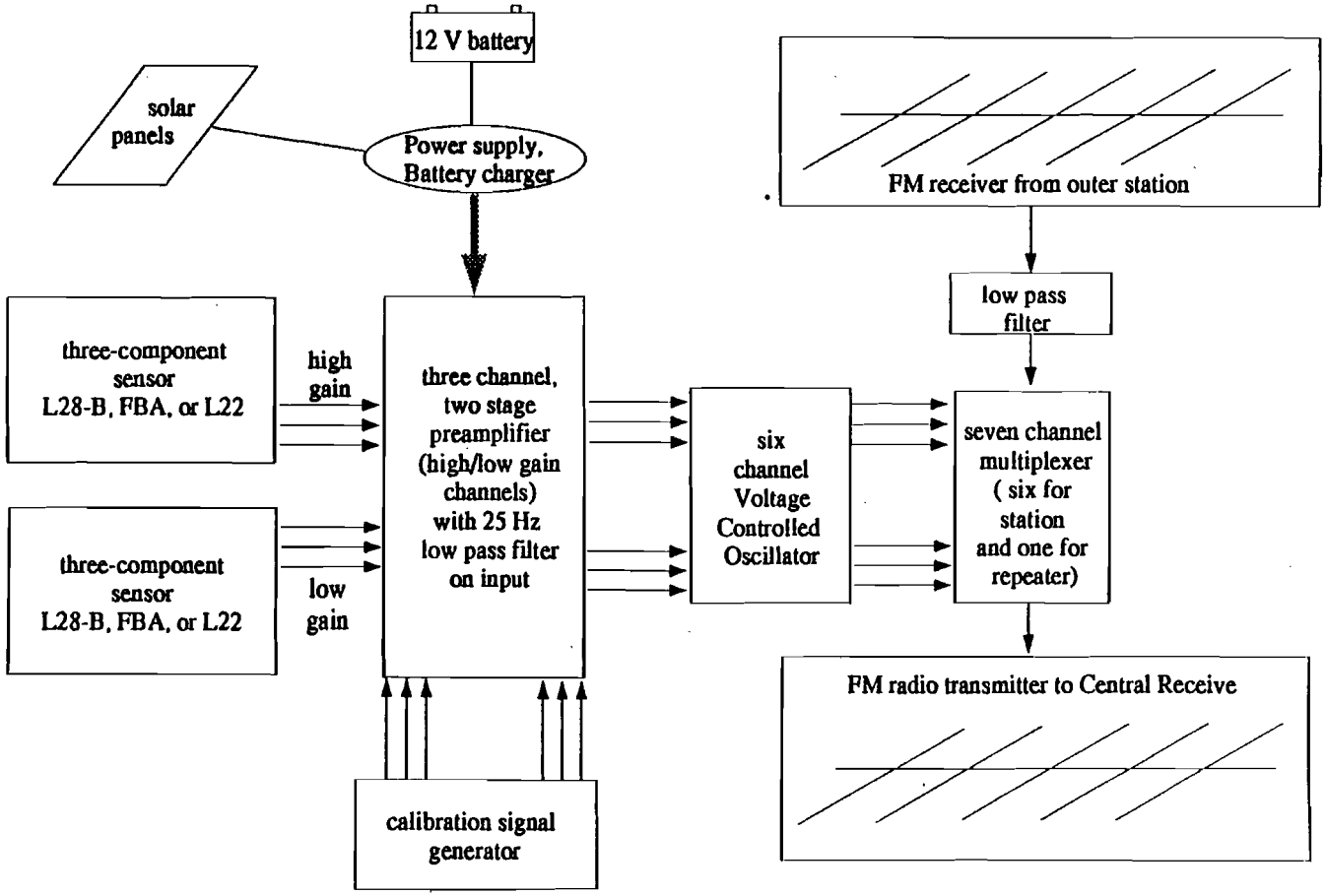

Figure 4. Data flow chart of an inner station, after Chiu et al., 1991.

computers, and recording equipment needed for data acquisition. Receiving antennae were mounted on a 75-foot tower from which the data were cabled into the lab for processing. The 17 continuous signals from the inner/outer station pairs were passed through discriminators and demultiplexed, producing 204 channels (17 station pairs at 12 channels per station; Figure 5). These data, along with timing signals from a satellite clock, were sent to a 12-bit 256-channel A/D converter. Each channel is sampled at 50 kHz for 100-Hz signal sampling, yielding a time lag of 20 msec between adjacent channels. The maximum time lag was 4.8 msec between channels 1 and 240, less than one-half of one sample.

The system response (geophone, filters, telemetry, and electronics) to velocity, as determined by technicians at Memphis State, shows a dominant recording frequency of about 20 Hz (Figure 6).

The continuous 100-Hz sampled data were cabled to a MASSCOMP™ MC660 workstation. "Events" were recorded in one-minute files by an event-detect algorithm using short- and long-term average ratios. Coincidence conditions between triggers at several previously specified stations (the trigger group) determined if an "event" had occurred (Chiu et al., 1991). The triggering process, in effect, the sensitivity of the array, is fine-tuned to eliminate false triggers by varying the stations within a trigger group and the accept level for the time-averaged ratios. In practice, a trade-off is necessary between the expected minimum event size and an acceptable number of false triggers. This array was configured to record events as small as M_D = -2.0. Many types of cultural noise,

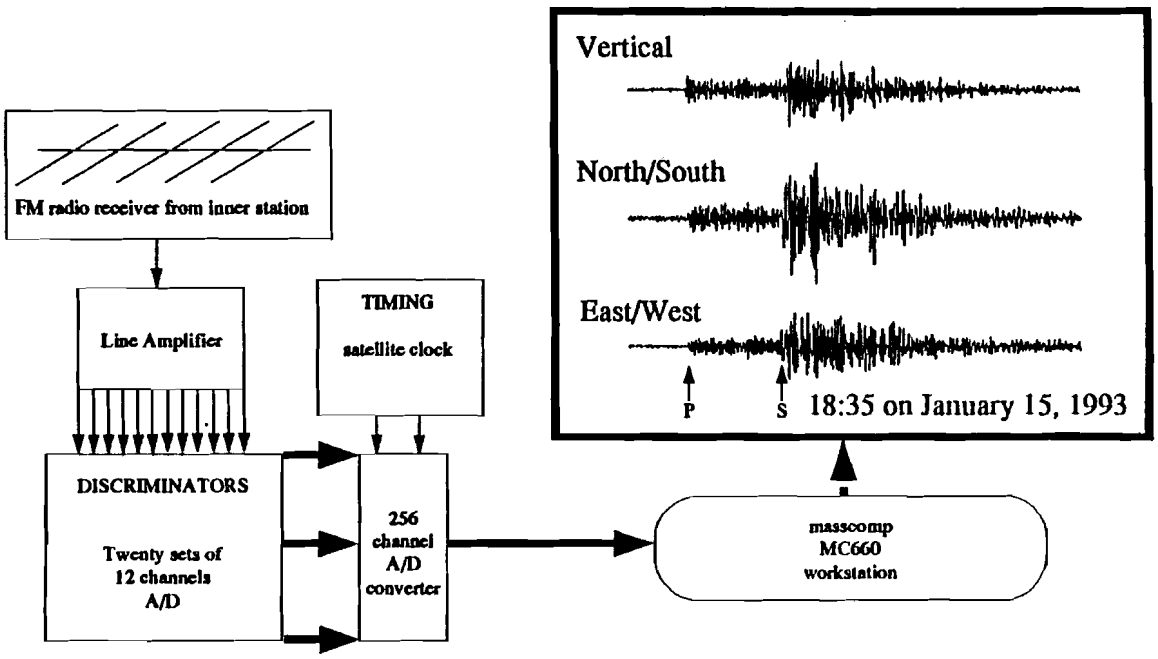

Figure 5. Data flow chart for the central receiving site established at the Puna Research Center, Puna, Hawaii, after Chiu et al., 1991.

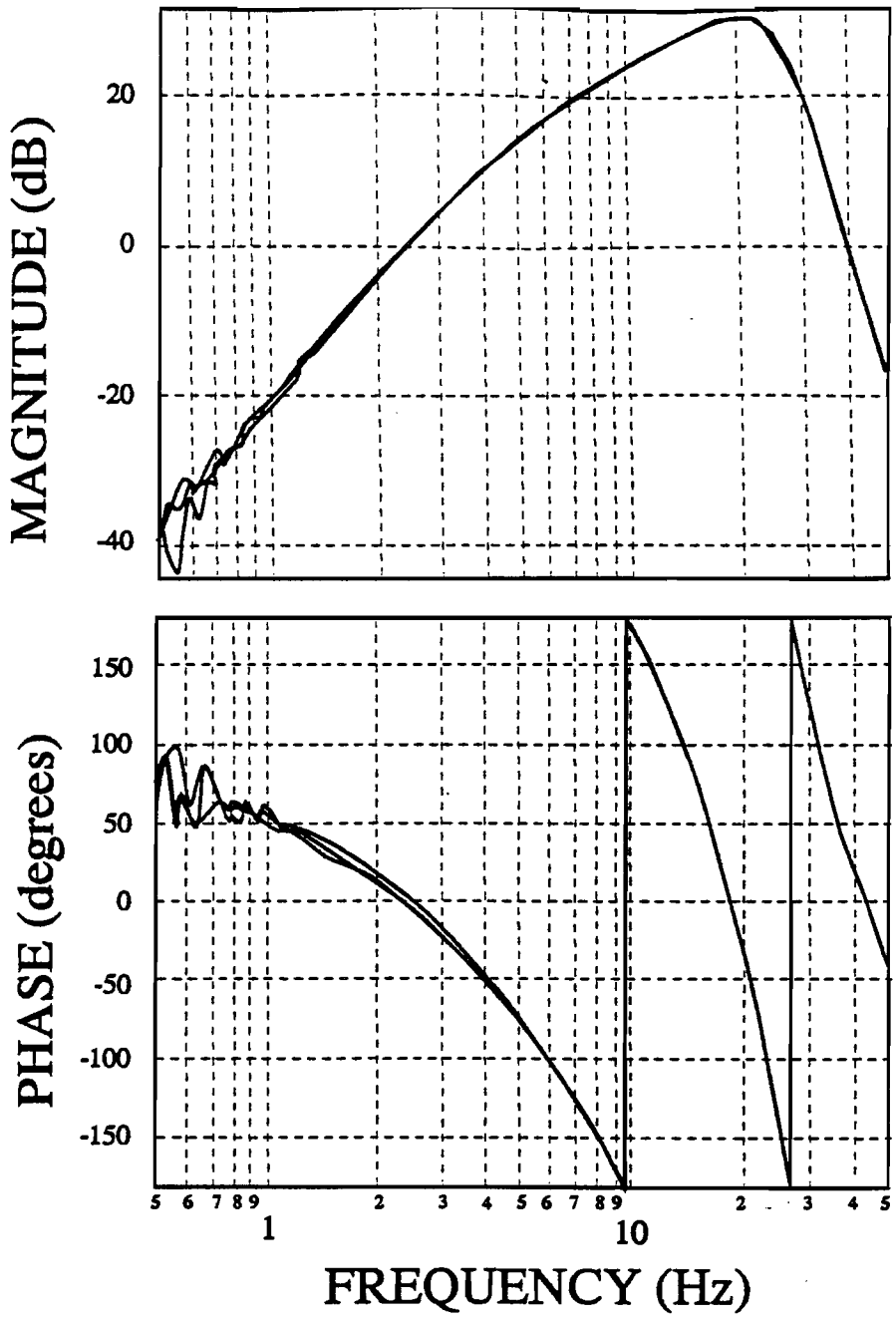

Figure 6. Frequency response to velocity as derived from a shake-table experiment at Memphis State University (personal communication, J. Bollwerk). These transfer functions represent the response of the entire PANDA acquisition system.

for example, helicopters, heavy machinery, and drilling at nearby PGV initiated false triggers. The triggered events were screened on a daily basis, and false triggers were removed from the data set.

Event files were recorded in one-minute files; a 20-second pre-trigger data buffer was used to ensure event capture, in other words, the saved event file began 20 seconds prior to the trigger time. Events, such as teleseisms, having durations longer than one minute were recorded as several one-minute files.

All saved files were archived to 9-track tape, written in PANDA format. Archived data was stored on-site, at the University of Hawaii at Manoa and at Memphis State University. Software for processing the data on a Sun SPARCsystem LX-4/30 EGX (x-windows operating system) was developed under this contract by Mike Simpson and is copyrighted to the University of Hawaii.

1.2.2. Station Installation

Stations were distributed as an elliptical array (Figure 1) centered on the PGV geothermal well KS-8, with the long axis parallel to the LERZ, and covering an area 9.5 x 7 km^2. Station spacing is smaller (0.3 to 0.5 km) in the center of the array to increase ray densities in the target region.

Station location selection was based on the following criteria:

1. Line-of-sight between transmitting and receiving sites was preferred for good signal quality and strength. Several stations, such as o-15, o-11, and i-05 (Figure 1) were not along line-of-sight because of topography, and required higher

transmitting power. This did not pose significant problems.

2. Noisy locations were avoided, if possible (e.g. wind, waves, roadways, heavy equipment).
3. Sites were required to be accessible by 4-wheel drive or by foot.
4. Stations were placed in secured or guarded locations whenever possible. In the months prior to this experiment Hawaii Volcano Observatory reported two of their stations vandalized (David Clague, personal communication). None of the PANDA stations were vandalized during the experiment.
5. Sites were to be placed in fully permitted locations only.

All sites were visited prior to installation to evaluate possible noise sources, check the availability of sunlight for battery recharge, and check for telemetry problems. Depth of burial of the instruments varied from 0.5 to 2 feet depending on soils conditions. Soil conditions ranged from soft soil to dense pahoehoe and a'a lavas. Station site characteristics are summarized in Appendix I. At locations where solid rock was present at the surface, pick-awls were used to break up as much rock as possible. The holes for the sensors were then backfilled with the excavated rock or soil and checked for abnormal noise levels.

Station locations were verified using both topographic maps, which have an accuracy of about ± 8 m horizontally and ± 3 m vertically, and Global Positioning System (GPS, Magellan™ 5000) hand-held instruments. The GPS positions would be adequate for locating the stations in a seismic array with dimensions on the order of a hundred kilometers; in this case, a horizontal uncertainty of 100 meters would constitute up to 30% of the actual interstation distance.

Station locations were measured several times throughout the experiment for accuracy.

Before burial, the geophones were aligned with the Earth's magnetic field (magnetic north, not geographic north) using a hand-held compass. United States Geological Survey maps (Anonymous, 1975) for the island of Hawaii show a magnetic north declination of 11°. This value should be used for all calculations dealing with the orientation of the instruments. Estimated uncertainty for azimuth is ±5°.

1.2.3. Field Problems

Several problems were encountered during the field portion of this experiment, largely due to increased noise levels at many stations, reducing the signal-to-noise ratio. The radio-telemetry system for the PANDA instrumentation was designed to transmit under local- to regional-scale conditions. "Local-scale" conditions was defined as from 10 to 50 km. For the Hawaii experiment, the longest transmittal distance was about 5 km and many of the distances were several hundred meters in length. Transmitting power had to be significantly reduced to avoid cross-talk. Telemetry problems permanently disabled station o-12. For station pairs with similar transmitting azimuths, the inner/outer configuration was reversed and the antennae polarizations were modified to alleviate interference.

Dominant cultural noise sources originated in drilling-related activity. A drilling rig, numerous heavy trucks, and steam-powered

generators were in use on the PGV property during daylight hours. This was particularly evident on the continuous drum recordings that were used to monitor the efficiency of the event detection system (Figure 7). The system recorded more than 200 events over the two-day period, February 28-29; during this time the bit was stuck in the hole (drilling log, on file at Department of Land and Natural Resources). Impacts and explosives were required to release the bit, resulting in the numerous triggers (Figure 8).

Other sources of cultural noise are passing vehicles, curious passing pedestrians, and helicopters flying at low altitudes.

1.4. Data Quality

A total of 1,002 event files were archived after visual inspection of the data and removal false triggers. This total includes 160 noise sample files, 762 earthquake files, 106 drill-bit impact/explosion files, and 2 files containing calibration signals. In many cases, a single one-minute earthquake file may contain multiple earthquakes. Additional files containing samples of cultural noise were archived.

Casual visual inspection of the digital data set demonstrates the very high quality of the data. Figures 9 through 11 each display a selected earthquake and its spectrogram for three orthogonal components - vertical, north-south, and east-west - uncorrected for instrument response. Compressional, or P-wave, arrivals typically have a frequency content in the band 12-16 Hz. shear, or S-wave, arrivals usually have a frequency content in the band 6-9 Hz.

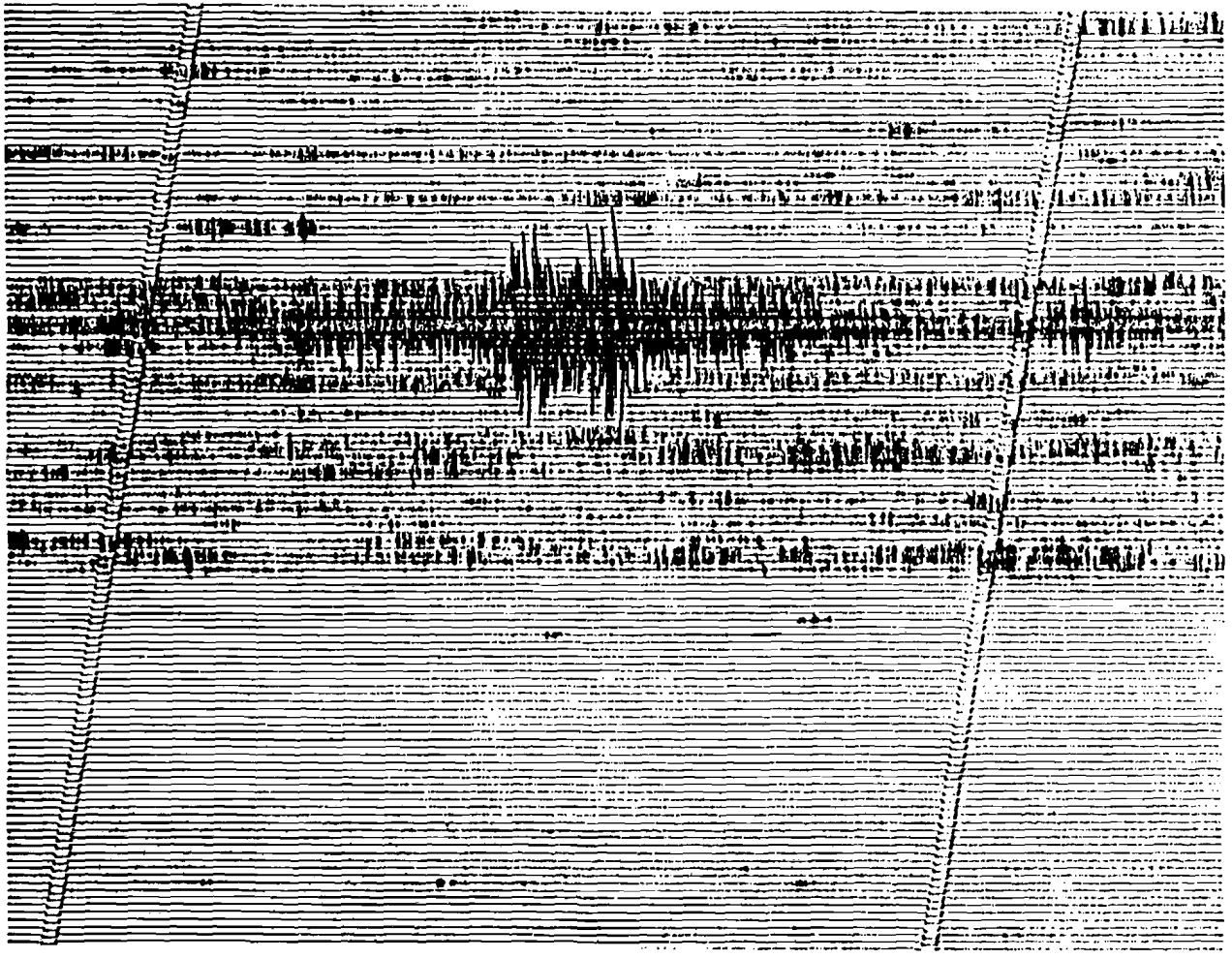

Figure 7. Sample traces of drum recording taken February 2, 1993 at station hulh (o-15), vertical component. Each large, rectangular tic marks one hour.

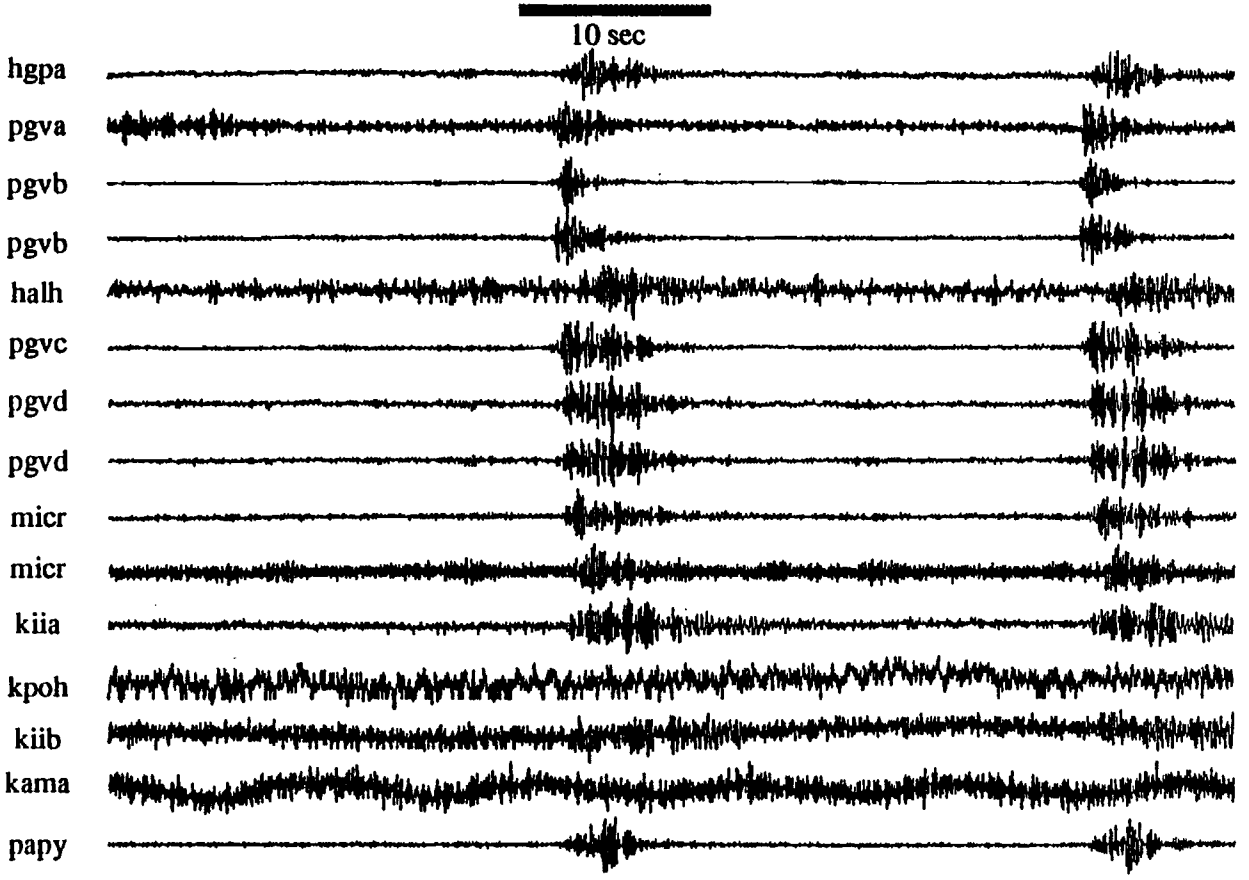

Figure 8. Sample digitized vertical seismograms of man-made, impulsive sources recorded on February 2, 1993 at 1603 GMT. All traces are scaled individually

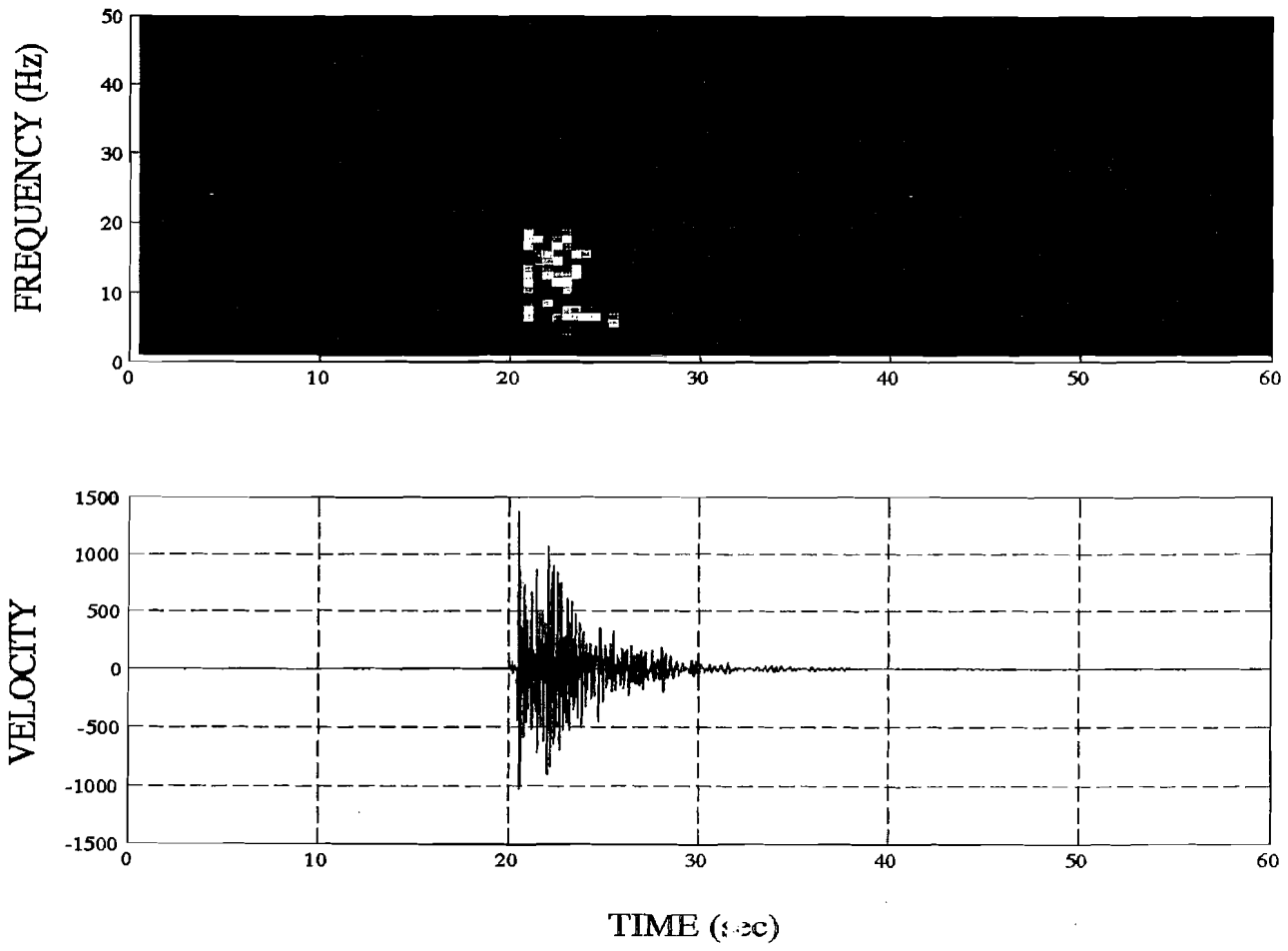

Figure 9. Vertical component and its spectrogram; earthquake occurred on February 18, 1993 at 0637 GMT. Color scale is gradational between blue and red for low- to high-frequency responses to velocity, respectively.

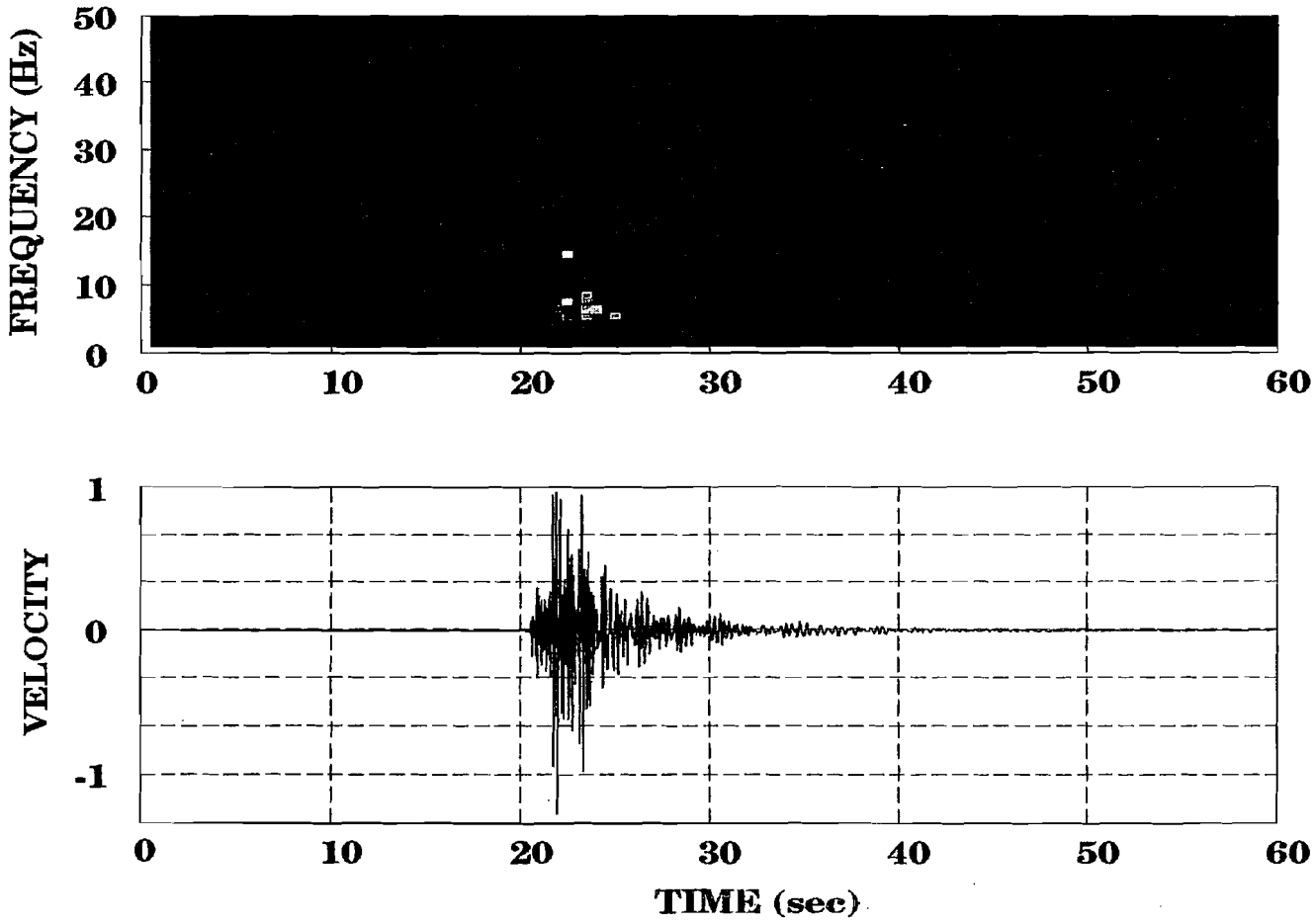

Figure 10. East-West component and its spectrogram; earthquake occurred on February 18, 1993 at 0637 GMT. Color scale is gradational between blue and red for low- to high-frequency responses to velocity, respectively.

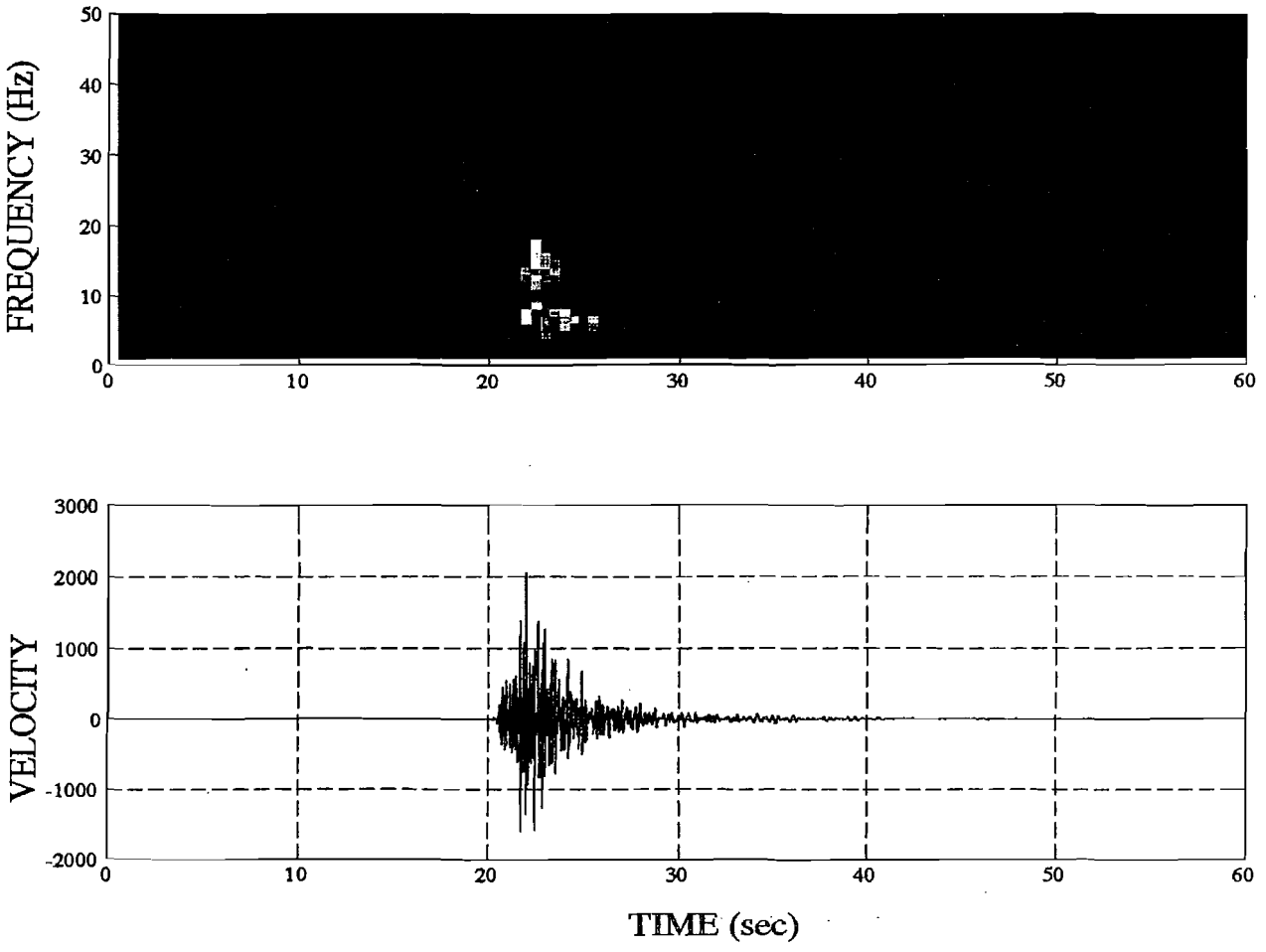

Figure 11. North-South component and its spectrogram; earthquake occurred on February 18, 1993 at 0637 GMT. Color scale is gradational between blue and red for low- to high-frequency responses to velocity, respectively.

P- and S-wave arrivals were picked using an interactive computer display and wave analysis program developed for the Sun SPARCsystem workstation. A total of 8,595 P-wave and 7,373 S-wave arrivals were picked. Onset of both types of arrivals was typically sharp or "impulsive" (Figure 12).

2. GRAVITY

Gravity data were collected along Kilauea's structurally complex LERZ to supplement HVO efforts in covering all of Kilauea. Gravity measurements for 374 stations (shown as open circles in Figure 13) were obtained using a LaCoste Romberg gravimeter with an estimated accuracy of ± 0.5 mgal. Station locations were obtained using a variety of methods including traditional leveling, hand-held altimeter, and hand-held global positioning computer; estimated accuracy for horizontal positioning is 50-100 m; estimated accuracy for vertical positioning is 0.5 to 1.0 m.

Tidal corrections were made to all the data and indicated a low long-term drift rate of < 0.3 mgal per month. A short-term drift of 0.1-0.2 mgal was observed, so there is an uncertainty of this order in the observed gravity values. This was borne out by repeat readings at field stations, which had shown differences of up to 0.2 mgal. The Bouguer anomaly values were calculated from the 1967 International Gravity Formula (I.A.G., 1971) and corrected for topography. Full terrain corrections to a radius of 166.7 km were computed automatically for all stations using digital topography data. Local terrain corrections (within 170 m of the station) in zones with rugged topography were included in the automatic computations be an

interpolation method. No correction was made for the "island effect," caused by the density contrast between the submarine island pedestal and the surrounding ocean.

The choice of density for gravity reductions in a survey in areas of high relief was a problem because it affects the short-range gravity patterns under study. As a rule we assumed a value that was based on the general nature and apparent age of the surface rocks so as to obtain a Bouguer map with as few as possible surface effects. The Bouguer anomaly map (Figure 13) was compiled using a reduction density of 2.3 g/cc.

The structural development of the LERZ has been complex, involving combinations of lava and cinder cones, and some emission fractures. The high-frequency gravity components that characterize Kapoho and other recent (1955) volcanic landforms are indicative of relative density variations, which may also be associated with a partly molten magma chamber below Kapoho. Contour lines of the residual gravity field associated with the volcanic constructs are concentric and suggest sources that lie within the volcanic edifice. A positive anomaly with wavelength of less than 20 km and amplitude up to 40 mgal characterize Kapoho; the smaller constructs have smaller amplitudes.

Even with the additional stations, the resulting complete Bouguer anomaly map cannot be used to define drilling targets because the resolution is not fine enough and because the ultimate cause of the observed gravity cannot be explored without some control over the density structure, such as seismic velocities.

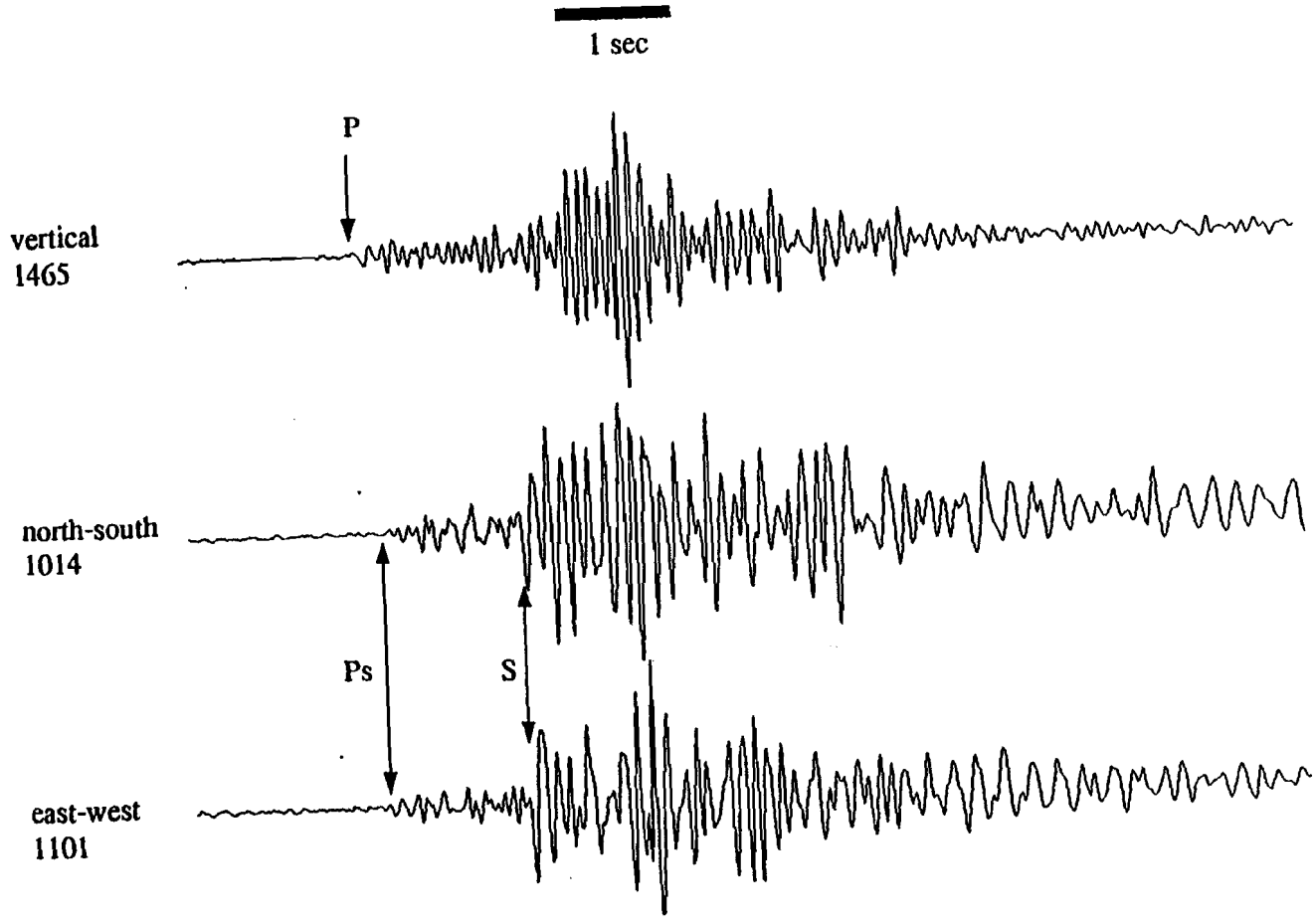

Figure 12. Seismograms for an earthquake that occurred on February 18, 1993 at 0637 GMT. P- and S-wave arrivals are identified, as is the P-to-S converted phase. Note impulsive character of arrivals. Scale is in millivolts.

Kapoho Area Complete Bouguer Gravity

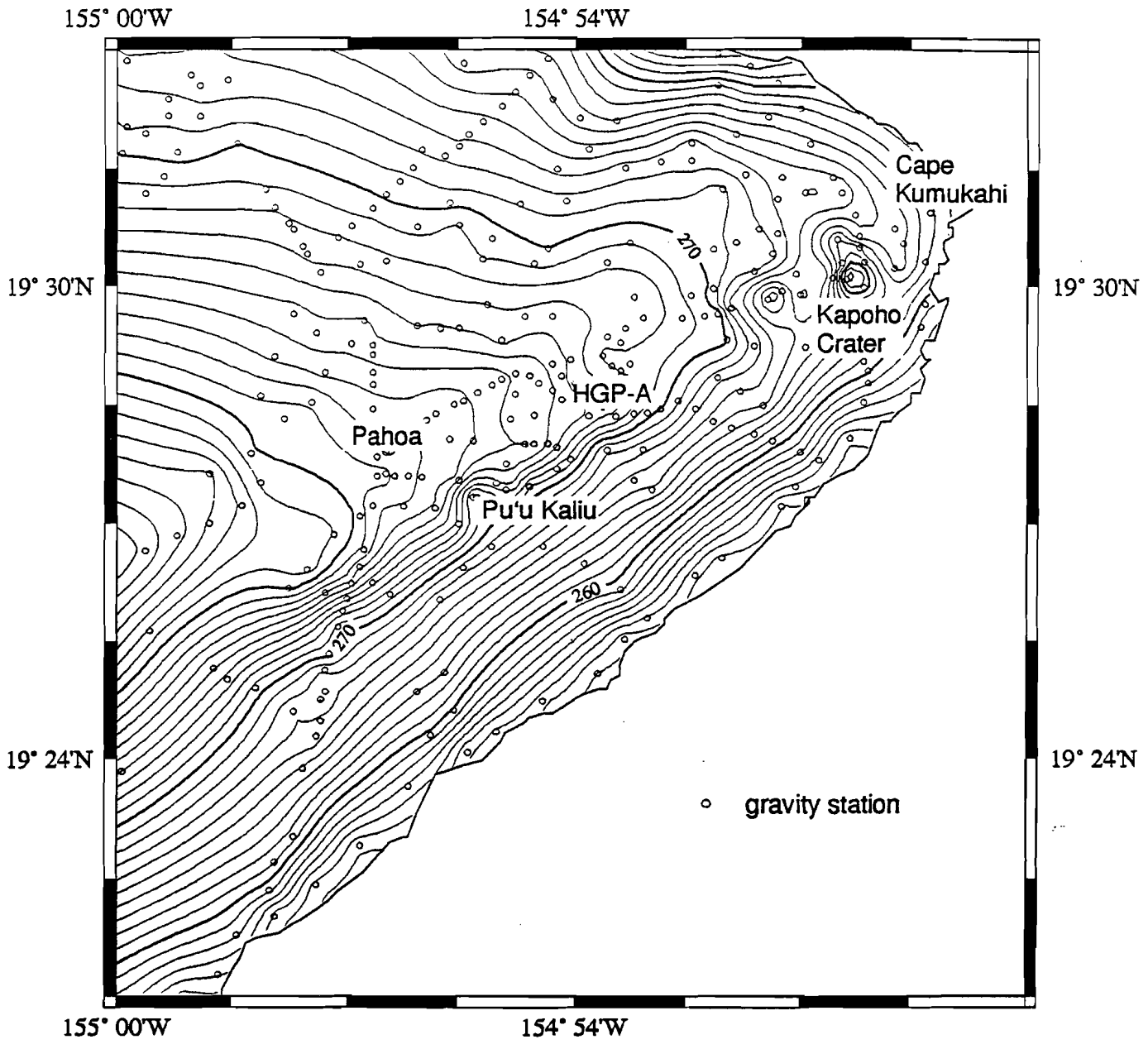

Map of the complete Bouguer anomaly for the Kapoho area of Kilauea Volcano. Reduction density is 2.3 g/cc. Data have been corrected for topography.

Figure 13.

3. SEISMICITY

3.1 Hawaii Velocity Models

Several one-dimensional velocity models (velocity dependent on depth only) have been derived for the island of Hawaii using both active (seismic refraction) and passive (seismic wave propagation) seismic techniques. One of the earliest models for Hawaii was determined using a large-scale seismic refraction experiment (Zucca and Hill, 1980). Crosson and Koyanagi (1979) used local earthquake arrival times to calculate jointly the hypocenters and one-dimensional velocity structure in the summit region of Kilauea. An important feature of the Crosson and Koyanagi model was a low-velocity zone from 9.5 to 13 km depth that may represent a low-velocity sedimentary layer sandwiched between the upper oceanic crust and the submarine lavas of the volcanic edifice. In 1981 Klein proposed an alternative to the layered models used previously. Klein's model used linear velocity gradients varying with depth to parameterize the velocity function. Hypocentral calculations using this model yielded residuals equal to or less than the models of Crosson and Koyanagi (1979), Eaton (1962), and several unpublished HVO models.

Shallow seismic velocities in Kilauea's LERZ are slightly different than those of the summit region. Broyles et al. (1979) performed a seismic refraction experiment that crossed the Puna geothermal region. The size of the shots and the geophone spacing for this survey limited sampling to depths above 5 km. Nevertheless, the authors were able to define five distinct velocity layers interpreted as

a very low-velocity upper layer, a water-saturated layer, two layers representing variable amounts of intrusive bodies and compacted lava flows, and the lowermost dike complex. A comparison of this model to the models of Crosson and Koyanagi (1979), Eaton (1970), and Klein (1991) is shown in Figure 14.

The most important difference between these models for our purposes is the location of the boundary between the surface lava flows and the dike complex, which is 1 km closer to the surface in the Broyles et al. (1979) model. Preliminary calculations of hypocenters using the Broyles velocity model resulted in significantly lower travel-time RMS residuals as compared to calculations using other models. The Broyles et al. (1979) velocity model was used in all subsequent hypocentral calculations.

Five small shots were detonated in an attempt to fix surface-layer velocities to nearby stations. Shooting was contracted to Earth Brothers Home Lot Improvement, which provided all equipment, explosives and permits. A six-foot-deep hole was bored to accept the charge; the hole was filled with excavated dirt and rocks, covered with a chain-tire net, and the charge was detonated. Five charges were detonated at four sites listed in Table 1. Charge size varied from 1 to 2 sticks of dynamite; larger charges were not possible because of the residential nature of the area. An average P-wave velocity of 0.97 km/s for the top 0.5 km, overlying a layer with a velocity of 2.25 km/s, was calculated from travel times for these shots (Table 2).

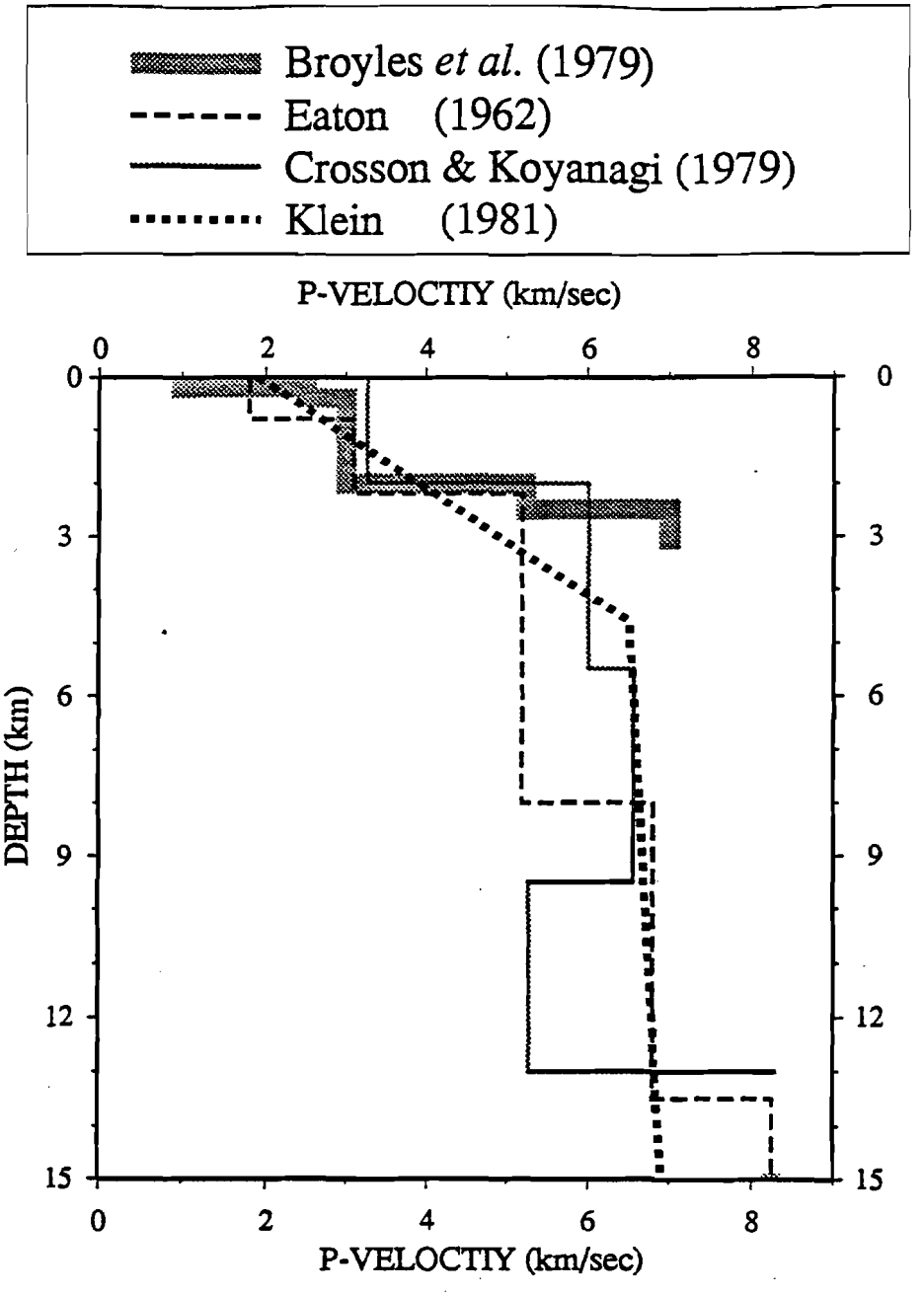

Figure 14. Summary of four velocity models used in Hawaii. The Broyles et al. (1979) model was used as the basis in forming the velocity model for the inversion for hypocenter and Vp/Vs structure.

Table 1. Blast Sites and Detonation Times, March 2, 1993.

Detonation Time (UT)	Blast Site	Elev. (ft)	Surface Geology
19:35:22.068	19° 28.043'N 154° 53.770'W	300	cinder over basalt
Operator error	19° 28.322'N 154° 53.216'W	500	cinder over basalt
21:14:12.119	19° 28.322'N 154° 53.216'W	500	cinder over basalt
00:27:44.274	19° 30.164'N 154° 49.707'W	100	basalt rubble
02:42:25.689	19° 30.164'N 154° 49.707'W	100	cinder over basalt

Table 2. Travel Times, March 2, 1993.

19:35:22.068	Station	Travel Time (s)	Distance (km)
	kaup	1.172	0.490
	potf	0.992	0.750
	maka	1.402	0.740
	bcoh	1.712	0.900
	kahu	0.692	0.670
	erni	0.052	0.017
	watr	1.452	1.570
21:14:12.119	Station	Travel Time (s)	Distance (km)
	micr	2.141	1.35
	kaup	1.351	1.29
	crck	0.831	0.81
	potf	0.331	0.31
	pila	0.541	0.36
	kahu	0.701	1.57
	uhes	0.741	1.24
	erni	0.871	1.09

3.2. Earthquake Locations

Hypocenters were calculated using the algorithm HYPOCENTER (Lienert et al., 1986) for P- and S-waves separately using the Broyles et al. (1979) velocity model with the addition of an 8.15 km/sec half-space beginning at 13.5 km. Arrivals with residuals greater than roughly twice the standard deviation of residuals were removed and the P- and S-wave data sets then were combined, producing a data set of 8,272 P- and 6,335 S-arrivals used for final calculations. Located events are tabulated in Appendix II.

A histogram of calculated RMS residual values (Figure 15) shows that more than 95% of the located earthquakes have RMS residuals less than 0.13 seconds. This is important because if the uncertainty in the velocity model for a particular ray is ± 200 m/s over a total path length of 5 km, then the uncertainty in travel time is 0.10 seconds. An acceptable earthquake location, therefore, should have an RMS residual less than or equal to the above uncertainty. Considering that significant lateral velocity variations appear to be common in the shallow crust, the velocity model used is a good approximation to the bulk vertical velocity structure beneath the array.

Although the authors of the HYPOCENTER program (Lienert et al., 1986) found that their method was less likely to leave the event depth at the a prior depth (5 km), 26 out of 504 events (5%) within 10 km hypocentral distance of the array remained at this depth. Hypocenters that cluster about the 2.7-km discontinuity (Figure 16) may indicate that the velocity contrast across the discontinuity is too high or that head-wave (refracted) travel times are present in the

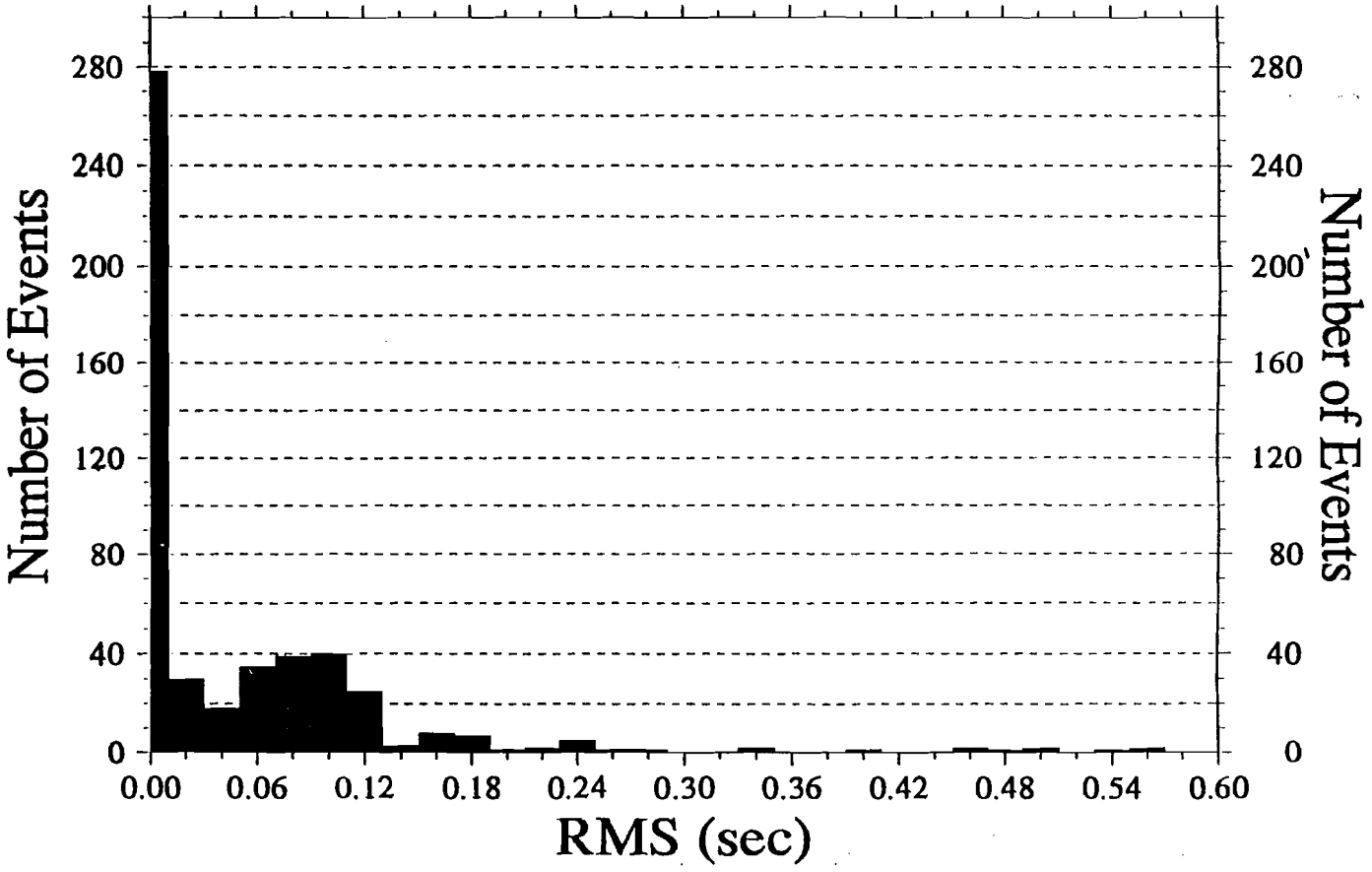

Figure 15. Histogram of earthquake location RMS residuals calculated using the program HYPOCENTER and all PANDA data within 10 km hypocentral distance of the PANDA array.

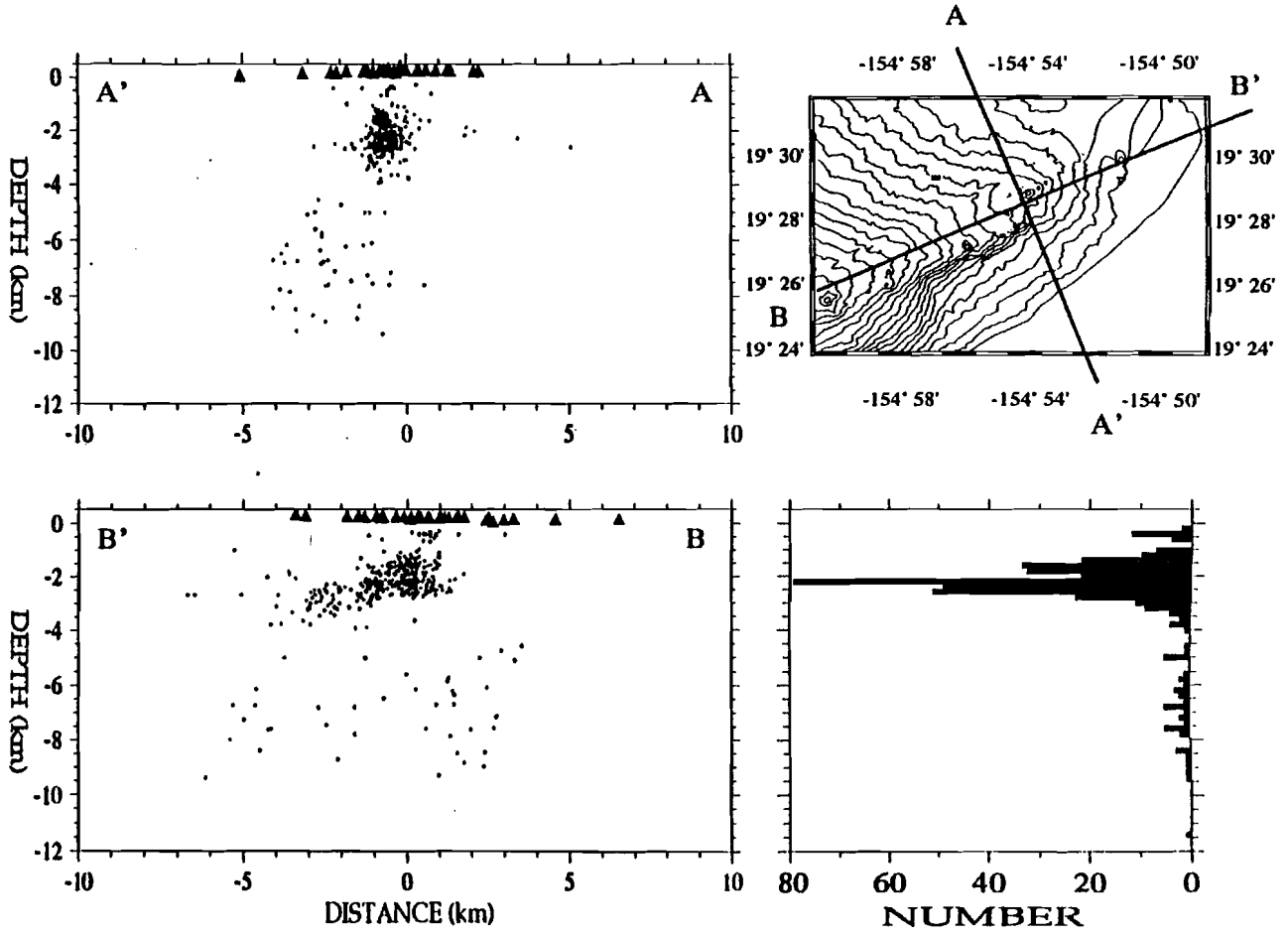

Figure 16. Cross-sections of seismicity A-A' and B-B'. Filled triangles denote PANDA stations and circles denote events (including drilling-related) with vertical errors less than 0.5 km. No vertical exaggeration. Contour interval equals 25 meters.

data. Estimates of location uncertainties (Appendix II, ERZ and ERH) show that 90% of the events within 10 km of the array center are located to a vertical uncertainty of 600 m and a horizontal uncertainty of 400 m or better (Figures 17 and 18).

In a plot of observed P-wave travel times vs. S-wave travel times, two distinct linear trends are evident (Figure 19). The primary trend intersects the origin and has a slope ($\Delta t_S/\Delta t_P$) of 1.78; this is consistent with the Vp/Vs ratio used by HVO and further validates our use of the Broyles et al. (1979) velocity model. The second trend intersects the S-wave travel-time axis at about 1.5 s and has a slope of 1.13. The cause of this second trend can be modeled by a refracted S-wave traveling along the top of the high-velocity dike complex as shown in Figure 19.

More than 85% of the epicenters are located within the array's boundaries (Figures 20 and 21). The main concentration of shallow (1-4 km) seismicity is confined to a roughly 1-km-wide (measured perpendicular to the LERZ) strip that is nearly vertical and striking parallel to the LERZ. This zone encompasses the locations of almost all geothermal wells in the region. Very shallow (0-3 km) hypocenters within the array (Figure 22) cluster into two general regions along the LERZ, one north of Pu'ulena Crater and another 0.5 km to the southwest of the first cluster. Deeper (4-10 km) hypocenters are located primarily in the south flank, seaward of the LERZ. The area to the northwest of the two zones of shallow hypocenters shows no seismic activity despite an adequate detection threshold. Also few earthquakes occur at depths shallower than 5 km in the area from Honuaulua to Kapoho Crater, again, despite adequate station coverage.

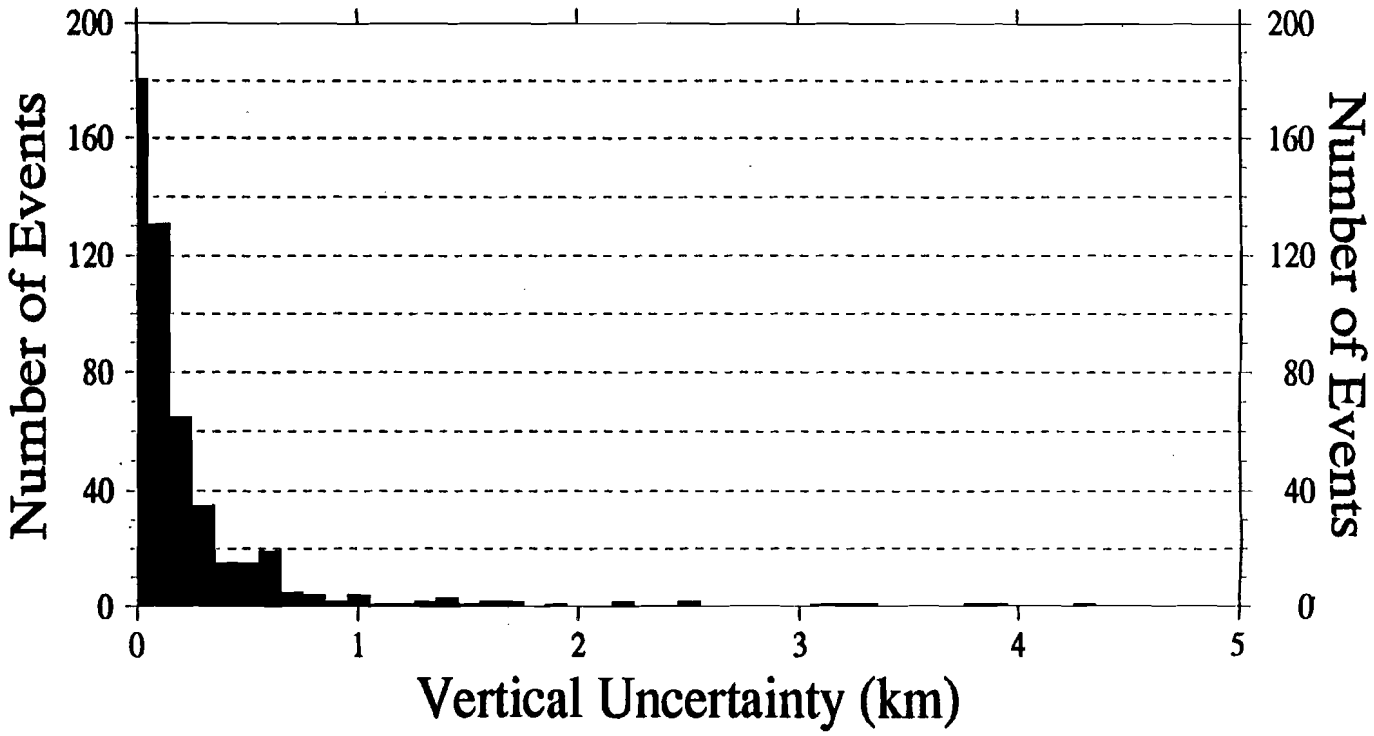

Figure 17. Histogram of vertical uncertainties calculated using the program HYPOCENTER and all PANDA data within 10 km hypocentral distance of the PANDA array.

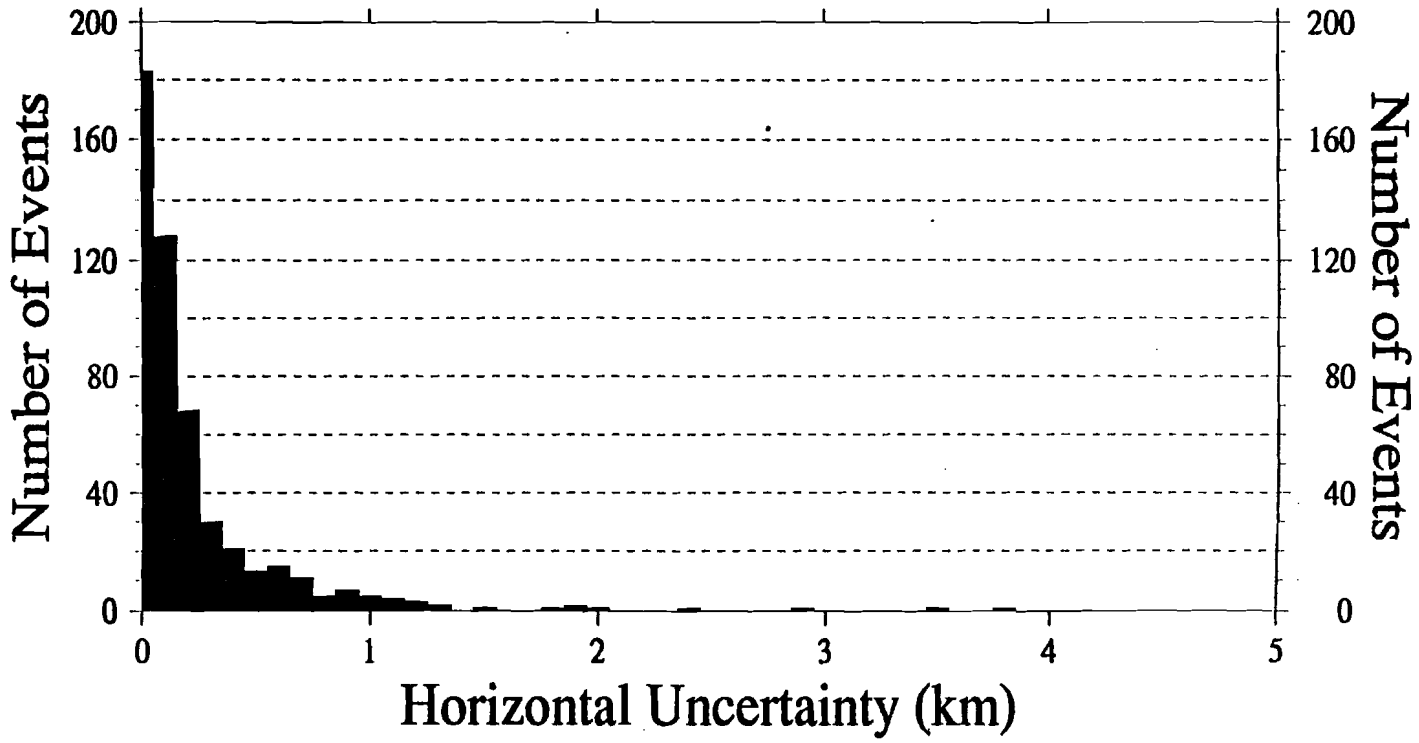

Figure 18. Histogram of Horizontal uncertainties calculated using the program HYPOCENTER and all PANDA data within 10 km hypocentral distance of the PANDA array.

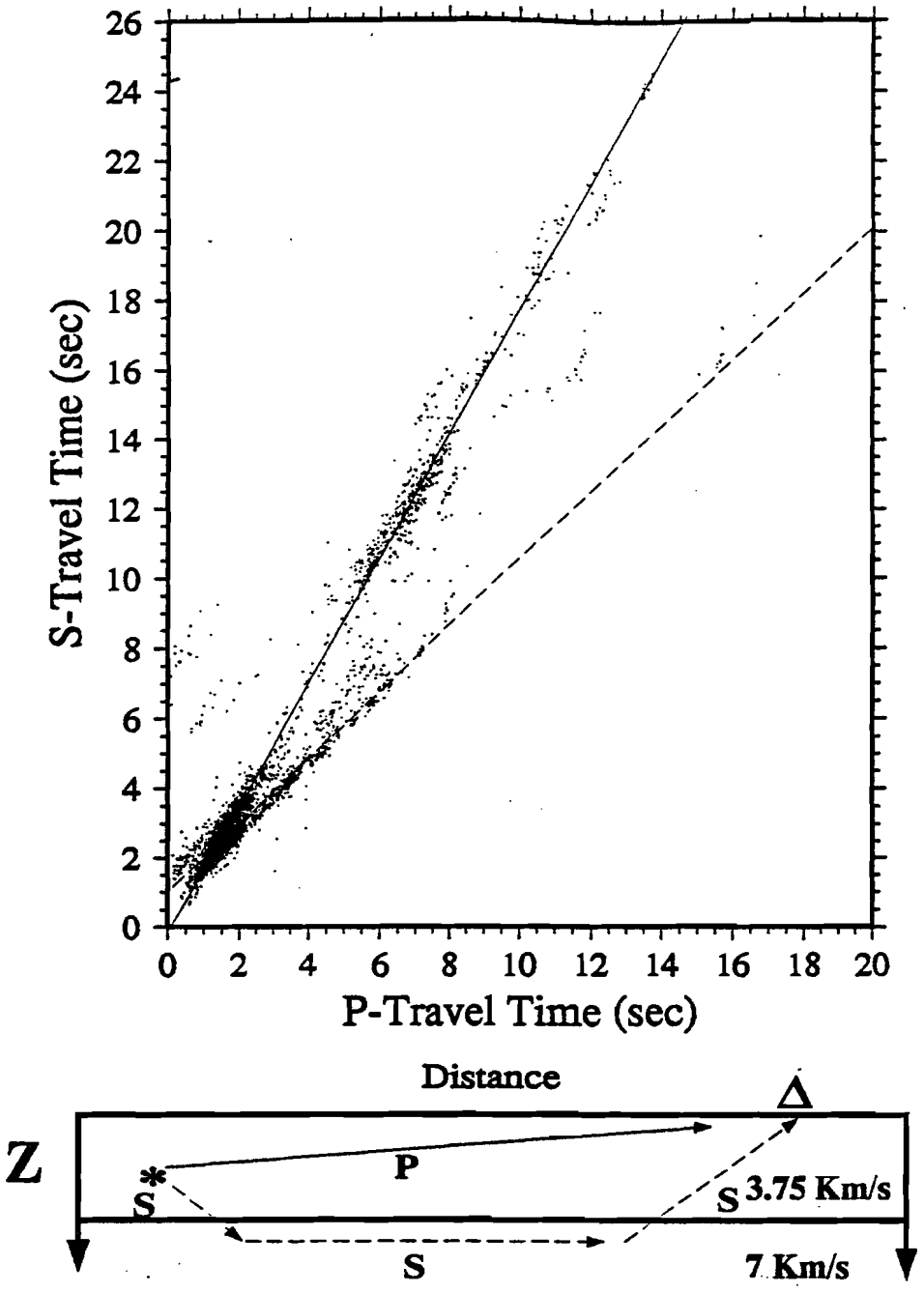

Figure 19. Observed P-wave travel times (top) vs. observed S-wave travel times. The solid line has a slope of 1.78 and the dotted line has a slope of approximately 1.1. At the bottom is a sketch of the velocity model and raypaths used to create the dotted line. Asterisk denotes hypocenter and triangle denotes receiver.

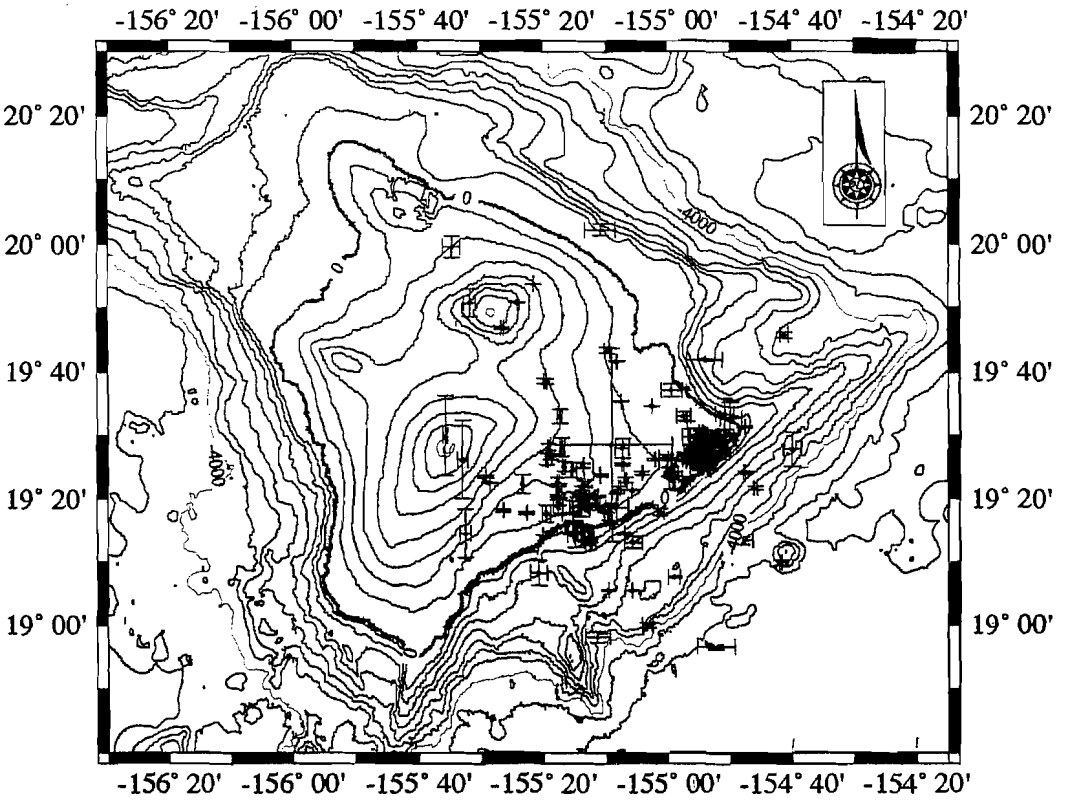

Figure 20. All located PANDA events. Green, red, and blue filled circles denote earthquakes with depth ranges of < 5 km, from 5 to 10 km, and > 10 km, respectively, referenced to station hulh (o-15) which is approximately 360 m above sea level. Contour interval is 500 m.

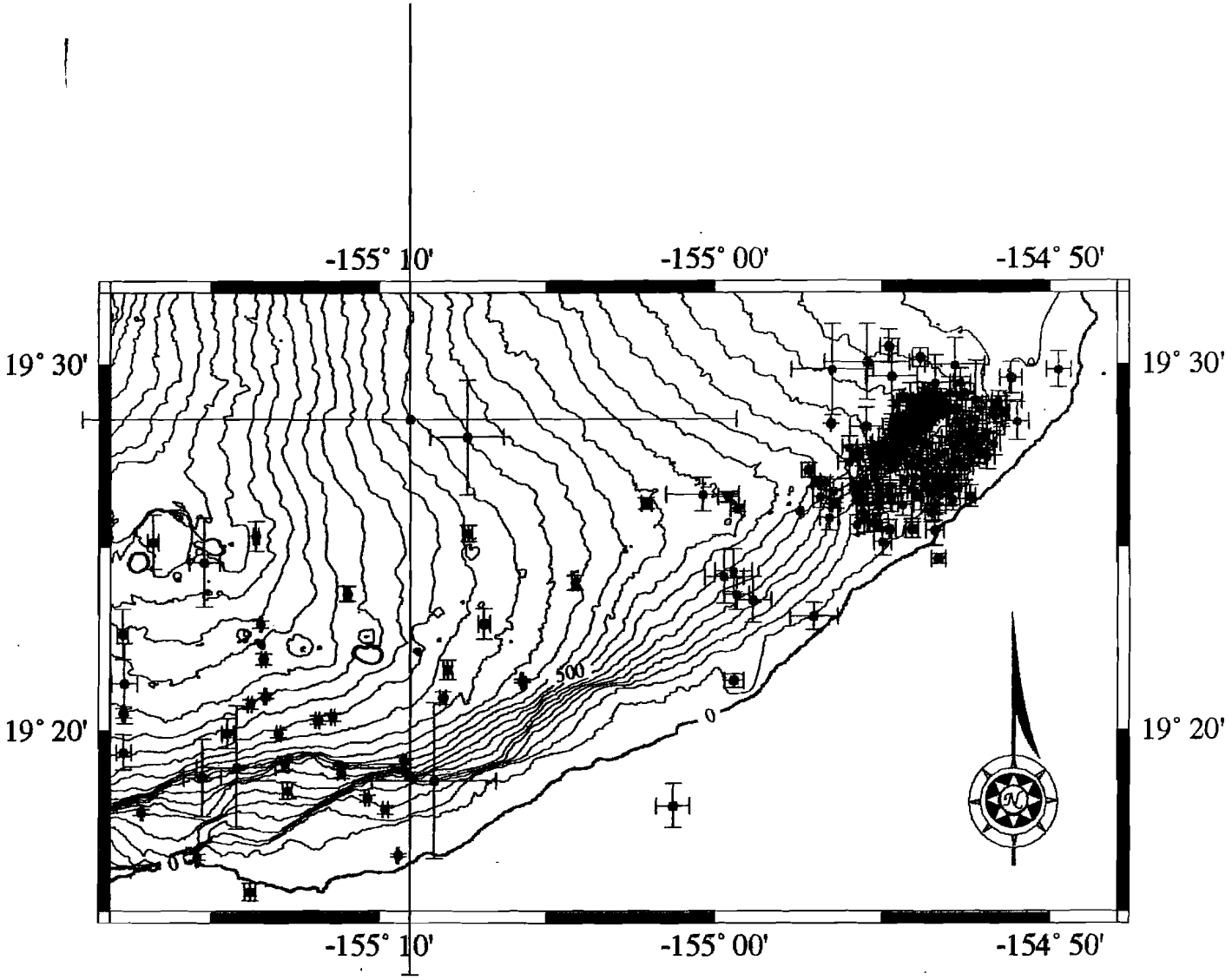

Figure 21. Plot of PANDA events. Error bars represent uncertainties in latitude and longitude. Green, red, and blue filled circles denote earthquakes with depth ranges of < 5 km, from 5 to 10 km, and > 10 km, respectively, referenced to station hulh (o-15) which is approximately 360 m above sea level. Contour interval is 500 m.

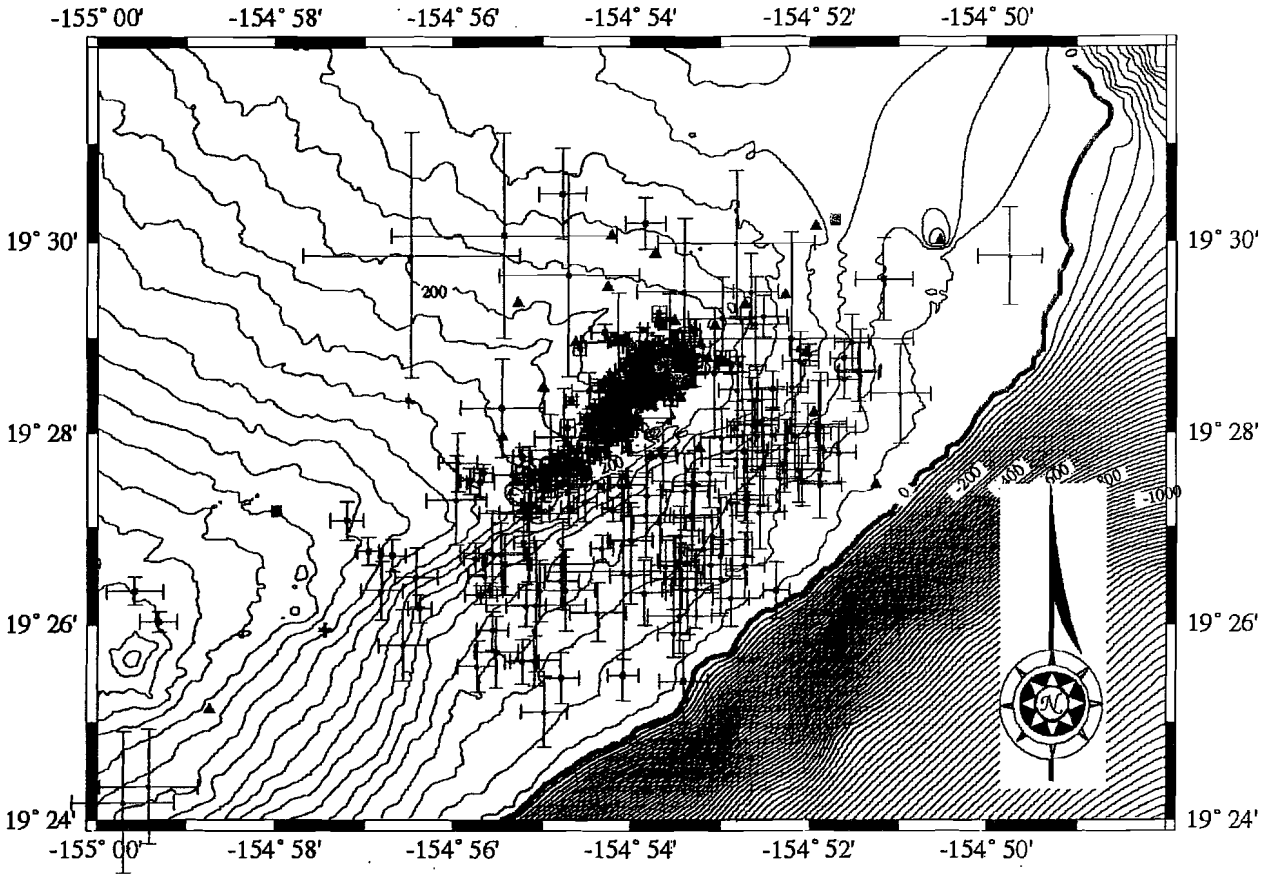

Figure 22. Close-up view of PANDA events. Green, red, and blue filled circles denote earthquakes with depth ranges of < 5 km, from 5 to 10 km, and > 10 km, respectively, referenced to station hulh (o-15) which is approximately 360 m above sea level. Contour interval is 500 m.

Looking from south to north, a three-dimensional view of the seismicity perpendicular to the LERZ (Figure 23a) shows the two elliptical zones of seismicity amidst the deeper, more diffuse seismicity of the south flank. Viewed in three dimensions the seismicity of zone 1 is associated with a nearly vertical fault, highlighted in yellow in Figure 23b (dip is exaggerated in Figure 23b because of scale). Confidential information provided by PGV indicates that this fracture probably provides the main channel along which hot water from depth reaches permeable horizons in the shallow subsurface. The producing KS-series wells intersect this fracture at various depths.

3.3. Temporal Variations in Seismicity

Figure 24 shows the number of operating stations plotted with respect to the number of events recorded. The level of seismic activity was typically about one or two potentially locatable microearthquakes per day, with occasional bursts of more frequent quakes. Figure 25 shows two sample 48-hour periods of "typical" seismic activity and a 24-hour period on March 31 during which a swarm of more than 40 locatable events occurred within a 2-hour period. Figure 26 is a three-dimensional display comparing a depth/perspective view of all located events with RMS < 0.10 with the same view of the events of the March 31 swarm. The swarm activity is tightly clustered in a nearly vertical distribution located (in geographical coordinates) at roughly 19.45° N 154.95° W and spanning a depth range of 0.48 to 4.19 km. The true frequency of

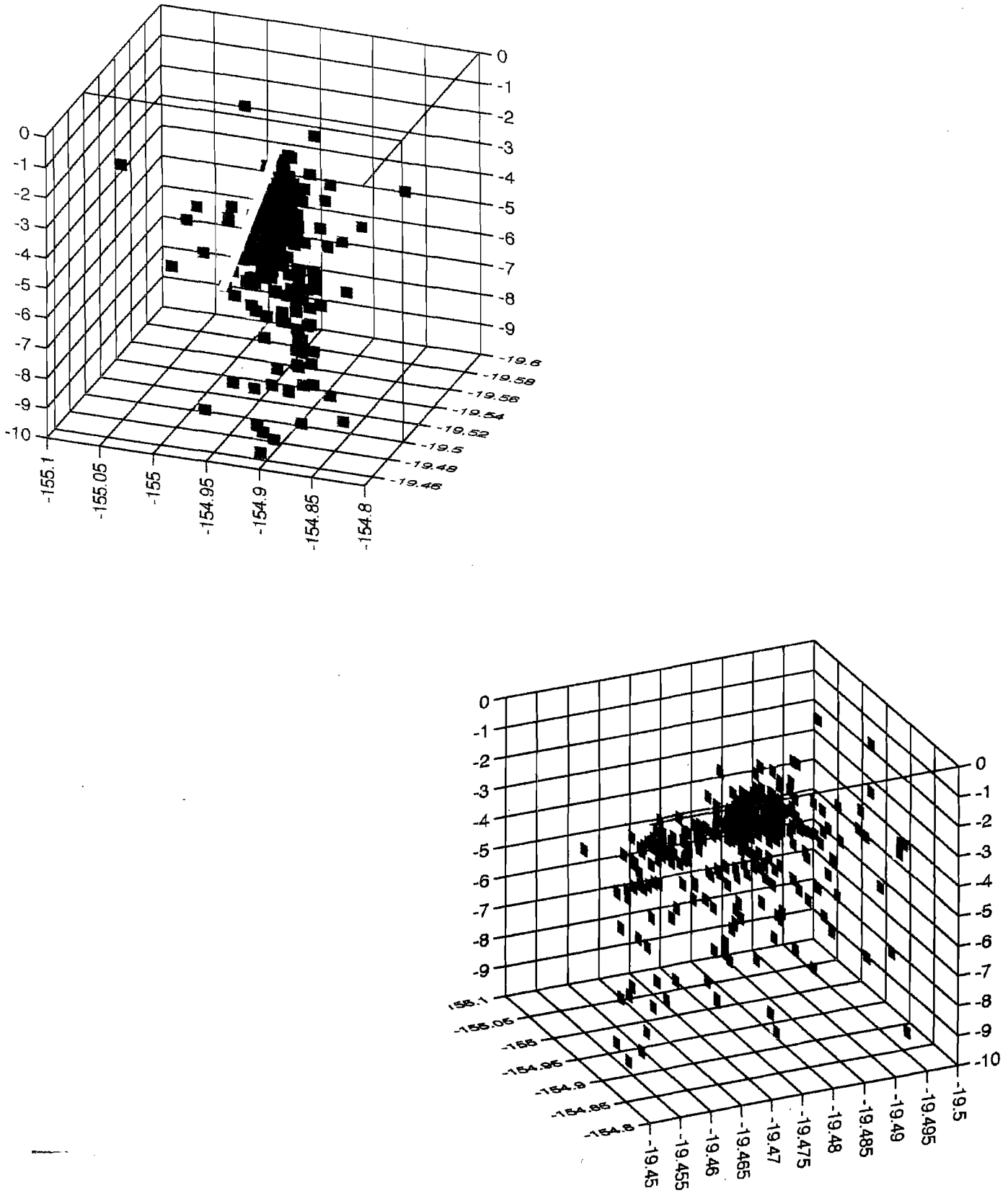

Figure 23. Three-dimensional perspectives of all earthquakes having RMS residuals less than 0.1 s. View is from the southeast looking north. Yellow bar in 23b denotes possible location of active fault.

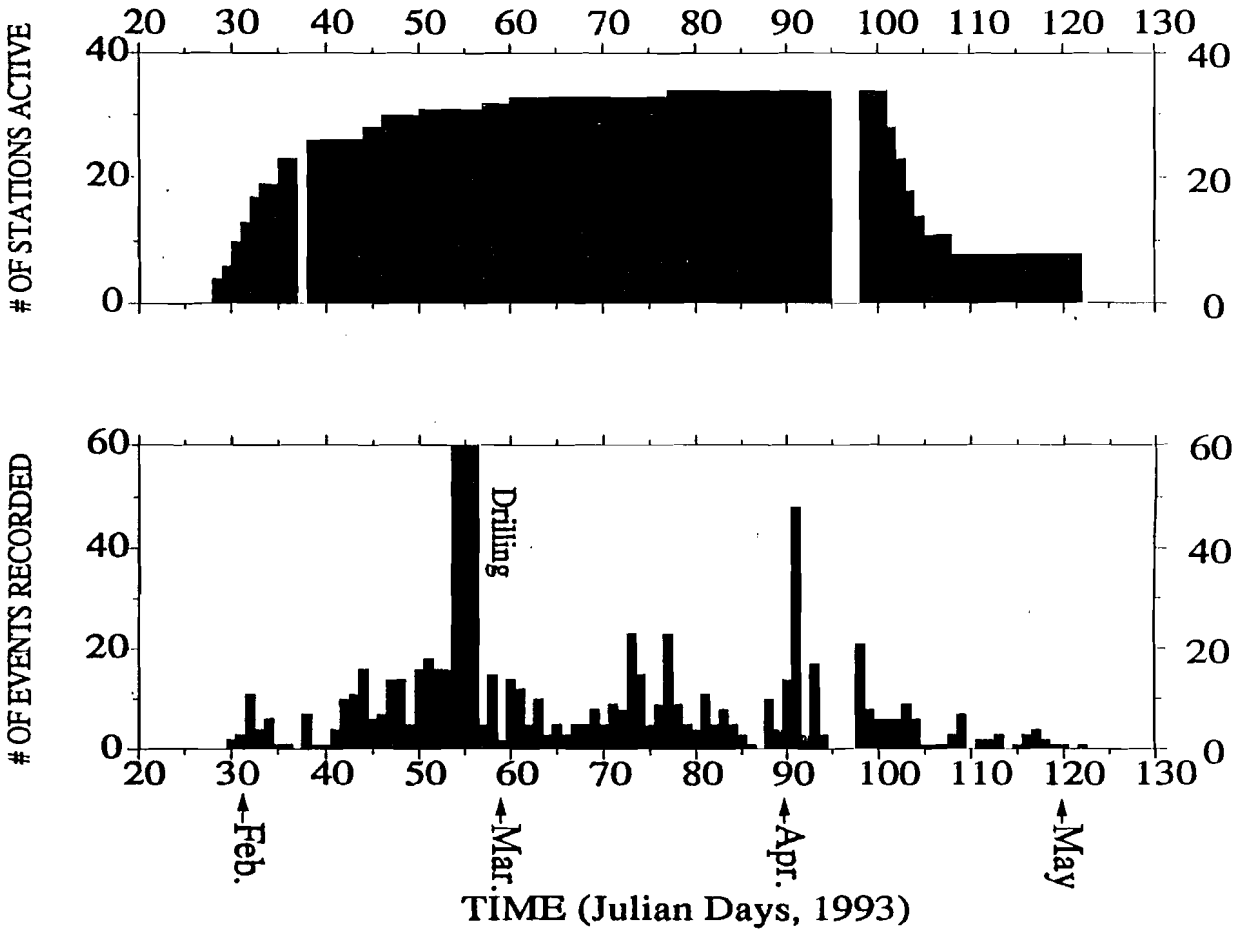

Figure 24. Number of earthquakes recorded including drilling-related events vs Julian day for the duration of the experiment (top). At the bottom is the total number of PANDA stations recording vs. Julian day.

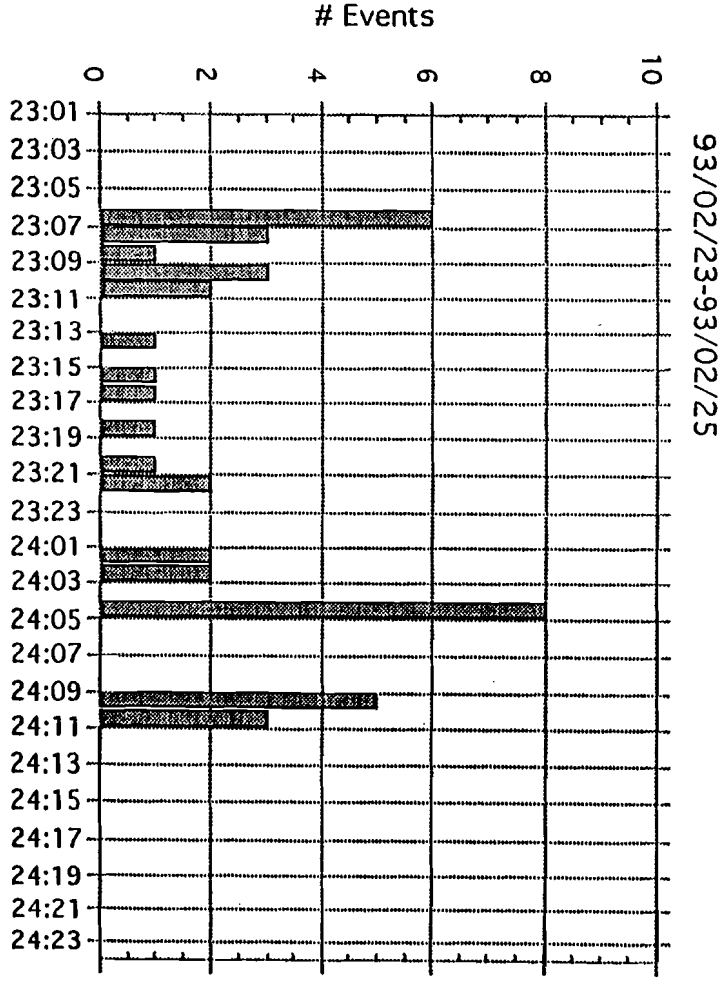
Events
0
2
4
6
8
10
23:01
23:03
23:05
23:07
23:09
23:11
23:13
23:15
23:17
23:19
23:21
23:23
24:01
24:03
24:05
24:07
24:09
24:11
24:13
24:15
24:17
24:19
24:21
24:23
93/02/23-93/02/25

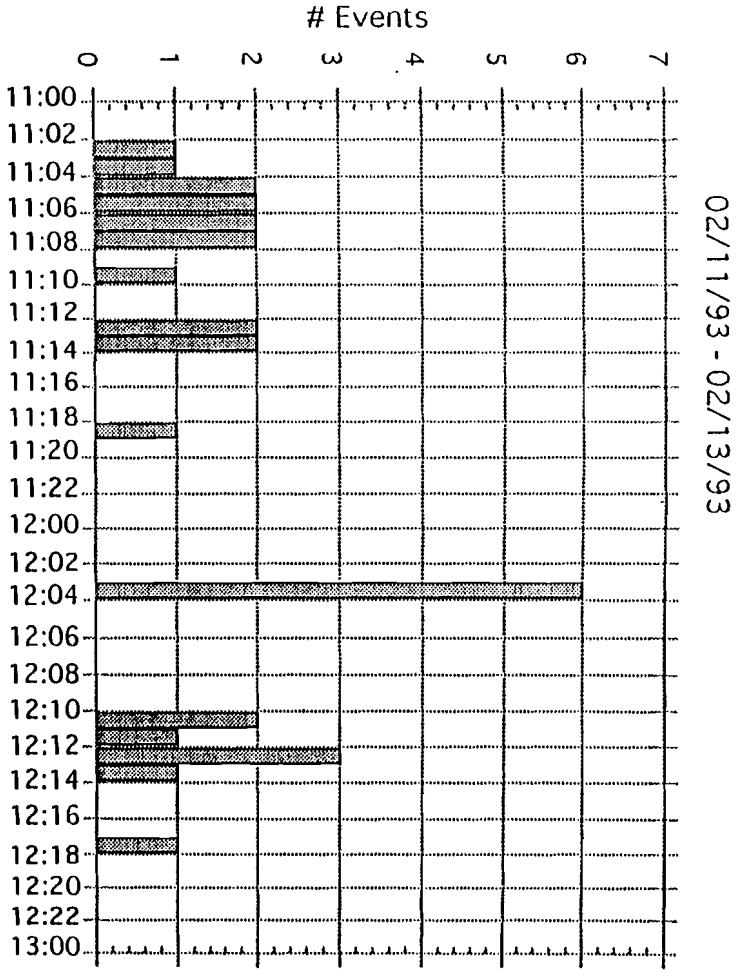
Events
0
1
2
3
4
5
6
7
11:00
11:02
11:04
11:06
11:08
11:10
11:12
11:14
11:16
11:18
11:20
11:22
12:00
12:02
12:04
12:06
12:08
12:10
12:12
12:14
12:16
12:18
12:20
12:22
13:00
02/11/93 - 02/13/93

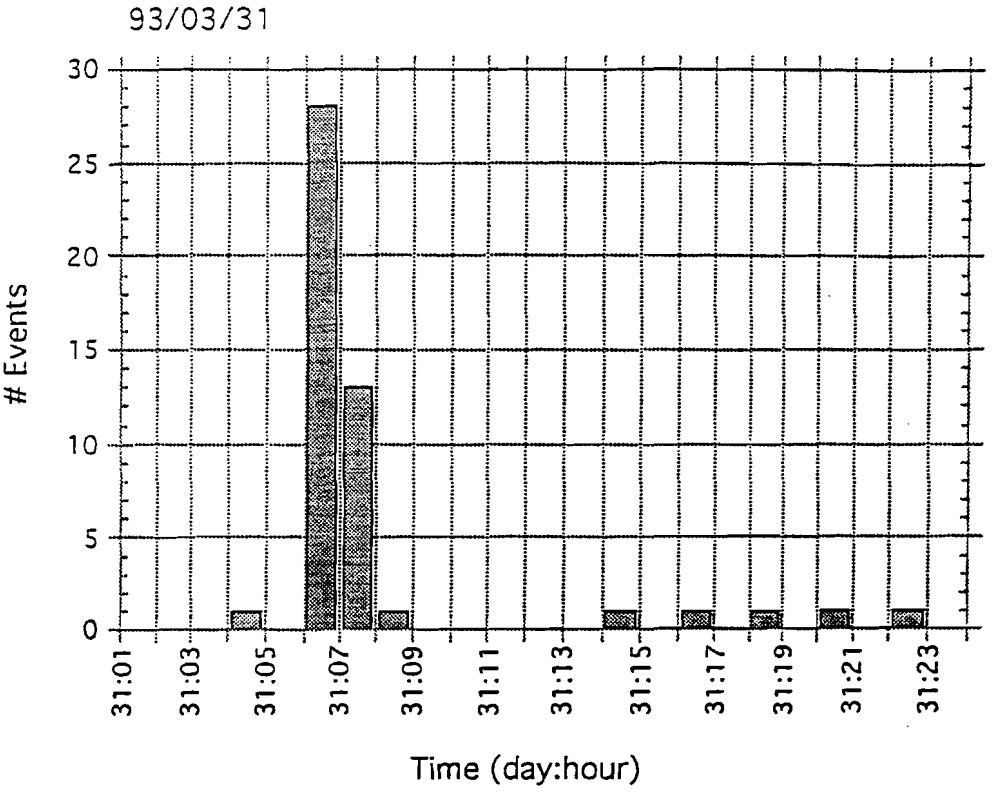

Figure 25. A and b each show two typical days' s seismicity. Seismicity rates are typically 1-2 locatable earthquakes per day with occasional swarm activity, as shown in Figure 25c.

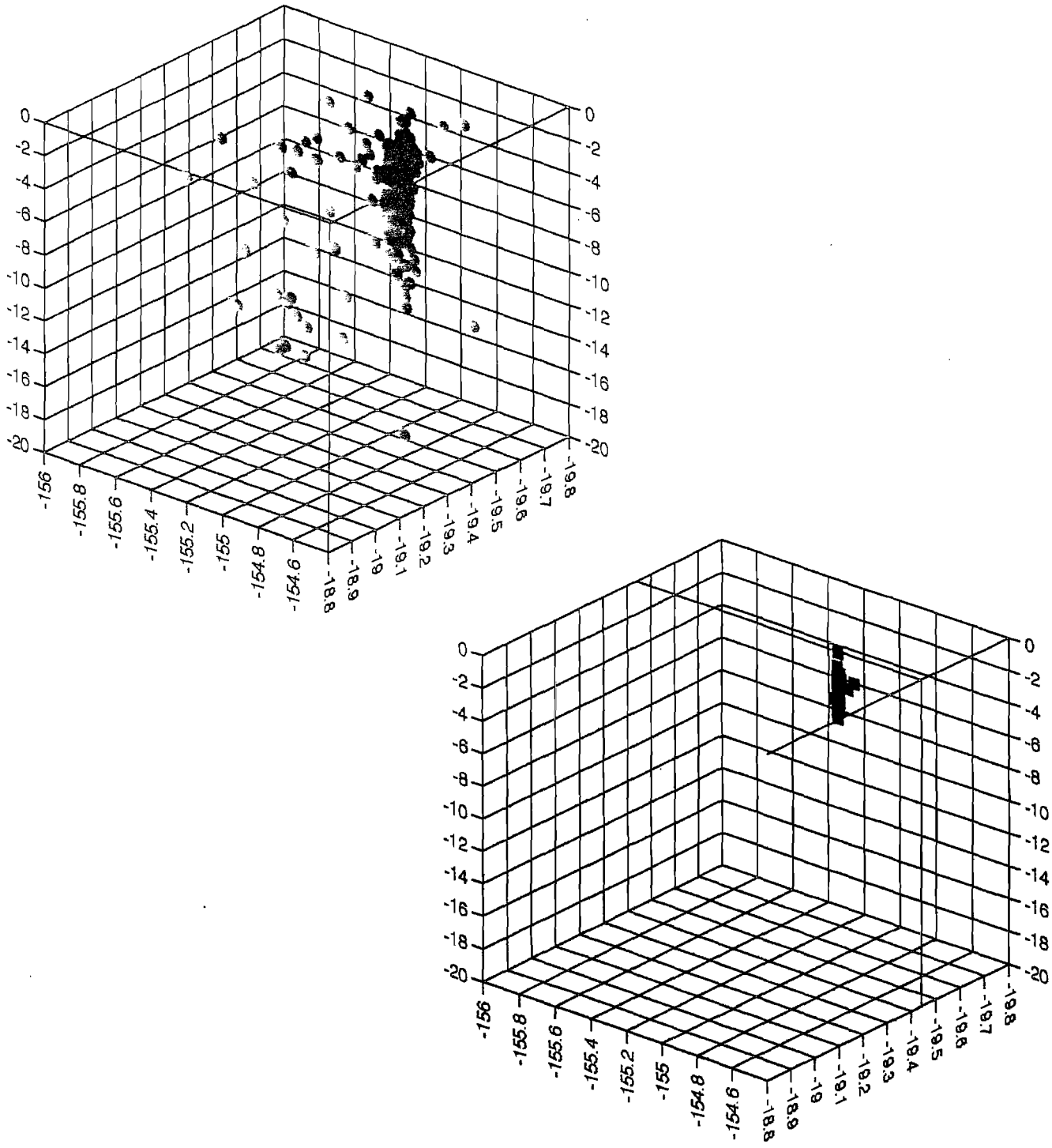

Figure 26. Three-dimensional display comparing a depth/perspective view of all located events with RMS < 0.10 with the same view of the events of the March 31 swarm.

occurrence of microearthquakes is unknown because of the short duration of the monitoring period; however, the above rates are probably typical of seismically quiet (i.e. no events larger than M = 2.0) periods along the LERZ.

3.4. Earthquake Magnitudes and b-Values

Magnitudes were calculated for the entire set of located earthquakes by a method using the coda length (Bisztricsany, 1958). The coda length, or time duration for the decaying seismic signal to return to within 10% of the pre-earthquake amplitude level, is related empirically to the magnitude using the following equation:

$$M_D = c_0 + c_1 \log t + c_2 D + c_3 Z,$$

where M_D is the duration magnitude, t is the coda duration in seconds as measured from the record, D is the epicentral distance from earthquake to station in km, Z is hypocentral depth in km, and c_0, c_1, c_2, and c_3 are constants. A simple average of the magnitude calculated at each station yields the earthquake magnitude.

Usually, duration magnitudes are first calibrated against the body-wave magnitudes by performing a simple regression to determine the constants in the above equation (Lee et al., 1972). We calibrated the PANDA coda durations to the HVO coda durations using an alternative regression method (Dustman, 1994). HVO is undertaking a revision of its coda duration-magnitude equation as of this writing, therefore, the magnitudes given in this report should be updated once that revision is complete.

Coda measurements for 7,869 vertical-component seismograms were measured (e.g., Figure 27). Results show that the distribution of earthquake magnitudes is not dependent on position except for earthquakes outside of the array boundaries (Figure 28). These earthquakes typically have high magnitudes ($0.5 < M_D < 3.1$). Within the array boundaries, where station spacing is small, smaller-magnitude earthquakes are more abundant (Figure 29), due largely to the detection threshold of the instrumentation.

The relationship governing the frequency of occurrence of earthquakes of certain magnitudes was documented by Gutenberg and Richter in 1954 and has been in use since that time as a measure of the state of stress in seismically active regions. Simply put,

$$\log N = a - bM$$

where a and b are constants, and N is the number of earthquakes larger than a given magnitude, M.

Numerous studies of the relationship of the b-value to the state of stress have been performed for geothermal regions (e.g. Coombs and Hadley, 1977 and Tryggvason, 1970) and for Kilauea Volcano (e.g., Koyanagi et al., 1981 and Klein, 1994). For tectonic earthquakes in Hawaii, b-values range from 0.9 to 1.0 (Klein, 1994), and for earthquakes near vents or active magma conduits, b-values range from 0.5 to 0.8. The 1991 Koyanagi et al. study of Kilauea's LERZ documented low b-values (0.71) during the earthquake swarm of February 1970. These lower b-values imply regions of higher stress (Gutenberg and Richter, 1954; Scholz, 1968).

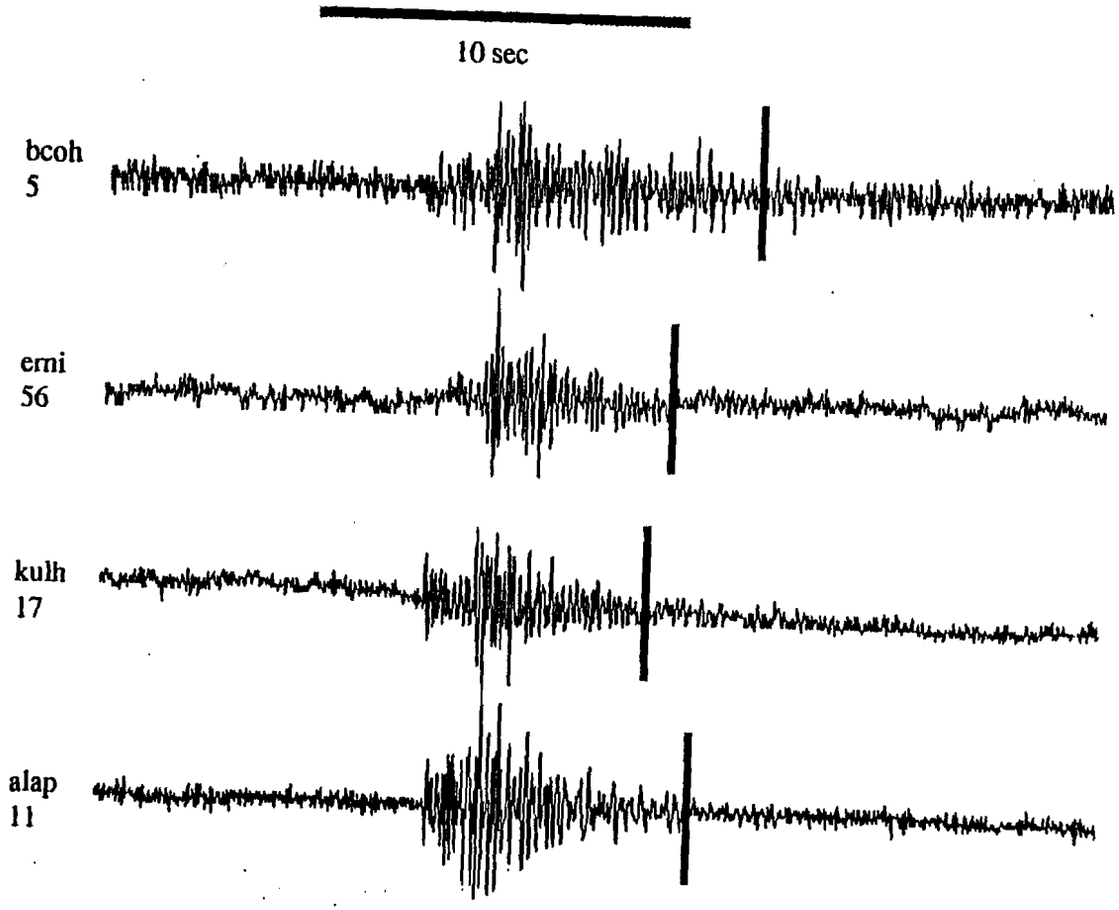

Figure 27. Four vertical seismograms from a selected earthquake showing coda duration picks. Scales are in millivolts.

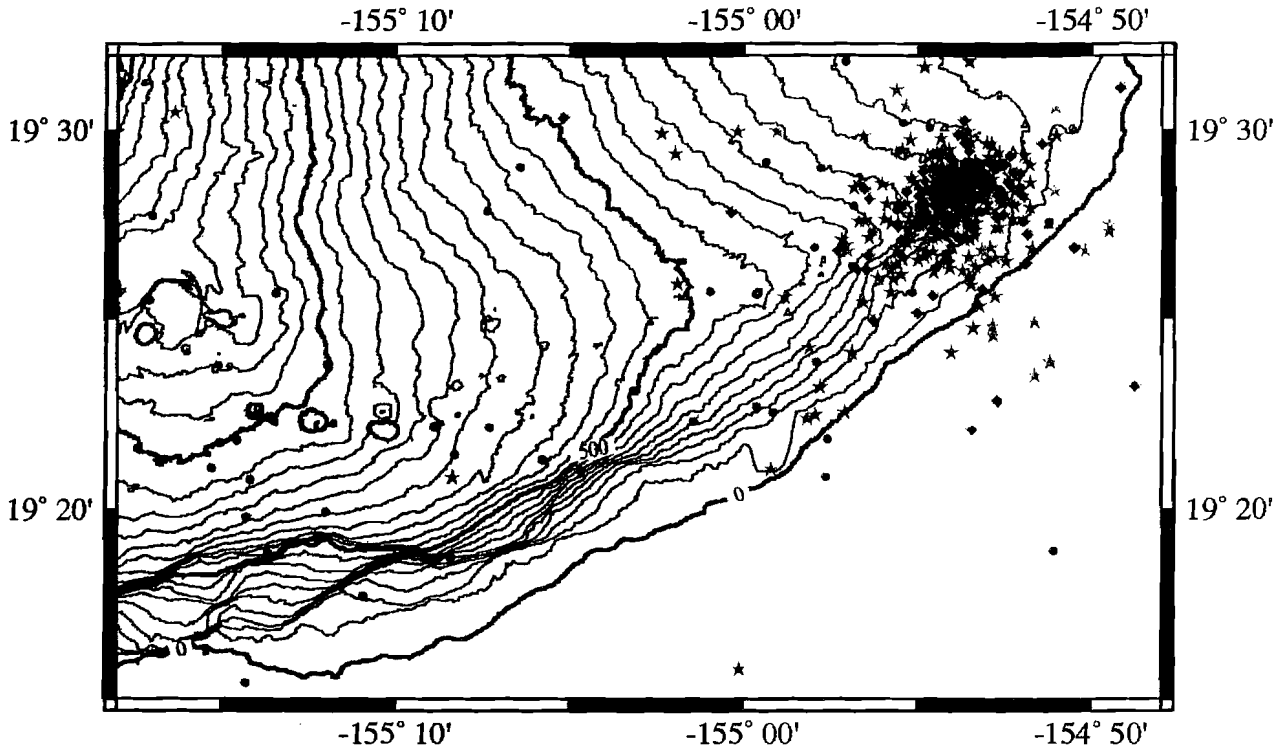

Figure 28. PANDA earthquakes sorted according to magnitude. Green, red, and blue filled circles denote earthquakes with depth ranges of < 5 km, from 5 to 10 km, and > 10 km, respectively.

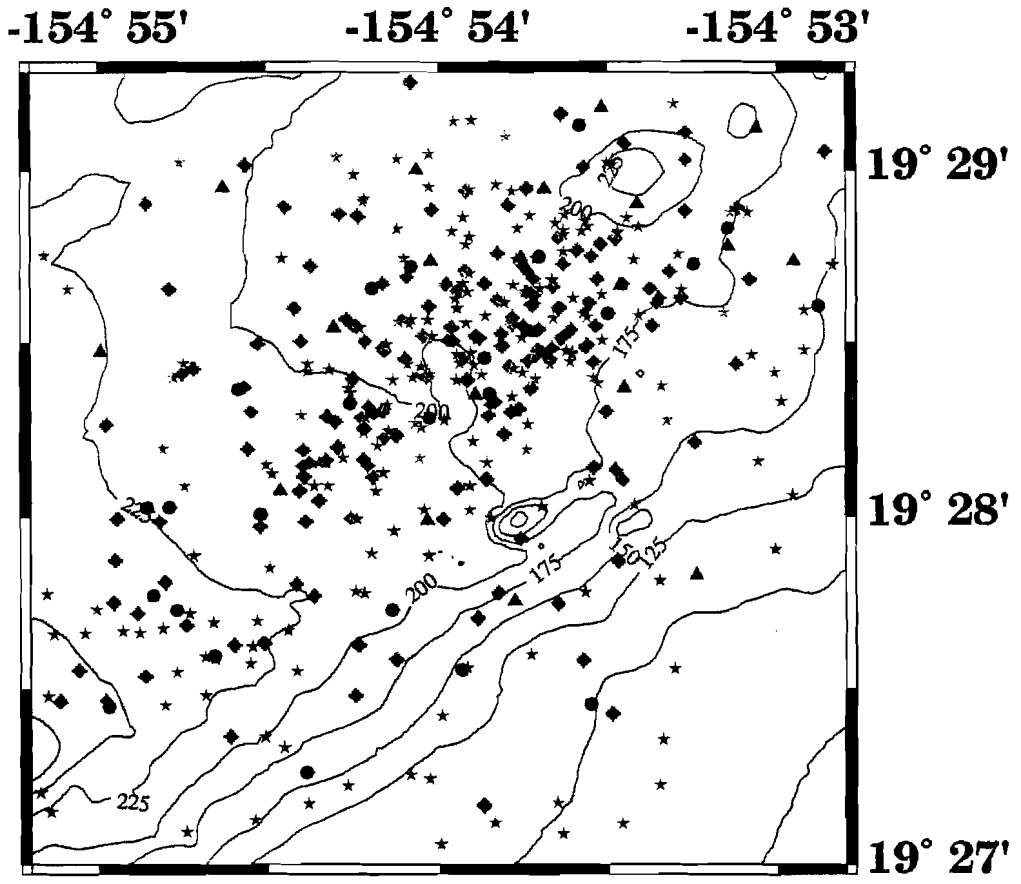

Figure 29. PANDA earthquakes sorted according to magnitude. Green, red, and blue filled circles denote earthquakes with depth ranges of < 5 km, from 5 to 10 km, and > 10 km, respectively.

A plot of the entire catalog of duration magnitudes (Figure 30) shows two distinct trends yielding b-values of 0.96 and 0.47 for events with magnitudes $M_D > 1.7$ and $-1.0 > M_D > 1.7$, respectively. A similar plot of earthquakes located within 4 km of the center of the array (Figure 31) was made to investigate the possibility of two distinct source regions. The resulting b-value (for earthquakes within 4 km of the array center) is 0.96, which agrees well with other values obtained for the south flank and LERZ (Koyanagi et al., 1981 and Klein, 1994). The lower b-value is probably a result of several factors: the inclusion in the catalog of higher-magnitude (>1.0) earthquakes from outside of the array; exclusion of low-magnitude earthquakes from outside the array because of the detection threshold; the limited time period of the experiment.

3.5. HVO/PANDA Joint Locations

Arrival-times, locations, and magnitude information for earthquakes occurring during the time period 1 February through 31 April were obtained from HVO. This data set included more than 640 earthquakes with magnitudes less than 1.5 within the area from 18° 40' to 20° 20'N and from 154° 20' to 156° 40'W. During the above time period the HVO telemetered network consisted of 52 single- and multi-component seismometers (Figure 32). Depths of solutions were greatest (down to 50 km) beneath Kilauea's summit region. A technical description of the HVO network instrumentation is given in Tomori et al. (1991).

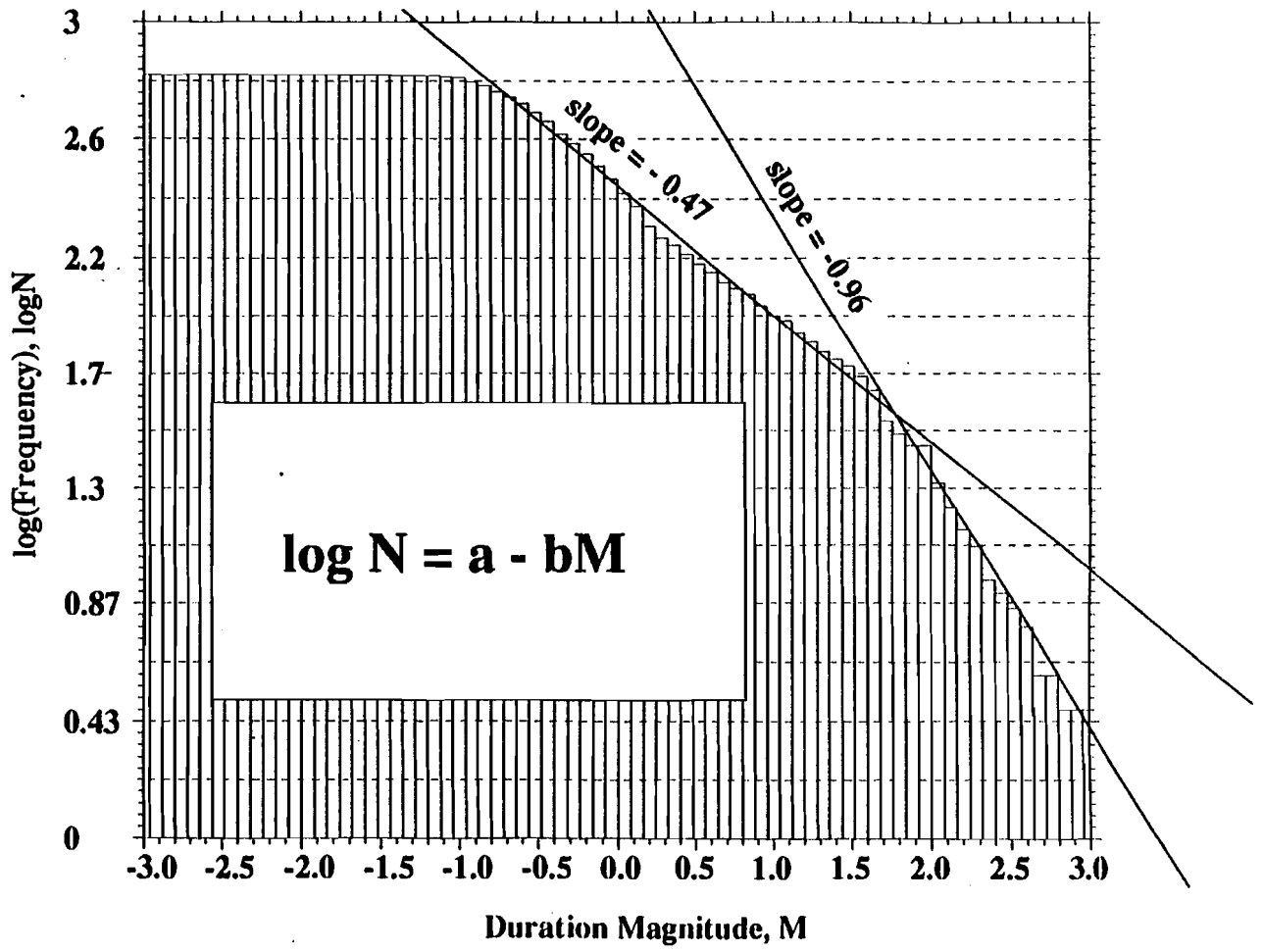

Figure 30. Frequency-magnitude relationship for the entire PANDA catalogue of events. Line fit is by eye and negative slope of the line fit is equal to the b-value (Gutenberg and Richter, 1954).

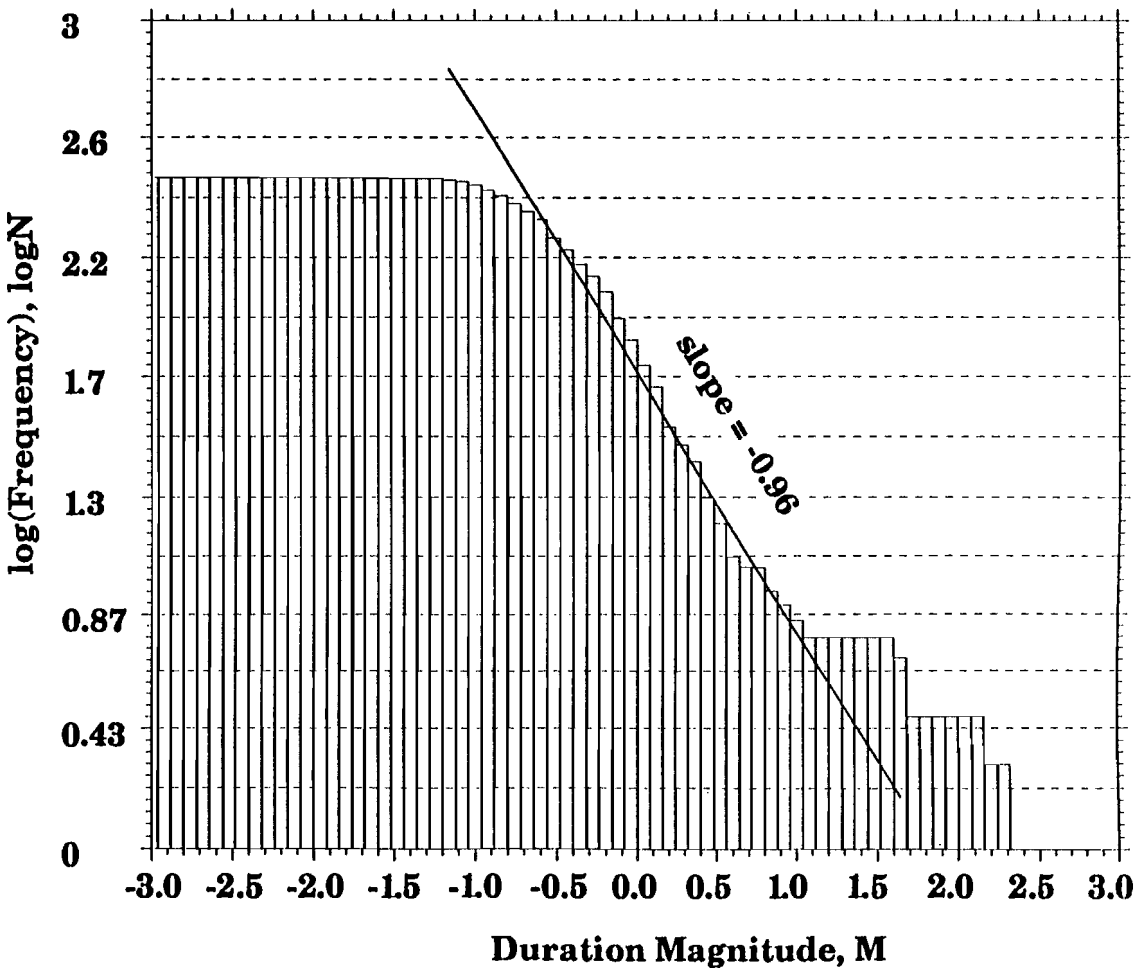

Figure 31. Frequency-magnitude relationship for PANDA events within 4 km hypocentral distance. Line fit is by eye and negative slope of the line fit is equal to the b-value (Gutenberg and Richter, 1954).

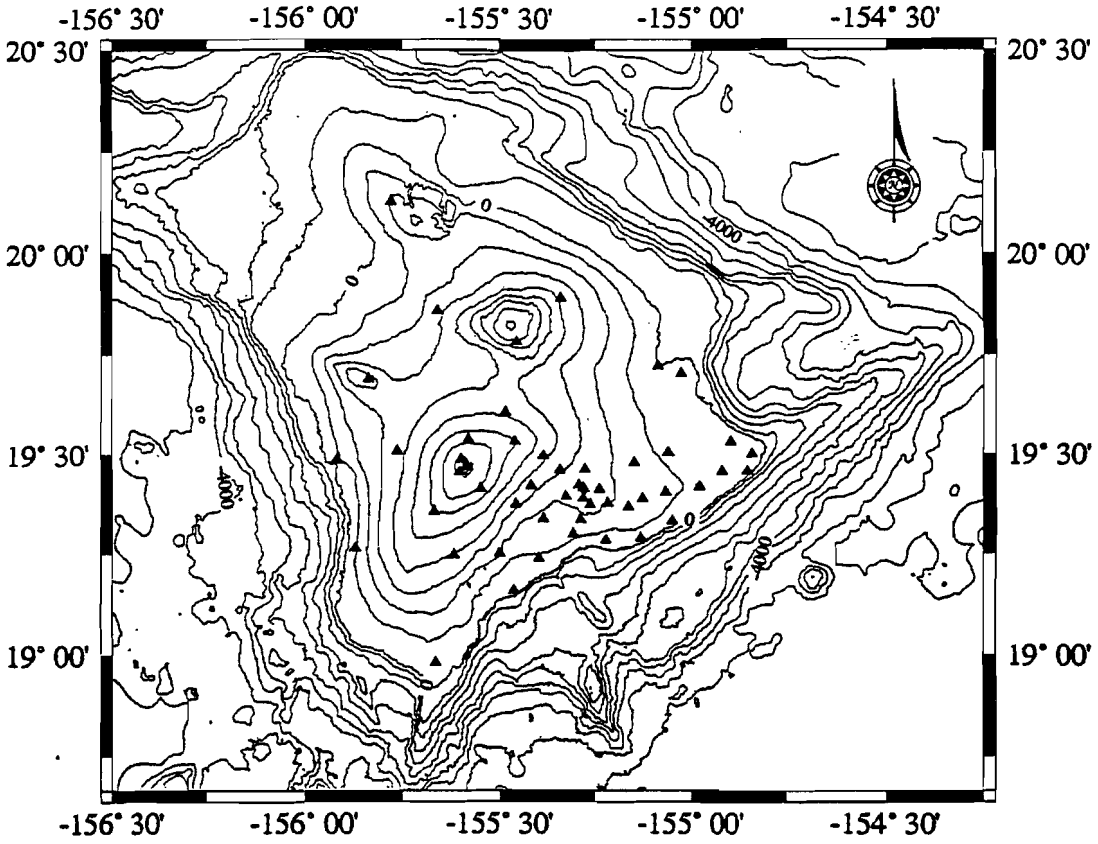

Figure 32. Map of seismograph stations operated by Hawaii Volcano Observatory (triangles) Contour interval is equal to 500 m.

A comparison of the HVO locations (Figure 33) with the PANDA array locations (Figure 20) reveals significant differences in the responses of the two systems. During the three-month period of this experiment, HVO located only six events within the PANDA array boundaries (HVO requires 6 "good" arrivals in order to locate and catalog and event - Paul Okubo, personal communication). The reasons for this are the sparse distributions of seismograph stations in the Puna region and the much higher amplifier-gain settings of the PANDA electronics. Almost all of the earthquakes located by HVO have hypocenters beneath the summit region and upper rift zones of Kilauea Volcano and the Kaoiki, Koae and Hilina fault systems.

Hypocenters calculated using combined HVO and PANDA travel-time data showed decreased uncertainties for earthquakes outside of the PANDA array bounds (Figure 34). Within the array, only four earthquakes had enough data to be located in this manner. (Since the tomographic inversion for Vp/Vs used only earthquakes within 10 km of the PANDA array, the HVO data was not included in the inversion.)

4. THREE-DIMENSIONAL TOMOGRAPHIC INVERSION FOR VP/VS STRUCTURE

Travel times for P- and S-waves were inverted for Vp/Vs structure using the SIMUL3SMP2 program (Eberhart-Philips, 1990; Thurber et al., 1991; and Thurber, 1993). This program is a modification of SIMUL3 (Thurber 1984) and SIMULPS12 (Evans et al., 1993), programs for the inversion of local earthquake travel-time

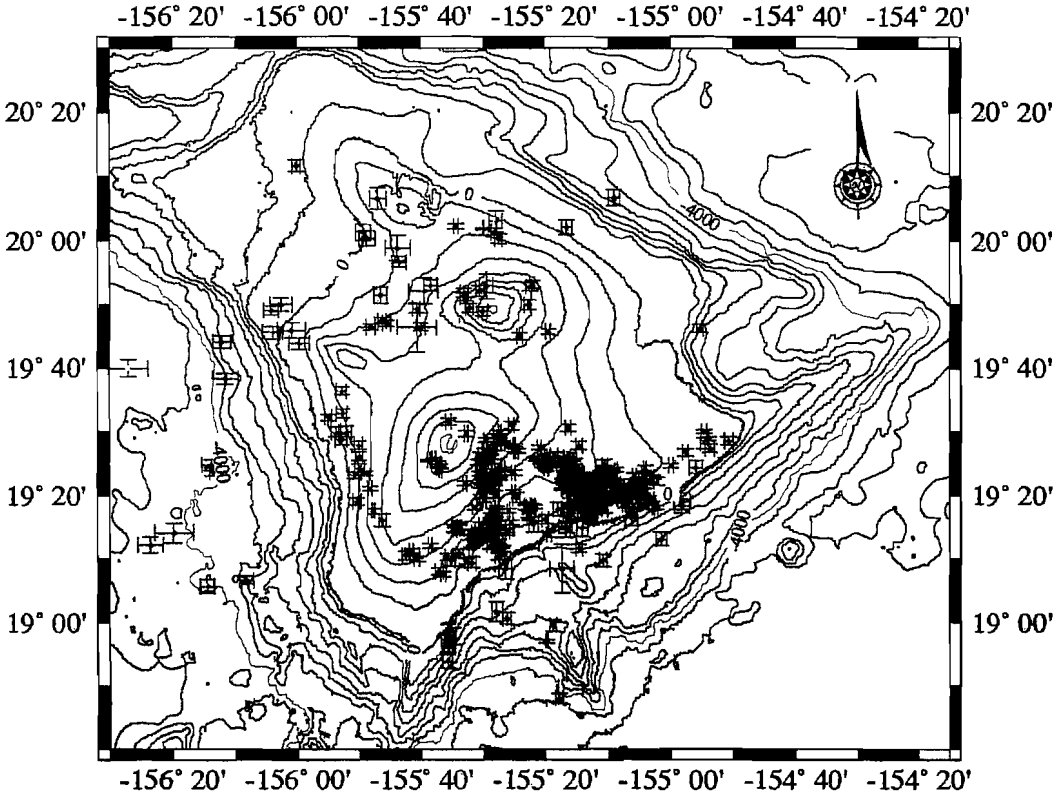

Figure 33. Earthquakes recorded by HVO during the PANDA field experiment; located using HYPOCENTER (Lienert et al., 1986.). Green, red, and blue filled circles denote earthquakes with depth ranges of < 5 km, from 5 to 10 km, and > 10 km, respectively.

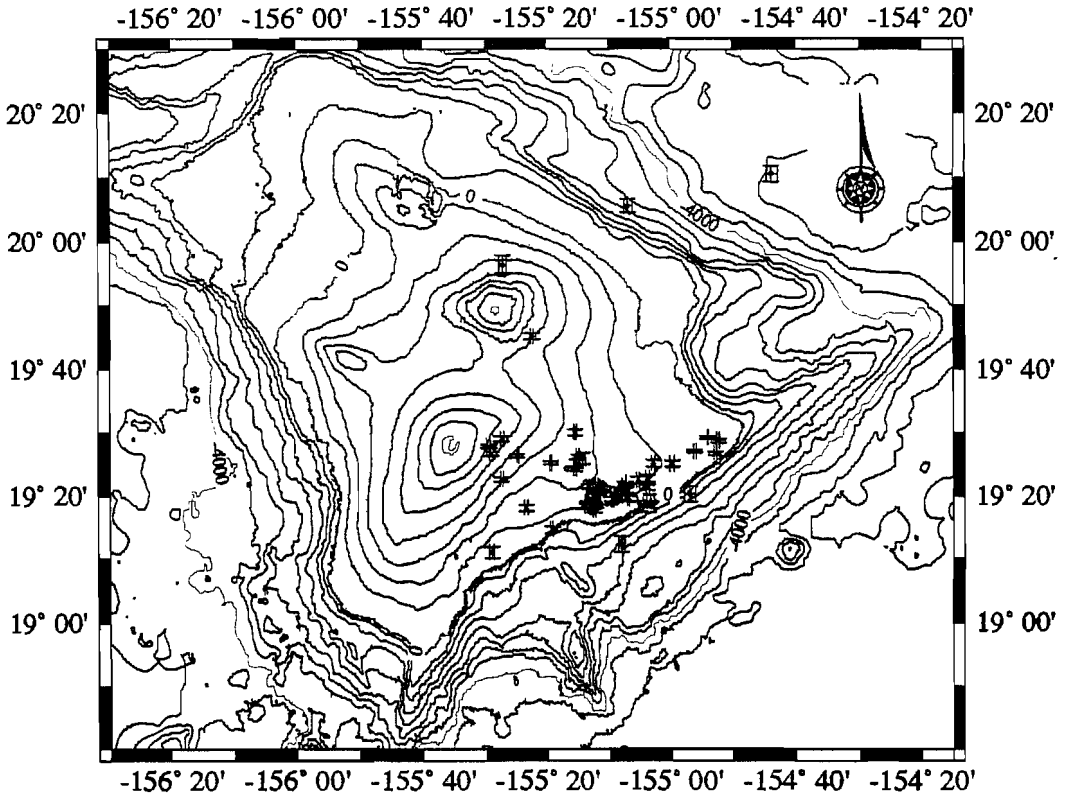

Figure 24. Earthquakes located by both the HVO and PANDA networks. Green, red, and blue filled circles denote earthquakes with depth ranges of < 5 km, from 5 to 10 km, and > 10 km, respectively.

data for 3-D velocity structure and hypocenter relocation. The reader is referred to the above-mentioned publications for details of the theoretical background. The procedure minimized travel-time residuals (the time difference between the calculated arrival time and the observed arrival time) of Vp/Vs at the recording sites. The final solution was achieved using an iterative procedure for earthquake relocation and simultaneous determination of velocity structure.

Travel times of first-arriving body waves were estimated from an initial crustal model by a three-dimensional, approximate ray-tracing technique. The crustal model was given as a set of points constituting a three-dimensional grid of nodes

4.1. Earthquake Selection Criteria

To ensure good quality of data for the velocity inversion, 93 earthquakes out of the PANDA data set satisfying the selection criteria listed below were selected for a one-dimensional velocity inversion. The selection criteria were (1) the reading weight for both P- and S-waves must be within quality levels 0 to 2 (the quality levels range from 0 to 4); (2) the largest azimuthal separation in degrees between stations (GAP) for each event must be less than or equal to about 100°; (3) the total number of both P- and S-wave readings must be greater or equal to 10; (4) the root mean square (RMS) travel-time residuals must be less than or equal to 0.1 second; (5) the epicenter locations must be located within 10 km of the array boundaries; and (6) the horizontal error (ERH) and the error in focal

depth (ERZ) must be less than or equal to 1.0 km, i.e. HYPOELLIPSE quality criterion of A or B.

4.2. Weighting and Nodal Spacing

Within the program SIMUL3SMP, two tapered weighting schemes were used to stabilize the algorithm. The first was the epicentral distance weight; for these calculations, earthquakes at distances < 5 km had a weight equal to 1, weights for earthquakes between 5 and 10 km were linearly distributed between 1 and 0, and events at distances > 10 km had zero weight. The second weighting scheme was based on station residuals and was similar to the distance weighting. After several trial inversions, station residuals less than 0.22 s were given weights of 1, residuals between 0.22 and 0.29 received weights linearly distributed between 1 and 0, and residuals greater than 0.29 were weighted zero (removed).

Aside from node spacing, the residual weighting was the most important factor in interpretation of the resultant inversion. If tapers were set too low, then all of the velocity variations due to lateral and vertical inhomogeneities would be removed. The station residuals were calculated as the difference between observed and calculated travel times based on initial velocity models. Conversely, allowing large residuals in the data set would produce large variations in the final model. The final weighting parameters were determined by gradually raising the cutoff until the model was no longer consistent with the previous model.

Calculations began with a node spacing of 4 x 4 km (Figure 35). Subsequent models were computed with reduced grid spacing until the minimum grid spacing allowed for the program was attained - 1 x 1 km (Figure 36). This lower limit exists because of computational limitations in the algorithm. Model variances and residuals decreased as grid spacing decreased. The grid was kept centered on the HGP-A well (19° 28.80'N, 154° 54.00'W) for all inversions. Figure 37 locates the grid with respect to local topographic features and the geothermal well sites. The final Vp/Vs model variations were significant compared to the calculated uncertainties (Figure 38), the area under investigation was well sampled (Figure 39), and the solution appeared stable at all nodal spacings. Final plots of the calculated uncertainties, observations, and Vp/Vs variations were made using the continuous curvature gridding routine GMT (Generic Mapping Tool; Wessel and Smith, 1992). False variations may appear where no node points exist to constrain the interpolation scheme; these are easily identified and commonly occur in the corners of plots.

4.3. Final Vp/Vs Model

Vp/Vs variations with depth are shown in Figures 38 and 39. The corresponding uncertainty and ray density for each node were also gridded and contoured and are shown in Figures 40 through 45.

Generally, the model shows relatively high Vp/Vs (above the background value of 1.78) at shallow depths along the LERZ to Pu'u Honuaulua with another relative high to the southeast, between Pu'u

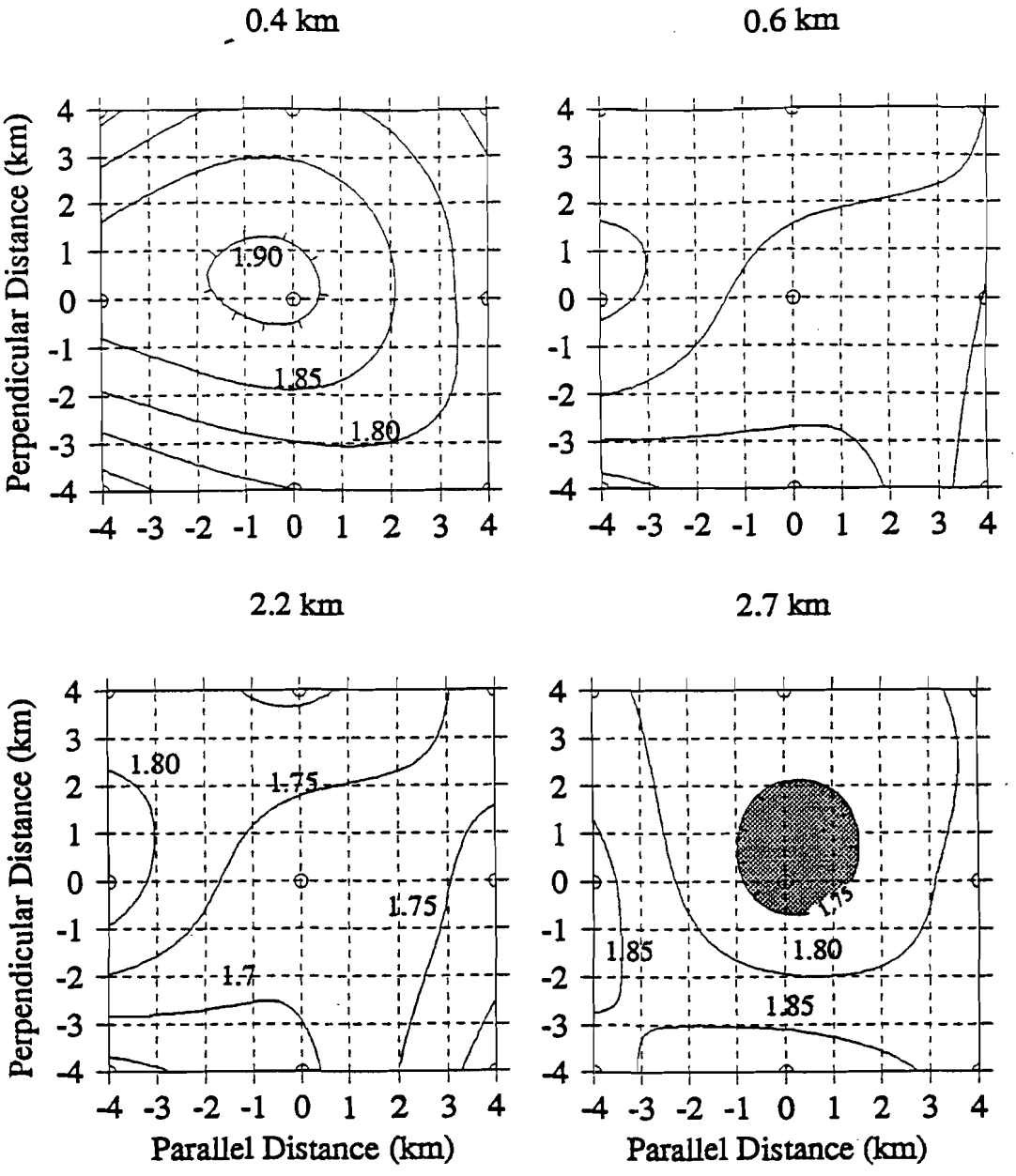

Figure 35. Plot of Vp/Vs variations for horizontal slices at 0.4, 0.6, 2.2, and 2.7 km depth. Grid is rotated 36 degrees west of north such that the horizontal axis is parallel to the LERZ and the vertical axis is perpendicular. Circles denote nodes used in this inversion. Contour interval equals 0.05 and closed lows are shaded.

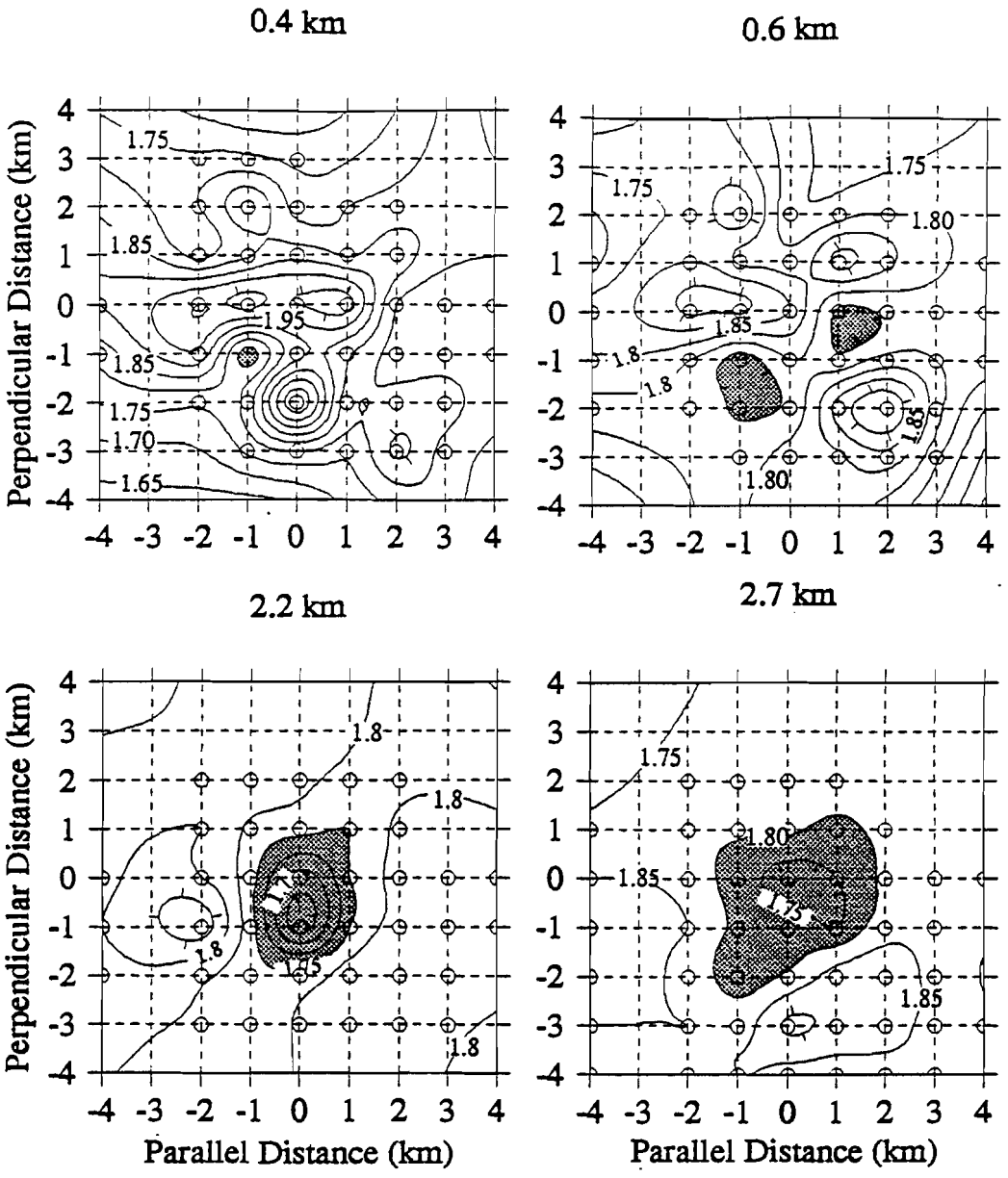

Figure 36. Plot of Vp/Vs cariations as horizontal slices are 0.4, 0.6, 2.2, and 2.7 km depth. Grid is rotated 36 degrees west of north such that the horizontal axis is parallel to the LERZ and the vertical axis is perpendicular. Circles denote nodes used in this incersion. Closed Vp/Vs lows are shaded.

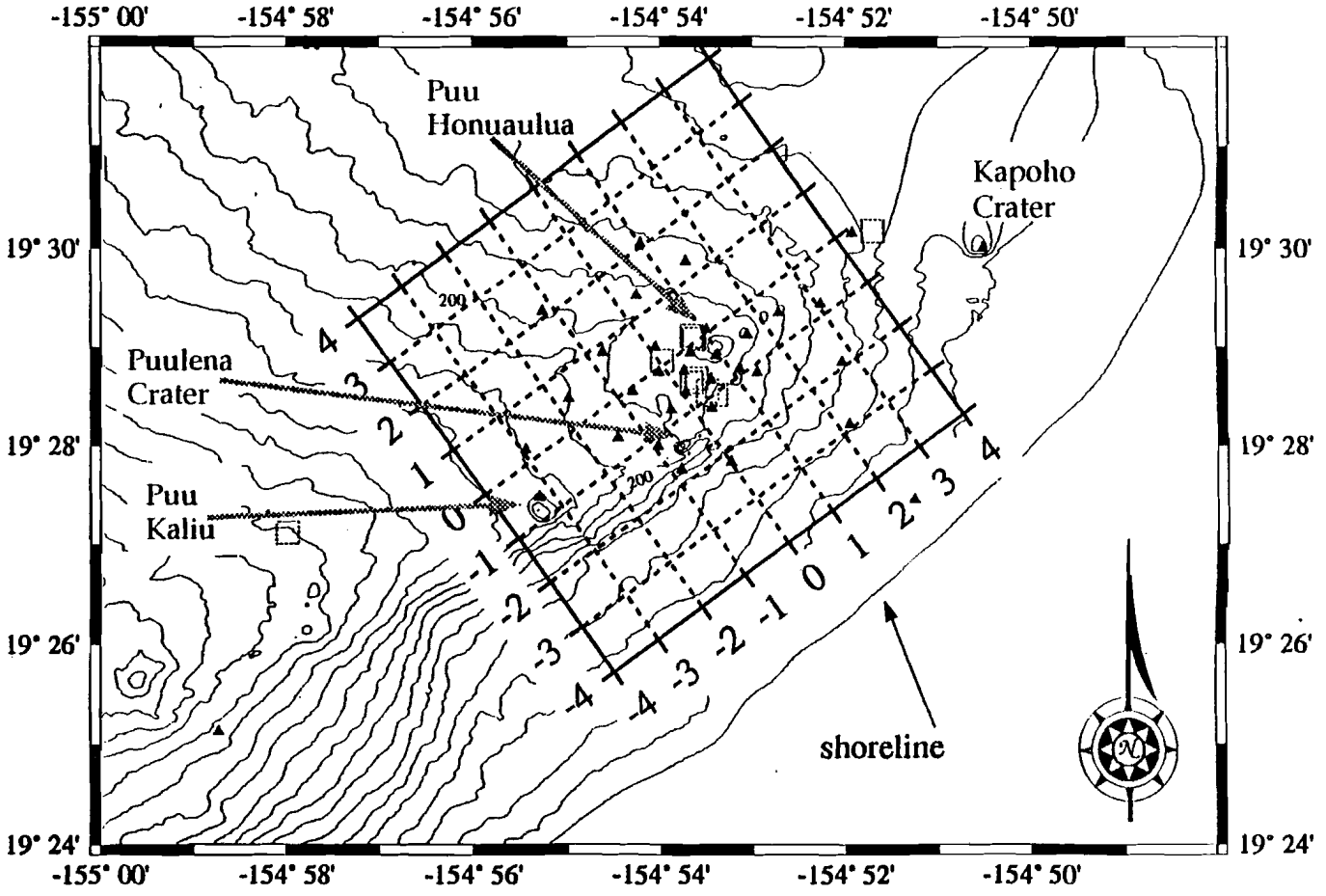

Figure 37. 1 x 1 km grid for Vp/Vs inversion. Triangles denote stations, squares denote geothermal wells, and grid scale units are in km.

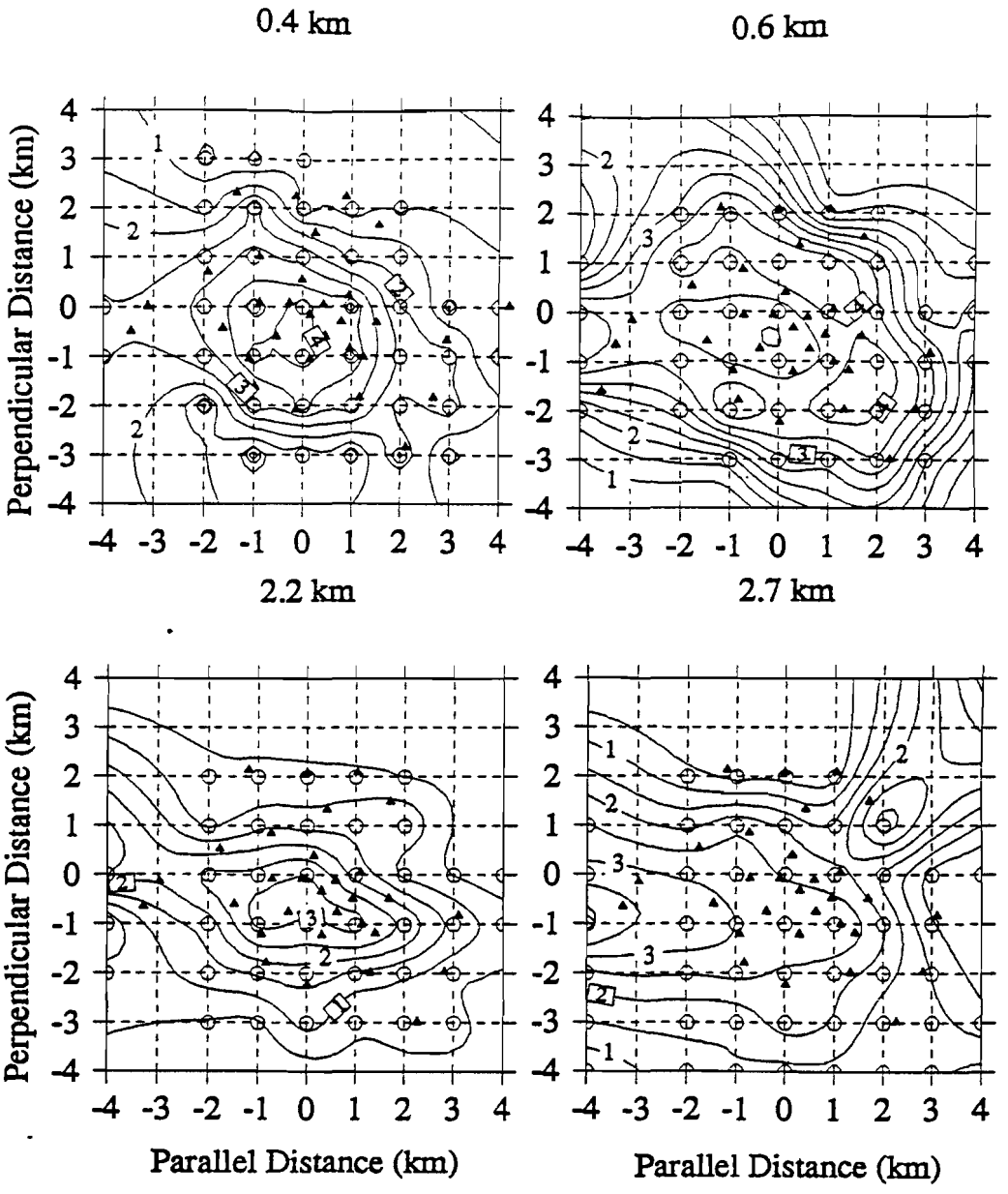

Figure 38. Model uncertainty for horizontal slices at 0.4, 0.6, 2.2, and 2.7 km depth. Grid is rotated 36 degrees west of north such that the horizontal axis is perpendicular to the LERZ and the vertical axis is perpendicular. Circles denote nodes used in the inversion. Contour interval equals 0.5%.

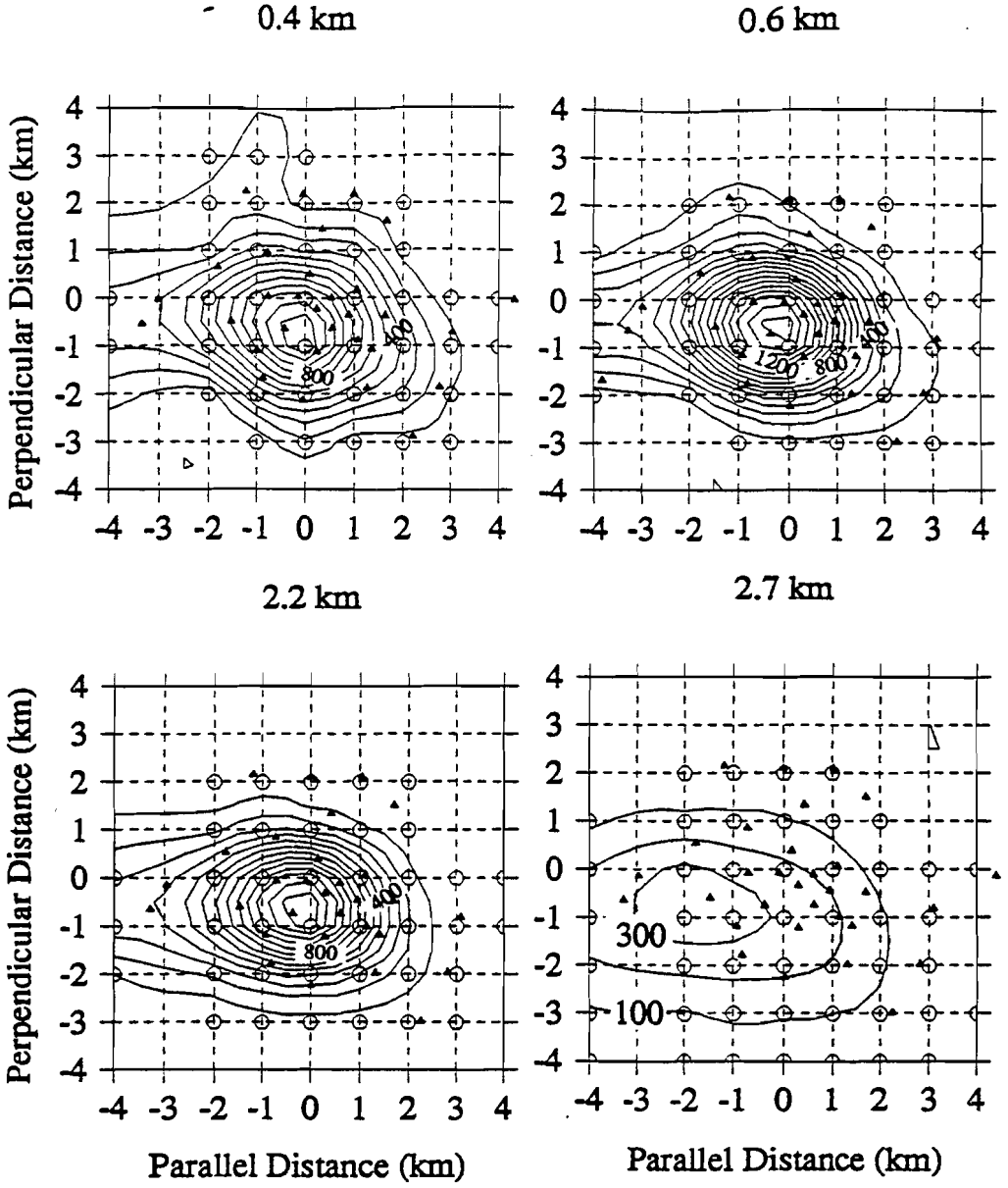

Figure 39. Ray hit-count for horizontal slices at 0.4, 0.6, 2.2, and 2.7 km depth. Grid is rotated 36 degrees west of north such that the horizontal axis is parallel to the LERZ and the vertical axis is perpendicular. Circles denote nodes used in this inversion and triangles denote stations. Contour interval is 100 events per square km.

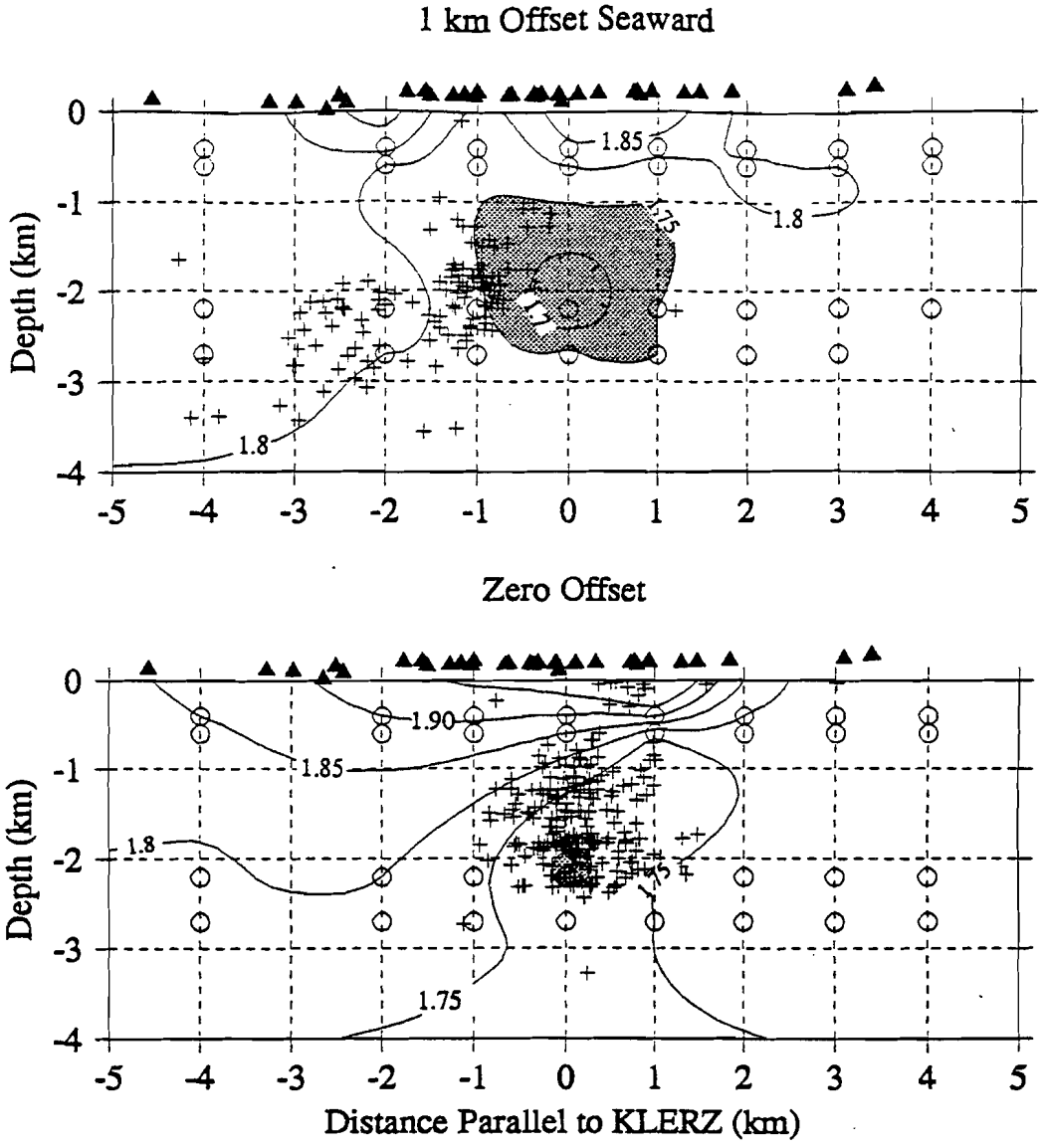

Figure 40. Plot of Vp/Vs variations for vertical slices striking parallel to the LERZ and centered on HGP-A geothermal well. Kapoho Crater is located at approximately 3.3 km, and Kilauea's summit is off-scale toward the negative end of the plot. Circles denote nodes used in this inversion, crosses denote earthquakes, and triangles denote stations. Contour interval equals 0.5% and closed Vp/Vs lows are shaded.

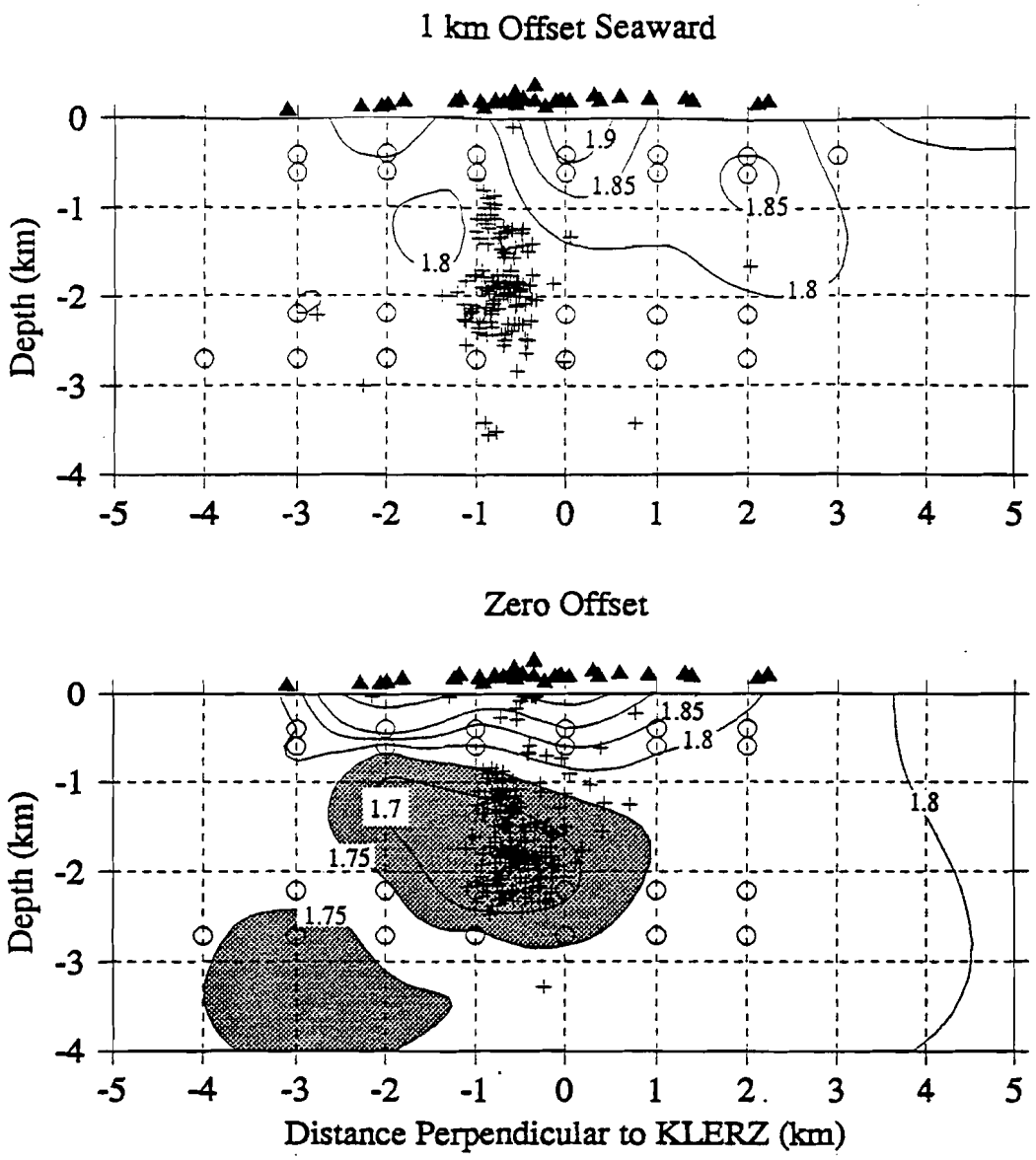

Figure 41. Plot of Vp/Vs variations for vertical slices striking perpendicular to the LERZ and centered on HGP-A geothermal well. View is looking toward Kilauea Volcano from Cape Kumukahi. Circles denote nodes used in this inversion, crosses denote earthquakes, and triangles denote stations. Contour interval equals 0.5% and closed Vp/Vs lows are shaded.

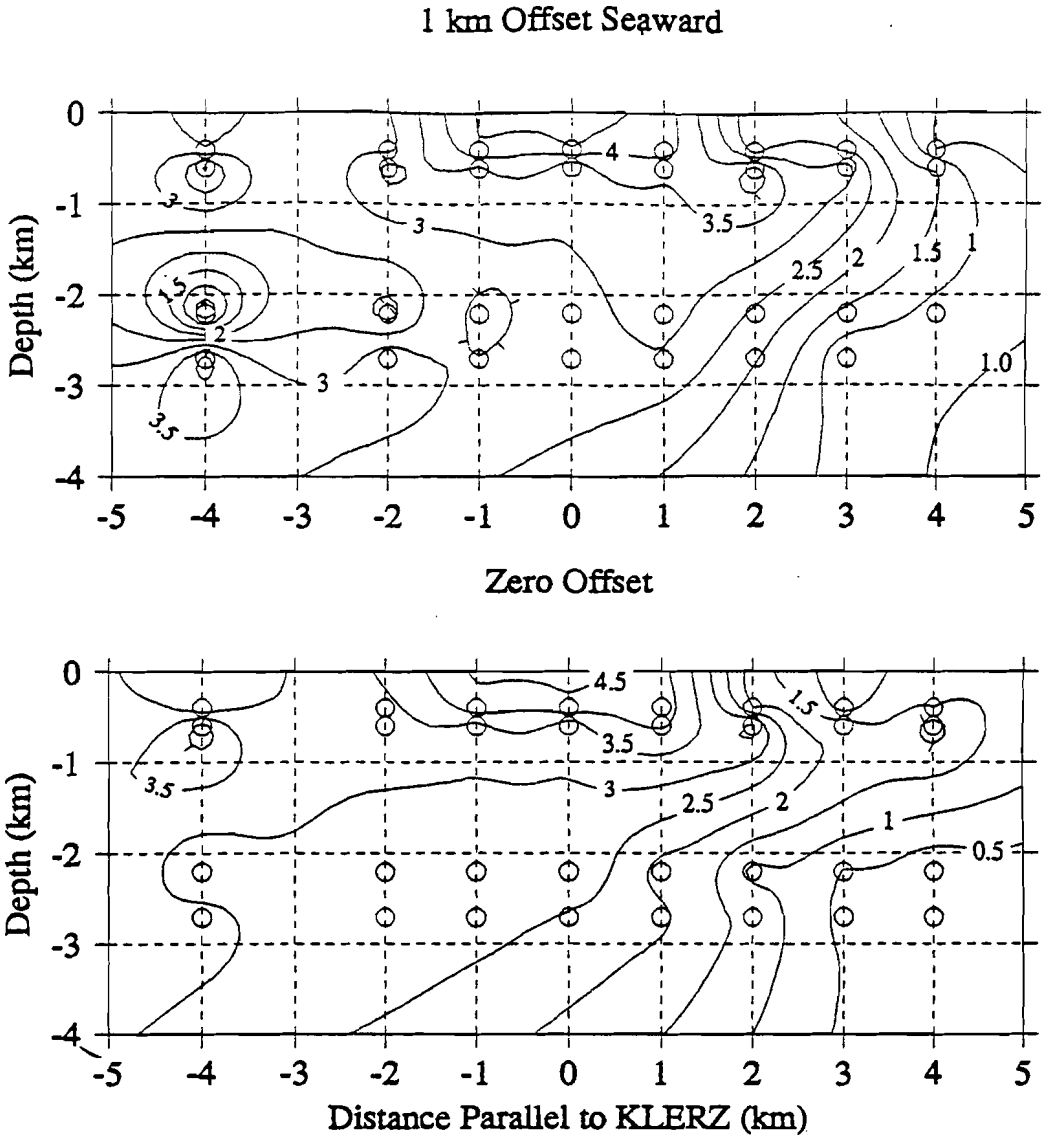

Figure 42. Model uncertainty for vertical slices striking parallel to the LERZ and centered on HGP-A geothermal well. View is looking toward Mauna Kea Volcano from the Puna coast. Circles denote nodes used in the inversion. Contour interval equals 0.5%.

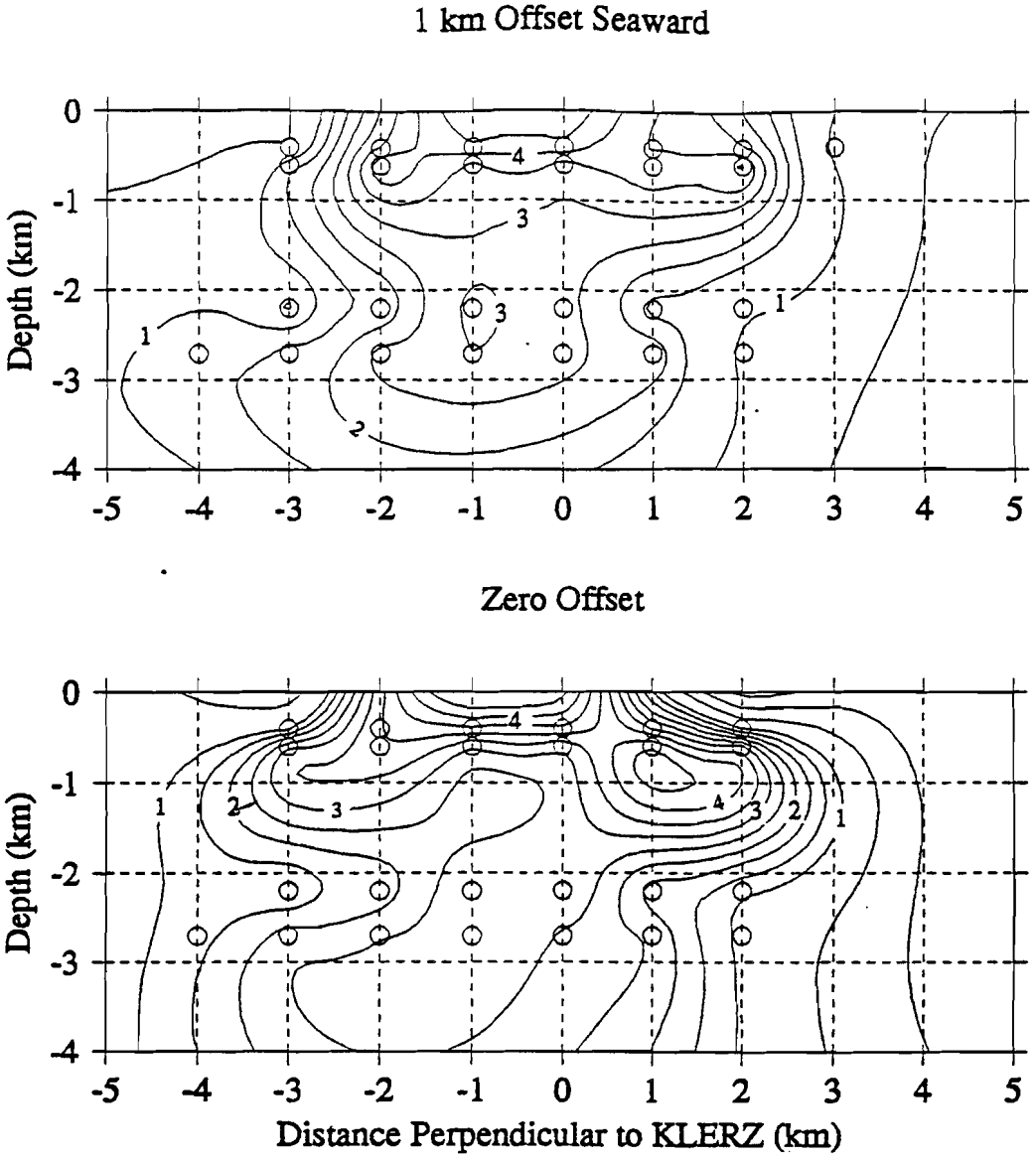

Figure 43. Plot of model uncertainty for vertical slices striking perpendicular to the LERZ and centered on HGP-A geothermal well. View is looking toward Kilauea Volcano from Kapoho Crater. Circles denote nodes used in the inversion. Contour interval equals 0.5%.

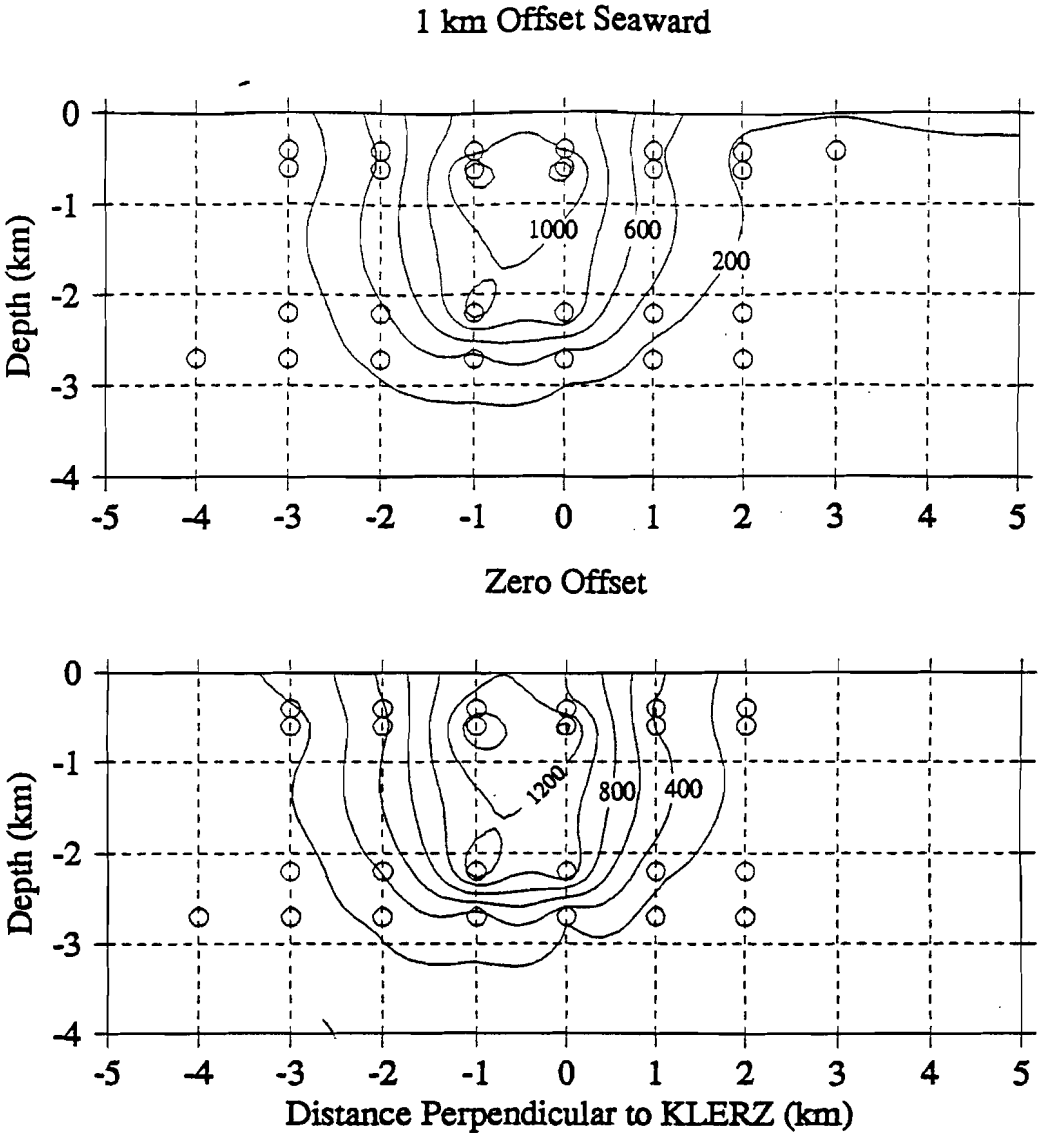

Figure 44. Plot of ray-path density for vertical slices striking perpendicular to the LERZ and centered on HGP-A geothermal well. View is looking toward the Kilauea summit region from Kapoho Crater. Circles denote nodes used in the inversion. Contour interval equals 200 observations per square km.

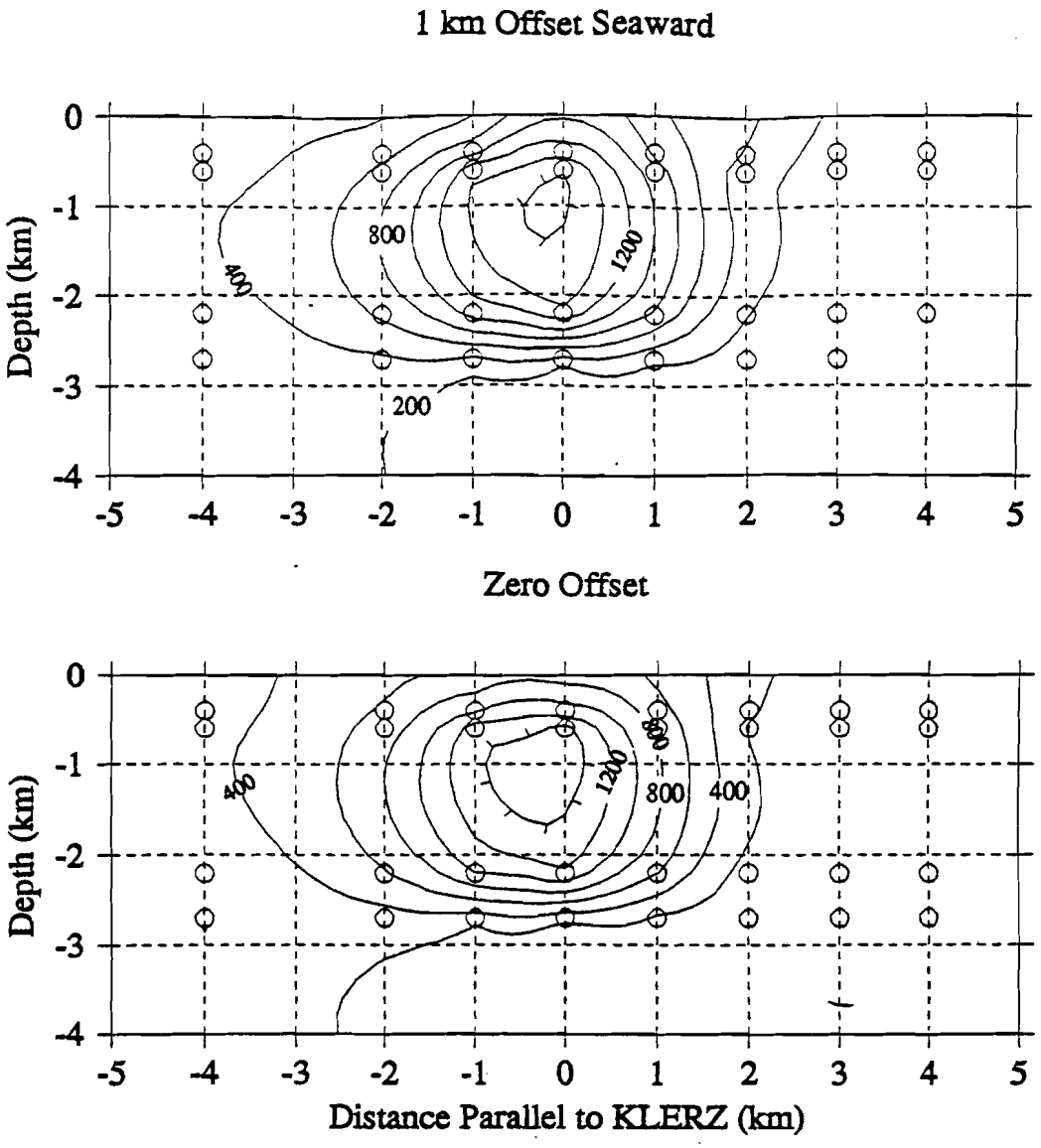

Figure 45. Plot of ray-path density for vertical slices striking parallel to the LERZ and centered on HGP-A geothermal well. View is looking toward Mauna Kea Volcano from the Puna coast. Circles denote nodes used in the inversion. Contour interval equals 200 observations per square km.

Honuaulua and Pu'ulena Crater (Figure 37). A roughly circular low Vp/Vs anomaly is centered about 1 km to the south of HGP-A. Superimposed on that feature is a smaller amplitude linear anomaly striking N 08° W.

Vertical cross-sections of Vp/Vs and seismicity in the upper 4 km perpendicular and parallel to the strike of the LERZ reveal the vertical extent of the anomaly (Figure 40 and 41). The velocity model determined from this study confirms the existence of a low-velocity zone for P-waves at shallow depths (from 2.0 to 5.0 km) beneath the Puna region and further suggests a relatively low Vp/Vs ratio within this zone. The results of the three-dimensional velocity inversion further show that seismically active areas appear to have a close spatial correlation with low velocity anomalies.

In three dimensions, we can approximate the shape of the low Vp/Vs anomaly as an oblate spheroid, centered between Pu'u Honuaulua and Pu'ulena Crater at a depth of 2 km. The total dimensions of the anomaly are 2.5 x 2 x 1.5 km (coordinates are parallel distance, perpendicular distance, and vertical distance with respect to the LERZ; see Figure 36). Vp/Vs reached a minimum of 1.66 in contrast to the background value of 1.78. Structures deeper than 4 km were not imaged well due to the reduced ray density (fewer observations) below 4 km. Information at the nodes to 13.5 km depth was included in the gridding of the data.

5. SOURCE MECHANISMS AND IMPLICATIONS FOR THE STRUCTURE OF THE RESERVOIR

Gravitationally driven dike-impounded meteoric waters flow from the upper and middle East Rift Zone toward the south coast (Ingebritsen and Scholl, 1993). Vertically dipping dikes are often laterally extensive along the rift zone; such dikes tend to impound groundwater in inter-dike compartments of more permeable rock, allowing water to flow along and parallel to the rift system (Macdonald et al., 1983; Ingebritsen and Scholl, 1993). Hot-water springs along the Puna coast (Lovenitti and D'Olier, 1990) indicate that, at some point along the rift zone, water escapes from the dike complex.

Upslope from the Puna coastal hot springs the LERZ appears to be slightly offset. The Vp/Vs low is roughly centered on this same offset. In order to determine that the apparent offset in the topographic expression of the LERZ reflects the rift structure and is not a surface effect of "repaving" by recent lava flows, we studied the source mechanisms of as many earthquakes as possible.

Composite fault-plane solutions for groupings of events located in a circular area within 0.1 degree of each other are shown in Figure 46. The focal sphere projections of the polarities of the first P-wave arrivals are plotted on lower-hemisphere equal-area projections (examples of solutions for individual events are shown in Appendix III). Quadrants with compressional arrivals are shaded, while quadrants displaying dilatations are left unshaded. A line is drawn

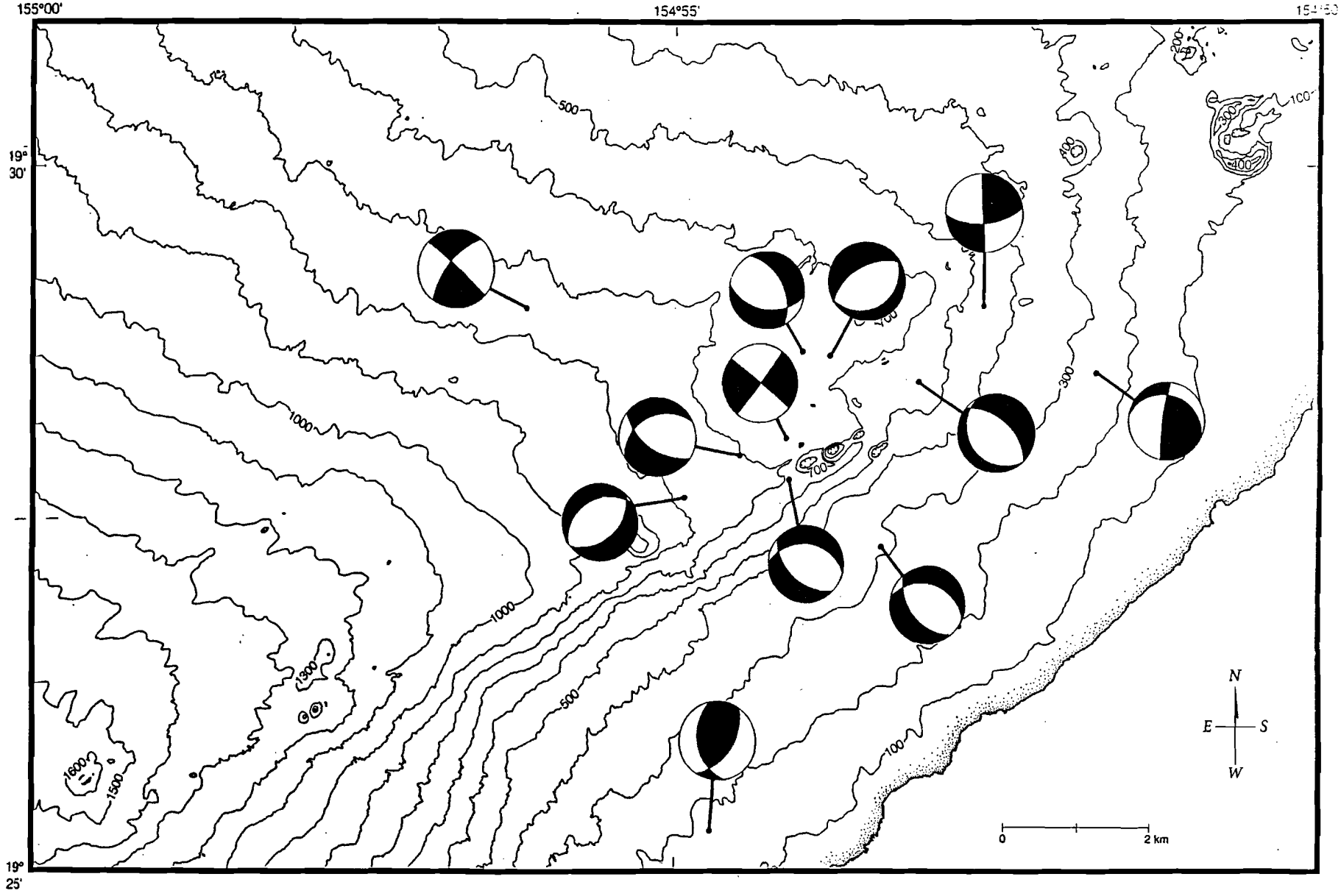

Figure 46. The focal sphere projections of the polarities of the first P-wave arrivals are plotted on lower-hemisphere equal-area projections (examples of solutions for individual events are shown in Appendix III). Quadrants with compressional arrivals are shaded, while quadrants displaying dilatations are left unshaded. A line is drawn from the solution to the approximate of center of the grouping of earthquakes for each solution.

from the solution to the approximate of center of the grouping of earthquakes for each solution.

Normal faulting in a direction roughly perpendicular to the rift zone is shown in three composites located within the structural boundaries of the rift (Figure 47), a 2- to 3-km-wide region marked by cinder cones and other volcanic constructs. Normal faulting oriented at an oblique angle to the rift zone is seen on the south flank, along with some thrust faulting. Strike-slip faulting occurs along the LERZ and to the northwest. The pattern suggests that seismic slip occurs in two directions - along faults parallel to and including the LERZ and along a system of faults oblique to the rift. Strike-slip faulting is associated with the apparent offset in the LERZ, indicating that this is a tectonic feature and the area is subject to ongoing deformation probably caused by differential motion of segments of the LERZ.

6. POLARIZATION OF SHEAR WAVES FROM CRACK-INDUCED ANISOTROPY

Seismic azimuthal anisotropy is an azimuthal variation of the physical properties of the transmitting medium. Shear waves, unlike P waves, have three-dimensional particle motions that are affected by the structural asymmetry of the medium through which they travel. Structural asymmetries along the raypath split the shear waves into several arrivals with different polarizations and different velocities. Theoretically, the fast shear wave is polarized in the plane of the cracks and the slow shear wave is polarized orthogonal to the

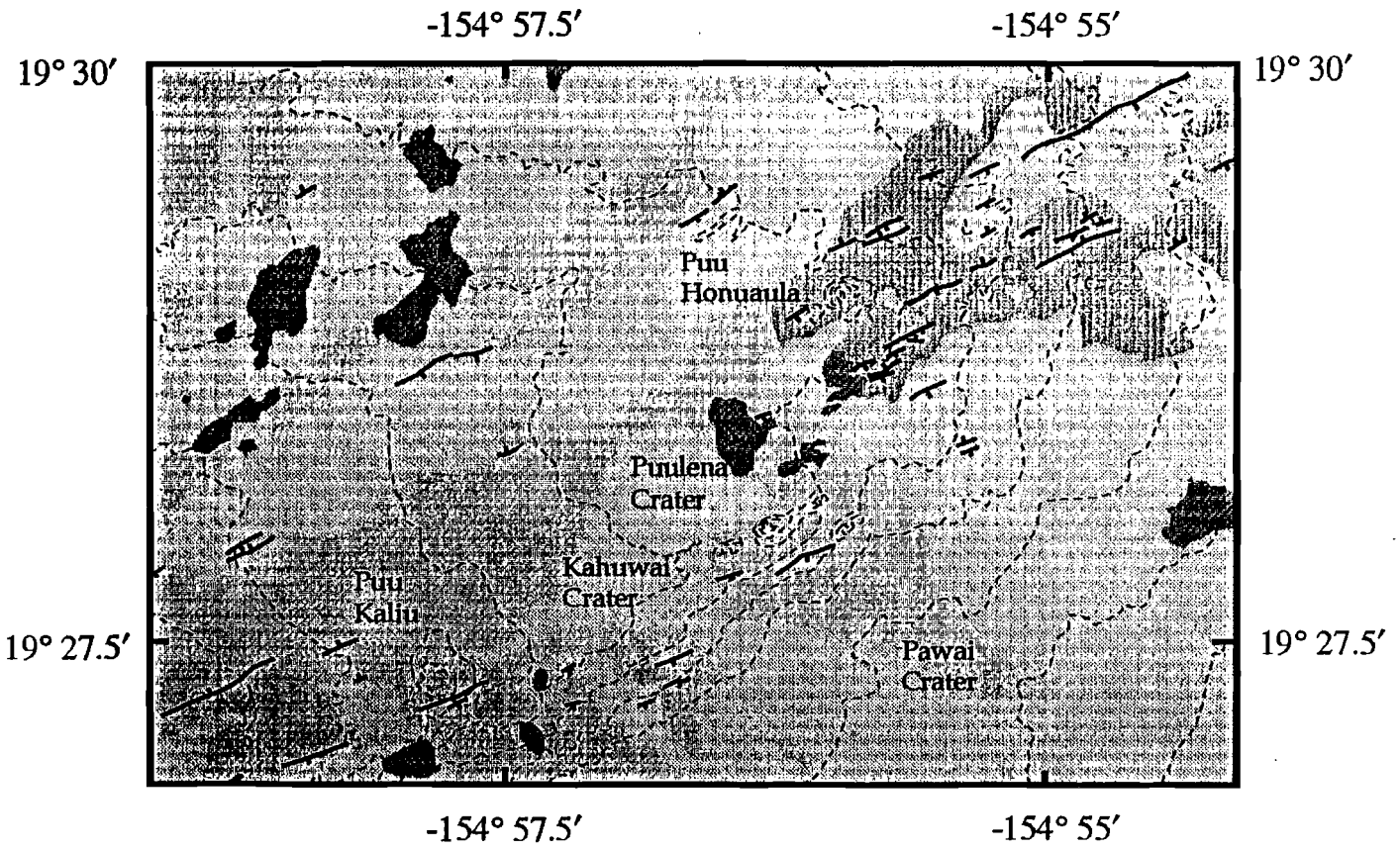

Figure 47. Geochronological map with topography and major surface features. Purple, gray, brown, and lavender areas denote lavas of ages 750-1500, 400-750, 200-400 and historic lava flows (younger than 1790 A.D.), respectively; after Moore and Trusdell, 1991.

fast shear and to the direction of propagation. The observed polarization direction of the shear waves yields information on the presence and geographical orientation of cracks and the delays between the arrivals give relative information about the amount of cracks present (Crampin, 1985).

The detection and analysis of S-wave splitting reveals useful information on the characteristics of crack distributions that cause seismic anisotropy along the propagation path. Shear-wave splitting has been used to characterize fracturing in numerous geothermal reservoirs (Sachpazi and Hirn, 1991; Sato et al., 1991; Booth et al., 1989; Crampin and Booth, 1989; Majer et al., 1988; Kaneshima et al., 1988; Roberts and Crampin, 1985).

A preliminary examination of unrotated particle motion plots of selected events revealed split shear waves at preferred azimuths (e.g., Figure 48), encouraging a more detailed analysis. The polarization direction of the fast shear wave is the azimuth of the particle motion associated with the first-arriving shear wave; here the fast shear direction is approximately parallel to the LERZ. The arrival of the slow shear wave is indicated by an abrupt change of particle motion in the diagram.

6.1. Aspect Ratio Method of Split Shear-Wave Analysis

The polarization of the fast split S-wave (S_1) is fixed by the symmetry of the anisotropic medium near the recording site (Crampin, 1985). The polarization direction and the time separation between the fast (S_1) and slow (S_2) S-wave arrivals are the two most useful

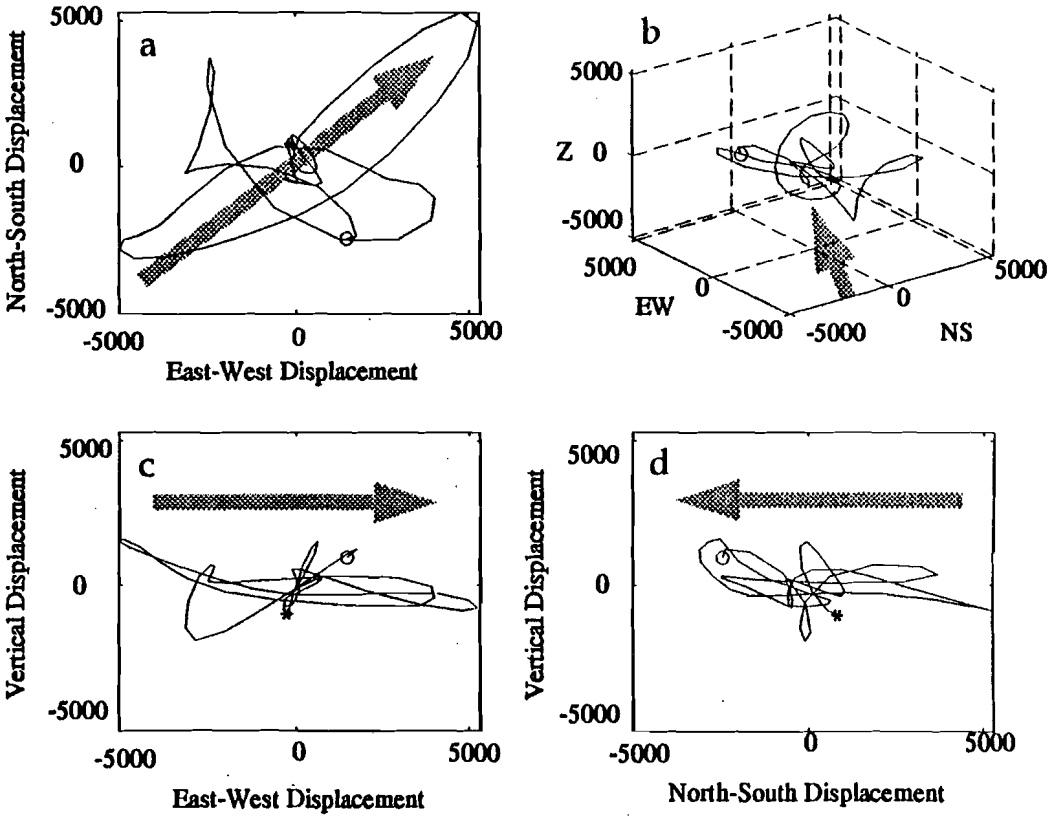

Figure 48. Hodograms of a selected S-wave arrival. Circle denotes start and the asterisk denotes end of data. Total time for this plot is 620 msec. Location of this earthquake is 19° 26.96' N 154° 57.04 W; depth is 1.94 km; magnitude is 1.31. Arrows indicate the approximate direction of propagation for this event. (a) map view; (b) 3-D perspective plot with positive up; (c) east-west cross-section, and (d) north-south cross-section

parameters derived from the study. The method used to extract these two parameters from the data is that of Shih et al. (1989).

Seismograms from ray paths with incident angles less than $\sin^{-1}$ (Vs/Vp), the "shear-wave window" of Nuttli (1961), were used to avoid S-P converted phases. The time window for analysis starts at the onset of S_1 and ends before the onset of S_2. In practice the size of the window cannot always be determined by visual inspection of the seismograms and has to be determined by trial and error. The aspect ratio is:

$$D_{xj}/D_{yj} = \sum d_i \, |\cos(\theta_j - e_i)| \, / \sum d_i \, |\sin(\theta_j - e_i)|$$

where n = the total number of samples at equal time intervals and θ = the rotation angle,

$e_i = \tan^{-1}[(y_i - y_{i+1})/(x_i + x_{i+1})]$ (i is the sample number),

and $d_i = [(y_i - y_{i+1})^2 + (x_i + x_{i+1})^2]^{1/2}$ is the displacement,

where x and y are amplitudes of the samples of the two orthogonal horizontal components (E-W and N-S). The aspect ratio is calculated at various azimuths by projecting the particle displacements onto axes that are rotated from 0° to 175° in 5° increments. The most linear particle motion, indicated by a maximum value of the aspect ratio, occurs when the angle of rotation of the projection axis is most nearly equal to the angle of polarization (Figure 49).

The horizontal components are then rotated (Figure 50) into the fast and slow directions, and the slow shear is advanced until it reaches maximum correlation with the fast shear; the amount of time advanced is equal to the time lag.

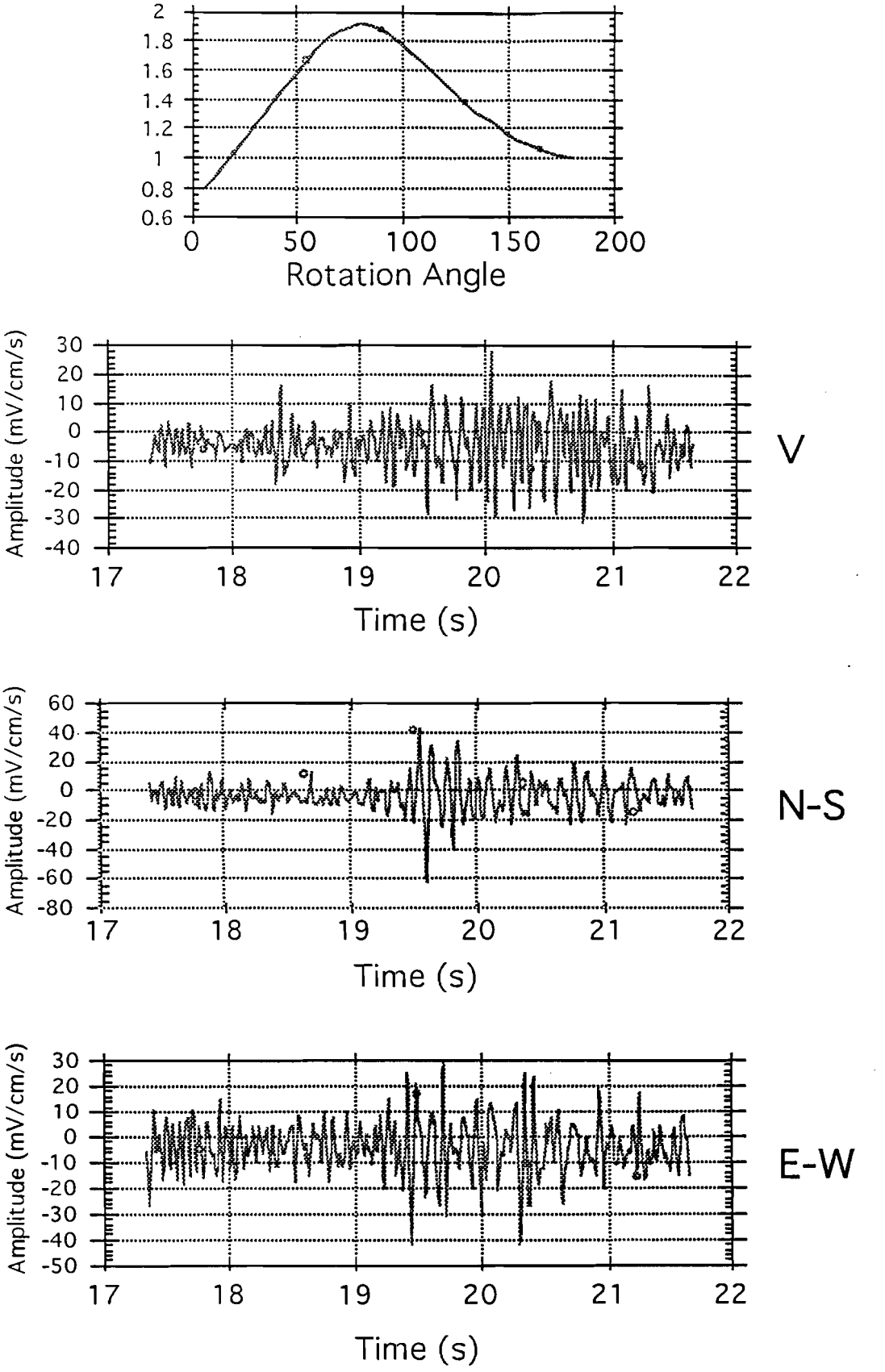

Figure 49. At the top is a sample plot of the aspect ratio calculated for an earthquake shown in the panels below indicating a polarization angle of about 80°. The p-wave arrival is clear only on the vertical component; shear-wave arrivals are high-amplitude and impusive on the N-S and E-W components.

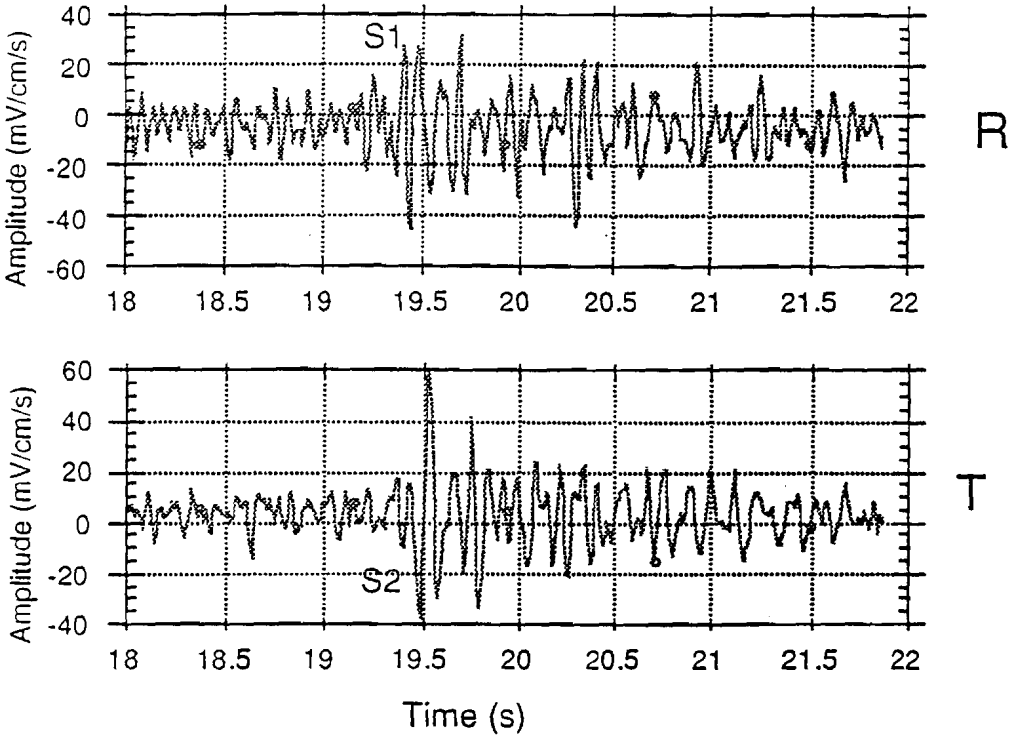

Figure 50. The two panels show the N-S and E-W seismograms of Figure 49 rotated into the fast (80°) and slow directions of polarization. S1 indicates the fast shear arrival; S2 indicates the slow shear arrival.

The crack density, or number of cracks per unit volume, can be related approximately to the time lag between S_1 and S_2 using the following equation (Sato et al., 1991):

$$\tau = (4\varepsilon / 7\beta)[\cos 4\theta - \cos 2\theta] D$$

demonstrating that the relative shear-wave lag time, τ, is proportional to the propagation distance, D, and the crack density, e (assuming that ε is small). Here, β is the shear-wave velocity in the isotropic medium with no cracks and θ is the angle of incidence measured from the vector normal to the crack face. Cracks were assumed to be parallel to the polarization directions. Alternatively, Hudson (1981) provides the following relation, assuming that the wavelength of the shear waves is large compared to crack dimensions and that the rays propagate vertically in a medium with parallel, vertical cracks:

$$\varepsilon = dT_S/T_S$$

where dT_S is the lag time and T_S is the shear-wave travel time.

6.2. Shear-Wave Polarization Directions

Almost all of the events used in this part of the study were located within or close to the boundaries of the PANDA array; 83 well located events ranging in depth from 1.8 to 10.2 km were chosen so as to provide propagation along different paths within the shear-wave window. The seismograms displayed complex P- and S-wave codas, reflecting the heterogeneity along the propagation paths, and in many cases it was difficult to identify the precise onset of S_1. Identification and elimination of S-to-P converted phases was

facilitated by including the vertical component into the particle motion analysis. Most of the identifiable shear-wave codas displayed the abrupt changes in polarization following the initial arrival that are characteristic of shear-wave splitting. P-wave polarities indicate that there are a number of different source mechanisms; i.e., not all of the events used have the same source.

The angular distributions of the observed polarization directions are shown as equal-area rose diagrams on the map in Figure 51. Uncertainties in the polarization direction of the fast shear wave and in the delay time between fast and slow shear arrivals are estimated to be about 20° and 10 ms, respectively. One persistent polarization orientation is observed regardless of the focal mechanisms and hypocentral locations of the individual events; 89% of the polarizations of the fast shear wave are roughly parallel (within 15°) to the strike of Kilauea Volcano's East Rift Zone (N64°E). The rift-parallel fast polarization direction prevails at 23 stations. Slight variations near the rift offset indicate that the near-surface contribution to splitting apparently does not predominate over pervasive anisotropy.

The overall polarization direction of the fast shear wave is consistent with independent information on stress orientation, supporting the contention that stress-aligned cracks are responsible for the shear-wave splitting.

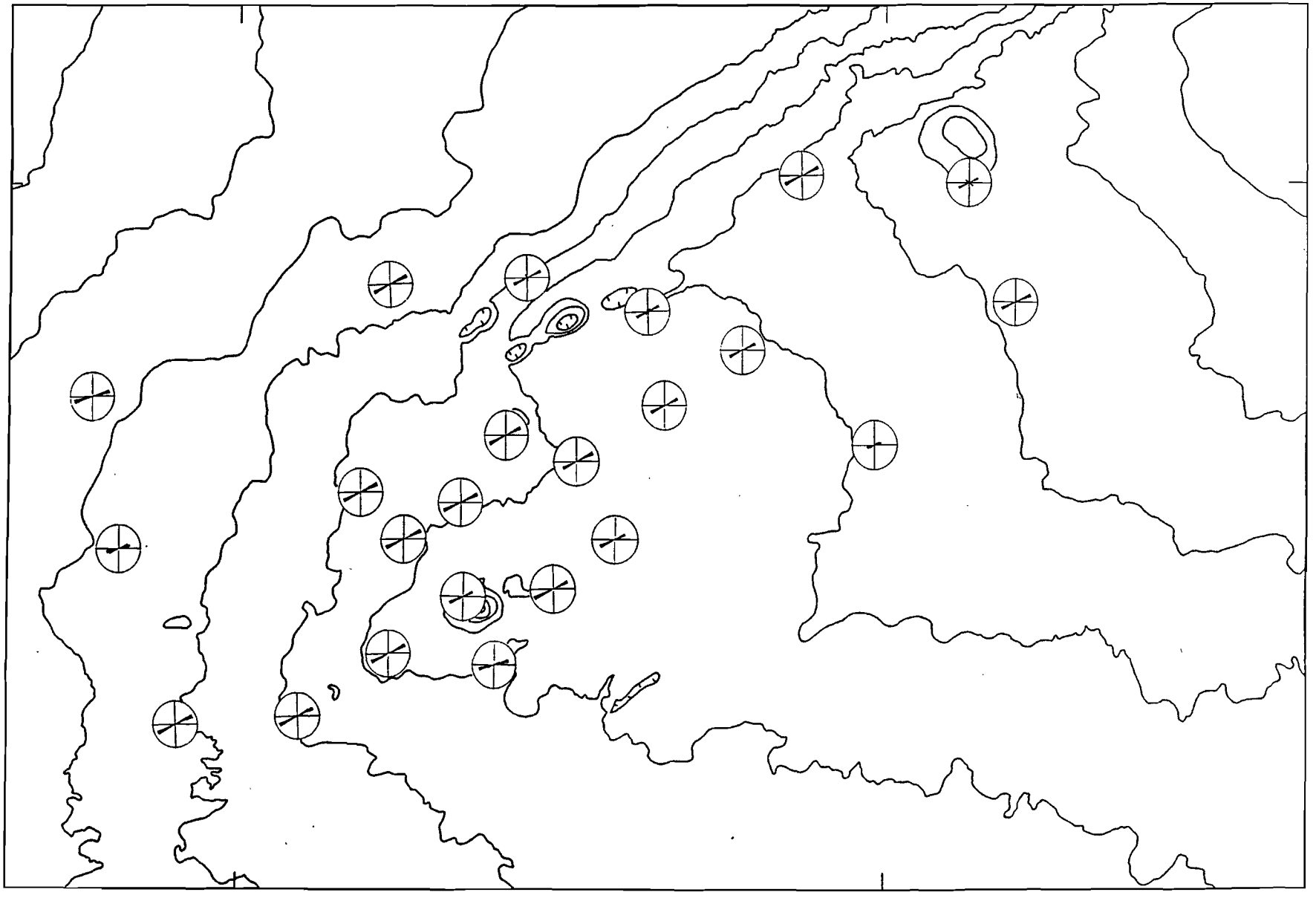

Figure 51. Angular distributions of observed polarization directions are shown as equal-area rose diagrams positioned over the station at which the measurements were made.

6.3. Estimated Crack Density

The time interval between the arrivals of fast and slow shear waves varies from 10 to 115 ms, and, for events within the array, appears to be related to hypocentral depth and location. The crack density estimated over the entire array from observed shear-wave splitting is 0.06 ±0.01. This is high compared to an average value of 0.04 for sedimentary (Crampin et al., 1986), metamorphic (Crampin and Booth, 1985), and igneous rocks (Booth and Crampin, 1986), and slightly lower than values from 0.5 to 1.0 calculated for the Kakkonda geothermal reservoir by Sato et al. (1991).

There is no apparent correlation between lag, or delay, time and azimuth (Figure 52). A weak correlation between individual lag times and event depth is evident in Figure 53. Keeping in mind that the number of earthquakes originating below 3.0 km is comparatively small, larger lag times are observed for earthquakes in the depth interval from 2.0 to 3.0 km.

7. AMBIENT NOISE AMPLITUDE SURVEY

Early studies of noise associated with geothermally active regions indicated that seismic noise amplitudes in such areas are higher than the average regional background noise level. Clacy (1968) and Whiteford (1970) found that large seismic noise amplitudes, in the frequency range of 1-10 Hz, occurred in the vicinity of known geothermal areas in the North Island of New

Delay times between fast and slow shear waves versus event azimuth

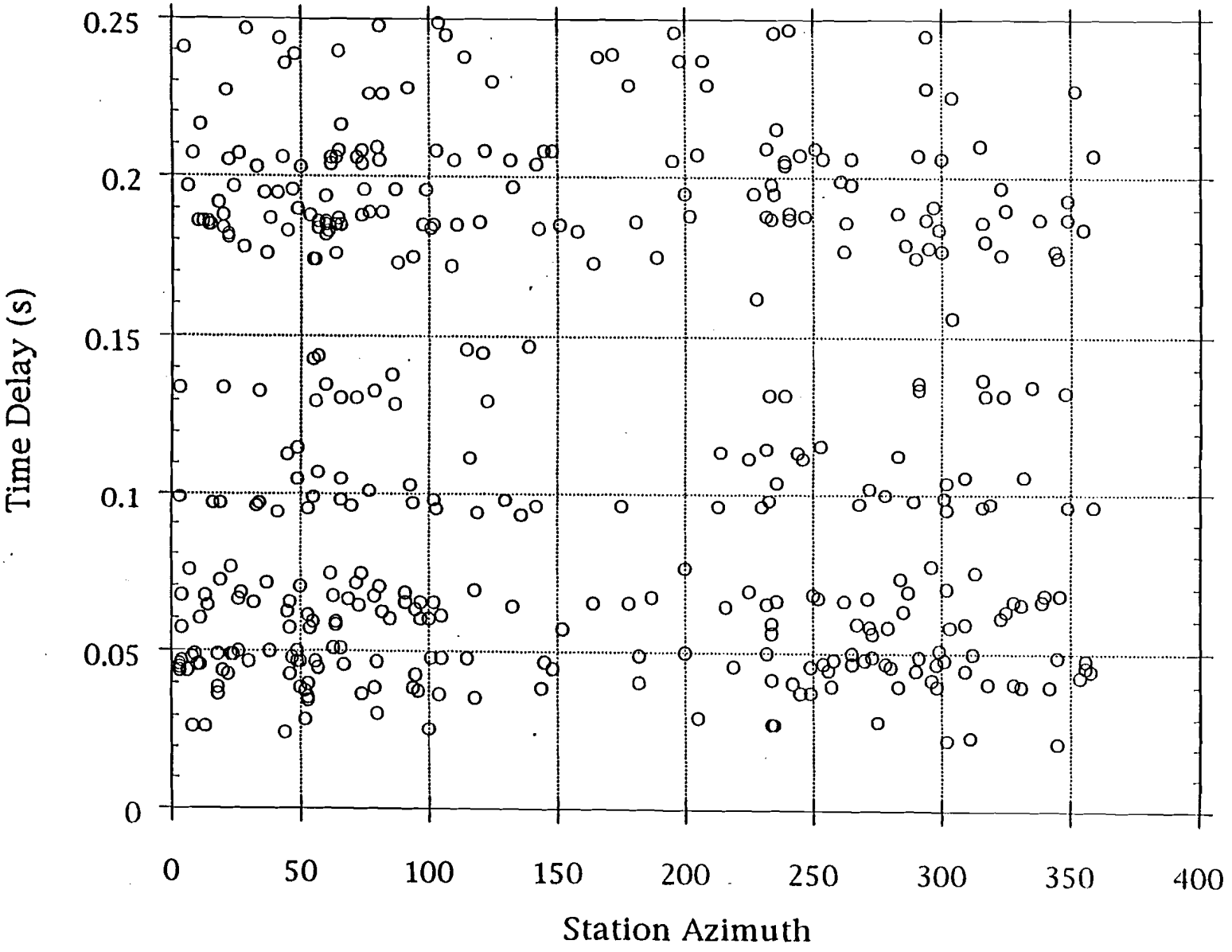

Figure 52.

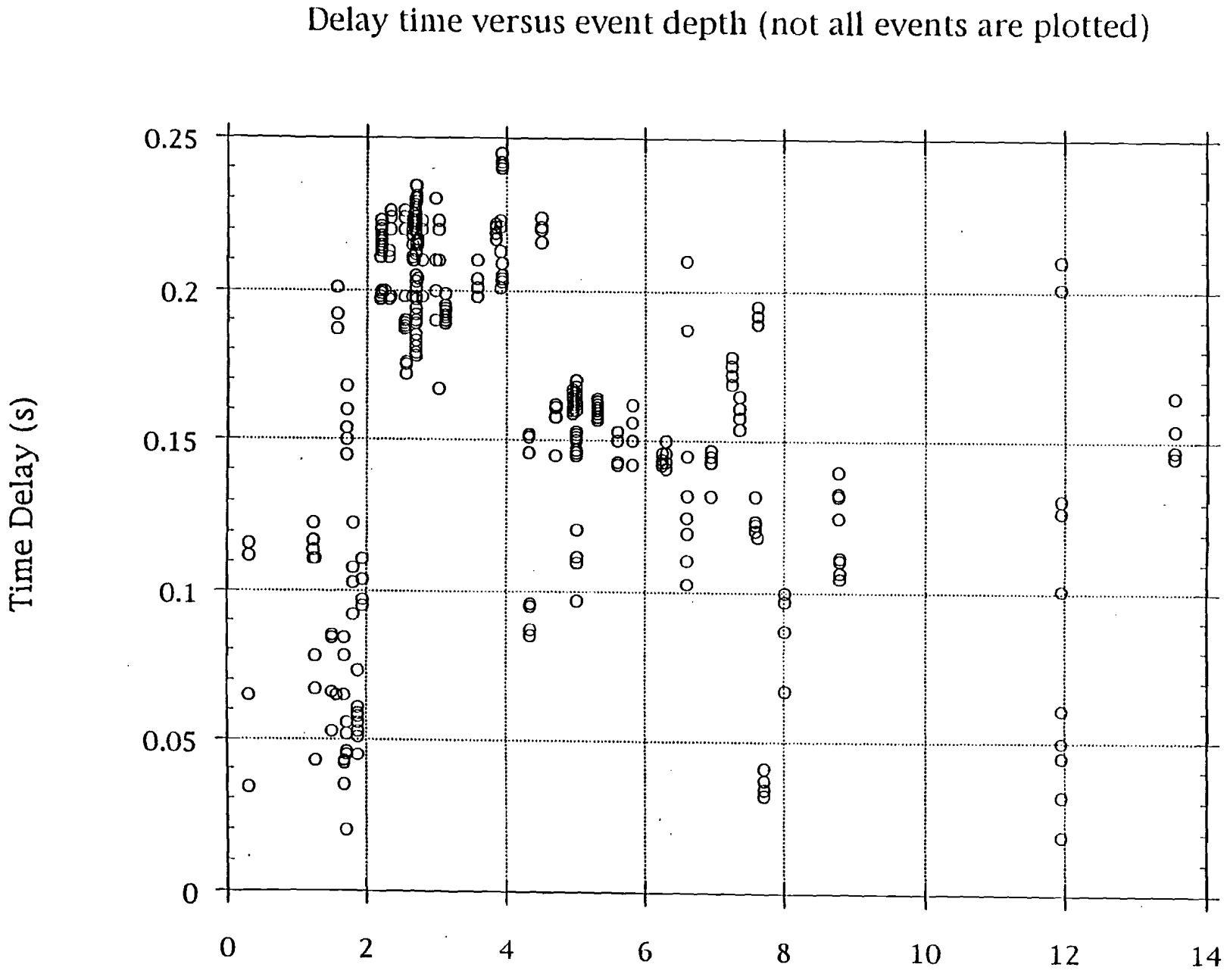
Delay time versus event depth (not all events are plotted)
Time Delay (s)
0.25
0.2
0.15
0.1
0.05
0
0
2
4
6
8
10
12
14
Hypocentral Depth (km)

Figure 53.

Zealand. Goforth et al. (1972) found a noise anomaly that nearly coincided with the pattern of thermal anomaly near the southeastern shore of the Salton Sea in Imperial Valley, California. The seismic energy in the anomalous region was an order of magnitude higher than in the surrounding region and was in the frequency band 1-3 Hz. The dominant frequency range of the noise in geyser basins of Yellowstone National Park is 2-8 Hz (Iyer and Hitchcock, 1974), however, hydrothermal eruptive activity produces only high-frequency noise above 8 Hz. Douze and Sorrells (1972) found high noise levels over the Mesa thermal anomaly in Imperial Valley.

Noise studies in many regions have not been entirely successful as exploration tools because of interference from cultural and meteorological noise, laterally heterogeneous and unquantifiable site amplifications due to local geology, poorly constrained crustal models, and partly because of instrumentation limitations. Geothermal noise is usually not coherent across moderate distances on the order of a few kilometers, prohibiting the location of sources. Further, high-amplitude surface sources (e.g. hot springs) mask weaker signals from deeper sources. Thus, amplitude mapping yields information about only the shallowest noise sources.

In some cases, repeat studies in the same area have produced contradictory results. Take, for example, early studies by Iyer (1975) and Teledyne Geotech (Douze and Sorrells, 1972; Geothermal Staff of Teledyne Geotech, 1972) in the same East Mesa area of Imperial Valley, California, produced conflicting results. Both Teledyne studies revealed that 3-5-Hz noise levels measured within the region of maximum thermal gradients and heat flow were 12-18

dB higher than in surrounding areas. Iyer (1975), however, reported that no noise anomaly could be detected due to a noise field dominated by cultural noise.

The method is actually very straight forward, which is why it survives. It consists of measuring the amplitude power spectrum of the vertical noise in the survey area. The presence of a geothermal resource is indicated by elevated noise levels at fairly low frequencies, 1-10 Hz. Resolving the main problems associated with the method - recognizing and eliminating interfering noise sources and evaluating near-site effects - is not so straight forward. For this study, all sources of interfering noise were identified and characterized by spectral content. Changes in noise level caused by near-site variations in acoustic impedance was not a serious problem because all stations were installed on similar lithology - volcanic rock.

With *a priori* knowledge of the location of this resource, the main purpose of this noise survey was to evaluate the potential for seismic noise measurements as a management/exploration tool in Hawaiian geothermal regions.

7.1. Data Analysis

One-minute digital noise samples were collected twice a day - one during daylight hours and a second during late-night/early morning - over a period of 90 days in order to monitor temporal variations of the regional noise. One of the biggest problems that we encountered was selection of representative noise samples. Noise samples containing small earthquakes recorded on a few of the

stations were eliminated. Periods of high winds, heavy rain, and high surf were avoided. There are many sources of cultural noise in the area; the well traveled roads cutting through the survey area, agricultural activity in the numerous papaya fields, drilling activity and heavy equipment movement at the geothermal development site (PGV) are the most common. Noise from agricultural activity was virtually absent at night, hence the 30 samples selected for study were those obtained between the hours of 7:00 PM and 5:00 AM, local time.

Spectra were calculated for ten-second data segments (100-Hz sample rate); the spectra were then averaged. The same time on the same day was used for all stations. Spectral analysis of the 30 "quietest" noise samples at the various stations revealed the presence of a noise source at approximately 2.5 Hz. A spectral high centered at this frequency can be detected in the spectra of the low-noise stations (o06 and o10, for example) with Type-D spectra (Figure 59; it is not noticeable in spectra of stations within the geothermal region with Type-A spectra (e.g. i01, i02; Figure 54). Noise of this frequency is attributed to wave action along the coast. Some of the noise spectra presented (uncorrected for seismic system response) show a small peak around 1 Hz that may be associated with oceanic microseisms. All of the spectra are contaminated by 60-Hz noise; these are the sharp peaks seen at 0, 20, and 40 Hz. The data are low-pass filtered at 25 Hz, which accounts for the amplitude fall-off observed in the spectra.

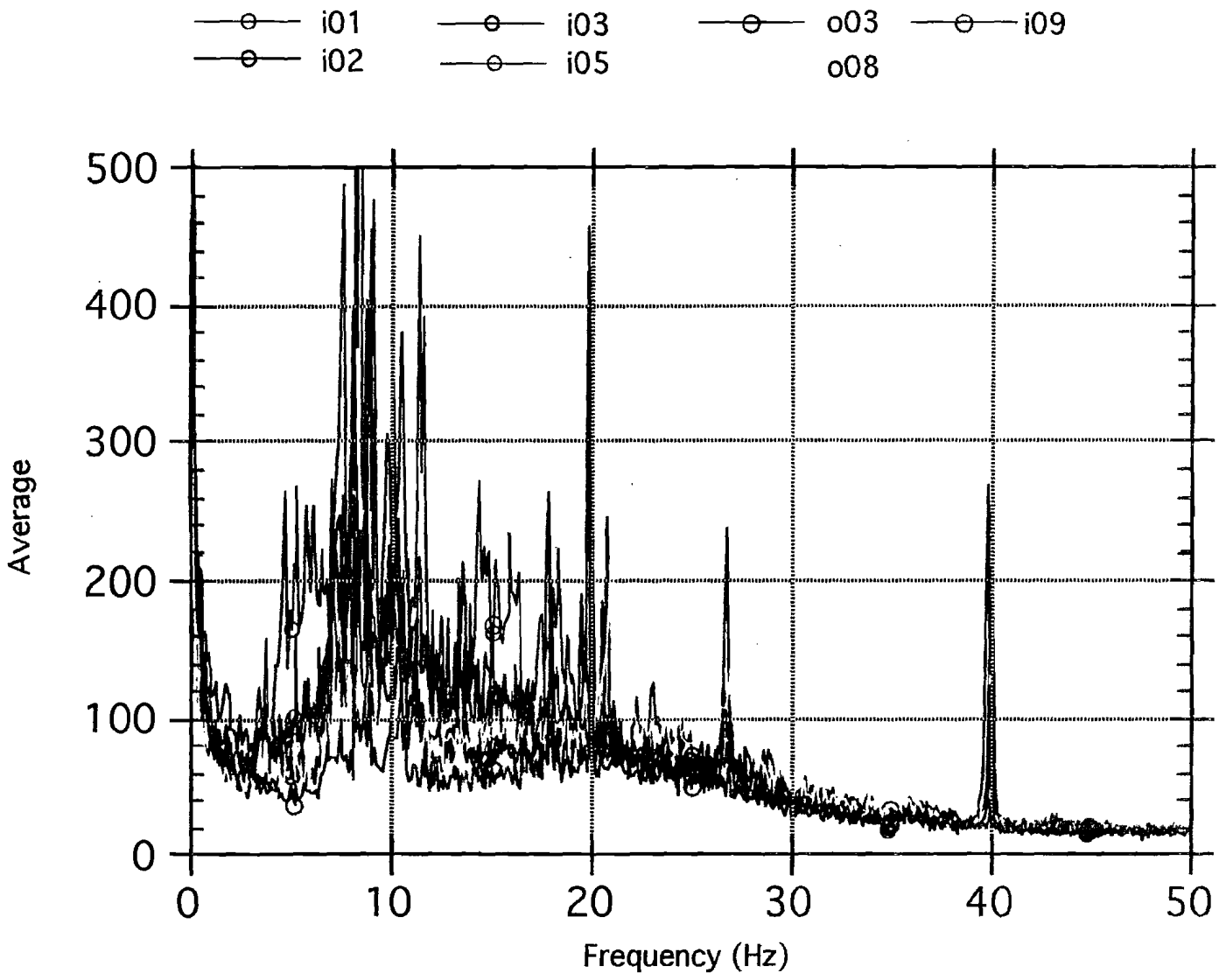

Figure 54. Type-A spectra. Stations are color-coded according to the key above the plot.

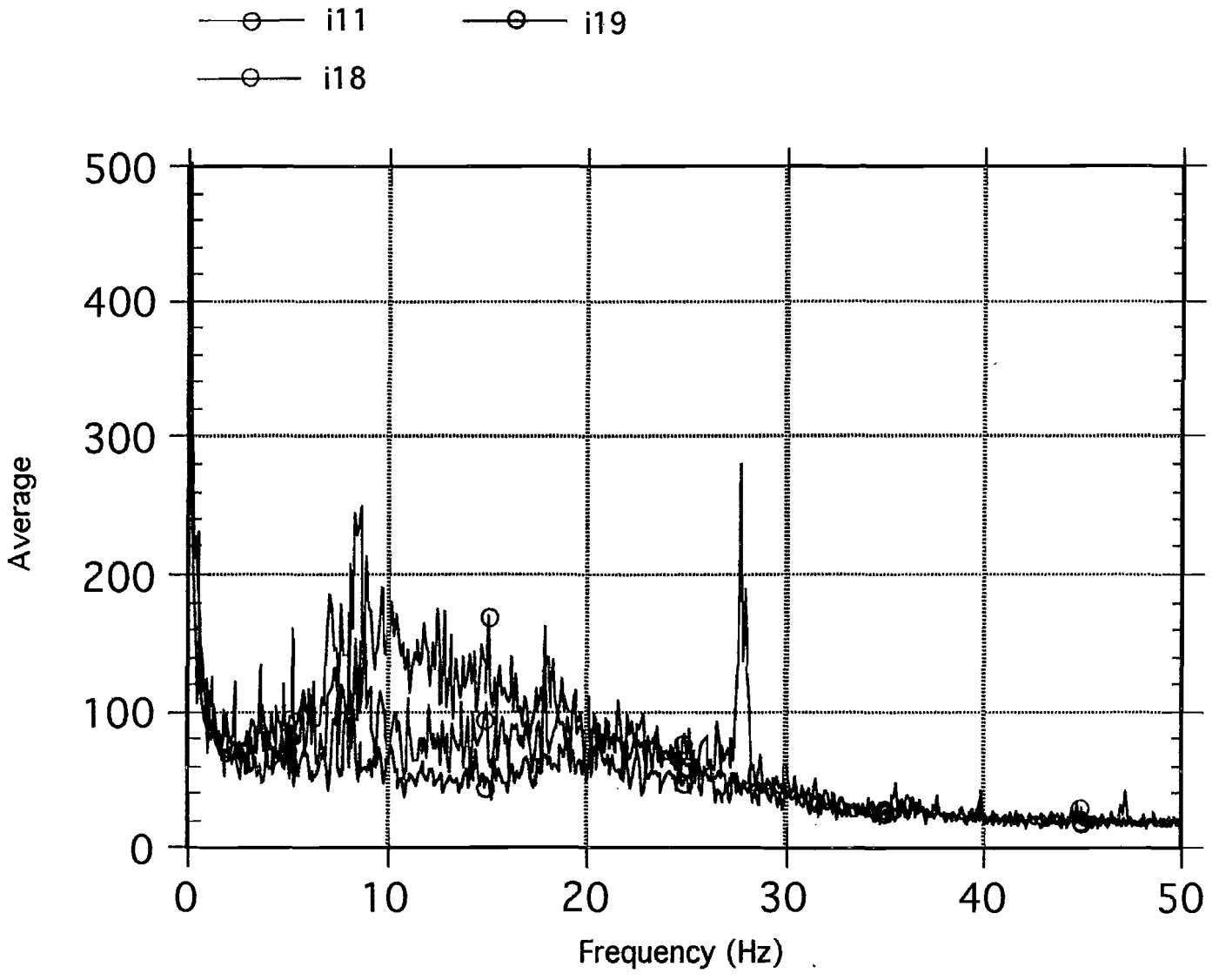

Figure 55. Type-A spectra, continued. Stations are color-coded according to the key above the plot.

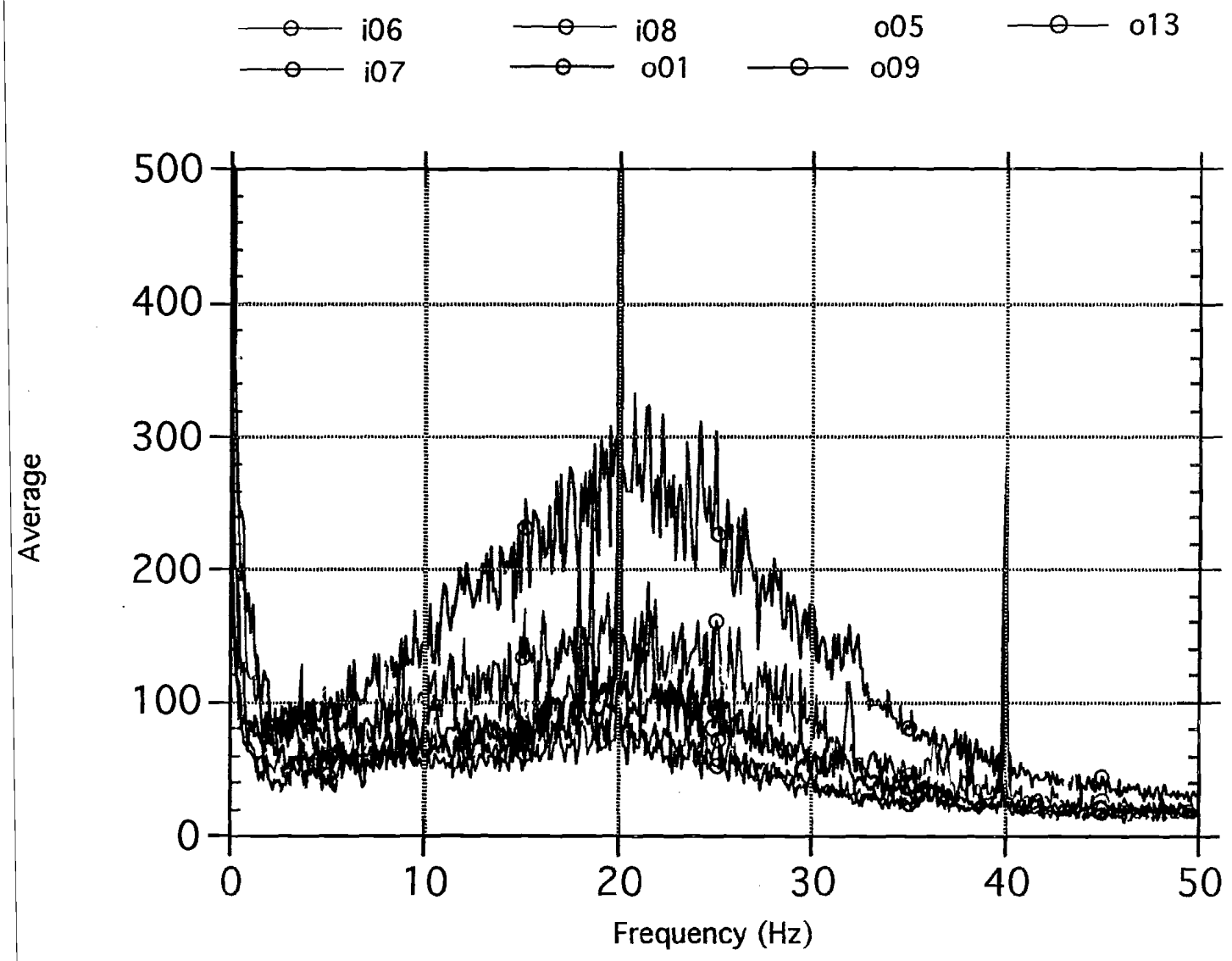

Figure 56. Type-B spectra. Stations are color-coded according to the key above the plot.

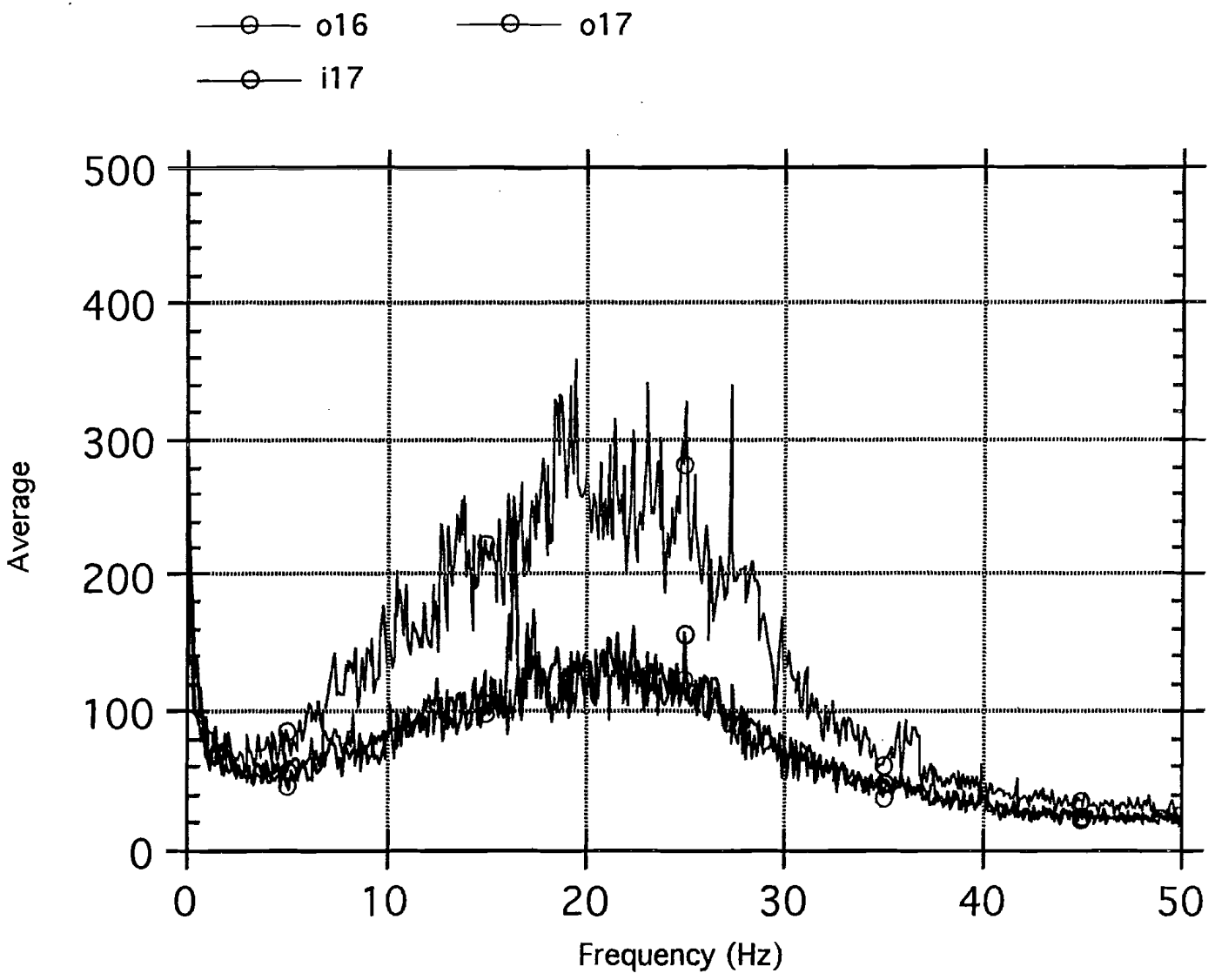

Figure 57. Type-A spectra, continued. Stations are color-coded according to the key above the plot.

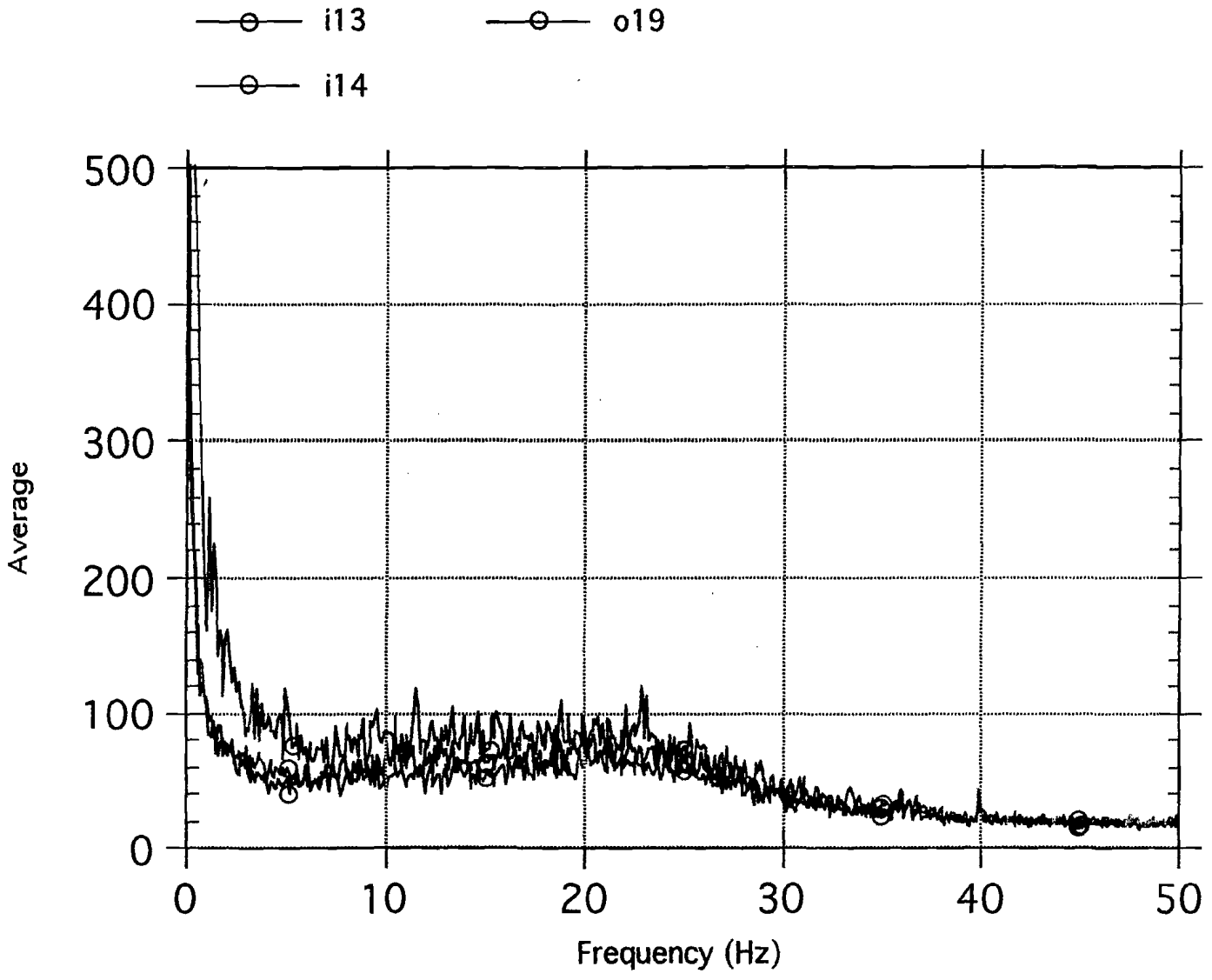

Figure 58. Type-A spectra, continued. Stations are color-coded according to the key above the plot.

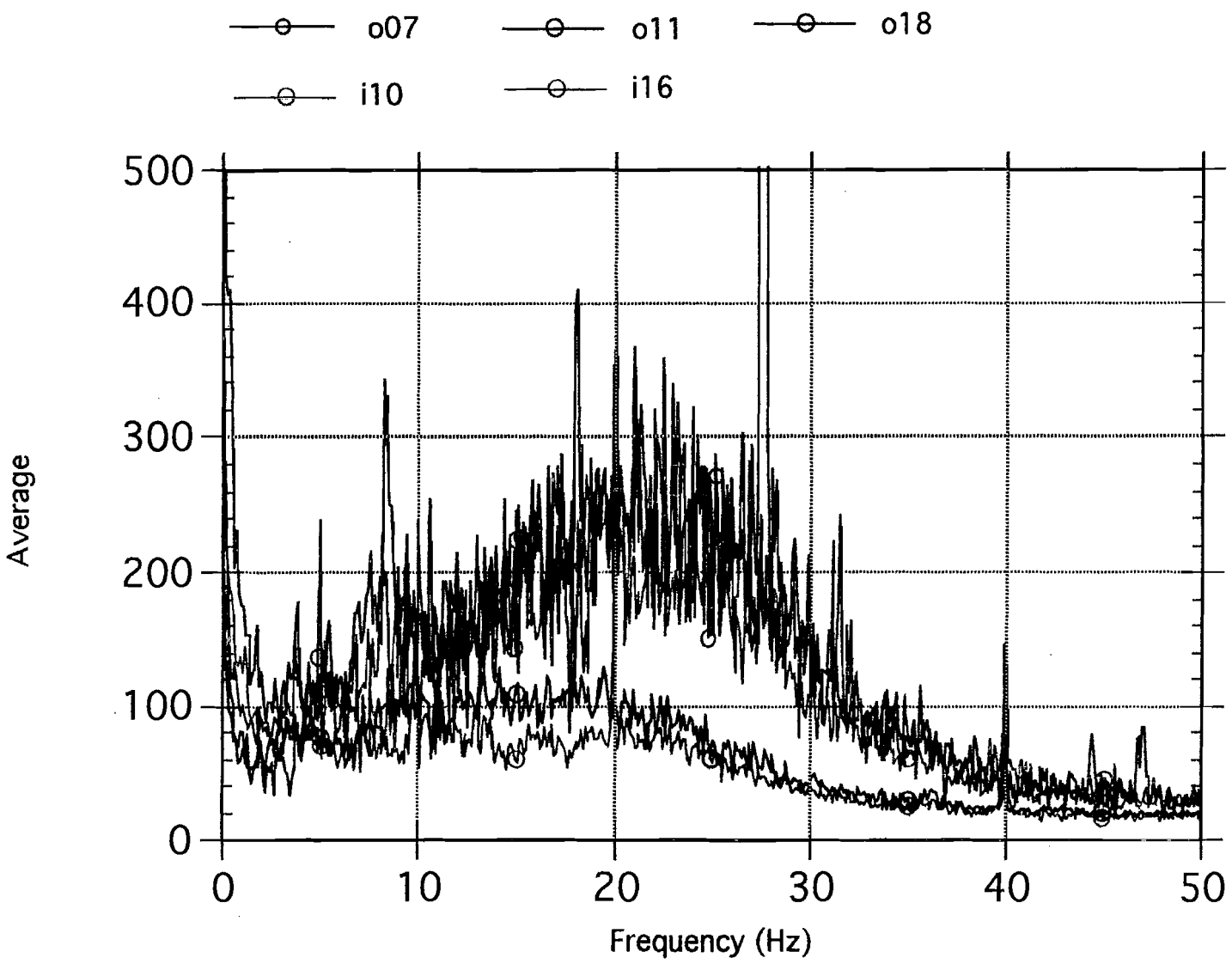

Figure 59. Type-C spectra. Stations are color-coded according to the key above the plot.

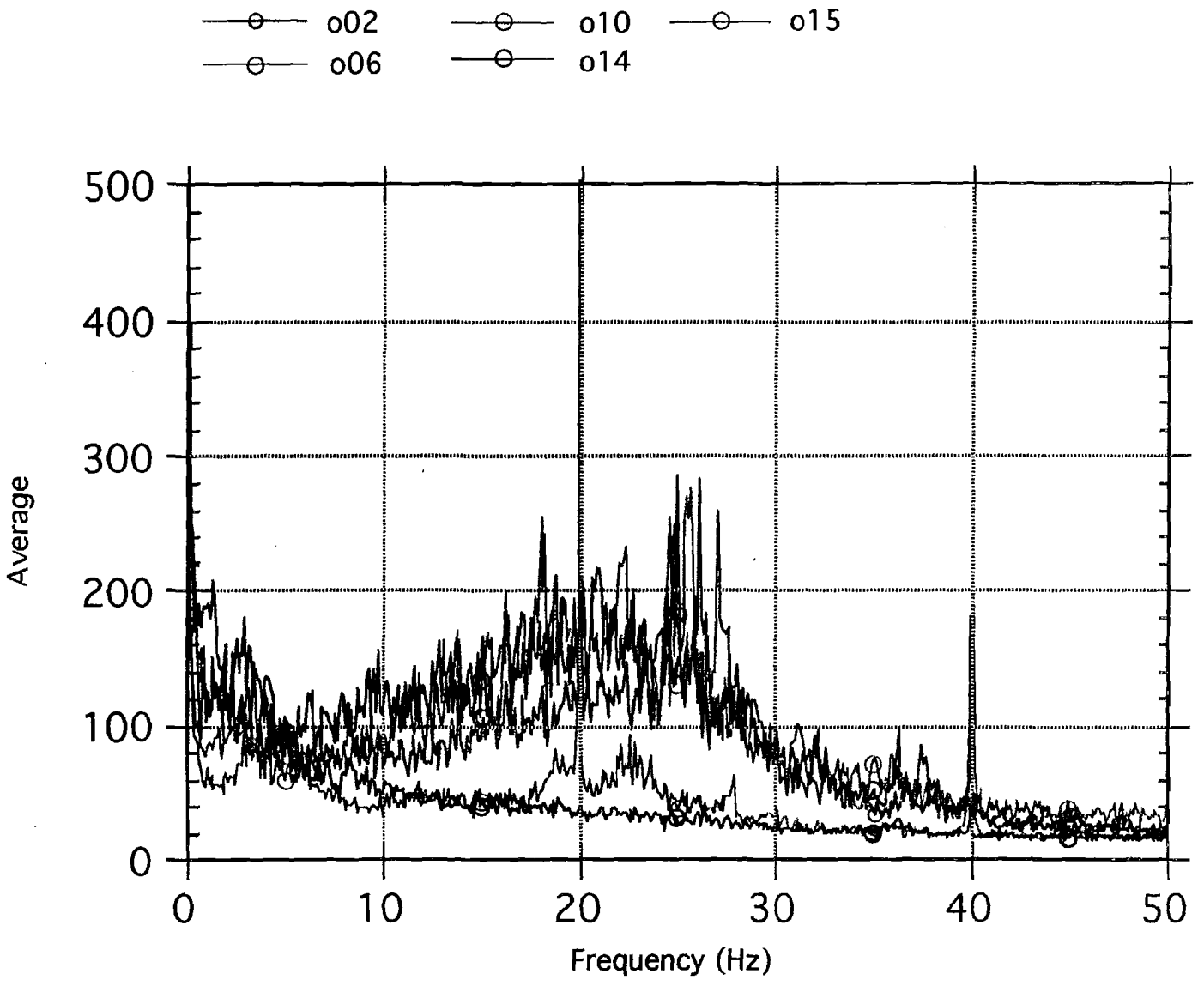

Figure 60. Type-D spectra. Stations are color-coded according to the key above the plot.

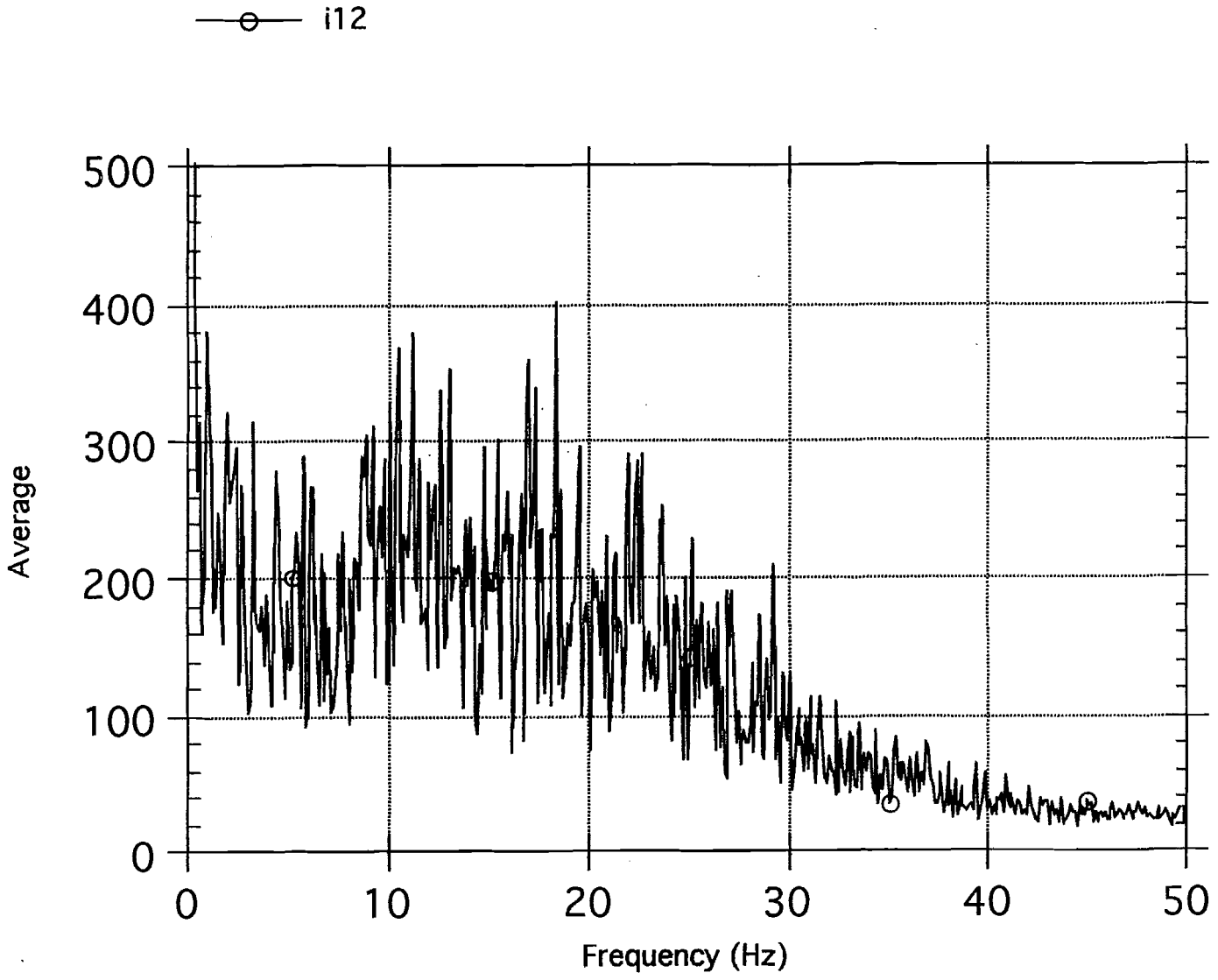

Figure 61. Station i-12 has an anomalous noise character that may be due to radio interference.

7.2 Spatial Variation of Noise

Thirty of the quietest data segments collected during the late night/early morning hours were used for calculating average spectral noise levels. The shape of the spectra changes significantly at the various stations. However, some characteristics allow a grouping into several different types:

Type-A spectrum is dominated by low-frequency high-amplitude noise within a frequency band of 5 to 12 Hz (Figures 54 and 55).

Type-B spectrum (Figures 56-58) shows no dominant peaks at any frequency. Sometimes a peak or peaks are seen between 1 to 3 Hz, associated with oceanic microseisms and wave action.

Type-C spectrum (Figure 59) shows low-amplitude noise within the same frequency band as Type A.

Type-D spectrum (Figure 60) shows very low frequency noise at about 2.5-3 Hz.

The areas with the Type-A spectra are areas located directly above the resource area as defined by the Vp/Vs study. Highest amplitudes are observed at the stations located closest to the production wells - i02, i03, and i05, but this feature can be seen in spectra from stations i01, o01, o03, o05, o07, o08, i09, i11, i12, i18, o18, and i19, as well. The energy decreases almost regularly moving away from KS-8. Stations o07, i18, and o18 are outside of this area, but also displayed Type-A spectra. Spectra from station o01, located approximately 100 m from the steam generators, are dominated by noise at 18-19 Hz. All other stations displayed Type-B, C, or D spectra.

Station i-12 shows high-amplitude noise that may result from radio interference; station o-12 was disabled because of this problem.

Peak frequencies in the 5-12 frequency band are present at most of the stations within a 1-km radius of the production site. Del Pezzo et al. (1975) attributed similar peaks observed at Solfatara, Italy, to agricultural activity, however, no agricultural activity was undertaken as the Puna samples were taken. Peak frequencies much higher than 5 Hz have been found by many authors, particularly near surface activity sources (fumaroles, geysers; Cappello et al, 1974). Three-Hz peak frequencies have also been reported in geothermal areas (Douze and Sorrells, 1972; Whiteford, 1970; Clacy, 1968). They appear related to the large size and relatively deep location of the fluid reservoir (the larger and deeper the reservoir, the lower the observed frequency; Douze and Sorrells, 1972). The dominant frequency range of the noise observed in geyser basins at Yellowstone National Park (Iyer and Hitchcock, 1974) is 3-8 Hz, very similar to that observed in Puna.

8. DISCUSSION

Correlations between shallow seismicity and surface structure for the PANDA earthquake data set and previous studies (Suyenaga and Furumoto, 1978; Koyanagi et al., 1981) imply that current seismicity may be related to shallow crustal thermal anomalies created by near-surface magmatic intrusions into the LERZ. Self-potential and resistivity anomalies (Kauahikaua, 1993) correlate well with the seismicity within the array boundaries, supporting the

notion of a localized hot-water upwelling or heat source (Kauahikaua, 1993). The sparse PANDA station distribution near the Opihikao anomaly (Figures 2 and 12) is the probable cause of a lack of seismicity in that area. Since HVO stations are absent, a further deployment would be required for confirmation of a similar geothermal system near that anomaly. The region of low Vp/Vs at Puna also correlates well with the self-potential and resistivity highs previously used to identify the lateral extent of the reservoir (Keller et al., 1977; Kauahikaua, 1993).

Vp/Vs is an important value because it can lead to insights into the mechanical properties of crustal materials (Thurber, 1993). Geothermal reservoirs with temperatures and pressures high enough to sustain steam-dominated systems are associated (usually) with low Vp/Vs values. This occurs because P-wave velocities are substantially slowed by the presence of steam-filled cracks while shear velocities remain less affected (Walck, 1988). In contrast, partially molten bodies exhibit high Vp/Vs values (Walck, 1988). The physical properties most affecting the Vp/Vs ratio are the sizes, aspect ratios, and distributions of cracks and pores (Tatham, 1982).

In a study similar to this one, O'Connell (1986) found that the geothermal reservoir at The Geysers, California, is associated with a Vp/Vs low. In this case as at Puna, high Vp/Vs values characterized the area directly above the main production zone. He speculated that high Vp/Vs was associated with condensation zones resulting from vapor upflow from the main reservoir. Vp/Vs values surrounding geothermal reservoirs generally decrease with depth. Nicholson and Simpson (1985) attributed this characteristic to saturated microcrack

closures due to higher confining pressures. Although the geology and tectonics of the Puna geothermal system are very different from those of Yellowstone or The Geysers, for example, fluid movement within existing fault systems and continued fracturing are reservoir characteristics common to all. It is not unreasonable, therefore, to assume that the comparably low Vp/Vs ratios calculated for the Puna geothermal system have a similar origin.

9. Conclusions

9.1 The background seismicity rate for the Puna geothermal region is about 8 earthquakes per day, consistent with seismicity levels at The Geysers and Yellowstone. Magnitudes vary from -1.0 to 2.0; earthquakes with magnitudes greater than 2.0 occur at an historical rate of 4-10 per year (averaged over 1987-1992). That rate is by no means constant; earthquakes typically occur as multiplets, i.e. 2-10 small-magnitude earthquakes with similar wave forms within a period of 2-20 minutes, and as swarms lasting for several hours.

9.2 No significant change in the background seismicity rate was observed during the 5 days after KS-9/10 was brought to full production levels. (A single seismometer left running at the Puna Research Center from August 1994 to June 1995 also detected no significant change in background seismicity.)

9.3 A b-value of 0.96, similar to that for Kilauea and Moana Loa, indicates that strain accumulation and stress release in the Puna region is primarily tectonic in origin.

9.4 Inversion of P- and S-wave arrival times for Vp/Vs structure resulted in a model that correlates very well with existing drilling data, surface geology, previous seismic surveys, and surface electrical studies for the geothermal area. By arbitrarily defining the boundary of the geothermal reservoir to be below background Vp/Vs, and estimate of 5 km is obtained for the geothermal source region.

9.5. Focal mechanisms show normal faulting in a direction roughly perpendicular to the rift zone within the structural boundaries of the rift. Normal faulting oriented at an oblique angle to the rift zone is seen on the south flank, along with some thrust faulting. Strike-slip faulting occurs along the LERZ and to the northwest. The pattern suggests that seismic slip occurs in two directions - along faults parallel to and including the LERZ and along a system of faults oblique to the rift. Strike-slip faulting is associated with the apparent offset in the LERZ, indicating that this is a tectonic feature and the area is subject to ongoing deformation probably caused by differential motion of segments of the LERZ.

9.6. A rift-parallel fast polarization direction prevails at 23 stations. Slight variations near the rift offset indicate that the near-surface contribution to splitting apparently does not predominate over

pervasive anisotropy. The overall polarization direction of the fast shear wave is consistent with independent information on stress orientation, supporting the contention that stress-aligned cracks are responsible for the shear-wave splitting.

A weak correlation between individual lag times and event depth was found. Keeping in mind that the number of earthquakes originating below 3.0 km is comparatively small, larger lag times are observed for earthquakes in the depth interval from 2.0 to 3.0 km.

9.7. Spectral analysis of noise samples may be used to estimate resource extent in Puna. The amplitude within a characteristic band of frequencies, here 5-9 Hz decreases systematically away from the area currently under develoment. Observed spectral amplitudes and frequencies of noise in Puna are similar to those observed at other geothermal fields.

10. REFERENCES

Anonymous, 1975. U.S.G.S. Topographic Map, NE 5-5, Series W532.

Bisztricsany, E., 1958. A new method for the determination of magnitudes of earthquakes. Geofiz. Kozl., 7:69-96.

Booth, D., Schleper, S., Crampin, S., Ochman, N., and Wholenberg, J., 1989. Shear-wave splitting observations in Milos, Greece. Geothermics, 18:597-610.

Broyles, M., Suyenaga, W., and Furumoto, A., 1979. Structure of the Lower East Rift Zone of Kilauea Volcano, Hawaii, from seismic and gravity data. J. Volcanol. Geotherm. Res., 5:317-336.

Brune, J., and Allen, C.R., 1967. A micro-earthquake survey of the San Andreas Fault system in Southern California. Bull. Seis. Soc. Am., 57:277-296.

Cappello, P., Lo Bascio, A., and Luongo, G., 1974. Seismic noise survey a Solfatara Crater, Phlegraean Fields, Italy. Geothermics, 3:76-80.

Chiu, J-M., Steiner, G., Smalley, R., and Johnston, A., 1991. PANDA: A simple, portable seismic array for local-to-regional-scale experiments. Bull. Seis. Soc. Am., 81:1000-1014.

Combs, J., and Hadley, D., 1977. Microearthquake investigation of the Mesa geothermal anomaly, Imperial Valley, California. Geophysics, 42:17-33.

Combs, J., and Rotstein, Y., 1976. Microearthquake studies at the Coso geothermal area, China Lake, California. Proc. 2nd U.N. Sympos., Develop. use of geothermal res., 2:909-916.

Crampin, S., 1985. Evaluation of anisotropy by shear-wave splitting. Geophysics, 50:142-154.

Crampin, S., and Booth, D., 1989. Shear-wave splitting showing hydraulic fractures dilating pre-existing joints. Scientific Drilling.

Crosson, T., and Koyanagi, R., 1979. Seismic velocity structure below the Islands of Hawaii from local earthquake data. J. Geophys. Res., 84:2331-2343.

Del Pezzo, E., Guerra, I., Luongo, G., and Scarpa, R., 1975. Seismic noise measurements in the Mt. Armiata Geothermal Area, Italy. Geothermics, 4:40-43.

Douze, E.J., and Sorrells, G., 1972. Geothermal ground-noise surveys. Geophysics, 37:813-824.

Dustman, M., Cooper, P., and Chiu, J-M., 1993. Microseismicity and crustal structure in the Lower East Rift Zone of Kilauea Volcano, Hawaii using the PANDA array. EOS, Trans. Am. Geophys. Union, 74:648.

Eaton, J., 1962. Crustal structure and volcanism in Hawaii, crust of the Pacific Basin. Geophys. Monogr., 6:13-29.

Eberhart-Philips, D., 1990. Three-dimensional P and S velocity structure in the Coalinga region, California. J. Geophys. Res., 95:15343-15363.

Evans, D., 1966. Man-made earthquakes in Denver. Geotimes, 10:11-18.

Evans, R., Eberhart-Philips, D., and Thurber, C., 1993. User's manual for SIMULPS12 ofr imaging Vp and Vp/Vs: A derivative of the Thurber tomographic inversion SIMUL3 for local earthquakes and explosions. U.S.G.S. Open File Report, 93.

Facca, G., and Tonani, F., 1964. Theory and technology of a geothermal field. Bull Volcanol., 27:143-189.

Fitch, T. and Rynn, 1976. Inversion of Vp/Vs in shallow source regions. Geophys. J. R. Astron. Soc., 44:253-267.

Fletcher, J., and Sykes, L., 1977. Earthquakes related to hydraulic mining and natural seismic activity in Western New York. EOS, Trans. Am. Geophys. Union, 57:289.

Furumoto, A., 1978. Thermal processes of Kilauea East Rift inferred from seismic data. Geothermal Resource Exploration in Hawaii, HIG-78-8, 5:123-136.

Geothermal Staff of Teledyne Geotech, 1972. Geothermal noise survey of the East Mesa area, Imperial Valley, California: Teledyne Tech. Rept. no. 72-19.

Goforth, T.T., Douze, E.J., and Sorrells, G., 1972. Seismic noise measurements in a geothermal area. Geophys. Prosp., 20:76-82.

Gupta, H.K., and Rastogi, B.K., 1976. Dams and Earthquakes, Elsevier Scientific Publishing Co., Amsterdam, 229p.

Gupta, H.K., Rastogi, B.K., and Narain, H., 1972. Common features of the reservoir-associated seismic activity. Bull. Seis. Soc. Am., 62:481-492.

Gutenberg, B., and Richter, C., 1954. Frequency of earthquakes in California. Bull. Seis. Soc. Am., 34:185-188.

Hamilton, R.M., and Muffler, L.J.P., 1972. Microearthquakes at the Geysers geothermal area, California. J. Geophys. Res., 77:2081-2086.

Healy, J.H., Rubey, W.W., Griggs, D.T., and Raleigh, C.B., 1968. The Denver earthquakes. Science, 161:1301-1310.

Hubbert, M.K., and Rubey, W.W., 1959. Role of fluid pressure in mechanics of overthrust faulting, 1. Mechanics of fluid-filled porous solids and its application to overthrust faulting. Bull. Geol. Soc. Am., 70:115-166.

Ingebritsen, S., and Scholl, M., 1993. The hydrology of Kilauea Volcano. Geothermics, 22:255-270.

Iyer, H.M., 1975. Search for geothermal seismic noise in the East Mesa area, Imperial Valley, California. Geophysics, 40:1066-1072.

Iyer, H.M., and Hitchcock, T., 1974. Seismic noise measurements in Yellowstone National Park. Geophysics, 39:389-400.

Kaneshima, S., Ito, H., and Sugihara, M., 1988. Shear-wave splitting observed above small earthquakes in a geothermal area of Japan. Geophys. J. R. Astron. Soc., 94:399-411.

Kauahikaua, J., 1993. Geophysical characteristics of the hydrothermal systems of Kilauea Volcano, Hawaii. Geothermics, 22:271-299.

Keller, G., Slokan, C., Slokan, J., Daniels, J., Kauahikaua, J., Klein, D., and Zablocki, C., 1977. Geoelectric studies on the East Rift, Kilauea Volcano, Hawaii Island. Geothermal Resource Exploration in Hawaii, HIG-78-8, 3, 161 pp.

Klein, F., 1991. Hypocenter location program HYPOINVERSE part 1: Users guide to versions 1, 2, 3, and 4. U.S.G.S. Open File Report 78-694.

Klein, F., 1994. Seismic Hazards at Kilauea and Mauna Loa Volcanoes, Hawaii. U.S.G.S. Open File Report, 94-216, in press.

Koyanagi, R., Nakata, J., and Tanigawa, W., 1981. Seismicity of the Lower East Rift Zone of Kilauea Volcano, Hawaii, 1960-1980. U.S.G.S. Open File Report, 81-984.

Lange, A.L., and Westphal, W.H., 1969. Microearthquakes near the Geysers, Sonoma County, California. J. Geophys. Res., 74:4377-4378.

Lee, W., and Lahr, J., 1972. HYPO71: A computer program for determining hypocenter, magnitude, and first motion pattern of local earthquakes. U.S.G.S. Open File Report, 75-311.

Lee, W., Bennet, R., and Meagher, K., 1972. A method for estimating magnitudes of local earthquakes from signal duration. U.S.G.S. Open File Report, 28 pp.

Lienert, B., Berg, E., and Frazer, L., 1986. HYPOCENTER: An earthquake location method using centered, scaled, and adaptively damped least squares. Bull Seis. Soc. Am., 76:771-783.

Lovenitti, J., and D'Olier, W., 1990. Shallow groundwater mapping in the Lower East Rift Zone, Kilauea Volcano. Geotherm. Resources Counc. Trans., 14:853-868.

Lund, J., 1986. The Puna Research Center. Geothermics, 15:423-424.

Macdonald, G., Abbott, A., and Cox, D., 1983. Volcanoes in the Sea, University of Hawaii Press, Honolulu, Hawaii, 517 pp.

Majer, E., and McEvilly, T., 1979. Seismological investigations at The Geysers Geothermal Field. Geophysics, 44:246-269.

Mattice, W., and Furumoto, A., 1978. Microearthquake study of the Opihikao anomaly, Puna, Hawaii. Geothermal Resource Exploration in Hawaii, HIG-78-8, 5:41-56.

Nicholson, and Simpson, 1985. Changes in Vp/Vs with depth: Implications for appropriate velocity models, improved earthquake locations, and material properties of the upper crust. Bull. Seis. Soc. Am., 75:1105-1123.

Nuttli, O., 1961. The effect of the Earth's surface on the s-wave particle motion. Bull. Seis. Soc. Am., 51:1429-1440.

O'Connell, D., 1986. Seismic Velocity Structure and Microearthquake Source Characteristics at The Geysers, California, Geothermal Area, Ph.D. Dissertation, Lawrence Berkeley Laboratory, Earth Sciences Division, 204 pp.

Ohtake, M., 1974. Change in Vp/Vs ratio related with occurrence of some shallow earthquakes in Japan. J. Phys. Earth, 21:173-184.

Raleigh, C.B., Healy, J.H., and Bredehoeft, J.D., 1972. Faulting and crustal stress at Rangely, Colorado. In, Heard, H.C., Borg, I.Y., Carter, N.L., and Raleigh, C.B. (Eds.), Flow and fracture of rocks, Geophys. Monogr. Ser., 16:275-284, Am. Geophys. Union, Washington, D.C.

Roberts, G., and Crampin, S., 1985. Shear-wave polarizations in a hot-dry-rock reservoir: anisotropic effects of aligned cracks. Int. J. Rock Mech. Min. Sci., 23:291-302.

Sachpazi, M., and Hirn, A., 1991. Shear-wave anisotropy across the geothermal field of Milos, Aegean volcanic arc. Geophys. J. Int., 107:673-685.

Sato, M., Matsumoto, N., and Niitsuma, H., 1991. Evaluation of geothermal reservoir cracks by shear-wave splitting of acoustic emission. Geothermics, 20:197-206.

Scholz, C., 1968. The frequency-magnitude relation of micro-fracturing in rock and its relation to earthquakes. Bull. Seis. Soc. Am., 58:399-415.

Shih, X., Meyer, R., and Schneider, J., 1989. An automated, analytical method to determine shear-wave splitting. Tectonophysics, 165:271-278.

Simpson, D.,1986. Triggered earthquakes. Ann. Rev. Earth Planet. Sci., 14:21-42.

Steiner, G., 1986. Site Installation and Initial Check. Unpublished Manual, Memphis State University.

Suyenaga, W., and Furumoto, A., 1978. Microearthquake study of the East Rift Zone of Kilauea, Puna, Hawaii. Geothermal Resource Exploration in Hawaii. HIG-78-8, 5:1-36.

Syles, L.R., Fletcher, P.J., Armbruster, J., and Davis, J.F., 1972. Tectonic strain release and fluid injection at Dale, N.Y. EOS, Trans. Am. Geophys. Union, 53:524.

Tatham, R., 1982. Vp/Vs and lithology. Geophysics, 47:336-344.

Teng, T., Real, C., and Henyey, T., 1973. Microearthquakes and water flooding in Los Angeles. Bull. Seis. Soc. Am., 63:859-875.

Thomas, D., 1986. Geothermal resources assessment in Hawaii. Geothermics, 14:435-514.

Thurber, C., 1983. Earthquake locations and three-dimensional crustal structure in the Coyote Lake area, Central California. J. Geophys. Res., 88:8826-8236.

Thurber, C., 1993. Local earthquake tomography: velocities and Vp/Vs -- Theory. In Iyer, H., and Hirahira, K., (Eds.) Seismic Tomography: Theory and Practice, Chapman and Hall, London, p. 563-583.

Thurber, C., 1984. SIMUL3. In Engdahl, E., (Ed.), Documentation of Earthquake Algorithms, Report SE-35, World Data Center A for Solid Earth Geophysics, Boulder, Colorado, p. 15-17.

Thurber, C., Atre, S., and Eberhart-Philips, D., 1991. Vp/Vs variations along the Loma Prieta Rupture Zone. In U.S.G.S. Redbook Conference on the Seismotectonic Significance of the Loma Prieta Earthquake, Asilomar, California, 12-15 May, 1991.

Tomori, A., Nakata, J., Okubo, P., Tanigawa, W., and Tokuuke, J., 1991. Hawaiian Volcano Observatory Summary 90, Part I: Seismic data, January to December 1990. U.S.G.S. Open File Report 91-578, 79 pp.

Tryggvason, E., 1970. Surface deformation and fault displacement associated with an earthquake swarm in Iceland. J. Geophys. Res., 75:4407-4422.

Walck, M., 1988. Three-dimensional Vp/Vs variations for the Coso Region, California. J. Geophys. Res., 93:2047-2052.

Ward, P.L., 1972. Microearthquakes: Prospecting tool and possible hazard in the development of geothermal resources. Geothermics, 1:3-12.

Ward, P.L., and Björnsson,S., 1971. Microearthquakes, swarms, and the geothermal areas of Iceland. J. Geophys. Res., 76:3953-3982.

Ward, P.L., and Jacob, K.H., 1971. Microearthquakes in the Ahuachapan geothermal field, El Salvador, Central America. Science, 173:328-330.

Ward, P.L., Palmáson, G., and Drake, C., 1969. Microearthquake survey and the Mid-Atlantic Ridge in Iceland. J. Geophys. Res., 74:664-684.

Wessel, P., and Smith, W., 1992. The GMT System, v. 2.1, Technical Reference and Cookbook, SOEST/SIO.

Zablocki, C., 1977. Self-potential studies in east Puna, Hawaii. Geothermal Resource Exploration in Hawaii, HIG-77-15, 3:172-198.

Zucca, J., and Hill., D., 1980. Crustal structure of the southeast flank of Kilauea Volcano, Hawaii, from seismic refraction experiments. Bull. Seis. Soc. Am., 70:1149-1159.

APPENDIX I: Listing of Stations and Station Information.

Station: I-01, hgpa

Date Installed: 01/28/93 Date Removed: 05/01/93

Instrumentation: hi/lo:L22/L28

Gains (dB): hi 72 (01/28/93-02/04/93), 54 (02/04/93-03/19/93),

30 (03/19/93-05/01/93)

lo 30 (01/28/93-02/04/93), 12 (02/04/93-05/01/93)

Coordinates, Elevation: 19° 28.533' N 154° 53.730'W, 185 m

Location/Driving Directions: None required; located in left rear of fenced area surrounding Puna Research Center.

Owner/Contact Person: NELHA/Tom Daniels (329-7341).

Site Characteristics: Instrument buried in cinders.

APPENDIX I: Listing of Stations and Station Information, continued.

Station: O-01, pgva

Date Installed: 01/28/93 Date Removed: 05/01/93

Instrumentation: hi/lo: L28/L28

Gains (dB): hi 72 (01/28/93-02/13/93), 60 (02/13/93-05/01/93)

lo 30 (01/28/93-02/13/93), 18 (02/13/93-05/01/93)

Coordinates, Elevation: 19° 28.905' N 154° 53.413'W, 217 m

Location/Driving Directions: Enter PGV premises through guarded gate. Take first left onto dirt road just past guard shack. Go past station O-03, through papaya field; road turns right twice. Go along the PGV side of Pu'u Honualua. Site is located on a bluff overlooking the PGV work yard, approximately 500 m from PGV generators.

Owner/Contact Person: PGV/Pete Hansen (961-2184).

Site Characteristics: Instrument buried in soil. Located on the cinder cone Pu'u Honualua.

APPENDIX I: Listing of Stations and Station Information, continued.

Station: I-02, pgvb

Date Installed: 02/01/93 Date Removed: 05/01/93

Instrumentation: hi/hi: L28/L22

Gains (dB): hi 66 (02/01/93-02/11/93), 54 (02/11/93-05/01/93)

hi 66 (02/01/93-02/11/93), 54 (02/11/93-05/01/93)

Coordinates, Elevation: 19° 28.750'N 154° 53.755'W, 197 m

Location/Driving Directions: Park at green gate just prior to entry to Puna Research Center off of route 137. Walk into station located 240 yards from drill rig.

Owner/Contact Person: PGV/Pete Hansen (961-2184).

Site Characteristics: Instrument buried in cinders. Two sets of components separated by distance of 50 m in N-S direction.

APPENDIX I: Listing of Stations and Station Information, continued.

Station: O-02, halh

Date Installed: 02/01/93 Date Removed: 05/01/93

Instrumentation: hi/lo: L28/L28
Gains (dB): hi 72 (02/01/93-05/01/93)
lo 30 (02/01/93-05/01/93)

Coordinates, Elevation: 19° 30.009'N 154° 53.717'W, 217 m

Location/Driving Directions: Station located in papaya field off of route 137. Go past the intersection of Rtes. 137 and 132; stay on 132 to just past the 4-mile marker. Turn left to enter via the gate to JC Farm, stay on dirt road, turn right then left (no other options) travel 8 field divisions along this section, then turn left; travel 4 field divisions along the field divider, then turn left. Work shack should be on your right. Take the first right; station is about 165 feet into the field along a row of dead and dying papaya trees.

Owner/Contact Person: Yamanaka Enterprises/Vern Yamanaka (935-9766).

Site Characteristics: Instruments buried in broken pahoehoe lava.

Comments: Location as given above is unreliable; data from this station were not used for locations.

APPENDIX I: Listing of Stations and Station Information, continued.

Station: I-03, pgvc

Date Installed: 01/28/93 Date Removed: 05/01/93

Instrumentation: hi/lo: L28/L28

Gains (dB): hi 72 (01/28/93-02/11/93), 60 (02/11/93-05/01/93)

lo 30 (01/28/93-02/11/93), 18 (02/11/93-05/01/93)

Coordinates, Elevation: 19° 28.948'N 154° 53.693'W, 189 m

Location/Driving Directions: Drive in main gate of PGV, past guard shack; take first right onto overgrown dirt road (road azimuth about 21°); station is 825 feet down the road, on the left side of the road across from telephone pole #6.

Owner/Contact Person: PGV/Pete Hansen (961-2184).

Site Characteristics: Instruments buried in soil and pahoehoe lava fragments. Location is on edge of a grass field near trees and other vegetation.

APPENDIX I: Listing of Stations and Station Information, continued.

Station: O-03, pgvd

Date Installed: 01/28/93 Date Removed: 05/01/93

Instrumentation: hi/hi: L28/L22

Gains (dB): hi 72 (01/28/93-02/11/93), 66 (02/11/93-05/01/93)

hi 72 (01/28/93-02/11/93), 66 (02/11/93-05/01/93)

Coordinates, Elevation: 19° 29.185'N 154° 53.515'W, 183 m

Location/Driving Directions: Drive through the main gate of PGV, turn left just past the guard shack; take the left fork and stay close to the trees. Station is on the right in the papaya field.

Owner/Contact Person: PGV/Pete Hansen (961-2184).

Site Characteristics: Instruments buried in soil and pahoehoe lava fragments. Location is on edge of papaya field near trees.

APPENDIX I: Listing of Stations and Station Information, continued.

Station: I-05, micr

Date Installed: 01/29/93 Date Removed: 04/17/93

Instrumentation: hi/lo: L28/L22

Gains (dB): hi 72 (01/29/93-02/13/93), 66 (02/13/93-04/17/93)

lo 60 (01/29/93-02/13/93), 54 (02/13/93-04/17/93)

Coordinates, Elevation: 19° 29.120'N 154° 53.063'W, 204 m

Location/Driving Directions: From HGP-A, turn right onto Rte. 137, at intersection turn right onto Rte. 132. From 132, take the 5th right turn after the PGV entrance, follow the telephone poles uphill to the cellular phone tower. Station is located near tower.

Owner/Contact Person: Zone 20/inactive lease; PGV has entry permission.

Site Characteristics: Instruments buried in soil. Location is near large microwave tower on a regional topographic high; home under construction nearby. Two sets of components separated by distance of 50 m in N-S direction.

APPENDIX I: Listing of Stations and Station Information, continued.

Station: O-05, kiia

Date Installed: 01/29/93 Date Removed: 04/17/93

Instrumentation: hi/lo: L28/L28

Gains (dB): hi 72 (01/29/93-04/17/93)

lo 30 (01/29/93-04/17/93)

Coordinates, Elevation: 19° 28.350'N 154° 52.725'W, 157 m

Location/Driving Directions: From HGP-A, turn right onto Rte. 137, at intersection turn right onto Rte. 132. Take 132 past PGV entrance, turn right onto dirt road between mile markers 5 and 4. Station is located beside a vent of the 1955 eruption.

Owner/Contact Person: Zone 32/no lease; PGV has entry permission.

Site Characteristics: Instruments buried in a'a flow fragments. Near 1955 eruption vent.

APPENDIX I: Listing of Stations and Station Information, continued.

Station: I-06, kiib

Date Installed: 01/30/93 Date Removed: 04/10/93

Instrumentation: hi/lo: L28/FBA

Gains (dB): hi 72 (01/30/93-02/12/93), 66 (02/12/93-04/10/93)

lo 30 (01/30/93-02/12/93), 24 (02/12/93-04/10/93)

Coordinates, Elevation: 19° 29.433'N 154° 52.293'W, 117 m

Location/Driving Directions: From HGP-A, turn right onto Rte. 137, at intersection turn right onto Rte. 132. Take 132 past PGV entrance, turn right onto dirt road between mile markers 5 and 4. Turn left at intersection with another dirt road; follow the road until you come to another intersection, turn right. Station is to the west of a large avocado tree, south of a guava orchard.

Owner/Contact Person: HVO (KPO); Murray Air (961-6601); HVO has key to gate

Site Characteristics: Instruments buried in soil. Location near macadamia nut tree in grassy field.

Comments: I/O-06 positions swapped 02/12/93 due to telemetry problems.

APPENDIX I: Listing of Stations and Station Information, continued.

Station: O-06, kpoh

Date Installed: 01/30/93 Date Removed: 04/10/93

Instrumentation: hi/lo: L28/L28

Gains (dB): hi 72 (01/30/93-02/12/93), 72 (02/12/93-04/10/93)

lo 30 (01/30/93-02/12/93), 24 (02/12/93-04/10/93)

Coordinates, Elevation: 19° 29.995'N 154° 50.525'W, 124 m

Location/Driving Directions: From HGP-A, turn right onto Rte. 137, take 137 about 0.4 miles. Turn right at locked gate (key is at Central Receive). Follow jeep trail about 0.4 miles, take left fork and follow it about 0.7 miles to station. The road may be washed out and low-hanging vines make driving hazardous.

Owner/Contact Person: Tony Freitas (959-9393).

Site Characteristics: Instruments buried in soil. Heavy vegetation with large trees nearby.

Comments: I/O-06 positions swapped 02/12/93 due to telemetry problems.

Co-sited with HVO station 'kpoh.'

APPENDIX I: Listing of Stations and Station Information, continued.

Station: I-07, kama

Date Installed: 02/13/93 Date Removed: 04/10/93

Instrumentation: hi/lo: L28/L28
Gains (dB): hi 72 (02/13/93-04/10/93)
lo 30 (02/13/93-04/10/93)

Coordinates, Elevation: 19° 30.148'N 154° 51.930'W, 124 m

Location/Driving Directions: From HGP-A, turn right onto 137; at the intersection, turn right onto 132. Go about 1.8 miles on 132, then turn left onto a dirt road that will take you past Pu'u Ki'i on your right. After about 0.6 miles, turn right onto another dirt road that leads to Halekamahina. Station should be on the west side-look for jeep trail.

Owner/Contact Person: Kapoho Land & Development/A. Lyman.

Site Characteristics: Instruments buried in pahoehoe lava fragments in papaya field. Two sets of components separated by distance of 15 m in N-S direction.

APPENDIX I: Listing of Stations and Station Information, continued.

Station: O-07, papy

Date Installed: 02/13/93 Date Removed: 04/10/93

Instrumentation: hi/hi: L28/L22

Gains (dB): hi 66 (02/13/93-04/10/93)

hi 66 (02/13/93-04/10/93)

Coordinates, Elevation: 19° 28.725'N 154° 53.143'W, 180 m

Location/Driving Directions: As you enter HGP-A premises from Rte. 137, take the dirt road on the immediate right (before you go through the gate). Follow the dirt road until you come to the air quality monitoring station. Station is nearby.

Owner/Contact Person: PGV/Pete Hansen (961-2184).

Site Characteristics: Instruments buried in soil. Northwest rim of Halekamahina Crater.

APPENDIX I: Listing of Stations and Station Information, continued.

Station: I-08, ahal

Date Installed: 02/15/93 Date Removed: 04/12/93

Instrumentation: hi/lo: L28/L28
Gains (dB): hi 72 (02/15/93-04/12/93)
lo 30 (02/15/93-04/12/93)

Coordinates, Elevation: 19° 28.845'N 154° 52.043'W, 105 m

Location/Driving Directions: From HGP-A, turn left onto Rte. 137, go about 1.6 miles, then turn left onto dirt road. Follow the dirt road about 1.2 miles. The station should be visible in the field on the right side of the road.

Owner/Contact Person: Kapoho Land & Development/A. Lyman.

Site Characteristics: Instruments buried in pahoehoe lava fragments in papaya field.

APPENDIX I: Listing of Stations and Station Information, continued.

Station: O-08, crck

Date Installed: 02/15/93 Date Removed: 04/12/93

Instrumentation: hi/lo: L28/L4

Gains (dB): hi 72 (02/15/93-04/12/93)

lo 54 (02/15/93-04/12/93)

Coordinates, Elevation: 19° 28.733'N 154° 52.950'W, 172 m

Location/Driving Directions: From HGP-A, turn left onto Rte. 137, turn left onto Hinalo St., go to end of road. Road is chained; keep away from the dogs - they are chained close to some storage shacks and may bite. If any of them are loose, call Ron Sewell, 965-8538. Station is visible from end of road.

Owner/Contact Person: Tolmie Properties/John Tolmie (961-6648).

Site Characteristics: Instruments buried in coarse cinders. Nearby surface crack on local topographic high.

APPENDIX I: Listing of Stations and Station Information, continued.

Station: I-09, pila

Date Installed: 02/03/93 Date Removed: 05/01/93

Instrumentation: hi/hi: L28/L22

Gains (dB): hi 42 (02/03/93-05/01/93)

hi 42 (02/03/93-05/01/93)

Coordinates, Elevation: 19° 28.670'N 154° 53.463'W, 180 m

Location/Driving Directions: As you enter HGP-A premises from Rte. 137, take the dirt road on the immediate right (before you go through the gate). Take the second left, fork right. Station is at the base of the palm tree (it's the only palm tree).

Owner/Contact Person: PGV/Pete Hansen (961-2184).

Site Characteristics: Instruments buried in rocky soil. In papaya field on topographic high (old cinder cone).

APPENDIX I: Listing of Stations and Station Information, continued.

Station: O-09, uhes

Date Installed: 02/03/93 Date Removed: 04/10/93

Instrumentation: hi/lo: L28/L22

Gains (dB): hi 72 (02/03/93-04/10/93)

lo 30 (02/03/93-04/10/93)

Coordinates, Elevation: 19° 27.825'N 154° 53.245'W, 107 m

Location/Driving Directions: From HGP-A, turn left onto Rte. 137; turn right into Malama Ki Experimental Station (University of Hawaii). Follow dirt road to end; park in parking area. Station in on grassy field above parking area. Gates are open during weekdays; keys at Central Receive.

Owner/Contact Person: Univ. Hawaii/Dennis Ida, supervisor (959-8477)

Site Characteristics: Instruments buried in very shallow soil over pahoehoe fragments. Nearby forested area.

APPENDIX I: Listing of Stations and Station Information, continued.

Station: I-10, poho

Date Installed: 01/31/93 Date Removed: 04/10/93

Instrumentation: hi/lo: L22/L28

Gains (dB): hi 72 (01/31/93-03/20/93), 54 (03/20/93-04/10/93)

lo 30 (01/31/93-04/10/93)

Coordinates, Elevation: 19° 28.213'N 154° 51.955'W, 84 m

Location/Driving Directions: From HGP-A, turn left onto Rte. 137, look for yellow gate along right side of road (always unlocked); turn right and go through gate. Fork left along dirt road parallel to Rte 137, go about 700 feet and park car. Turn right, walk to station, about 90 feet along a stand of trees bordering an abandoned papaya field (white box in center front of field).

Owner/Contact Person: AMFAC-Puna Sugar/Ann Shimazu, 945-8363 or Dennis Maeda (966-7435).

Site Characteristics: Instruments buried in soil and pahoehoe lava fragments. In field along wind break of tall trees.

APPENDIX I: Listing of Stations and Station Information, continued.

Station: O-10, poih

Date Installed: 01/31/93 Date Removed: 04/10/93

Instrumentation: hi/lo: L28/FBA

Gains (dB): hi 72 (01/31/93-02/04/93), 60 (02/04/93-04/10/93)

lo 24 (01/31/93-02/04/93), 12 (02/04/93-04/10/93)

Coordinates, Elevation: 19° 27.450'N 154° 51.225'W, 17 m

Location/Driving Directions: From HGP-A, turn left onto Rte. 137, follow 137 about 2 miles past Leilani Estates. Turn right through a yellow gate, go about 25 yards, then turn left onto a dirt road that parallels Rte. 137. Go along this road, passing 9 field dividers. At the 10th divider, turn right; go straight, passing 2 field dividers. Station is on top of the 3rd field divider, next to HVO station.

Owner/Contact Person: AMFAC-Puna Sugar/Ann Shimazu, 945-8363 or Dennis Maeda (966-7435).

Site Characteristics: Instruments buried in soil and pahoehoe lava fragments. In papaya field along man-made ridge 3 meters high.

Close to shore; surf is audible at times. Co-sited with HVO station 'poih.'

APPENDIX I: Listing of Stations and Station Information, continued.

Station: I-11, potf

Date Installed: 02/04/93 Date Removed: 04/12/93

Instrumentation: hi/hi: L28/L22
Gains (dB): hi 66 (02/04/93-04/12/93)
hi 66 (02/04/93-04/12/93)

Coordinates, Elevation: 19° 28.368'N 154° 53.453'W, 168 m

Location/Driving Directions: TMK 1-3-8 parcel 6. From HGP-A, turn left onto Rte. 137, go past Hinalo St. Turn right along a dirt road lined with Norfolk pines. A field of macadamia nut trees is on the right. Station is in the weeds on the left side of road, on the strip between Rte 137 (Pohoiki) and Old Pohoiki Rd.

Owner/Contact Person: Wayne DeLus (935-2920).

Site Characteristics: Instruments buried in soil and pahoehoe lava fragments. Location about 10 meters from frequently used roadway.

APPENDIX I: Listing of Stations and Station Information, continued.

Station: O-11, bcoh

Date Installed: 02/04/93 Date Removed: 04/12/93

Instrumentation: hi/lo: L28/L28
Gains (dB): hi 72 (02/04/93-04/12/93)
lo 30 (02/04/93-04/12/93)

Coordinates, Elevation: 19° 27.763'N 154° 53.783'W, 165 m

Location/Driving Directions: TMK 1-3-007-029. From HGP-A, turn left onto Rte. 137, go past Hinalo St. Turn right at dirt road lined with Norfolk pines. Follow the road to its end at Robert Kochy's house. Attempt this only in 4-wheel drive; narrow road, precipitous. Station is in front yard. DOGS.

Owner/Contact Person: Robert Kochy (965-7646).

Site Characteristics: Instruments buried in soil. Nearby dwelling and sugar cane field; between Pu'ulena and Kahuwai Craters.

APPENDIX I: Listing of Stations and Station Information, continued.

Station: I-12, erni

Date Installed: 02/06/93 Date Removed: 04/12/93

Instrumentation: hi/lo: L28/L28

Gains (dB): hi 54 (02/06/93-04/12/93)

lo 12 (02/06/93-04/12/93)

Coordinates, Elevation: 19° 28.350'N 154° 53.920'W, 198 m

Location/Driving Directions: From HGP-A, turn left onto Rte. 137, turn right onto Leilani Ave. Go about 200 feet past the intersection of Kahukai and Leilani, turn right into home site. Station in left rear of property. Army-green van marked 'vehicle-in-tow' visible from street.

Owner/Contact Person: Ernie Hicks (965-6095).

Site Characteristics: Instruments buried in coarse cinders. Nearby home under construction; near frequently used roadway.

APPENDIX I: Listing of Stations and Station Information, continued.

Station: I-13, kulh

Date Installed: 01/30/93 Date Removed: 04/11/93

Instrumentation: hi/lo: L28/L22

Gains (dB): hi 72 (01/30/93-02/04/93), 66 (02/04/93-04/11/93)

lo 24 (01/30/93-02/04/93), 18 (02/04/93-04/11/93)

Coordinates, Elevation: 19° 27.475'N 154° 55.300'W, 287 m

Location/Driving Directions: From HGP-A, turn left onto Rte. 137, turn right onto Leilani Ave. Turn left onto Moku St. and go to end of street. Turn right onto dirt road, go past house, turn left, and park near the cinder pit. Station is on a bluff overlooking Leilani Estates near to HVO station.

Owner/Contact Person: Jussi Makrisen (965-7121).

Site Characteristics: Instruments buried in coarse cinders. Large trees nearby. On rim of Pu'u Kaliu. Co-sited with HVO station 'kluh.'

APPENDIX I: Listing of Stations and Station Information, continued.

Station: O-13, alap

Date Installed: 01/30/93 Date Removed: 04/11/93

Instrumentation: hi/lo: L22/L28

Gains (dB): hi 72 (01/30/93-03/20/93), 54 (03/20/93-04/11/93)

lo 30 (01/30/93-04/11/93)

Coordinates, Elevation: 19° 27.790'N 154° 55.320'W, 247 m

Location/Driving Directions: TMK 1-3-017-058; 13-3547 Alapai St., Pahoa, HI. From HGP-A, turn left onto Rte. 137, turn right onto Leilani Ave. Turn left onto Alapai St. Station is at 13-3547 Alapai, home of Ira Earll, in back yard.

Owner/Contact Person: Ira Earll (965-6546).

Site Characteristics: Instruments buried in coarse cinders. Nearby home and infrequently used roadway.

APPENDIX I: Listing of Stations and Station Information, continued.

Station: I-14, maka

Date Installed: 02/06/93 Date Removed: 04/11/93

Instrumentation: hi/lo: L28/L28
Gains (dB): hi 66 (02/06/93-04/11/93)
lo 24 (02/06/93-04/11/93)

Coordinates, Elevation: 19° 28.073'N 154° 54.480'W, 212 m

Location/Driving Directions: 13-3471 Makamae St., Pahoa, Hi. From HGP-A, turn left onto Rte. 137, turn right onto Leilani Ave. Turn right onto Makamae St. Take first driveway on right, 13-3471 Makamae; station is at the rear of lot.

Owner/Contact Person: Myra Neiga (964-8234).

Site Characteristics: Instruments buried in coarse cinders. Nearby house and frequently used roadway.

APPENDIX III. CATALOGUE OF LOCATED EARTHQUAKES

DATE = date (year month day)
ORIGIN = origin time (hour minute second)
LAT N = north latitude
LONG W = west longitude
DEPTH = depth (km) referenced to 360 m above sea level; increases down
MAG = duration magnitude (magnitude units)
NO = number of arrival times used for location
GAP = azimuth from event to array center (degrees)
DMIN = minimum station-to-event distance (km)
RMS = root-mean-square sum of residuals (sec)
ERH = estimated horizontal error (km)
ERZ = estimated vertical error (km

DATE	ORIGIN	LAT N	LONG W	DEPTH	MAG	NO	GAP	DMIN	RMS	ERH	ERZ
930129	0455 18.02	19-29.04	154-58.07	2.71	1.48	10	351	7.7	0.00	1.1	99.9
930129	0705 19.83	19-28.92	154-53.81	1.13	-0.83	6	314	0.2	0.00	0.0	0.0
930129	1129 19.08	19-28.60	154-53.77	1.75	-0.38	7	270	0.7	0.04	0.2	0.1
930129	2130 31.39	19-28.71	154-53.78	2.49	-0.33	10	272	0.5	0.00	0.0	0.2
930129	2244 49.44	19-44.02	154-40.07	2.96	0.94	6	356	36.0	0.39	1.0	67.4
930129	2304 59.62	19-28.91	154-53.86	1.19	-0.44	4	320	0.3	0.00	0.0	0.0
930130	0838 25.82	19-28.61	154-52.74	9.12	-0.11	12	58	0.5	0.00	0.3	0.2
930130	1857 26.47	18-51.39	154-53.50	5.00	-0.21	3	2	66.8	0.04	0.9	0.1
930131	0310 39.32	19-26.56	154-53.00	5.01	-0.28	13	17	4.3	0.00	0.1	0.0
930131	0335 39.73	19-27.85	154-54.84	2.76	-0.72	10	140	1.1	0.00	0.0	0.1
930131	0620 38.49	19-18.32	155-02.50	2.70	1.26	19	339	14.3	0.28	1.6	4.9
930131	0620 57.19	19-30.89	155-30.87	2.69	2.58	15	352	57.2	0.90	0.0	0.2

930131	1202	03.54	19-28.95	154-54.17	2.77	-0.28	21	201	3.0	0.01	0.0	0.5
930131	1215	10.12	19-07.15	154-57.61	10.64	1.08	12	8	41	0.01	1.1	2.7
930131	1314	06.85	19-28.64	154-53.31	2.7	-0.54	9	139	4.3	0.00	0.1	0.0
930131	1615	00.43	19-23.55	154-51.72	5.00	0.72	12	11	10.3	0.00	0.0	0.0
930131	2130	16.90	19-29.44	154-52.26	2.99	-0.73	17	269	2.7	0.01	0.5	0.5
930201	0746	47.15	19-15.85	155-00.04	7.06	0.01	14	335	26.9	0.00	0.0	1.0
930201	1056	24.29	19-02.20	155-31.79	150.01	2.42	21	356	72.3	0.00	0.2	0.3
930201	1446	28.41	19-26.04	155-16.35	5.00	1.61	18	347	40.6	0.01	2.1	4.3
930201	2101	33.46	19-42.69	154-59.16	2.76	0.21	19	335	32.5	0.07	0.0	4.8
930202	0744	50.44	19-27.15	154-49.24	2.72	-0.21	18	280	8.3	0.15	0.7	31.5
930202	0756	15.61	19-31.94	154-56.68	5.00	0.39	25	271	8.6	0.01	0.0	0.9
930202	0922	36.71	19-27.93	154-59.58	4.14	-0.67	15	334	10.5	0.08	0.6	0.1
930202	1454	21.28	19-18.03	155-29.37	2.42	0.92	17	354	66.4	1.36	0.3	1.6
930202	1932	09.31	19-27.80	154-54.97	4.99	-0.41	8	26	3.1	0.00	0.0	0.0
930204	0700	38.66	19-25.75	154-53.09	5.00	-0.50	13	6	6.2	0.00	0.0	0.0
930204	2110	45.57	19-37.31	156-10.15	5.00	0.95	10	356	132.1	1.37	21.0	3.2
930206	0351	20.90	19-25.68	154-58.79	2.95	-0.44	28	342	10.6	0.17	0.1	3.1
930206	0717	04.40	19-28.23	154-53.57	5.63	-0.09	25	112	2.8	0.01	0.0	0.0
930206	0842	13.61	19-21.05	155-24.44	7.48	1.38	28	353	56.0	0.01	0.3	1.2
930206	1013	39.35	19-15.40	155-00.26	2.63	0.68	20	342	18.2	1.06	0.0	0.0
930206	1158	54.21	19-21.62	154-42.08	8.69	-1.02	19	351	24.3	0.04	0.5	2.1
930206	1722	57.79	19-19.89	155-20.30	11.79	2.07	19	353	50.0	0.00	0.6	0.1
930206	1724	16.40	19-07.59	154-59.02	12.52	1.82	12	348	32.4	0.10	1.9	0.5
930207	1307	27.04	19-25.17	154-53.22	5.46	-0.11	23	3	5.5	0.01	0.8	1.7
930207	1259	36.42	19-30.24	154-53.75	2.21	-0.41	34	241	2.4	0.06	0.0	0.9
930207	2203	08.57	19-19.34	155-14.20	10.86	1.70	15	352	38.2	0.19	1.1	2.0
930209	0241	56.44	19-28.24	154-54.32	2.96	-0.83	32	26	0.7	0.21	0.2	0.2
930209	0246	26.24	19-21.61	155-04.95	13.46	0.92	21	348	12.8	0.01	0.2	0.0
930209	1905	28.67	19-26.68	154-55.69	1.72	0.02	35	127	1.6	0.04	0.0	0.0
930210	0325	00.50	19-26.94	154-53.49	9.55	-0.49	21	33	7.7	0.00	0.1	0.1
930210	0506	55.26	19-17.88	154-47.29	39.48	-0.63	13	335	21.4	0.03	0.2	3.5

930210	0703	18.71	19-27.47	154-54.24	3.41	-0.54	5	69	1.0	0.01	0.2	0.3
930210	0755	25.38	19-25.08	154-54.96	5.34	-0.95	11	6	5.4	0.00	0.2	0.1
930210	0904	16.98	19-25.79	154-56.34	2.71	0.40	6	341	5.5	0.02	0.4	73.8
930210	1440	40.35	19-27.51	154-51.86	4.38	-0.53	24	101	4.7	0.14	0.7	0.7
930210	2123	37.08	19-21.64	154-57.50	5.00	0.26	16	33	14.5	0.01	0.1	0.0
930211	0007	14.21	19-15.07	155-08.53	2.74	1.92	18	352	35.2	0.01	0.2	81.0
930211	0220	48.86	19-29.98	155-22.66	5.00	0.60	23	349	42.8	0.01	3.2	5.9
930211	0323	11.86	19-29.76	154-51.23	9.49	-0.21	31	301	4.7	0.06	1.1	1.6
930211	0401	11.53	19-04.96	155-13.13	2.65	1.29	15	355	54.2	0.14	0.0	0.0
930211	0458	17.22	19-31.86	155-16.82	2.69	1.06	15	345	41.1	0.01	0.2	0.5
930211	0526	29.95	19-24.67	154-52.81	2.83	-0.11	27	19	6.7	0.01	0.2	4.3
930211	0558	39.32	19-12.23	155-15.43	2.53	0.69	21	354	47.9	0.39	1.8	2.0
930211	0600	39.04	19-28.63	154-53.80	2.20	-1.27	25	88	0.6	0.00	0.1	0.0
930211	0613	11.93	19-28.62	154-53.37	2.21	0.49	22	179	0.5	0.00	0.0	0.0
930211	0703	08.62	19-25.02	155-14.07	6.78	0.74	21	347	26.9	0.00	0.2	0.0
930211	0712	13.64	19-08.79	155-06.15	3.01	1.58	14	351	42.6	0.00	0.5	46.9
930211	0743	20.68	19-08.42	155-09.41	5.00	1.15	21	353	46.1	0.01	2.2	18.2
930211	0922	27.42	19-19.25	155-19.74	5.00	1.13	14	355	48.5	0.00	2.6	15.6
930211	1210	18.55	19-28.48	154-54.05	2.19	-0.13	20	85	1.1	0.17	0.1	0.0
930211	1237	53.19	19-26.28	154-56.77	5.30	0.56	28	146	4.1	0.01	0.4	0.6
930211	1251	38.88	19-28.50	154-53.94	1.98	-0.61	26	86	0.9	0.11	0.1	0.1
930211	1318	29.63	19-28.65	154-54.01	2.75	-1.15	19	101	1.3	0.23	0.4	0.4
930211	1334	53.31	19-33.06	155-13.11	2.00	0.83	23	341	29.0	1.53	0.2	0.6
930211	1842	23.58	19-35.62	155-00.99	2.73	0.92	8	329	16.5	0.01	1.8	***
930212	0343	47.56	19-28.17	154-54.32	3.13	-0.85	15	22	2.2	0.19	0.6	0.7
930212	0344	07.59	19-28.60	154-54.28	0.34	-0.21	13	169	2.4	***	0.1	0.0
930212	0344	13.89	19-28.44	154-54.48	3.13	1.63	16	74	0.7	0.13	0.5	0.5
930212	0344	19.29	19-30.08	154-54.62	11.95	1.96	15	322	3.1	0.01	3.5	1.5
930212	0344	25.66	19-28.03	154-54.54	2.70	1.66	20	28	0.9	0.00	0.0	0.0
930212	0347	13.35	19-27.80	154-54.22	4.00	-0.05	18	32	1.1	0.00	0.0	0.0
930212	0622	07.64	19-07.66	155-31.74	0.25	1.99	11	357	66.7	0.09	11.3	13.9

930212	0741	18.87	19-26.18	154-53.54	3.86	-0.24	15	16	9.3	0.00	0.0	0.1
930212	1010	33.41	19-25.33	154-54.71	5.00	0.15	16	11	4.1	0.01	0.0	0.2
930212	1033	43.37	19-46.70	155-35.25	5.00	0.87	17	358	78.8	0.00	1.6	1.6
930212	1156	40.95	19-26.74	154-53.29	5.00	-0.93	28	5	4.0	0.4	1.0	0.1
930212	1227	16.64	19-15.25	155-13.79	3.28	1.64	26	353	32.3	0.01	0.2	4.7
930212	1230	00.56	19-14.62	155-12.66	2.71	2.04	34	351	31.4	0.01	0.0	68.9
930212	1232	46.45	19-14.75	155-14.65	11.12	0.90	16	355	34.1	0.07	0.6	0.2
930212	1330	58.42	19-11.25	155-12.59	13.50	2.06	11	355	35.6	0.10	4.5	0.4
930212	1710	23.36	19-28.74	154-54.07	1.13	-0.84	16	192	0.6	0.14	0.2	0.3
930213	0217	13.33	19-28.13	154-54.19	1.94	-0.97	13	153	0.5	0.11	0.3	0.2
930213	0417	19.03	19-28.40	155-31.21	2.14	2.20	26	352	57.2	0.46	2.0	0.6
930213	0431	38.56	18-45.41	155-01.98	5.00	3.01	34	351	73.7	0.55	34.7	58.3
930213	0651	10.78	19-24.74	155-19.51	2.75	1.92	27	350	46.1	0.01	0.5	91.4
930213	0823	33.98	19-27.34	154-53.37	9.10	-0.47	22	17	1.9	0.00	0.0	0.1
930213	1125	55.90	19-23.54	155-01.11	2.69	-0.01	14	347	5.1	0.09	0.4	0.2
930213	1812	21.02	19-33.43	154-50.84	21.16	-1.02	10	344	11.6	0.09	5.6	3.2
930214	0250	59.35	19-26.52	154-56.57	2.71	-1.12	16	161	4.6	0.49	1.0	99.9
930214	0912	24.47	19-24.63	154-53.28	2.72	0.10	17	277	7.0	0.15	0.5	91.0
930214	1426	18.78	19-26.58	154-54.98	6.25	0.23	18	4	5.2	0.08	0.7	0.7
930214	1531	56.21	19-28.47	154-53.07	10.45	-0.24	37	16	1.8	0.02	1.0	0.3
930214	1755	30.03	19-26.67	154-50.37	1.69	0.12	18	285	3.9	0.01	0.3	0.2
930214	1845	23.81	19-29.06	154-52.57	5.49	-0.52	14	111	0.8	0.00	0.0	0.0
930215	0213	48.94	19-27.58	154-52.22	6.61	0.10	38	7	1.3	0.01	0.5	0.1
930215	0405	03.05	19-27.54	154-56.24	4.34	0.17	29	313	4.0	0.05	0.2	0.0
930215	0703	05.85	19-26.02	155-03.04	2.11	2.06	12	328	7.7	0.12	13.4	0.0
930215	0840	40.41	19-28.97	154-51.17	0.59	2.17	27	97	2.1	****	0.2	0.2
930215	1017	25.64	19-27.65	154-54.94	2.97	-0.67	19	15	0.7	0.01	0.1	0.1
930215	1115	43.05	19-25.78	154-53.33	5.32	-0.31	16	5	4.7	0.01	0.4	0.3
930215	1319	08.41	20-30.81	154-12.77	5.00	2.58	17	357	****	****	9.2	6.8
930215	1420	34.51	19-27.98	154-54.38	2.71	-1.07	7	54	0.2	0.02	0.2	0.2
930215	1423	16.47	19-29.76	155-18.50	9.85	1.16	35	346	45.9	0.01	0.2	0.6

930215	1834	56.92	19-23.28	155-19.85	2.71	1.96	48	350	37.2	0.02	0.4	99.9
930215	1909	18.94	19-27.51	154-54.68	2.70	-0.23	17	18	2.1	0.00	0.2	0.1
930215	1948	34.07	19-29.79	154-53.56	7.41	-0.42	19	250	3.00	0.00	0.4	0.5
930215	2309	26.81	19-27.64	154-54.95	2.70	-0.98	26	16	0.7	0.00	0.1	0.0
930215	2333	17.28	19-22.57	154-57.73	4.99	0.03	33	38	14.0	0.68	3.5	2.7
930216	0218	16.24	19-26.01	154-55.57	5.01	0.17	34	111	2.7	0.00	0.0	0.1
930216	0321	30.68	19-28.66	154-53.75	2.02	-0.71	18	94	1.0	0.09	0.1	0.1
930216	0511	44.42	19-28.76	154-54.19	4.00	-0.75	31	116	0.8	0.01	0.0	0.0
930216	0520	42.12	19-28.64	154-53.69	0.64	-0.62	12	82	1.0	0.00	0.0	0.1
930216	0620	11.83	19-28.32	154-55.12	2.75	-0.93	17	45	8.7	0.00	0.3	0.4
930216	0701	10.97	19-27.98	154-54.42	2.19	-0.27	10	142	0.2	0.00	0.1	0.0
930216	0742	00.80	19-28.41	154-53.00	1.51	0.09	39	12	1.5	0.12	0.0	0.1
930216	0803	29.73	19-28.51	154-51.97	3.94	-0.84	21	306	4.1	0.01	0.1	0.0
930216	1009	41.29	19-16.36	155-12.22	1.35	0.65	17	357	39.9	0.55	3.1	3.1
930216	1210	41.76	19-19.83	155-11.16	2.87	0.63	19	352	24.0	0.01	0.1	12.2
930216	1335	41.70	19-28.90	154-53.49	2.69	-0.72	26	63	2.2	0.01	0.0	0.0
930216	1342	03.77	19-29.51	154-52.60	0.01	-0.33	51	109	3.2	0.08	0.1	0.2
930216	1344	47.87	19-28.69	154-53.54	2.67	-1.10	30	71	0.4	0.11	0.1	0.1
930216	1521	50.60	19-27.54	154-53.92	1.82	0.54	51	12	0.8	0.48	0.1	0.2
930216	2100	49.72	19-27.91	154-54.11	2.31	-0.35	10	69	0.6	0.00	0.0	0.1
930216	2121	25.51	19-28.51	154-52.86	3.94	0.79	14	72	1.4	0.00	0.0	0.1
930217	0709	44.00	19-29.11	154-54.49	7.71	0.04	36	111	3.4	0.01	0.0	0.1
930217	1049	50.22	19-29.68	154-51.20	3.46	-0.84	9	181	3.0	0.00	0.5	1.0
930217	1836	43.39	19-23.12	154-50.63	2.99	-0.10	41	10	11.8	0.39	0.1	1.8
930217	1846	08.46	19-28.48	154-53.88	2.01	-0.13	8	193	0.7	0.13	0.4	0.4
930217	2023	33.08	19-28.08	154-54.29	3.89	-0.79	20	71	9.6	0.10	0.4	0.4
930217	2134	19.88	19-27.62	154-54.78	1.89	0.18	49	19	8.4	0.02	0.0	0.0
930217	2148	19.87	19-28.66	154-53.73	2.74	0.05	51	12	0.7	0.01	0.0	0.0
930218	0627	11.76	19-26.52	154-56.90	1.58	1.29	55	157	6.3	0.47	0.1	0.0
930218	0631	38.77	19-26.08	154-56.31	2.70	-0.70	12	129	3.6	0.07	0.4	0.4
930218	0643	49.81	19-26.75	154-57.12	2.04	-0.62	14	170	3.5	0.00	0.2	0.1

930218	0708 54.43	19-26.13	154-56.60	3.85	0.07	31	137	3.4	0.01	0.1	0.1
930218	0744 41.70	19-27.07	154-57.19	3.07	-0.39	12	181	3.6	0.06	0.5	2.2
930218	0922 09.29	19-19.09	155-22.31	2.69	0.97	22	354	54.7	0.77	0.0	0.1
930218	1218 35.68	19-29.11	154-54.32	3.18	-0.62	46	139	1.7	0.01	0.0	0.0
920218	1441 01.95	19-28.56	154-54.05	1.25	0.08	51	67	3.0	0.03	0.0	0.0
930218	1525 31.51	19-28.21	154-53.26	2.54	-0.98	28	26	0.4	0.01	0.0	0.0
930218	1608 08.19	19-14.73	155-36.65	5.00	2.13	9	358	77.8	0.08	5.0	3.9
930218	2000 35.76	19-28.41	154-53.59	2.46	-0.13	46	9	0.7	0.01	0.0	0.0
930218	2003 31.19	19-30.37	154-53.97	2.69	-0.89	39	249	3.0	0.08	0.1	1.7
930218	2008 30.89	19-28.62	154-53.81	1.93	-0.37	16	127	1.3	0.00	0.1	0.0
930219	0016 12.23	19-28.22	154-52.61	4.50	0.60	18	45	1.1	0.01	0.5	0.7
930219	0346 07.18	19-29.21	154-53.99	2.99	0.21	23	175	1.8	0.01	0.0	0.0
930219	0408 23.60	19-28.74	154-53.71	2.70	-0.54	25	61	0.4	0.01	0.0	0.0
930219	0535 27.22	19-26.94	154-55.42	2.90	-0.68	18	123	1.0	0.00	0.2	0.4
930219	0620 34.32	19-27.44	154-54.01	5.81	0.12	11	65	0.7	0.00	0.0	0.0
930219	0708 52.97	19-28.41	154-54.01	1.89	0.41	54	57	0.8	0.46	0.1	0.1
930219	0727 25.95	19-57.12	155-58.29	0.00	3.17	54	354	121.0	0.94	4.6	2.5
930219	0951 42.17	19-32.81	154-59.93	4.91	1.67	32	295	14.8	1.10	2.4	12.0
930219	1006 17.46	19-27.09	154-57.14	8.01	0.12	6	198	5.7	0.03	0.9	0.4
930219	1148 53.68	19-27.37	154-54.82	3.97	-0.46	23	14	0.9	0.00	0.0	0.1
930219	1307 07.71	19-26.23	155-32.90	4.66	2.10	22	353	69.3	0.44	10.8	1.2
930219	1612 19.94	19-29.07	154-55.06	3.94	-1.00	19	139	2.1	0.01	0.1	0.1
930219	1623 18.89	19-27.69	154-54.17	2.98	-0.32	16	52	0.9	0.15	0.5	0.6
930219	1640 42.08	19-28.66	154-53.90	1.47	-0.15	49	69	0.3	0.01	0.0	0.0
930219	1659 01.35	19-28.41	154-53.60	2.64	-0.17	44	9	0.3	0.01	0.0	0.0
930219	1734 15.57	19-26.92	154-54.72	5.00	-0.21	31	11	2.3	0.01	0.0	0.0
930219	2057 33.53	19-27.64	154-54.49	1.56	-0.02	50	24	1.0	0.24	0.0	0.0
930219	2100 47.78	19-25.52	154-54.65	2.70	-0.67	22	6	4.7	0.04	0.5	0.3
930219	2116 49.81	19-28.68	154-53.68	2.60	-0.81	25	20	0.2	0.00	0.0	0.0
930219	2122 51.36	19-28.40	154-53.81	2.46	-0.61	12	148	0.2	0.11	0.2	0.1
930220	0015 19.34	19-28.62	154-53.05	2.66	-0.31	25	23	0.3	0.01	0.0	0.0

930220	0018	53.84	19-27.81	154-53.92	3.04	0.24	53	25	2.2	0.03	0.0	0.0
930220	0019	55.46	19-28.91	154-53.21	2.63	-0.69	34	56	0.5	0.01	0.0	0.0
930220	0020	31.62	19-28.83	154-53.11	2.32	0.99	32	77	0.2	0.01	0.2	0.1
930220	0245	55.92	19-29.81	154-57.72	2.68	-0.49	52	253	7.9	0.78	0.4	0.2
930220	0530	33.21	19-28.52	154-53.25	2.13	-1.04	22	46	0.7	0.00	0.1	0.0
930220	0838	28.22	19-29.00	154-52.47	5.00	-0.39	15	279	2.3	0.01	0.4	0.0
930220	0918	41.14	19-28.61	154-53.60	2.20	-0.52	30	22	0.5	0.02	0.0	0.0
930220	1009	38.62	19-28.26	154-55.44	3.82	-0.33	14	143	0.9	0.33	1.2	1.1
930220	1109	21.45	19-26.23	154-53.96	4.83	-0.01	41	1	3.7	0.01	0.0	0.0
930220	1253	28.63	19-28.47	154-53.77	1.73	0.03	15	61	0.9	0.00	0.0	0.1
930220	1601	12.52	19-27.23	154-53.62	5.00	0.09	28	13	3.6	0.01	0.0	0.2
930220	1614	17.94	19-27.14	154-56.18	5.00	-0.28	17	305	4.2	0.01	0.9	0.1
930220	1744	58.89	19-31.80	154-54.93	5.00	-0.31	30	264	8.0	0.01	0.0	0.0
930220	1836	22.21	19-28.32	154-53.77	1.59	-1.48	11	164	0.9	0.00	0.0	0.0
930220	1941	13.64	19-27.37	154-53.58	3.71	-0.52	37	4	3.4	0.01	0.0	0.0
930220	1954	16.33	19-28.09	154-54.13	2.51	-0.75	23	28	0.3	0.00	0.0	0.1
930220	2050	18.90	19-28.67	154-54.07	2.79	-0.56	15	144	2.4	0.00	0.0	0.0
930220	2354	44.28	19-24.96	154-52.85	2.68	0.04	51	1	7.2	0.13	0.0	0.3
930221	0121	29.30	19-28.34	154-52.76	3.10	-0.99	34	33	0.8	0.01	0.0	0.0
930221	0122	04.71	19-27.97	154-54.92	4.31	2.25	27	23	1.1	0.01	0.0	0.3
930221	0438	45.14	19-28.64	154-53.79	2.14	-0.58	34	65	0.6	0.01	0.0	0.0
930221	0446	35.63	19-28.52	154-53.71	2.21	-0.42	28	54	1.1	0.01	0.0	0.0
930221	0704	43.45	19-21.60	155-00.72	13.54	0.94	19	343	20.8	0.44	12.9	14.2
930221	0737	37.93	19-28.77	154-51.96	5.00	-0.77	33	203	2.7	0.11	0.2	0.0
930221	0739	48.90	19-28.30	154-53.83	2.48	-0.84	31	26	0.9	0.01	0.0	0.0
930221	0756	56.77	19-27.52	154-53.99	1.95	-0.74	35	4	1.3	0.01	0.0	0.0
930221	0757	25.70	19-27.70	154-54.15	2.35	2.13	12	62	0.9	0.06	0.2	0.1
930221	0816	41.63	19-27.43	154-54.34	2.52	-1.09	10	13	1.7	0.04	0.2	0.3
930221	0821	51.42	19-27.60	154-54.65	3.94	0.56	17	37	1.5	0.00	0.0	0.0
930221	0844	26.80	19-28.39	154-54.77	2.66	0.00	35	39	1.9	0.15	0.3	0.1
930221	1228	19.37	19.28.61	154-53.93	2.34	-0.34	29	44	0.3	0.01	0.1	0.0

930221	1637 33.01	19-37.40	154-47.20	2.69	-0.33	35	343	19.8	0.57	0.3	1.4
930221	1725 03.70	19-28.59	154-53.55	1.95	-0.09	34	23	0.5	0.01	0.0	0.0
930221	1919 36.31	19-28.67	154-53.68	2.62	-0.49	31	1	0.5	0.01	0.2	0.0
930221	2051 47.29	18-52.50	155-01.12	7.77	2.63	36	349	68.7	0.03	4.3	0.9
930221	2208 15.65	19-28.66	154-53.37	1.73	-1.19	20	46	0.7	0.12	0.1	0.1
930221	2215 41.66	19-28.81	154-53.56	1.07	-0.28	21	62	1.4	0.01	0.0	0.0
930221	2358 36.93	19-28.36	154-54.21	2.42	-0.41	32	50	0.8	0.01	0.0	0.0
930222	0443 27.85	19-18.57	155-10.23	2.66	1.49	14	354	23.7	1.13	6.9	70.3
930222	0748 18.30	19-28.31	154-53.85	1.37	-1.05	8	101	0.8	0.05	0.1	0.1
930222	0802 48.43	19-29.12	154-59.06	2.71	-0.45	22	264	7.2	0.05	0.1	8.3
930222	0841 25.22	19-28.49	154-53.78	1.34	-1.00	14	63	0.6	0.08	0.1	0.2
930222	0927 18.96	19-28.27	154-54.07	1.65	-0.93	11	44	1.1	0.06	0.1	0.1
930222	1118 15.46	19-23.26	154-48.02	5.00	0.22	16	349	13.6	0.23	0.6	0.1
930222	1120 04.53	19-28.22	154-54.20	2.33	-0.45	14	35	0.5	0.06	0.2	0.2
930222	1156 39.69	19-11.61	155-24.06	0.67	2.08	15	357	51.3	0.20	0.8	99.9
930222	1216 35.43	19-31.75	153-44.17	5.00	2.62	23	356	****	****	52.0	93.8
930222	1440 08.07	19-28.16	154-54.25	2.71	-0.26	20	27	0.4	0.55	0.2	0.2
930222	1454 23.38	19-28.87	154-52.12	4.72	-0.37	12	23	0.2	0.03	0.3	0.5
930222	1601 29.22	19-36.47	154-55.45	4.80	0.04	14	351	14.5	0.14	6.0	12.3
920222	1611 36.54	19-28.74	154-53.71	0.97	-0.12	9	99	0.4	0.02	0.1	0.1
930222	1620 55.49	19-53.72	155-21.02	2.58	0.63	10	359	65.8	0.10	0.0	10.2
930222	1632 04.71	19-28.85	154-53.57	0.32	0.34	11	60	0.4	0.08	0.0	0.0
930222	1641 37.25	19-28.81	154-53.47	0.51	-0.12	8	93	0.2	0.06	0.1	0.1
930222	1650 58.21	19-29.02	154-53.50	1.08	-0.21	7	190	0.6	0.05	0.2	0.3
930222	1701 11.47	19-27.19	154-54.00	2.10	-0.01	9	327	2.9	0.12	1.3	3.9
930222	1712 31.84	19-33.48	155-00.87	1.96	0.09	11	350	15.1	0.11	0.7	99.9
930222	1724 09.37	19-30.60	154-56.59	0.89	-0.07	10	340	6.0	0.18	3.7	0.0
930222	1800 12.32	19-36.98	155-01.00	1.17	-0.39	7	356	19.7	0.10	0.2	99.9
930222	2118 30.95	19-17.23	154-53.04	5.00	-0.24	18	1	20.6	0.63	4.0	0.4
930223	0604 09.19	19-25.10	154-51.85	2.68	-0.37	20	344	7.7	0.03	0.2	3.1
930223	0626 45.39	19-21.99	154-53.50	2.69	-0.71	26	1	10.6	0.13	0.3	0.1

930223	0658 07.54	19-27.92	154-54.90	3.10	-0.61	37	22	1.1	0.01	0.0	0.1	
930223	0658 23.86	19-28.15	154-54.50	1.76	-0.48	32	34	2.9	0.08	0.1	0.1	
930223	0658 31.31	19-27.06	154-54.00	1.95	0.06	31	10	2.0	0.22	0.1	0.0	
930223	0659 13.38	19-27.78	154-54.42	1.83	-0.58	12	17	1.6	0.13	0.3	0.4	
930223	0700 37.94	19-28.55	154-56.83	2.69	-0.25	47	212	4.2	0.12	0.2	3.3	
930223	0701 19.30	19-27.50	154-54.53	2.70	0.15	36	7	1.3	0.01	0.0	0.3	
930223	0730 38.26	19-27.93	154-54.41	4.07	-0.78	14	20	1.4	0.07	0.4	0.3	
930223	0740 03.87	19-28.07	154-54.73	2.42	-0.33	16	71	0.4	0.09	0.2	0.2	
930223	0830 14.61	19-27.63	154-54.52	2.99	0.46	22	9	1.4	0.08	0.2	0.2	
930223	0921 10.58	19-28.70	154-53.75	2.18	-0.34	29	67	0.5	0.09	0.1	0.0	
930223	0933 40.54	19-28.47	154-53.77	2.34	-0.78	30	45	0.5	0.01	0.1	0.2	
930223	0945 40.10	19-32.89	154-46.94	2.70	-0.52	33	343	17.9	0.12	0.0	0.3	
930223	1029 23.67	19-20.35	155-13.65	2.71	1.70	24	353	27.7	0.01	0.1	61.1	
930223	1047 29.26	19-26.57	154-55.41	5.59	0.30	13	117	7.5	0.10	1.2	1.4	
930223	1302 26.96	19-28.08	154-53.95	2.47	-0.55	7	159	0.2	0.02	0.2	0.1	
930223	1508 40.13	19-27.73	154-53.65	3.12	-0.62	15	23	1.2	0.15	0.6	0.6	
930223	1649 05.53	19-16.58	155-26.64	1.66	1.67	20	354	51.6	0.27	0.0	99.9	
930223	1812 58.79	19-28.55	154-53.75	1.48	-0.71	20	55	1.2	0.04	0.0	0.1	
930223	2036 52.81	19-28.09	154-58.72	2.69	-0.99	36	333	8.8	0.23	0.3	0.5	
930223	2048 18.87	19-28.12	154-54.10	2.70	0.15	23	30	0.5	0.00	0.0	0.0	
930223	2150 29.87	19-25.05	154-56.17	2.69	-0.80	39	325	7.3	0.61	0.2	0.7	
930223	2151 15.92	19-28.31	154-53.77	1.50	-1.13	12	108	0.6	0.07	0.1	0.1	
930224	0127 23.96	19-28.45	154-54.03	2.27	-0.96	13	49	0.5	0.00	0.0	0.3	
930224	0132 44.78	19-27.92	154-53.75	2.24	-1.27	16	49	1.6	0.01	0.0	0.0	
930224	0215 23.59	19-27.51	154-54.52	5.00	-0.54	18	7	2.5	0.03	0.7	0.1	
930224	0254 52.84	19-28.56	154-53.67	2.17	-1.23	14	137	0.5	0.13	0.2	0.1	
930224	0406 11.99	19-32.32	154-57.06	2.67	-1.21	7	350	8.5	0.24	1.5	99.9	
930224	0406 35.00	19-29.94	154-52.83	4.99	-0.32	20	271	2.2	0.22	1.9	1.4	
930224	0411 00.13	19-31.36	154-55.60	2.59	-0.44	10	352	5.9	0.01	0.7	0.3	
930224	0411 11.75	19-12.63	155-02.72	5.00	-0.31	12	358	33.9	1.29	2.5	2.6	
930224	0411 39.00	19-28.73	154-53.67	0.41	-0.05	7	24	0.6	****	0.1	0.1	

930224	0411	58.89	19-28.71	154-53.74	1.04	-0.61	10	22	0.1	0.23	4.0	0.3
930224	0412	32.15	19-28.77	154-53.62	0.25	-0.49	14	77	0.2	0.18	0.1	0.0
930224	0412	32.34	19-28.83	154-53.63	0.40	-0.46	15	98	0.3	0.13	0.1	6.1
930224	0413	24.96	19-28.85	154-53.67	0.41	-0.42	11	37	0.2	0.17	0.0	0.2
930224	1022	40.93	19-31.12	154-49.45	2.76	-0.51	51	325	8.8	0.45	0.4	15.8
930224	1022	52.52	19-28.62	154-53.55	2.53	-1.01	33	25	0.6	0.00	0.0	0.0
930224	1023	28.94	19-28.65	154-53.90	1.84	-0.95	30	63	0.3	0.12	0.1	0.2
930224	1026	30.18	19-27.83	154-53.81	2.75	-0.70	29	17	1.7	0.01	0.1	0.2
930224	1031	26.73	19-28.76	154-53.97	2.44	-0.39	47	76	0.1	0.01	0.0	0.0
930224	1101	15.72	19-28.65	154-53.94	1.72	-0.71	29	52	0.4	0.01	0.0	0.0
930224	1102	0905	19-28.58	154-53.82	2.61	-0.34	28	54	0.3	0.01	0.1	0.0
930224	1123	53.48	19-25.68	154-55.74	6.30	0.17	31	108	3.4	0.01	0.1	0.0
930225	0043	45.54	19-28.39	154-54.05	2.21	-0.91	16	54	0.6	0.15	0.2	0.3
930225	0053	45.04	19-28.01	155-07.40	29.01	0.69	23	332	16.0	0.09	3.4	1.6
930225	0408	54.46	19-28.56	154-51.61	5.08	-0.46	16	72	4.1	0.07	0.5	0.5
930225	0552	27.32	19-28.89	154-54.54	5.00	-0.53	14	329	1.9	0.07	0.8	0.1
930225	0604	50.56	19-28.51	154-53.64	0.39	-1.01	21	33	0.5	0.08	0.0	1.6
930225	0705	45.80	19-26.79	154-53.29	7.35	-0.28	37	7	2.5	0.00	0.1	0.1
930225	0945	27.55	19-26.63	154-55.42	6.91	-0.55	20	118	5.8	0.11	0.7	0.6
930225	1307	48.92	19-23.28	154-48.80	4.82	-0.65	37	334	12.5	0.25	1.7	9.8
930226	0434	04.64	19-09.97	155-08.66	53.73	1.70	44	349	33.2	1.08	60.0	60.0
930226	0550	07.55	19-24.57	155-02.77	5.00	2.16	42	335	20.6	0.82	10.6	0.8
930226	0553	28.48	19-28.75	154-54.04	2.44	-0.44	50	76	0.5	0.01	0.1	0.1
930226	0725	56.35	19-28.66	154-53.32	2.03	-1.02	24	46	1.0	0.13	0.1	0.1
930226	0958	41.14	19-28.55	154-52.34	5.82	-0.59	18	93	1.6	0.01	0.8	0.5
930226	1246	06.58	19-28.15	154-54.50	2.43	-0.94	16	56	1.9	0.00	0.1	0.2
930226	1321	54.41	19-24.59	154-57.80	7.56	-0.04	34	85	6.9	0.06	1.2	0.6
930226	1341	48.76	19-27.94	154-54.21	2.55	-0.86	16	19	0.5	0.08	0.2	0.1
930226	1409	06.43	19-27.69	154-54.19	3.01	-0.10	21	15	0.9	0.00	0.1	0.3
930226	1738	16.12	19-28.88	154-54.33	5.00	-0.60	31	89	0.6	0.10	0.4	0.0
930226	1839	42.36	19-28.81	154-53.42	1.90	-0.99	16	60	0.9	0.00	0.1	0.0

930226	1925	29.86	19-28.19	154-52.70	5.20	-0.54	33	23	2.3	0.01	0.6	0.2
930227	0008	27.44	19-28.41	154-53.54	2.55	0.09	29	61	1.2	0.54	0.6	0.3
930227	0202	06.10	19-29.12	154-54.54	2.74	1.57	38	111	2.8	0.17	0.1	0.3
930227	0223	05.85	19-27.13	154-53.33	7.17	-0.42	12	40	1.4	0.10	1.0	0.7
930227	0544	15.57	19-26.47	154-52.99	7.25	0.16	25	9	5.1	0.12	0.8	0.6
930228	0032	44.42	19-11.26	155-20.60	2.63	1.12	36	353	57.1	0.42	0.1	0.6
930228	0057	54.61	19-28.47	154-53.68	2.17	-0.96	19	119	1.4	0.15	0.2	0.1
930228	0257	39.83	19-35.32	154-52.06	3.70	-0.88	28	341	13.1	0.25	0.4	1.2
930228	0339	43.68	19-28.49	154-53.58	2.51	-0.18	12	327	4.9	0.23	3.0	1.8
930228	0536	14.61	19-27.99	154-53.38	3.54	-0.02	50	20	1.2	0.06	0.0	0.0
930228	0735	08.41	19-27.20	155-17.29	2.63	1.11	35	346	45.7	0.20	3.1	3.9
930228	0736	49.03	19-29.24	155-00.74	3.18	-0.40	51	288	12.0	1.19	0.1	0.2
930228	1002	15.43	19-29.44	154-53.81	5.00	-0.89	19	236	2.1	0.02	0.4	0.0
930228	1200	19.76	19-28.42	154-54.03	2.70	-0.70	21	53	2.0	0.13	0.2	0.2
930228	1512	02.39	19-27.69	154-55.95	7.59	-0.42	20	178	5.8	0.07	0.7	0.3
930228	1905	37.45	19-27.13	154-53.84	8.79	0.25	34	8	1.6	0.14	0.9	0.6
930228	1928	35.26	19-28.68	154-53.83	3.99	-0.33	25	149	0.9	0.01	0.1	0.0
930228	1943	50.49	19-28.15	154-53.10	3.97	-0.76	23	259	2.4	0.00	0.0	0.1
930228	1945	56.74	19-26.00	154-46.28	5.00	-0.06	15	348	14.0	0.28	1.2	0.3
930228	1958	30.12	19-28.26	154-53.47	2.01	-0.94	17	81	1.5	0.00	0.0	0.1
930228	2203	18.40	19-25.66	154-52.71	6.96	-0.46	30	3	4.9	0.00	0.0	0.0
930301	0237	46.15	19-27.92	154-57.72	8.77	0.68	12	232	7.8	0.01	0.1	0.1
930301	0354	15.63	19-22.87	154-56.73	2.69	0.09	27	54	8.9	****	0.1	1.6
930301	0508	41.01	19-28.78	154-53.31	1.28	0.02	14	129	0.6	0.08	0.1	0.1
930301	0738	27.31	19-28.37	154-53.52	2.55	0.02	8	303	3.6	0.18	0.9	0.3
930301	1425	29.75	19-28.47	154-53.71	1.48	-1.76	12	63	0.5	0.05	0.1	0.1
930301	1433	36.89	19-20.59	155-10.40	28.93	0.02	21	351	35.9	0.00	0.9	2.1
930301	1705	59.31	19-00.69	154-59.16	8.01	0.71	17	345	50.1	0.01	0.9	1.9
930301	2313	36.73	19-29.54	154-59.62	2.70	-0.47	44	334	10.4	0.89	0.9	0.2
930301	2320	29.35	19-19.57	154-51.09	2.66	0.81	49	3	16.3	0.13	0.2	1.1
930302	0506	05.34	19-26.47	154-54.11	7.59	0.46	20	5	2.5	0.00	0.0	0.1

930302	0735	53.45	19-19.56	155-17.50	2.69	-0.07	26	353	34.6	0.12	0.2	0.3
930302	1459	10.99	19-26.56	154-54.12	7.62	0.58	45	6	4.5	0.01	0.1	0.1
930302	2015	57.09	19-41.69	154-52.53	2.75	0.09	17	351	23.4	0.01	5.3	61.7
930302	2133	04.26	19-23.36	154-46.09	35.08	1.22	24	310	22.3	0.01	0.6	1.1
930302	2326	08.03	19-27.53	154-55.04	4.06	-0.58	22	8	0.5	0.00	0.0	0.0
930302	2347	06.75	19-31.32	154-56.79	19.99	0.60	35	264	7.8	0.04	0.3	0.6
930303	0022	47.57	19-27.62	154-54.86	2.77	-0.73	9	35	1.1	0.06	0.3	0.3
930303	0141	12.10	19-27.25	154-54.58	2.73	-0.15	11	23	2.9	0.00	0.3	0.4
930303	0258	23.44	19-28.36	154-55.39	5.00	-0.22	26	142	1.7	0.01	0.0	0.0
930303	0914	41.08	19-29.11	154-53.28	2.85	-0.99	19	168	0.4	0.01	0.0	0.1
930303	1242	22.14	19-28.69	154-53.09	5.23	-0.69	8	159	0.9	0.00	0.0	0.1
930303	1337	31.66	19-26.51	155-00.38	2.69	0.12	49	336	13.7	0.55	0.9	0.9
930303	1354	09.62	19-28.47	154-53.92	1.67	-0.64	14	82	0.6	0.08	0.1	0.2
930304	0602	32.83	19-27.30	154-54.47	7.46	-0.16	32	4	1.5	0.00	0.0	0.2
930304	0604	47.31	19-28.68	154-54.36	2.70	-0.56	18	68	1.2	0.18	0.0	0.0
930304	0915	41.36	19-27.37	154-55.62	4.51	-0.61	12	137	0.9	0.00	0.0	0.0
930304	1022	12.88	19-35.70	155-07.49	9.05	0.25	27	327	27.4	0.34	9.5	15.2
930304	1439	33.00	19-28.86	154-53.46	0.46	-0.46	11	54	0.1	0.04	0.0	0.0
930304	1940	03.99	19-28.56	154-53.77	2.07	-0.69	35	32	0.6	0.01	0.1	0.0
930304	2049	50.72	19-28.45	154-53.67	1.54	-0.98	16	73	0.4	0.13	0.2	0.2
930305	0243	25.27	19-26.81	154-53.08	4.73	-0.08	24	11	10.4	0.01	0.0	0.0
930305	0329	19.19	19-28.47	154-54.10	1.93	-0.43	11	50	0.4	0.12	0.2	0.2
930305	0943	44.01	19-51.50	156-07.28	5.00	-0.24	31	355	136.8	0.01	0.4	0.3
930305	2123	05.31	19-26.08	155-01.91	2.70	0.34	13	315	18.1	0.01	0.9	1.1
930306	0418	22.78	19-21.92	155-10.87	0.33	1.38	41	349	32.7	0.29	0.1	0.0
930306	0841	58.41	19-25.63	154-55.09	6.95	0.61	15	3	3.4	0.05	0.7	0.5
930306	0916	20.46	19-11.08	155-43.52	4.97	1.56	28	357	83.1	0.01	0.3	0.7
930306	1922	13.45	19-29.58	154-53.52	1.89	0.49	16	259	5.6	0.00	0.0	0.0
930307	0859	53.13	19-28.62	154-53.71	1.36	-0.76	8	58	0.7	0.01	0.0	0.0
930307	1239	19.33	19-28.18	154-54.16	2.18	-0.40	21	26	1.6	0.00	0.0	0.0
930307	1607	35.78	19-26.35	154-52.38	3.67	-0.26	25	10	5.5	0.13	0.6	1.3

930307	1650	10.98	19-28.72	154-54.10	2.57	0.54	42	67	3.4	0.49	0.3	0.2
930307	2055	18.68	19-26.66	154-54.71	7.36	0.41	11	12	1.8	0.4	0.5	0.4
930308	0311	10.64	19-14.05	155-15.87	5.00	2.35	25	354	36.6	4.89	0.7	0.2
930308	0839	57.71	19-21.35	154-43.10	2.70	0.86	37	338	22.5	0.46	0.6	1.9
930308	0930	59.44	19-27.98	154-52.72	4.55	-0.60	16	284	1.5	0.00	0.0	0.0
930308	0949	39.41	19-28.51	154-56.62	2.20	-0.64	13	225	7.3	0.00	0.2	0.1
930308	1029	48.18	19-16.92	155-20.26	0.00	2.07	48	353	51.6	0.34	4.5	2.0
930308	1327	43.99	19-28.51	154-53.81	2.21	-0.54	20	47	0.4	0.00	0.0	0.0
930308	1950	30.75	19-23.56	154-58.33	0.01	1.06	29	39	13.5	0.18	0.1	0.1
930308	2211	18.94	19-28.99	154-53.52	2.67	-0.45	20	81	1.2	0.00	0.0	0.0
930309	0656	07.97	19-28.49	154-53.79	1.73	-1.10	18	46	1.4	0.00	0.0	0.1
930309	0829	28.36	19-28.66	154-53.30	1.56	0.21	14	47	0.6	0.00	0.0	0.0
930309	0918	39.76	19-33.87	155-28.72	5.00	1.96	13	349	54.8	0.01	3.3	6.4
930309	1122	26.19	19-29.48	154-52.66	7.14	-0.43	20	208	1.6	0.09	0.9	0.4
930309	1304	49.28	19-23.67	154-53.51	5.00	0.17	22	4	10.2	0.00	0.1	0.1
930309	2316	57.45	19-29.36	154-51.93	2.01	-0.33	35	69	0.6	0.02	0.0	0.0
930310	0006	08.00	20-02.29	155-10.93	5.62	1.51	22	346	69.1	0.17	4.8	1.6
930310	0940	19.08	19-28.44	154-54.18	2.03	-0.30	17	50	0.9	0.11	0.1	0.2
930310	1244	40.26	19-29.86	154-53.48	3.77	-0.56	16	285	3.1	0.00	0.1	0.0
930310	1327	07.10	19-28.50	154-53.66	2.20	-0.01	29	17	0.5	0.18	0.0	0.0
930310	1333	43.23	19-28.44	154-53.74	2.69	-0.59	29	27	1.5	0.01	0.0	0.0
930310	1450	18.13	19-27.63	154-54.81	2.61	-0.55	15	18	0.9	0.07	0.2	0.1
930310	1548	31.17	19-27.96	154-55.72	3.59	0.20	36	236	1.2	0.01	0.0	0.1
930310	1617	25.65	19-27.93	154-55.31	3.17	-0.34	17	176	0.8	0.00	0.2	0.3
930310	2144	07.41	19-28.79	154-53.00	4.18	-0.60	22	96	2.3	0.02	1.3	0.0
930311	0247	50.68	19-28.32	154-53.56	2.16	-0.79	15	80	3.0	0.00	0.2	0.1
930311	0631	04.61	19-07.16	155-01.30	10.19	1.71	40	343	33.6	0.03	0.3	0.0
930311	0650	42.08	19-26.47	154-59.10	2.80	2.39	44	245	11.0	0.45	0.7	2.9
930311	1058	26.20	19-28.78	154-52.13	4.32	0.42	24	20	2.5	0.00	0.1	0.0
930311	2125	48.46	19-26.65	154-53.98	5.00	-0.20	22	6	2.5	0.00	0.0	0.0
930311	2232	57.42	19-29.61	154-54.89	2.71	-1.33	5	326	3.4	0.03	0.3	23.2

930312	0412	36.10	19-29.11	154-53.63	3.32	-0.85	19	139	1.4	0.01	0.0	0.0
930312	0801	56.82	19-28.89	155-06.33	32.10	0.81	19	327	21.1	0.00	0.3	0.4
930312	0825	52.96	19-23.14	154-54.42	2.33	-0.53	24	49	9.5	0.01	0.0	0.0
930312	0826	10.36	19-27.95	154-54.06	2.90	-0.27	24	20	9.8	0.00	0.0	0.0
930312	1102	19.15	19-28.59	154-54.02	1.99	-0.48	28	43	0.5	0.09	0.1	0.1
930312	1152	51.47	19-28.48	154-54.22	2.14	-0.85	22	64	10.1	0.00	0.0	0.0
930312	1310	24.93	19-25.65	154-55.80	4.70	0.20	37	108	9.4	0.00	0.0	0.0
930312	1716	24.68	19-27.20	154-54.03	5.00	-0.21	26	10	2.4	0.05	0.5	0.0
930212	1716	35.60	19-27.92	154-54.10	0.63	-0.64	27	17	3.3	47.64	0.1	0.0
930312	1754	42.19	19-27.57	154-54.84	3.94	-0.45	21	17	3.8	0.00	0.0	0.0
930312	1757	17.29	19-31.71	154-37.32	0.00	0.94	32	349	23.4	0.02	0.3	0.1
930312	2146	21.47	19-28.32	154-54.05	2.20	0.66	11	40	0.9	0.00	0.0	0.0
930312	2324	45.08	19-28.67	154-53.57	2.25	-0.13	13	59	0.9	0.00	0.1	0.1
930313	0026	10.07	19-28.34	154-52.94	2.91	-0.23	39	30	1.1	0.01	0.0	0.0
930313	0131	18.40	19-28.73	154-53.94	2.25	-0.50	16	105	2.6	0.01	0.0	0.4
930313	0429	05.87	19-27.50	154-55.82	3.77	-0.21	24	146	3.7	0.07	0.3	0.3
930313	0437	26.03	19-28.05	154-54.57	3.98	-0.24	30	28	2.3	0.00	0.0	0.0
930313	0545	48.15	19-27.76	154-53.44	5.00	-0.49	15	24	3.2	0.03	0.4	0.0
930313	0633	05.33	19-26.88	154-54.00	3.32	-0.18	30	9	2.2	0.16	0.1	0.2
930313	0734	21.14	19-28.10	154-54.75	5.00	0.15	13	65	1.5	0.00	0.0	0.1
930313	0914	43.68	19-27.62	154-54.46	2.79	-0.52	18	11	1.7	0.00	0.0	0.0
930313	1152	19.34	19-27.26	154-53.55	4.06	0.53	25	3	1.6	0.01	0.4	0.1
930313	1403	52.10	19-28.72	154-55.14	3.92	0.16	38	56	3.0	0.01	0.0	0.0
930313	1440	18.16	19-27.88	154-54.66	2.26	1.48	4	125	1.4	0.01	0.1	0.3
930313	1503	39.08	19-27.68	154-54.54	2.90	0.03	12	36	1.4	0.00	0.3	0.5
930313	1615	29.62	19-28.88	154-53.79	2.32	-0.83	20	103	0.2	0.12	0.2	0.2
930313	1623	09.28	19-28.70	154-53.91	3.00	-0.54	29	32	1.0	0.00	0.0	0.0
930313	1750	00.36	19-27.12	154-51.80	6.41	-0.67	14	29	4.8	0.00	0.3	0.3
930313	2028	19.76	19-28.45	154-54.05	1.87	-0.25	13	47	0.5	0.10	0.2	0.2
930313	2336	48.60	19-30.44	155-15.90	12.68	-0.09	11	343	38.3	0.00	1.9	0.4
930314	0036	34.37	19-13.78	155-16.10	2.64	1.80	39	355	49.1	0.55	0.1	0.1

930314	0117	27.66	19-28.51	154-53.82	1.27	-1.11	10	135	0.7	0.00	0.1	0.2
930314	0122	36.61	19-28.71	154-53.90	5.57	-0.22	32	63	3.1	0.05	0.4	1.9
930314	0211	55.29	19-27.39	154-54.93	3.16	-1.01	12	19	0.7	0.02	0.1	0.2
930314	0305	46.88	19-32.01	155-02.87	2.67	0.49	47	337	16.2	0.66	0.4	1.3
930314	0312	20.29	19-28.41	154-53.73	2.57	0.16	44	3	0.6	0.18	0.0	0.0
930314	0312	49.31	19-21.13	154-54.51	17.12	-0.40	43	2	17.9	0.31	7.2	5.7
930314	0335	02.04	19-27.23	154-56.53	2.69	0.86	48	157	5.4	0.40	0.1	1.2
930314	0335	56.20	19-26.67	154-53.42	2.46	-0.76	35	1	5.9	0.04	0.0	0.0
930314	0355	32.92	19-28.54	154-53.89	1.71	-0.05	16	47	0.4	0.00	0.0	0.1
930314	0401	23.92	19-28.44	154-53.79	2.70	0.48	23	26	0.9	0.00	0.1	0.0
930314	0409	40.06	19-28.85	154-53.86	2.65	-0.49	13	92	2.6	0.00	0.1	0.0
930314	0427	17.41	19-28.41	154-54.20	1.67	-0.16	13	48	0.3	0.00	0.1	0.1
930314	0546	17.64	19-28.72	154-53.88	2.48	-0.24	19	65	1.0	0.10	0.2	0.2
930314	0709	33.60	19-26.78	154-54.60	6.71	0.07	20	18	2.4	0.00	0.0	0.0
930314	0820	15.92	19-28.48	154-53.63	1.55	-0.28	8	45	1.2	0.02	0.0	0.1
930314	2104	29.89	19-28.41	154-50.97	7.94	0.15	20	65	1.8	0.12	1.1	0.6
930315	0008	08.85	19-28.27	154-53.83	2.04	-0.85	7	76	1.0	0.00	0.2	0.1
930315	0207	51.83	19-28.40	154-54.08	2.20	-0.49	21	45	0.5	0.08	0.1	0.2
930315	0301	31.04	19-28.75	154-53.91	2.69	-0.26	10	67	0.8	0.09	0.3	0.1
930315	0302	49.52	19-29.05	154-53.19	4.68	-0.55	36	168	2.2	0.07	0.1	0.0
930315	0343	06.19	19-27.64	154-55.19	3.31	-0.13	10	139	7.8	0.00	0.0	0.0
930315	0755	38.12	19-29.72	154-54.12	5.31	-0.13	24	162	0.9	0.01	0.2	0.1
930315	1003	26.10	19-28.66	154-56.95	2.69	0.24	16	321	4.6	0.02	0.4	2.5
930315	1757	46.14	19-28.86	154-54.24	2.24	-0.66	19	207	1.6	0.01	0.0	0.0
930315	1937	19.60	19-27.83	154-55.68	3.34	0.87	44	147	4.0	0.13	0.4	0.5
930315	2012	58.26	19-28.70	154-53.49	1.60	-1.57	18	45	0.6	0.00	0.0	0.0
930315	2152	18.75	19-27.91	154-53.91	2.66	-0.08	35	6	1.6	0.01	0.3	0.1
930316	0110	12.81	19-28.47	154-53.68	0.60	-0.88	6	101	1.2	0.04	0.1	0.2
930316	0208	20.69	19-03.71	155-00.35	11.52	1.37	20	346	39.7	0.01	0.4	0.1
930316	0444	46.20	19-28.49	154-54.33	1.91	-0.66	12	56	1.1	0.07	0.1	0.2
930316	1445	19.38	19-28.40	154-53.89	0.16	-0.24	32	19	0.8	0.03	0.0	0.0

930316	1641	41.32	19-27.97	154-52.43	5.91	-0.35	18	32	5.6	0.10	0.6	0.6
930316	1656	08.05	19-27.15	154-53.66	4.92	-0.27	3	40	1.2	0.01	0.2	0.0
930316	1659	15.11	19-21.16	154-45.86	2.65	-0.16	5	356	20.3	0.26	1.0	0.5
930316	1757	08.66	19-27.39	154-52.57	7.46	-0.41	13	33	5.9	0.01	0.8	0.5
930316	2139	12.08	19-27.54	154-54.81	3.31	-0.68	15	17	1.1	0.00	0.1	0.1
930316	2152	26.61	19-28.40	154-53.67	1.35	-0.28	14	41	0.4	0.00	0.0	0.2
930316	2203	12.47	19-28.59	154-53.49	2.38	0.96	8	125	1.0	0.00	0.0	0.0
930316	2212	06.20	19-28.64	154-53.52	2.20	-0.40	24	8	1.2	0.10	0.1	0.0
930316	2215	33.30	19-28.55	154-53.42	2.31	-0.20	42	8	0.7	0.06	0.0	0.0
930316	2215	58.79	19-28.55	154-53.46	1.62	-5.03	9	72	0.3	0.05	0.1	0.1
930316	2247	11.94	19-01.92	155-19.68	0.00	1.62	24	356	66.8	0.06	0.4	0.2
930316	2300	05.57	19-28.19	154-53.74	3.56	-0.02	49	19	0.6	0.01	0.0	0.0
930316	2357	19.17	19-28.52	154-53.75	2.16	-0.60	17	31	0.6	0.12	0.1	0.1
930317	0100	06.61	19-28.51	154-53.74	2.67	-0.49	28	2	1.4	0.01	0.0	0.0
930317	0209	18.49	19-28.57	154-53.04	6.37	-0.11	19	23	2.1	0.00	0.0	0.0
930317	0336	08.68	19-29.01	154-53.27	1.82	0.53	17	82	0.4	0.06	0.1	0.1
930317	0336	16.19	19-29.11	154-53.31	2.70	-0.33	14	93	1.9	0.11	0.3	0.1
930317	0432	53.99	19-18.83	155-12.76	2.77	1.04	12	353	36.5	0.13	0.4	86.9
930317	0547	32.66	19-32.54	155-04.63	2.69	-0.38	19	352	21.0	0.21	0.0	0.2
930317	0626	09.26	19-26.25	154-53.80	5.75	-0.01	28	5	3.2	0.00	0.1	0.0
930317	0653	35.82	19-29.15	154-53.20	4.30	-0.62	15	187	0.9	0.00	0.0	0.2
930317	0913	40.31	19-27.81	154-53.32	5.00	-0.77	28	17	3.0	0.07	0.4	0.0
930317	1356	25.21	19-28.52	154-53.49	4.90	-0.41	19	35	0.9	0.00	0.2	0.0
930317	1403	30.90	19-28.46	154-53.91	2.24	-0.02	29	20	0.8	0.08	0.1	0.2
930317	1405	49.35	19-29.46	154-53.51	3.05	-0.87	12	287	3.1	0.01	0.1	0.1
930317	1407	20.72	19-27.27	154-54.43	3.92	-0.31	15	8	2.7	0.00	0.0	0.0
930317	1410	17.37	19-32.06	154-54.75	2.69	-0.81	21	321	7.0	0.10	0.2	0.1
930317	1620	15.38	19-28.79	154-54.13	2.16	0.31	33	79	2.1	0.01	0.0	0.0
930317	1750	06.96	19-28.46	154-53.81	1.30	0.16	10	127	0.7	0.00	0.0	0.1
930317	1848	36.91	19-28.94	154-54.19	2.65	0.26	44	90	1.9	0.01	0.0	0.0
930317	2220	58.45	19-28.42	154-53.82	2.03	-0.95	7	158	0.9	0.00	0.2	0.1

930317	1959	40.74	19-28.33	154-55.19	5.00	-0.74	9	312	3.5	0.01	1.9	0.3
930318	0200	34.79	19-26.58	154-52.72	8.15	0.00	25	12	3.5	0.09	0.7	0.6
930318	0322	29.86	19-26.56	154-54.10	7.12	0.81	8	5	3.1	0.08	2.4	1.4
930318	0435	47.51	19-28.02	154-49.75	4.20	0.10	37	267	4.3	0.01	0.1	0.0
930318	0437	08.10	19-29.07	154-51.59	3.37	0.24	29	63	7.0	0.01	0.3	0.0
930318	1058	43.35	19-28.44	154-54.10	1.70	-0.56	10	53	0.4	0.00	0.0	0.1
930318	1206	24.33	19-29.34	154-54.12	3.51	-0.11	33	120	1.1	0.01	0.0	0.0
930318	1320	57.33	19-28.81	154-53.61	2.75	-0.75	26	18	2.8	0.01	0.2	0.1
930318	1503	48.56	19-28.13	154-52.54	6.37	-0.69	11	60	2.0	0.07	0.7	0.5
930318	2245	53.73	19-28.17	154-53.52	2.71	-0.58	32	5	1.1	0.23	0.0	0.0
930319	0531	15.30	19-28.24	154-53.99	2.69	0.08	34	13	0.9	0.00	0.0	0.0
930319	0933	04.00	19-24.52	155-13.39	0.01	1.42	34	346	34.9	0.07	1.1	0.3
930320	0127	35.52	19-24.11	154-54.07	5.13	0.39	40	2	8.0	0.01	0.1	0.1
930320	0410	33.37	19-28.59	154-54.02	1.84	0.10	9	5	0.8	0.04	0.1	0.1
930320	0929	34.45	19-28.42	154-52.88	6.61	0.04	7	129	0.3	0.00	0.0	0.0
930320	1404	18.51	19-26.64	154-54.78	7.35	0.47	13	9	6.3	0.11	0.9	0.8
930320	1413	03.83	19-28.34	154-54.17	2.28	-0.32	18	39	0.4	0.07	0.1	0.1
930320	2042	24.62	19-27.79	154-53.28	2.52	-0.07	28	14	1.8	0.01	0.0	0.0
930320	2351	37.40	19-21.67	155-07.94	2.57	1.31	14	352	17.4	0.50	0.5	0.2
930321	0141	29.20	19-28.34	154-53.35	3.49	-0.19	31	29	1.0	0.01	0.3	0.3
930321	0158	55.91	19-36.11	155-15.96	3.47	1.20	6	357	39.2	0.00	0.6	9.1
930321	0357	25.37	19-28.09	154-52.62	5.73	0.17	11	31	2.0	0.06	0.5	0.4
930321	0424	26.97	19-28.46	154-53.01	3.11	-0.02	21	45	1.4	0.00	0.0	0.1
930321	0700	19.67	19-28.24	154-53.41	2.52	-0.24	36	26	3.0	0.01	0.0	0.0
930321	0832	07.12	19-28.46	154-53.83	1.71	1.67	8	125	0.8	0.05	0.1	0.2
930321	2131	18.10	19-25.20	154-56.23	1.40	-0.03	20	333	4.5	1.85	0.3	0.0
930321	2316	08.75	19-27.65	154-54.68	2.82	0.65	22	20	1.1	0.00	0.1	0.1
930321	2316	17.46	19-27.74	154-54.89	2.71	1.68	13	18	1.8	0.00	0.1	0.0
930322	0002	18.53	19-27.52	154-54.64	3.51	-0.19	23	18	8.5	0.00	0.1	0.1
930322	0012	09.97	19-26.79	154-55.64	6.18	0.38	11	325	4.0	0.00	0.6	0.4
930322	0247	16.86	19-28.19	154-52.00	6.99	0.06	21	40	3.4	0.11	0.6	0.6

930322	0811	52.04	19-26.22	154-54.34	6.20	0.07	15	15	7.1	0.00	0.3	0.1
930322	1306	05.77	19-30.23	154-55.45	2.70	1.96	17	289	5.9	0.04	0.1	6.4
930322	1455	58.08	19-28.45	154-54.31	2.70	0.36	47	32	1.0	0.02	0.1	0.1
930322	1806	27.30	19-28.80	154-53.10	3.02	-0.44	29	32	0.2	0.01	0.0	0.0
930322	1806	46.12	19-23.20	154-52.74	2.78	-0.99	24	1	10.4	0.10	0.5	24.5
930322	1956	37.11	19-28.56	154-53.78	2.51	-0.61	24	80	0.7	0.10	0.1	0.1
930323	0352	35.04	19-28.26	154-54.13	2.09	-0.69	14	38	1.1	0.00	0.2	0.0
930323	0452	57.56	19-28.07	154-52.30	6.03	0.02	23	51	1.7	0.00	0.5	0.3
930323	0614	00.76	19-29.00	154-53.58	11.09	0.28	33	27	2.4	0.01	0.0	0.1
930323	0942	39.94	19-27.24	154-54.24	5.00	-0.41	19	17	2.5	0.04	0.6	0.0
930323	1114	54.43	19-28.58	154-53.47	2.20	-0.47	41	12	1.0	0.01	0.1	0.0
930323	1244	58.24	19-27.33	154-54.59	2.20	-0.70	21	17	1.4	0.01	0.0	0.0
930323	1329	01.10	19-27.90	154-54.73	2.48	-0.48	9	24	0.5	0.03	0.1	0.1
930323	2054	32.14	19-22.26	155-01.44	2.98	1.04	20	346	17.3	0.01	0.1	3.1
930324	0753	18.05	19-28.47	154-53.94	1.74	-0.32	14	113	2.0	0.09	0.1	0.2
930324	0950	05.45	19-28.67	154-53.69	2.31	-0.40	25	45	1.3	0.12	0.2	0.3
930324	1032	06.24	19-27.47	154-54.44	8.80	-0.04	19	7	3.9	0.00	0.8	0.4
930324	1048	35.46	19-28.24	154-54.37	2.48	-0.53	13	48	0.6	0.00	0.0	0.0
930325	0702	13.77	19-23.91	155-11.43	2.61	0.85	11	346	29.2	0.46	0.0	0.0
930325	1325	25.27	19-26.36	154-53.27	7.35	-0.13	11	7	5.1	0.00	0.3	0.3
930325	1514	19.73	19-28.38	154-53.80	1.56	0.20	16	31	0.6	0.00	0.0	0.1
930325	1746	30.98	19-30.12	154-31.93	11.68	1.66	25	348	37.1	0.02	0.4	0.3
930326	1414	03.80	19-29.42	154-55.52	2.74	0.99	19	215	8.8	0.05	0.0	2.2
930326	1623	17.32	19-28.52	154-53.61	1.99	-0.81	12	48	1.2	0.00	0.0	0.0
930328	0536	33.38	19-29.04	154-54.01	3.03	-0.18	42	42	1.1	0.01	0.0	0.0
930328	1132	23.88	19-29.15	154-53.94	2.34	-0.20	22	124	1.6	0.00	0.0	0.0
930328	1206	44.64	19-32.72	155-13.43	0.00	1.69	36	339	29.2	0.46	4.3	1.0
930328	1257	39.93	19-28.27	154-54.35	1.87	0.45	15	58	1.6	0.08	0.1	0.2
930328	1259	43.48	19-58.97	154-48.73	6.65	-0.69	18	356	56.8	0.29	3.2	39.3
930328	1259	53.81	19-27.76	154-55.48	0.11	-1.57	8	307	0.3	****	0.4	0.1
930328	1302	48.26	19-28.17	154-54.29	3.92	-0.18	34	21	0.4	0.00	0.0	0.0

930328	1309	20.58	19-28.44	154-54.28	4.07	-0.10	21	30	0.6	0.00	0.0	0.0
930329	0252	52.15	19-28.15	154-53.56	2.20	0.38	42	10	0.7	0.01	0.0	0.0
930329	0300	04.13	19-28.60	154-53.54	2.91	0.10	10	121	2.7	0.12	0.3	0.6
930329	0350	07.43	19-27.93	154-51.57	7.38	-0.12	22	49	5.5	0.00	0.0	0.1
930329	0417	53.46	19-27.93	154-54.47	2.15	-0.46	19	22	1.5	0.00	0.0	0.0
930329	0512	18.36	19-28.90	154-54.63	5.00	-0.62	14	211	2.3	0.02	3.0	0.2
930329	1159	01.27	18-25.02	154-54.09	91.30	2.72	26	3	111.3	0.00	0.4	0.3
930329	1935	53.60	19-28.64	154-53.88	2.19	-0.35	21	30	3.5	0.08	0.1	0.0
930330	0251	55.24	19-27.64	154-55.17	3.06	-0.41	21	14	0.4	0.00	0.0	0.0
930330	0353	57.72	19-27.55	154-54.70	2.43	-0.39	10	36	2.0	0.00	0.1	0.0
930330	0439	55.19	19-27.52	154-55.04	2.62	-0.82	14	9	7.9	0.06	0.3	0.1
930330	1020	59.04	19-29.21	154-52.85	4.96	0.03	19	112	3.6	0.00	0.0	0.0
930330	1037	07.19	19-13.43	155-29.84	5.00	1.68	3	357	67.8	0.15	1.5	0.2
930330	1455	47.04	19-27.99	154-53.82	4.55	0.24	14	74	0.4	0.00	0.0	0.0
930330	2254	34.20	19-28.45	154-53.90	1.49	-0.71	10	116	2.1	0.00	0.0	0.0
930331	0406	10.97	19-28.61	154-53.67	2.07	-0.72	22	107	0.7	0.10	0.1	0.1
930331	0601	55.69	19-28.63	154-54.48	3.96	-0.74	17	68	2.0	0.00	0.0	0.0
930331	0614	11.35	19-26.42	154-51.88	2.69	-0.65	11	326	4.1	0.05	0.1	3.3
930331	0618	39.71	19-28.17	154-54.33	0.48	-0.57	10	46	1.2	0.12	0.1	0.1
930331	0622	58.08	19-28.19	154-54.24	2.20	-1.03	13	37	1.1	0.08	0.2	0.0
930331	0632	12.91	19-31.57	154-53.22	2.68	-0.55	26	309	5.9	0.04	0.1	2.5
930331	0635	57.38	19-29.32	154-54.15	2.30	-0.90	24	39	0.7	0.09	0.1	0.1
930331	0636	28.60	19-28.37	154-53.86	2.07	1.59	15	148	1.2	0.00	0.0	0.0
930331	0636	44.69	19-28.36	154-54.24	2.41	0.79	10	45	2.2	0.08	0.2	0.3
930331	0637	01.54	19-28.38	154-53.99	2.38	-0.42	18	73	0.6	0.09	0.1	0.2
930331	0637	47.98	19-28.51	154-54.04	3.50	0.15	32	7	1.7	0.03	0.1	0.0
930331	0638	12.76	19-28.56	154-54.93	4.06	-0.45	29	54	2.3	0.01	0.0	0.1
930331	0638	58.26	19-27.93	154-53.95	2.63	-0.80	29	10	2.3	0.01	0.0	0.0
930331	0639	06.42	19-28.55	154-53.95	3.88	-0.30	24	21	1.1	0.00	0.0	0.1
930331	0639	50.27	19-28.35	154-54.55	3.93	-0.57	19	46	1.7	0.00	0.0	0.0
930331	0640	10.68	19-28.34	154-54.10	2.72	0.00	27	41	0.8	0.00	0.1	0.1

930331	0640 40.35	19-28.07	154-54.44	2.83	-0.71	12	103	1.1	0.26	0.7	1.0
930331	0641 42.99	19-28.22	154-53.92	2.69	-0.02	11	130	1.0	0.00	0.1	0.1
930331	0641 52.17	19-28.14	154-54.17	3.74	-0.44	11	34	0.4	0.00	0.0	0.0
930331	0642 38.10	19-27.96	154-54.23	2.15	-0.04	12	56	1.9	0.06	0.1	0.1
930331	0642 50.10	19-28.06	154-54.38	1.29	-0.70	7	109	1.3	0.00	0.0	0.2
930331	0643 18.00	19-28.36	154-54.53	4.19	-0.60	19	68	0.5	0.00	0.1	0.1
930331	0644 51.11	19-28.20	154-54.08	2.24	-0.87	13	44	0.8	0.07	0.2	0.2
930331	0645 30.43	19-28.23	154-54.15	2.20	-0.39	18	30	0.6	0.01	0.1	0.0
930331	0650 26.07	19-28.24	154-54.23	2.28	-0.53	12	23	0.6	0.07	0.1	0.2
930331	0650 51.90	19-29.16	154-52.22	2.69	-0.45	8	311	2.6	0.57	1.8	1.4
930331	0654 19.14	19-28.74	154-54.20	2.46	0.13	29	78	1.3	0.01	0.0	0.0
930331	0656 33.88	19-28.25	154-54.25	2.27	-0.61	24	21	0.5	0.00	0.0	0.0
930331	0658 01.09	19-27.72	154-54.55	3.29	0.11	19	12	1.6	0.00	0.2	0.0
930331	0659 19.88	19-28.40	154-54.08	2.61	-0.51	10	142	1.1	0.11	0.3	0.1
930331	0702 07.82	19-29.87	155-03.82	2.08	-0.77	9	351	17.5	0.15	0.5	0.1
930331	0702 42.91	19-27.86	154-53.67	4.41	0.14	5	270	0.7	0.00	0.0	0.0
930331	0707 49.70	19-28.30	154-54.18	2.47	-0.49	23	34	2.6	0.09	0.1	0.1
930331	0708 01.66	19-28.31	154-54.23	1.79	-0.90	15	55	0.6	0.07	0.1	0.1
930331	0710 38.77	19-27.69	154-53.87	2.80	-0.75	17	34	1.3	0.00	0.0	0.0
930331	0736 52.69	19-28.27	154-54.06	1.85	0.07	14	37	0.7	0.09	0.1	0.2
930331	0742 59.27	19-27.80	154-53.92	2.17	-0.87	13	112	1.5	0.00	0.0	0.0
930331	0743 12.58	19-28.26	154-54.26	2.20	-0.84	13	54	1.3	0.00	0.1	0.2
930331	0744 20.84	19-28.47	154-54.09	2.70	-0.09	15	54	0.4	0.04	0.0	0.0
930331	0745 03.41	19-28.14	154-54.32	1.63	-0.04	12	21	1.9	0.09	0.1	0.1
930331	0745 15.28	19-28.29	154-54.21	2.37	-1.03	17	42	0.6	0.10	0.2	0.3
930331	0745 31.48	19-26.79	154-50.51	5.00	-1.23	3	339	8.6	0.00	0.3	0.5
930331	0745 54.80	19-28.24	154-54.14	1.88	-0.32	13	49	2.3	0.10	0.2	0.2
930331	0802 16.48	19-27.80	154-55.05	5.00	-0.23	14	113	1.1	0.03	0.6	0.1
930331	1434 19.55	19-26.38	154-55.50	7.47	0.07	13	116	5.5	0.00	0.1	0.1
930331	1609 28.27	19-28.14	154-54.37	2.24	-0.68	12	20	2.1	0.08	0.2	0.2
930331	1804 07.13	19-25.73	155-00.22	3.28	1.25	25	302	14.1	0.27	3.8	0.5

930331	2059 45.40	19-28.44	154-53.96	1.75	-0.41	11	140	0.6	0.06	0.1	0.2
930331	2205 38.99	19-28.36	154-54.71	1.63	-0.05	10	155	2.3	0.06	0.1	0.1
930401	1854 35.15	19-28.03	154-51.99	5.00	-0.49	11	263	3.2	0.02	0.9	0.1
930401	1855 53.94	19-28.20	154-52.67	4.75	-0.55	21	60	1.4	0.01	0.2	0.0
930401	1906 20.82	19-28.82	154-53.18	1.53	-0.73	7	130	1.6	0.00	0.2	0.2
930401	2149 01.63	19-28.43	154-54.43	1.92	-1.11	11	135	2.0	0.07	0.1	0.1
930401	2149 21.05	19-27.51	154-54.94	5.00	1.35	7	328	1.8	0.01	0.5	0.2
930401	2157 51.62	19-28.49	154-53.97	2.20	-0.69	20	46	2.0	0.12	0.1	0.2
930401	2159 40.69	19-28.53	154-54.36	1.86	-0.80	6	171	1.8	0.04	0.3	0.2
930401	2224 43.73	19-28.70	154-53.66	2.29	-0.75	25	54	0.7	0.01	0.0	0.1
930402	0724 34.97	19-28.36	154-53.88	1.23	-0.89	6	103	0.7	0.01	0.0	0.0
930402	0911 57.73	19-29.49	154-54.35	5.00	-0.93	9	302	2.6	0.01	2.9	0.3
930402	1015 45.82	19-26.59	154-53.46	7.77	-0.15	13	13	2.7	0.07	0.6	0.5
930402	1213 15.37	19-18.10	155-10.37	2.51	1.18	12	357	35.2	0.23	0.0	0.0
930402	1223 46.77	19-27.27	154-54.11	9.56	-0.30	27	4	8.1	0.01	1.2	0.1
930402	1306 40.33	19-27.25	154-52.69	5.10	-0.26	14	8	3.5	0.07	0.6	0.6
930402	1324 29.15	19-29.64	154-50.06	2.84	-0.80	10	339	9.9	0.05	0.6	0.4
930402	1343 11.29	19-28.67	154-54.45	3.00	-0.21	30	41	1.5	0.01	0.2	0.2
930402	1412 20.10	19-28.84	154-53.60	0.40	-0.03	5	101	0.3	0.13	0.1	0.4
930402	1633 23.42	19-28.48	154-54.16	1.84	-0.82	17	14	1.9	0.10	0.1	0.2
930402	1910 18.95	19-28.85	154-54.13	2.68	-0.35	31	28	1.0	0.02	0.0	0.0
930402	1940 31.54	19-29.04	154-52.67	5.00	-0.84	3	296	2.4	0.00	0.0	0.0
930403	0255 06.95	19-05.63	155-16.80	6.95	2.26	17	356	60.0	0.00	0.2	0.5
930403	0524 44.39	19-28.14	154-54.08	2.50	0.42	13	29	0.8	0.07	0.2	0.2
930403	0652 18.59	19-27.45	154-55.07	2.78	0.39	18	38	0.4	0.06	0.3	0.3
930406	2333 14.30	19-21.94	155-14.27	2.69	1.80	36	350	37.9	0.26	0.3	0.1
930407	0237 09.24	19-28.61	154-54.20	1.68	-1.13	12	21	0.4	0.00	0.0	0.0
930407	0420 42.28	19-26.83	154-51.64	7.36	0.39	34	265	4.7	0.01	0.0	0.2
930407	0452 11.94	19-29.39	154-54.29	5.00	-0.92	10	313	2.5	0.02	0.9	0.1
930407	0522 33.38	19-29.86	154-56.59	2.70	-0.23	32	297	6.1	0.18	0.0	0.2
930407	0718 38.39	19-28.48	154-54.11	2.22	-0.90	12	51	0.9	0.07	0.2	0.2

930407	0840	37.67	19-21.09	154-59.19	37.05	0.03	8	325	19.2	0.03	2.3	0.5
930407	1008	18.47	19-28.02	154-53.57	2.23	-0.66	17	27	0.7	0.01	0.0	0.0
930407	1125	22.19	19-28.59	154-53.79	2.35	0.82	42	28	0.7	0.01	0.0	0.0
930407	1126	23.79	19-28.30	154-54.34	1.31	0.32	12	30	2.5	0.00	0.0	0.0
930407	1223	19.16	19-28.82	154-53.55	1.48	-0.38	31	12	0.4	0.01	0.1	0.0
930407	1320	29.74	19-28.90	154-59.45	3.06	1.45	33	268	7.1	0.01	0.2	0.8
930407	1403	47.03	19-24.00	154-58.11	4.98	1.09	24	53	14.0	0.01	0.5	0.7
930407	1619	39.11	19-30.29	154-51.26	5.00	0.05	22	276	4.2	0.01	0.0	0.2
930407	1953	21.77	19-25.96	154-55.60	4.99	-0.02	12	111	6.3	0.05	0.5	0.6
930407	2041	38.28	19-43.29	155-09.81	11.54	1.13	9	355	39.1	0.09	1.2	0.4
930407	2309	38.91	19-27.65	154-54.80	2.29	0.42	25	19	1.8	0.08	0.2	0.1
930407	2310	57.66	19-27.39	154-55.13	2.52	-2.51	16	10	0.3	0.05	0.2	0.1
930407	2311	40.90	19-27.37	154-54.96	3.19	-0.04	12	7	2.5	0.05	0.3	0.3
930407	2315	08.03	19-27.92	154-55.53	3.55	0.89	11	216	2.5	0.00	0.0	0.0
930407	2317	07.77	19-27.53	154-54.76	2.55	0.09	13	18	1.8	0.00	0.2	0.1
930407	2319	13.72	19-27.18	154-54.54	3.96	0.91	36	5	1.4	0.01	0.0	0.0
930407	2323	35.97	19-27.68	154-54.79	3.01	-0.46	6	50	2.0	0.00	0.2	0.1
930407	2335	30.67	19-27.66	154-54.81	2.58	-0.33	19	19	0.9	0.00	0.1	0.0
930408	0026	19.16	19-28.46	154-53.55	1.05	-0.95	7	104	1.0	0.04	0.1	0.1
930408	0029	43.22	19-28.41	154-53.67	1.50	-0.97	13	42	0.8	0.00	0.1	0.0
930408	0237	53.06	19-27.47	154-55.07	2.90	-0.45	19	9	1.5	0.00	0.1	0.1
930408	0537	03.28	19-28.80	154-52.83	6.48	-0.11	10	119	1.9	0.00	0.7	0.3
930408	1053	20.06	19-29.14	154-52.61	6.07	-0.14	12	260	2.1	0.08	1.1	0.5
930408	1259	06.65	19-27.98	154-52.16	7.47	0.33	26	12	1.9	0.13	0.9	0.6
930408	1805	47.21	19-22.30	155-06.95	2.69	1.62	14	347	15.4	0.12	0.9	0.3
930408	2303	17.44	19-29.74	154-52.83	4.70	0.18	25	155	4.3	0.01	0.4	0.4
930409	0050	41.55	19-27.84	154-51.58	6.65	0.69	39	32	3.4	0.01	0.0	0.1
930409	0427	12.93	19-21.50	155-14.37	8.89	1.28	16	354	37.7	00.0	1.4	1.7
930409	0639	04.91	19-29.28	154-54.06	3.08	-0.83	14	187	1.0	0.00	0.0	0.1
930409	0813	35.74	19-32.90	154-49.74	20.08	1.56	24	319	5.6	0.11	6.4	7.4
930409	1114	49.19	19-28.37	154-54.49	2.70	-0.81	20	68	1.5	0.01	0.0	0.0

930409	1302	35.22	19-32.80	155-16.23	10.41	1.55	30	341	33.6	0.01	0.1	0.3
930410	0550	53.81	19-28.45	154-52.41	3.38	0.02	19	44	1.1	0.11	0.5	0.8
930410	0615	03.87	19-28.38	154-53.58	3.43	0.11	19	62	2.4	0.01	0.0	0.0
930410	1348	37.38	19-24.87	154-53.96	5.00	-0.44	14	7	6.8	0.00	0.0	0.1
930410	2319	55.60	19-28.32	154-53.79	1.50	-1.12	8	36	1.0	0.06	0.1	0.1
930410	2324	16.29	19-28.19	154-53.47	3.15	-1.14	6	110	1.4	0.00	0.0	0.0
930411	0215	06.82	19-26.77	154-52.87	5.69	-0.30	12	6	3.6	0.00	0.6	0.5
930411	0333	38.34	19-27.65	154-55.12	2.77	-0.32	17	12	2.6	0.00	0.1	0.2
930411	0554	17.60	19-26.96	154-55.25	3.70	-0.18	15	3	3.9	0.08	0.2	0.3
930411	1552	38.08	19-26.09	154-53.45	8.59	0.00	22	2	3.6	0.10	0.9	0.8
930411	2037	29.25	19-27.47	154-53.30	7.79	0.36	1	39	1.0	0.07	1.1	0.6
930412	0003	39.84	18-51.92	154-53.67	1.31	-0.83	4	359	68.4	0.10	0.4	82.4
930412	0124	41.24	19-15.12	155-16.07	5.00	0.23	3	358	46.4	0.04	11.4	73.0
930412	0242	37.28	19-35.35	155-07.57	2.60	0.78	6	357	25.6	0.34	0.5	0.2
930412	0549	07.23	19-27.41	155-18.62	10.63	2.53	32	354	41.5	0.01	0.3	0.5
930412	0957	08.65	19-27.27	154-53.84	3.51	0.10	14	10	0.9	0.01	0.0	0.0
930412	1001	27.50	19-28.05	154-54.00	2.49	-0.50	26	10	0.6	0.11	0.1	0.0
930412	1014	05.59	19-28.14	154-53.95	2.08	-0.64	12	12	0.4	0.00	0.0	0.0
930412	1020	33.12	19-45.26	154-59.62	12.99	1.27	28	351	31.8	0.01	2.1	0.2
930412	1028	26.10	19-28.12	154-53.00	2.64	-0.10	29	6	1.7	0.33	2.0	0.1
930412	1301	58.82	19-28.75	154-53.31	1.22	-0.97	11	56	2.2	0.09	0.1	0.3
930412	1518	45.03	19-28.60	154-53.62	1.52	-1.03	9	21	0.7	0.06	0.1	0.1
930413	0434	05.53	19-28.67	154-53.73	1.65	-0.58	8	33	0.2	0.02	0.1	0.1
930413	0925	59.79	19-28.73	154-53.70	2.19	-0.24	20	33	0.4	0.09	0.1	0.0
930413	1057	26.10	19-28.51	154-53.74	2.20	-0.01	11	7	0.4	0.00	0.0	0.0
930413	2105	43.57	19-28.46	154-53.57	1.71	-0.63	6	44	0.9	0.04	0.1	0.2
930414	0254	43.74	19-13.42	155-04.27	39.48	1.94	10	355	33.7	0.00	0.1	0.1
930414	0514	38.13	19-28.15	154-54.54	2.65	-0.32	7	332	1.4	0.01	0.1	0.1
930415	0335	00.72	19-21.89	155-13.85	2.73	1.98	9	355	37.1	0.08	0.2	99.8
930415	0404	17.30	19-25.85	154-54.59	2.70	0.45	6	336	5.4	0.06	0.2	99.9
930415	1146	18.09	19-28.74	154-53.33	0.00	1.01	5	58	0.3	****	0.1	1.2

930416	0532	27.34	19-28.24	154-55.16	2.53	-0.19	14	311	2.2	0.00	0.6	0.2
930416	1553	58.60	19-28.65	154-53.16	1.73	0.14	13	40	0.8	0.00	0.0	0.0
930417	1346	15.28	19-28.39	154-51.95	7.00	0.75	16	312	2.4	0.00	0.1	0.2
930418	0324	02.36	19-28.97	154-54.18	1.60	-0.21	10	267	0.9	0.05	0.2	0.1
930418	0737	00.12	19-28.79	154-53.52	0.67	-0.64	4	48	0.2	0.00	0.0	0.0
930418	0737	57.22	19-21.65	154-58.68	2.69	0.00	6	355	15.8	0.03	0.7	99.9
930418	0738	07.50	19-28.28	154-53.41	3.69	0.09	8	5	1.0	0.00	0.5	0.1
930418	0741	47.99	19-28.83	154-54.62	0.61	-0.59	5	301	1.5	0.04	0.3	52.2
930418	0748	11.71	19-28.88	154-53.88	1.50	-0.25	102	232	0.3	0.05	0.2	0.1
930418	2043	17.31	19-26.10	154-55.42	2.73	0.61	7	352	6.6	0.00	0.3	15.4
930420	1255	21.77	19-09.47	154-45.98	11.45	0.84	4	358	38.0	0.01	4.9	0.1
930420	2141	35.45	19-05.81	155-12.05	0.81	-0.45	4	360	53.5	0.04	0.3	0.0
930421	0207	44.30	19-27.69	154-54.52	0.60	0.01	7	344	2.4	0.22	0.2	0.1
930421	1227	36.74	19-28.88	154-53.94	1.29	-0.34	11	246	0.4	0.06	0.1	0.1
930423	0209	27.48	19-28.81	154-54.13	5.00	-0.40	9	277	0.7	0.56	14.4	0.1
930424	1126	39.34	19-28.81	154-53.65	2.69	-0.50	5	21	0.2	0.00	0.0	0.0
930425	1414	18.31	19-27.84	154-53.21	5.00	0.20	12	341	1.9	0.01	0.4	0.0
930425	1543	39.90	19-27.89	154-54.08	3.99	-0.50	5	333	1.7	0.01	0.8	0.6
930426	0111	43.57	19-29.09	154-53.86	1.41	0.30	9	205	0.6	0.04	0.1	0.1
930426	0432	19.60	19-28.98	154-54.00	1.56	-0.27	7	241	0.6	0.05	0.3	0.2
930426	0447	09.35	19-28.65	154-53.75	2.82	-0.42	5	275	0.2	0.00	0.1	0.0
930426	0809	02.37	19-21.77	154-57.64	4.99	0.94	8	357	14.7	0.20	1.1	0.2
930426	1351	55.18	19-28.94	154-53.92	2.27	-0.59	5	232	0.4	0.01	0.1	0.1
930426	2111	57.48	19-25.18	154-56.63	2.67	0.37	6	349	8.4	0.02	0.7	99.9
930427	0303	22.35	19-27.79	154-51.65	1.79	-0.29	4	337	3.5	0.01	0.3	0.0
930427	0535	55.33	19-12.13	154-43.48	2.38	-0.45	4	358	35.4	0.01	0.0	0.0
930428	1023	25.54	19-27.14	154-55.22	1.83	-0.15	6	340	4.0	0.02	0.4	0.0

APPENDIX III. Selected Focal Mechanisms, Kilauea Lower East Rift Zone

Compressional (up) arrivals on the vertical component are plotted as filled circles on an equal area stereographic projection, lower hemisphere; dilatational (down) arrivals are plotted as open squares. Date and time of earthquake, epicenter and depth are listed at the top of each diagram. Strike and dip of the nodal planes is given at the bottom of the diagram, together with azimuth and plunge of poles. Nodal planes separate quadrants of predominantly compression motion from those with predominantly dilational motion.

93/01/30 0838:25.82 19 28.71 N 154 53.78 W 2.49 km

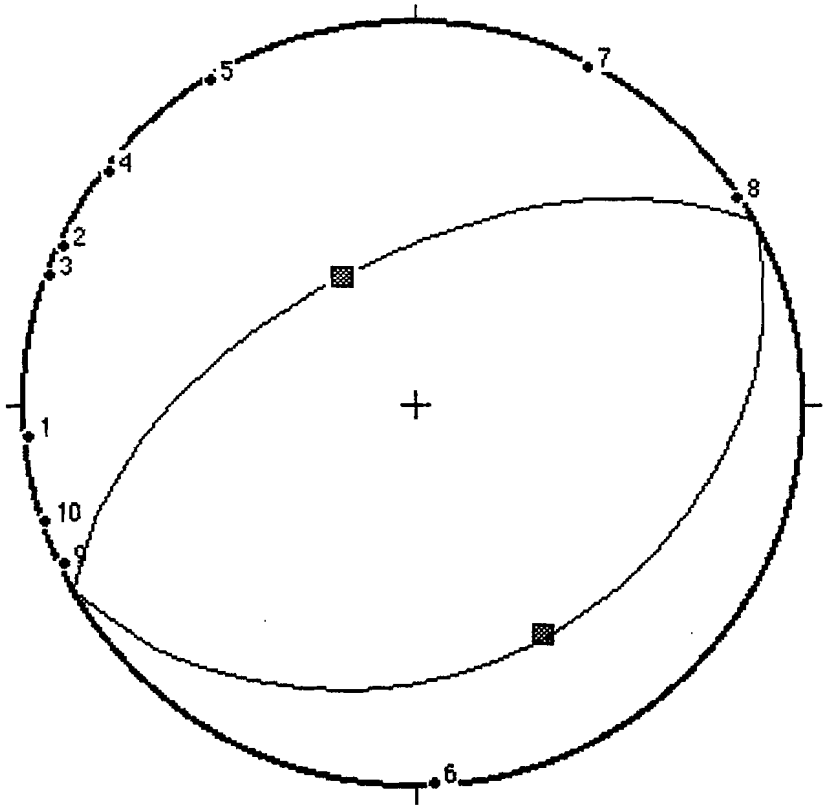

Nodal Plane-1: 241/58 N
Pole-1: 151/32
Nodal Plane-2: 062/31 S
Pole-2: 333/59

93/01/30 1615:00.43 19 23.55 N 154 51.72 W 5.00 km

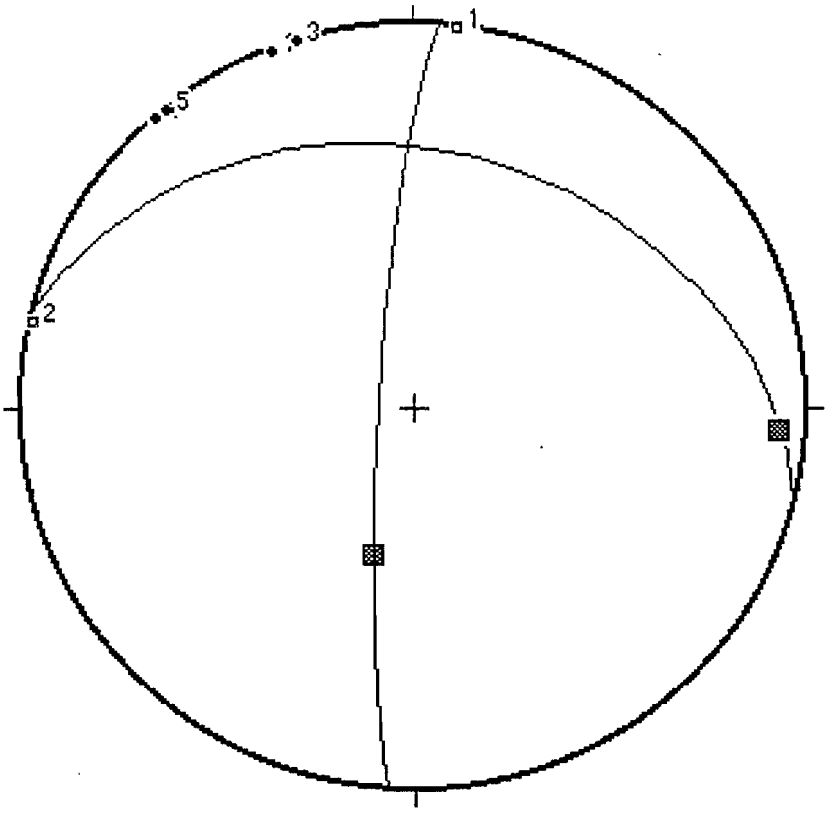

Nodal Plane-1: 285/33 N
Pole-1: 195/57
Nodal Plane-2: 184/83 W
Pole-2: 094/07

93/02/12 0344:25.66 19 28.03 N 154 54.54 W 2.70 km

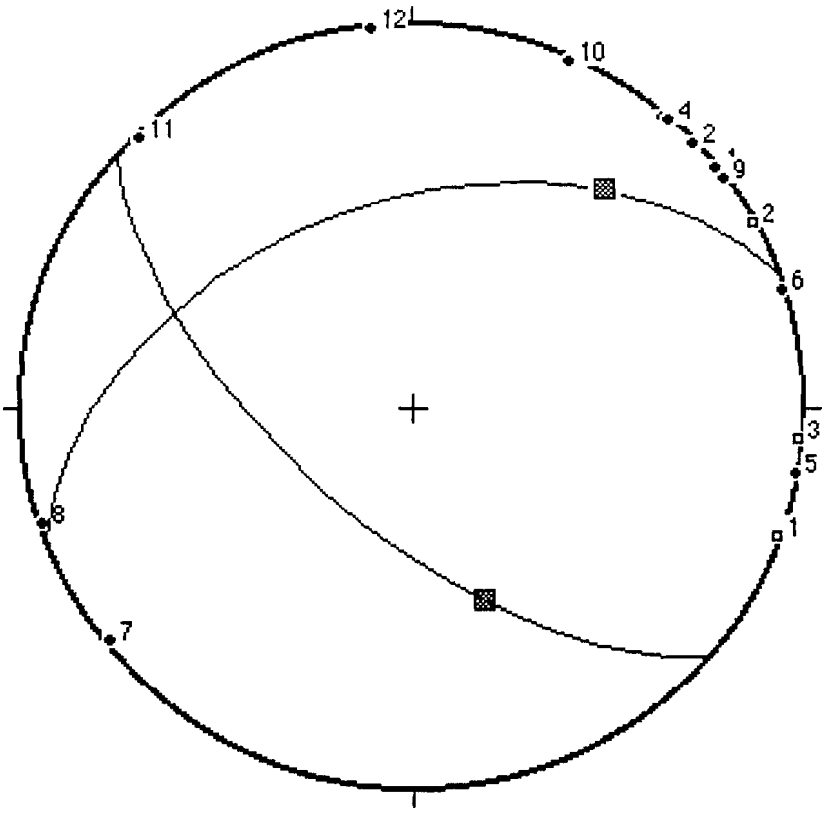

Nodal Plane-1: 250/45 N
Pole-1: 160/45
Nodal Plane-2: 131/64 S
Pole-2: 041/26

93/02/12 0347:13.35 19 27.80 N 154 54.22 W 4.00 km

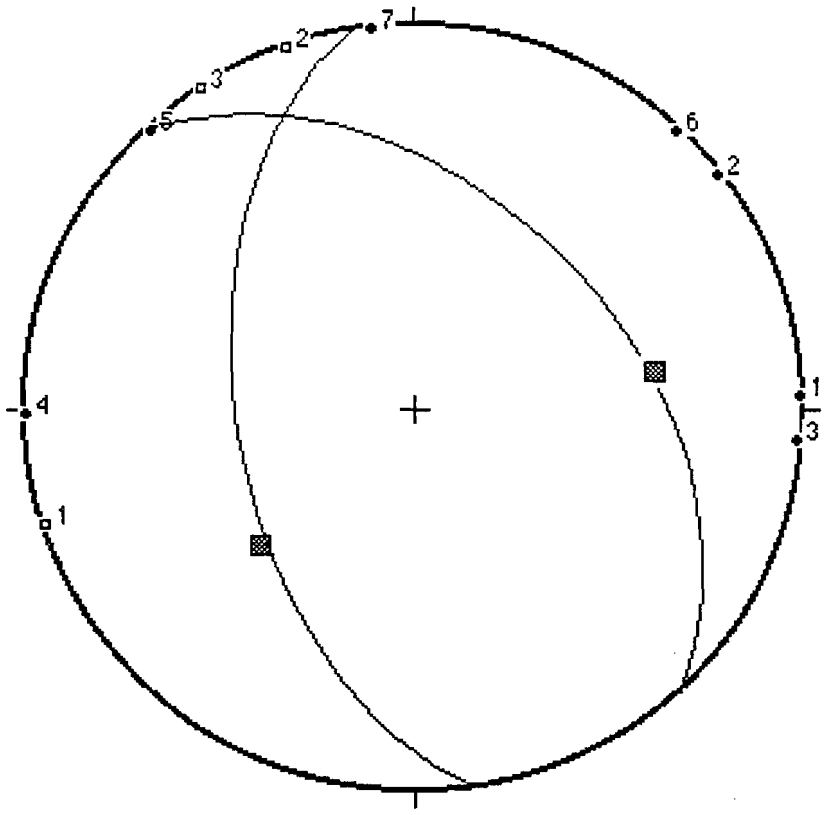

Nodal Plane-1: 317/44 E
Pole-1: 227/46
Nodal Plane-2: 171/53 W
Pole-2: 081/37

93/02/12 1010:33.41 19 25.33 N 154 54.71 E 5.00 km

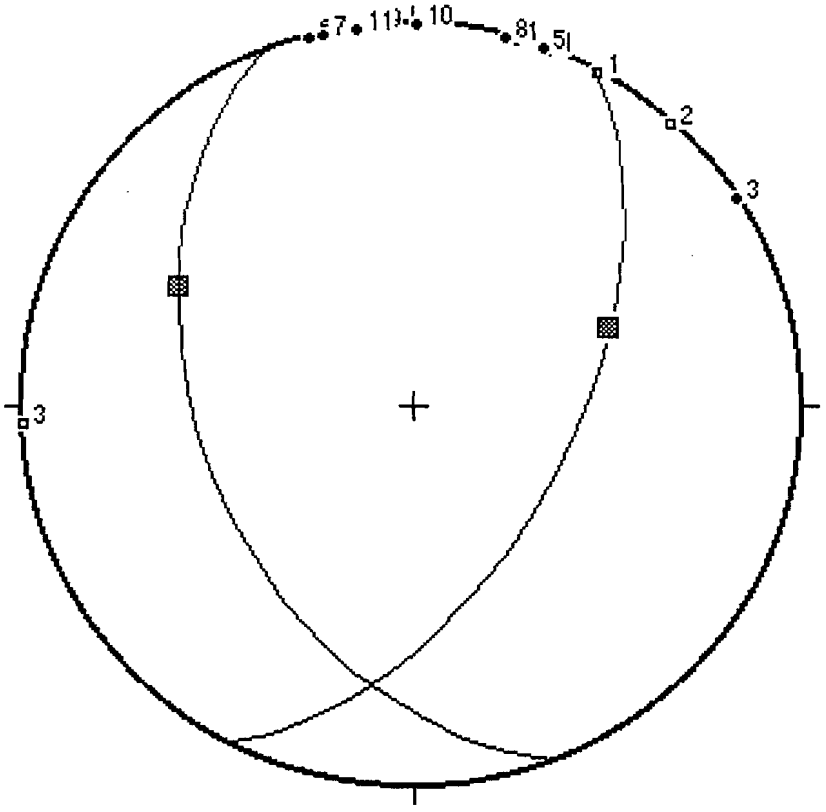

Nodal Plane-1: 028/58 E
Pole-1: 298/34
Nodal Plane-2: 158/45 W
Pole-2: 068/45

93/02/12 1710:23.36 19 28.74 N 154 54.07 W 1.13 km

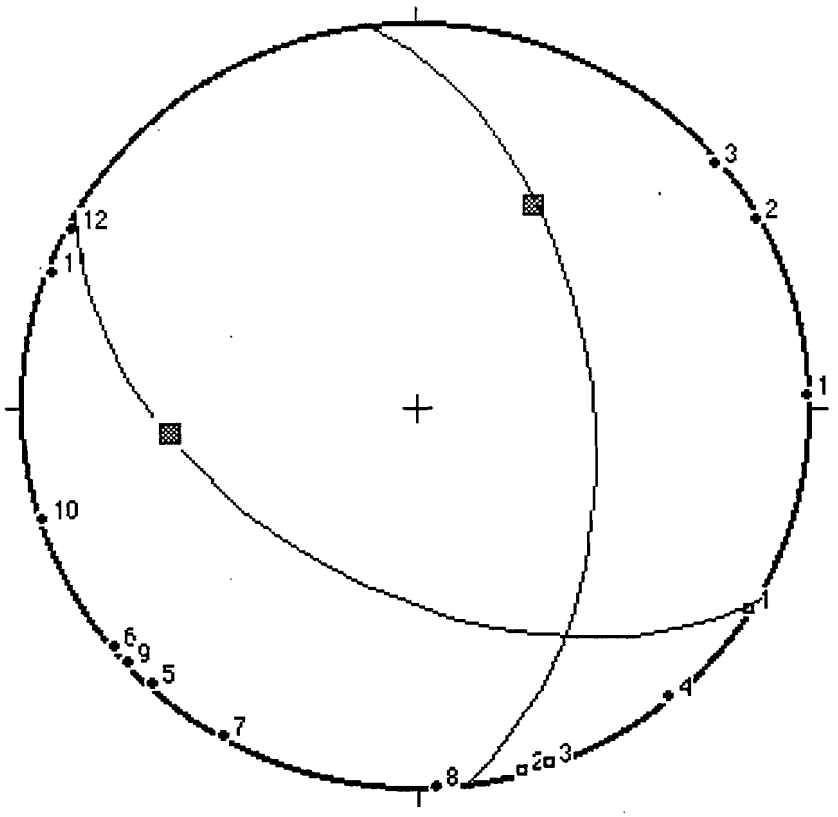

Nodal Plane-1: 121/51 S
Pole-1: 030/39
Nodal Plane-2: 354/53 E
Pole-2: 264/37

93/02/13 0217:13.33 19 28.13 N 154 54.19 W 1.94 km

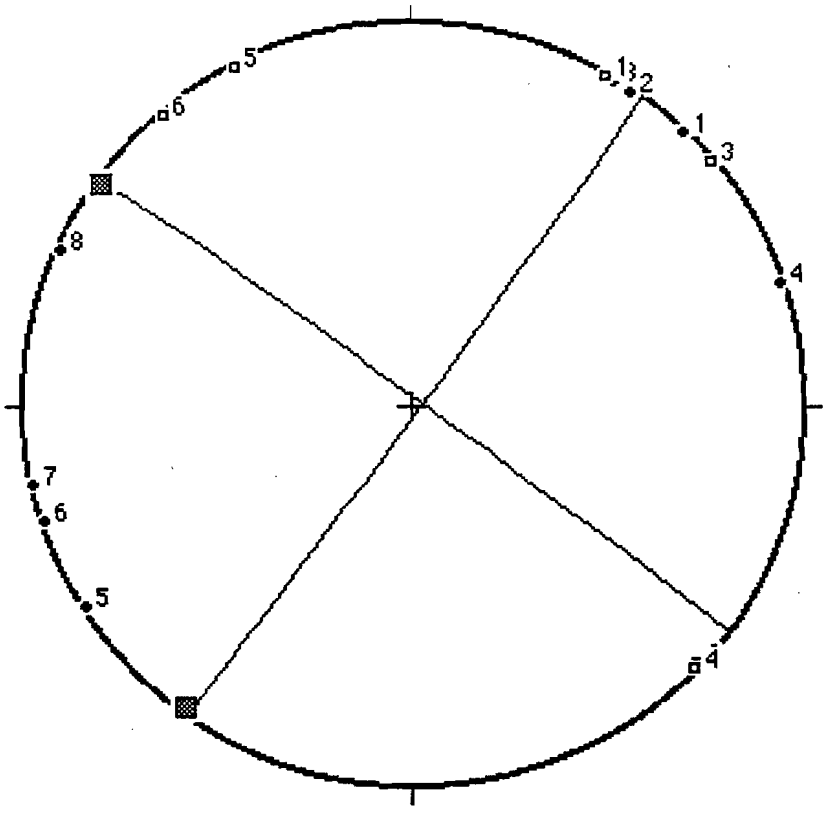

Nodal Plane-1: 306/88 N
Pole-1: 216/02
Nodal Plane-2: 036/88 W
Pole-2: 306/02

93/02/13 0823:33.98 19 27.34 N 154 53.37 W 9.10 km

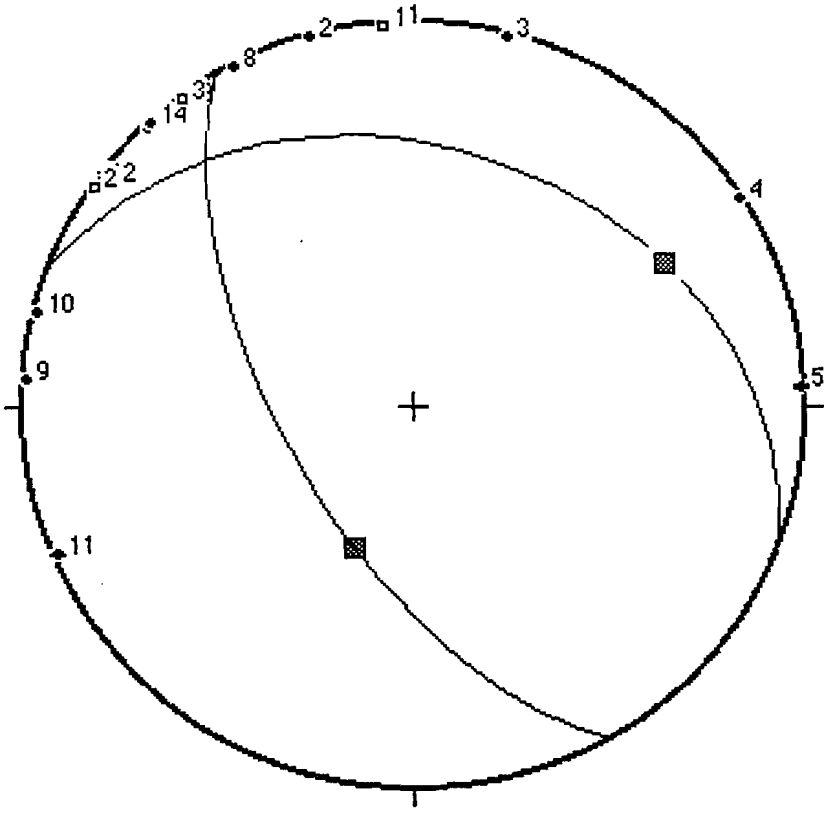

Nodal Plane-1: 291/33 N
Pole-1: 201/57
Nodal Plane-2: 150/63 W
Pole-2: 060/27

93/02/14 0912:24.47 19 24.63 N 154 53.28 W 2.72 km

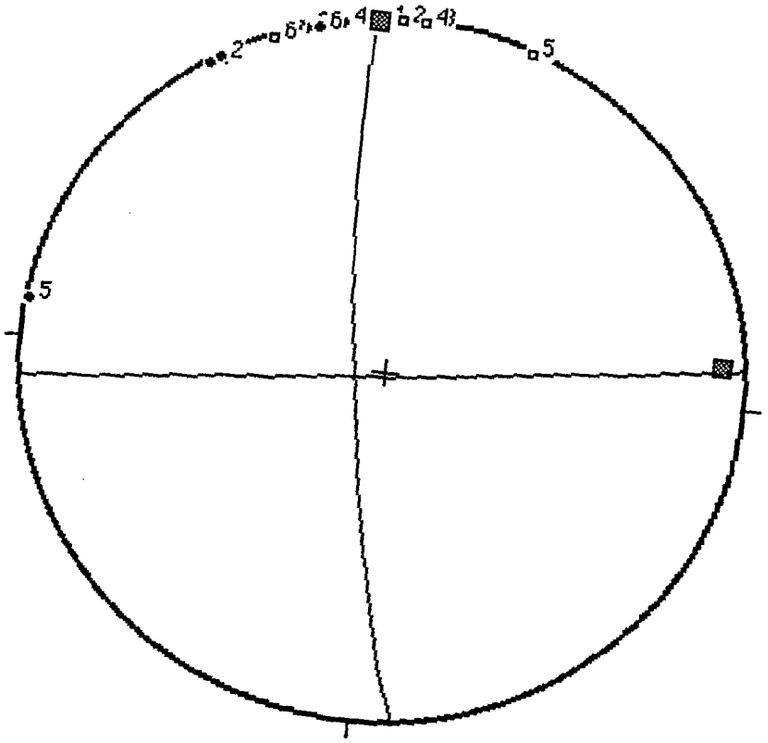

Nodal Plane-1: 173/83 W
Pole-1: 083/07
Nodal Plane-2: 084/89 S
Pole-2: 354/01

93/02/14 1531:56.21 19 28.47 N 154 53.07 W 10.45 km

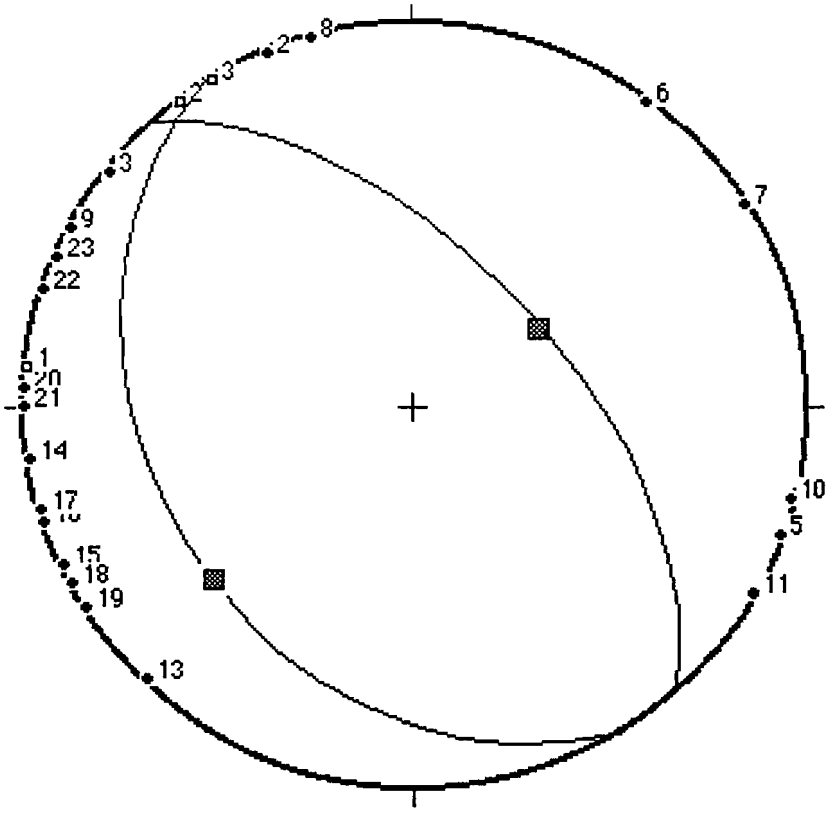

Nodal Plane-1: 148/31 W
Pole-1: 058/59
Nodal Plane-2: 318/58 E
Pole-2: 228/32

93/02/14 1845:23.81 19 29.06 N 154 52.57 W 5.49 km

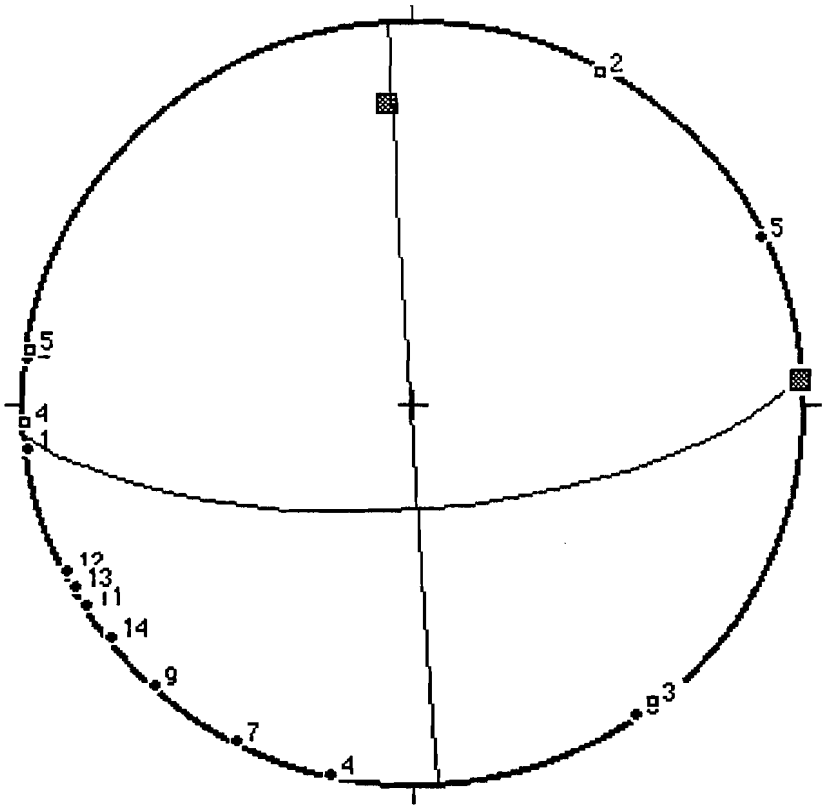

Nodal Plane-1: 085/68 S
Pole-1: 355/22
Nodal Plane-2: 176/89 W
Pole-2: 086/01

93/02/15 0405:03.05 19 27.54 N 154 56.24 W 4.34 km

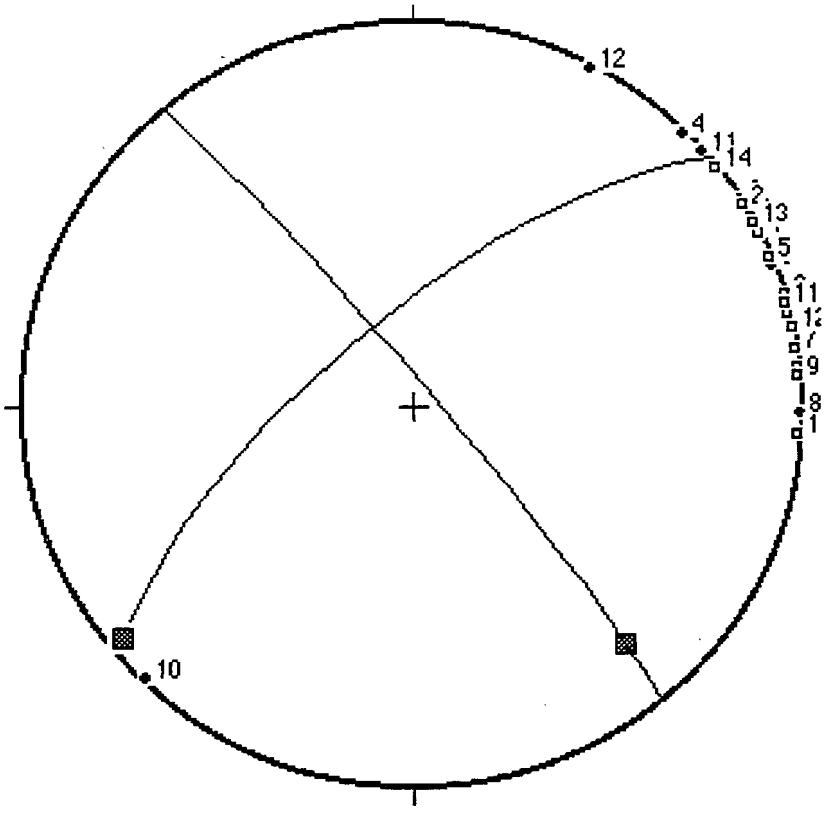

Nodal Plane-1: 229/72 N
Pole-1: 139/18
Nodal Plane-2: 321/86 E
Pole-2: 231/04

93/02/15 1017:25.64 19 27.65 N 154 54.94 W 2.97 km

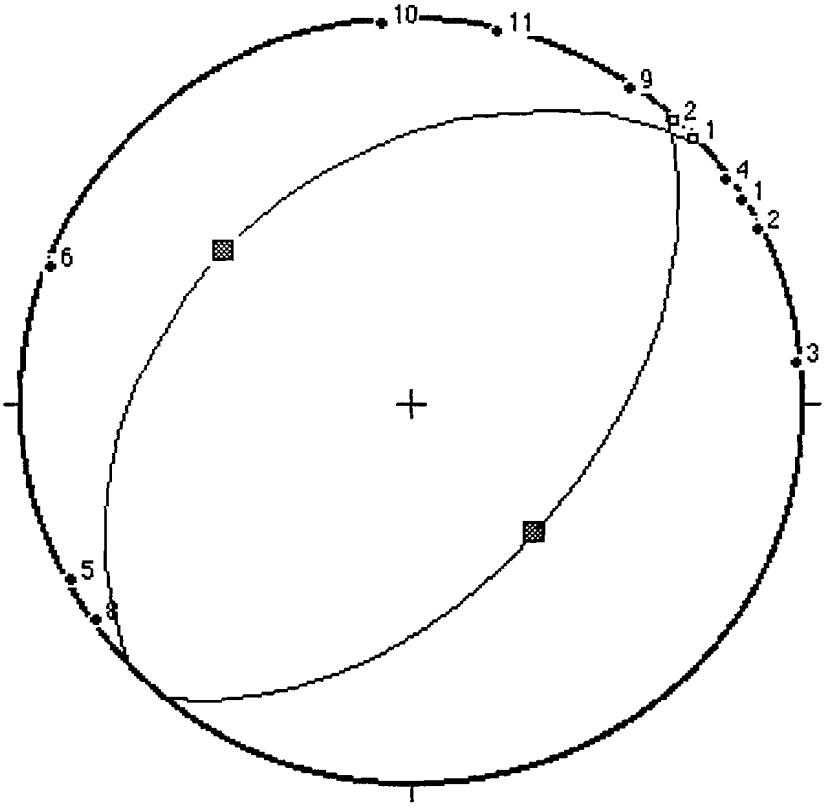

Nodal Plane-1: 227/38 N
Pole-1: 137/52
Nodal Plane-2: 040/52 E
Pole-2: 310/38